

FOR INFORMATION ONLY
PRELIMINARY DRAFT

REPORT NO.

SUBWAY ENVIRONMENTAL DESIGN HANDBOOK
VOLUME II

SUBWAY ENVIRONMENT SIMULATION (SES) COMPUTER PROGRAM
VERSION 3

PART I: USER'S MANUAL

Parsons Brinckerhoff Quade & Douglas, Inc.
One Penn Plaza
250 West 34th Street
New York NY 10001



NOVEMBER 1980
FINAL REPORT

DOCUMENT IS AVAILABLE TO THE PUBLIC
THROUGH THE NATIONAL TECHNICAL
INFORMATION SERVICE, SPRINGFIELD,
VIRGINIA 22161

Prepared for

U.S. DEPARTMENT OF TRANSPORTATION
URBAN MASS TRANSPORTATION ADMINISTRATION
Office of Technology Development and Deployment
Washington DC 20590

This file contains extracts of the SES version 3 User's Manual.

The scan was made because some of these sections do not appear in the SES version 4.1 User's Manual. They may still be of use, so here they are:

Section 13 (building a sample system, pages 3–24 of this file). It is Section 16 of the v4.1 Manual.

Section 14 (calculating with example systems, pages 25–130 of this file) was deleted from the v4.1 Manual. It may be useful for those learning to calculate station cooling using SES.

Section 15 (Montreal Metro tests and SES calculations, pages 131–246 of this file) was deleted from the v4.1 Manual. Aerodynamic, transient pressure and temperature tests. Shows how to use the pressure transient calculation in Section 3.4 of the SEDH volume 1.

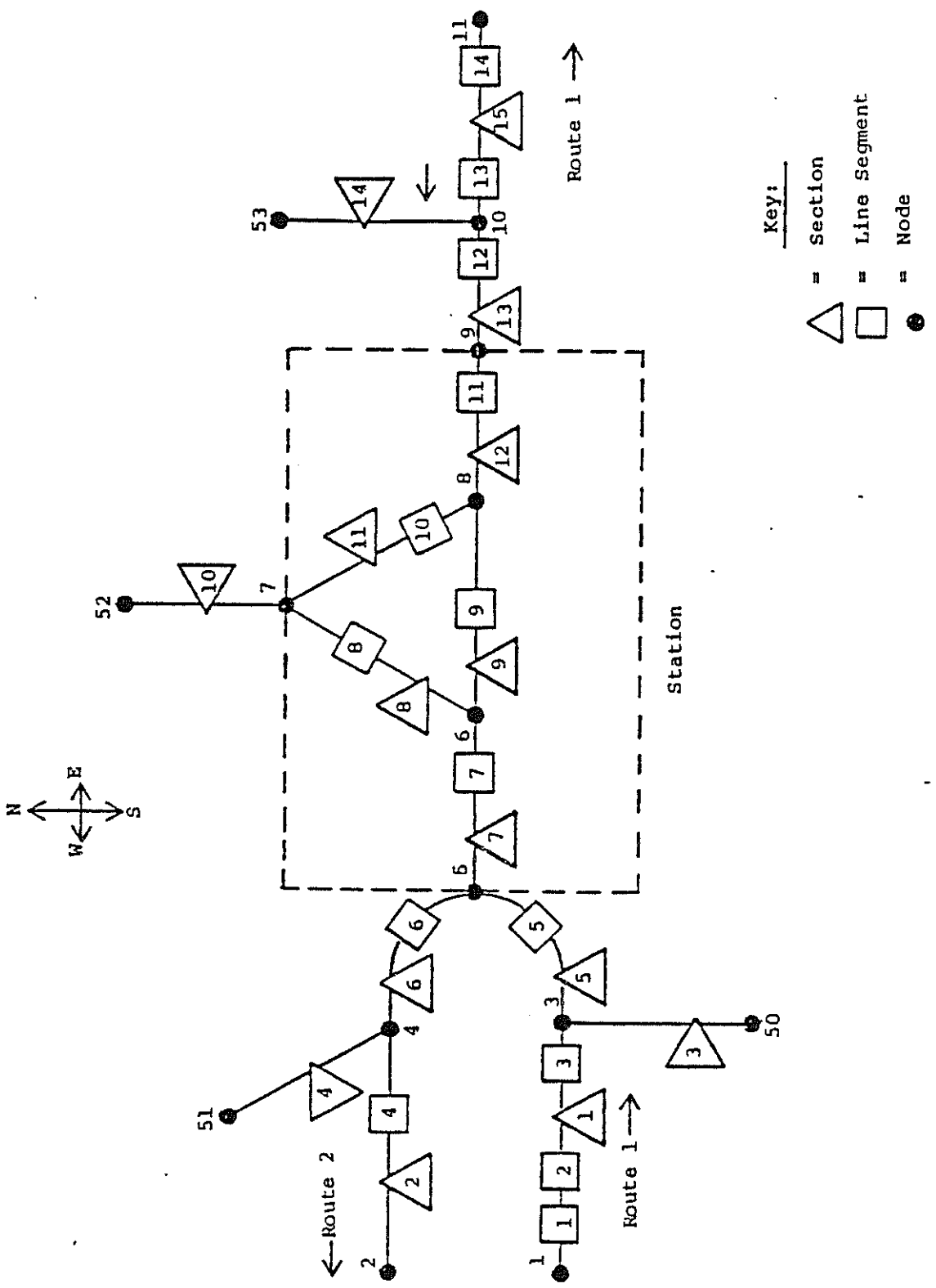
Section 16 (description of the SES fire model, pages 247–261 of this file) was deleted from the v4.1 Manual.

Ewan Bennett, November 2024.

13. SAMPLE PROBLEMS

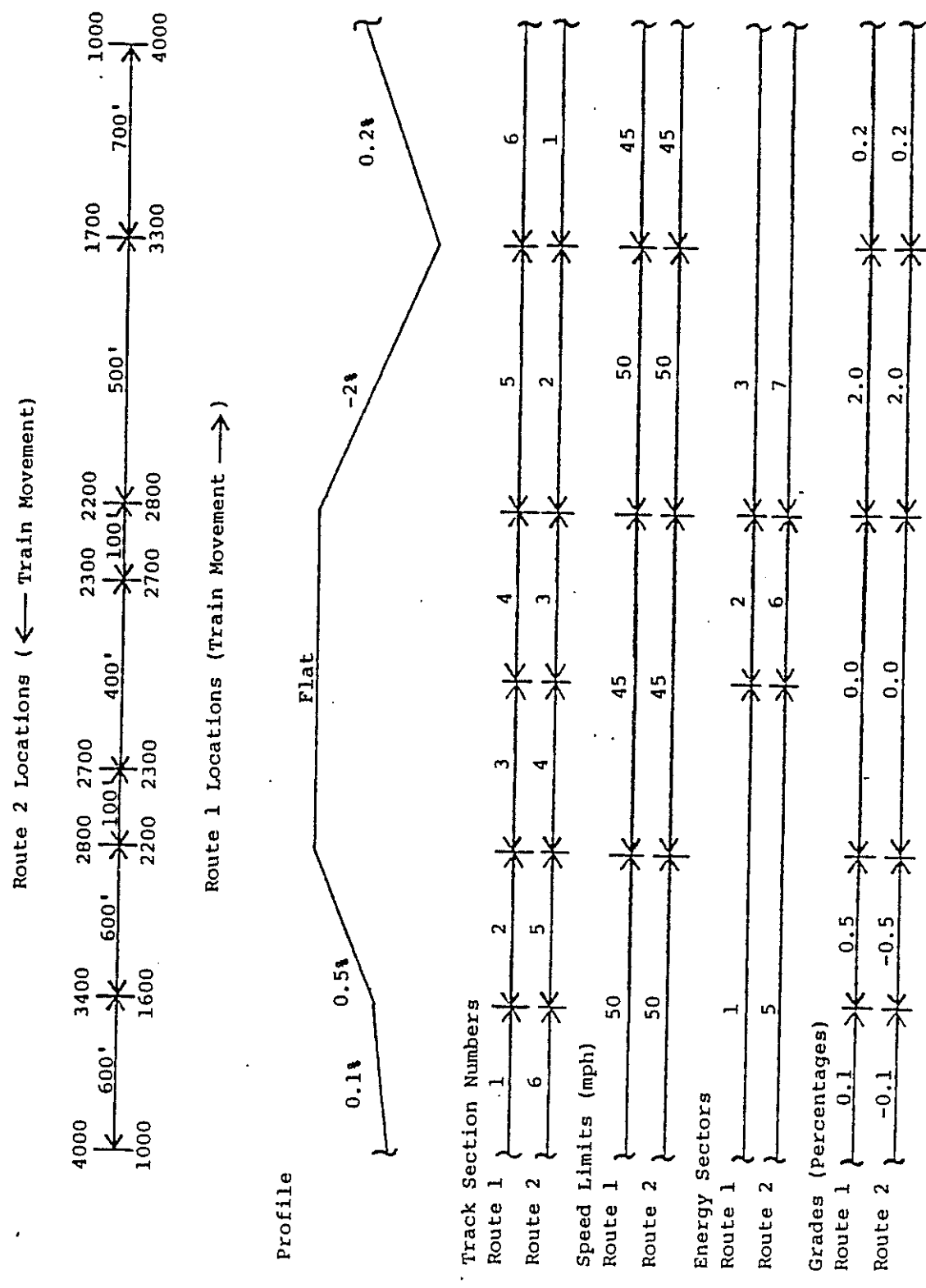
The SES program is very flexible and can accommodate many different types of subway systems. These sample problems are given to illustrate the use of the major program options available to the user. The user should realize that in some cases this has led to unlikely situations such as having coasting and regenerative braking on one route and not on another. Both of the sample problems use the exact same subway geometry and train types.

Figure 13.1 shows the system simulated by the sample problems. It consists of a one-station subway with adjoining tunnels at both ends of the station. The station has a mezzanine with two stairways connecting the platform and the mezzanine, and one stairway connecting the mezzanine with the street. The adjoining tunnels at the west end of the station are single-track tunnels with one-way traffic. The tunnel adjoining the east end of the station is a double-track tunnel with two-way traffic. Each of the two single-track tunnels has a ventilating shaft halfway between the west end of the station and the portals at the west end of the system. The ventilation shaft on the incoming single-track tunnel (Route 1) forms a "T" junction with the tunnel, and the ventilation shaft on the outgoing single-track tunnel (Route 2) forms an "angled" junction with the tunnel. There is a ventilation shaft with an exhaust fan 500 feet beyond the east end of the station in the double-track tunnel. This fan shaft forms a "T" junction with the double-track tunnel. There are also two impulse fans, one located in the outbound single-track tunnel, the other in the inbound single-track tunnel, between the station and the vent shafts.



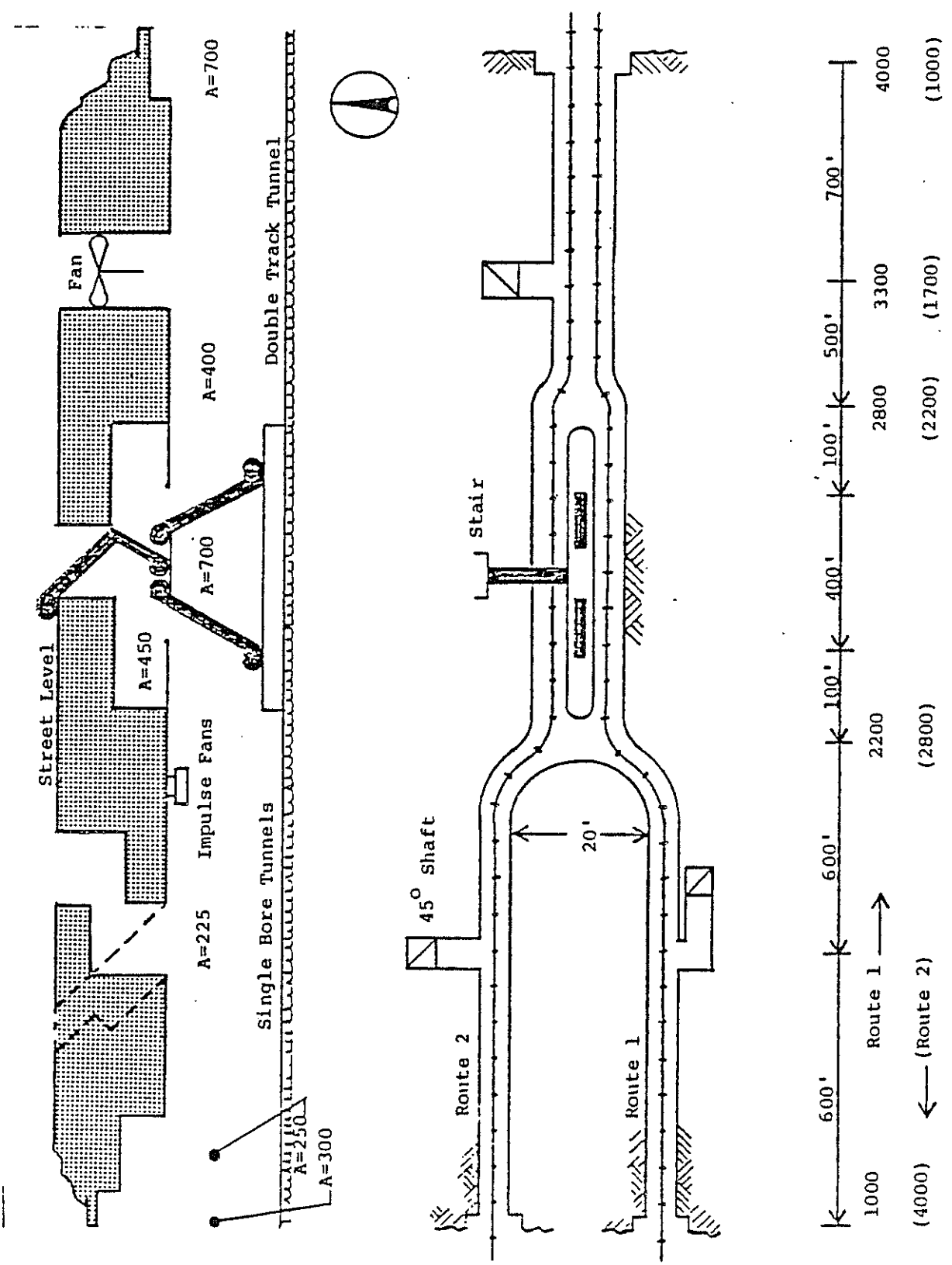
13-1(A)

FIGURE 13-1 SAMPLE PROBLEM SCHEMATIC DIAGRAM



13-1(B)

FIGURE 13-2 SAMPLE PROBLEM TRACK SECTION GEOMETRY



13-1 (c)

FIGURE 13-3 SAMPLE PROBLEM SYSTEM

As shown in Figure 13.2, there are six track sections of various grades and speed restrictions. Energy sectors are assigned to separately tabulate the amount of energy required to travel from the beginning of the system to the station, and from the station to the end of the system. Coasting is permitted on Route One (Eastbound) but not on Route Two (Westbound).

13.1 Obtaining the Input Data

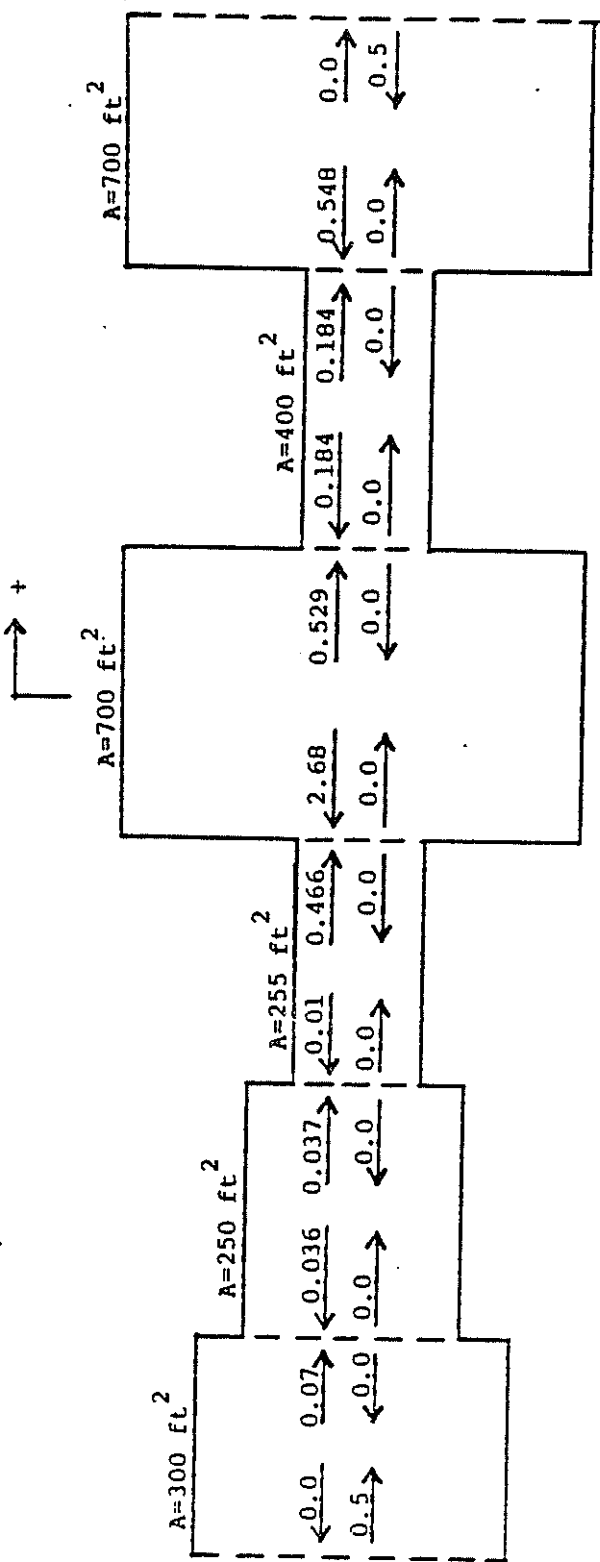
An outline of the methods used to obtain some of the input data for the sample system is discussed briefly below.

Figure 13.3 provides a schematic diagram of the base system. The schematic diagram is an extremely helpful aid when entering the system geometry in the input data. The vent shaft identification numbers have been arbitrarily set equal to the vent shaft section identification numbers plus 100. A "dummy" node (node 9) has been placed at the east end of the station to allow for a future addition of a stairway at that end of the station.

The calculations for the tunnel velocity head loss coefficients due to changes in the tunnel area are shown in Figure 13.4. It was assumed that all the losses are either square edge abrupt contraction or square edge abrupt expansion losses.

The steady-state heat source calculations are given for both the tunnels and the station in Appendix D. The tunnel lighting is a constant 7.0 Btu (hr-foot) of tunnel. This number is simply a function of the number and power of the lights within the tunnels.

All calculations based on ASHRAE Equipment
Guide and Data Book (1969 Edition)
(Tables 4.3 and 4.4)



13-2(A)

NOTE: All losses are either square edge
abrupt contraction or square edge
abrupt expansion losses.

KEY:

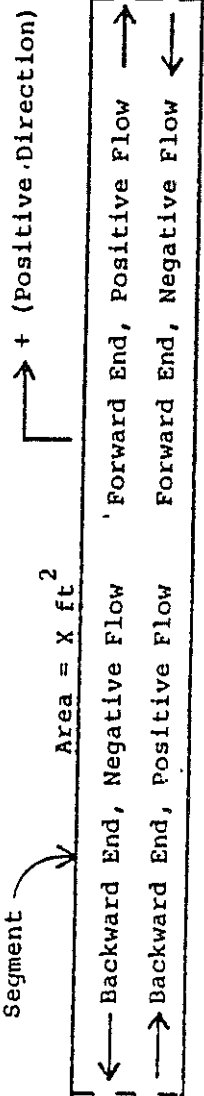


FIGURE 13-44 SAMPLE PROBLEM TUNNEL SEGMENT HEAD LOSSES

Third rail losses are also considered to be steady-state heat sources if they are averaged over the entire simulation, but they exist only in the line segments where trains are providing substantial amounts of power to their propulsion systems. This is due to the fact that trains draw relatively little power from the third rail when braking or maintaining speed on level trackway. Power is always being drawn from the third rail to provide power for train lighting, air conditioning and auxiliaries, but the third rail losses involved are very small in comparison to the losses that occur when a train is accelerating or maintaining speed against a large grade. Therefore, the user must determine where in his system trains will be drawing substantial amounts of power from the third rail to provide power to the trains' propulsion systems. It is only in these line segments that third rail losses are to be entered as steady-state heat sources.

It was determined that trains on Route 1 (West to East) only draw substantial amounts of power when they accelerate from the station after making their scheduled stop in the station. The trains on Route 1 accelerate to speed outside the tunnel system and enter the system at speed. Therefore, while the trains on Route 1 approach the station within the tunnel, the only power being drawn from the third rail is for the purpose of overcoming air drag to maintain speed and to power the train's lights, air conditioners and auxiliaries.

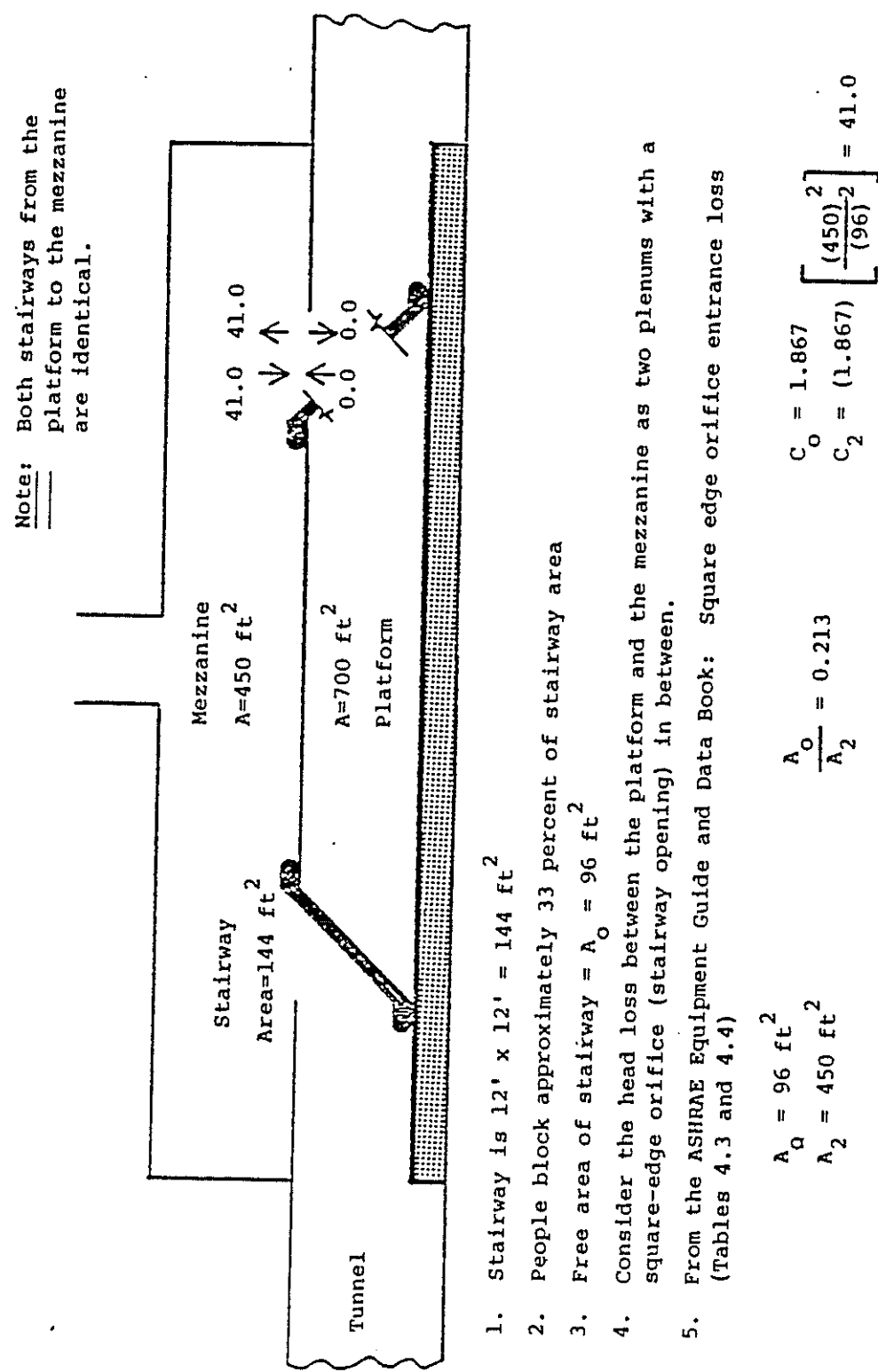
Similarly, it was determined that the trains on Route 2 (East to West) only draw substantial amounts of power when they accelerate from the station, as they also enter the tunnel system at speed and require relatively little power while approaching the station within the tunnel system.

Therefore, each tunnel segment has a steady-state heat source entitled "3rd Rail Loss, Tunnel Lighting." This number includes the rate of heat release from both tunnel lighting and third rail losses—if the segment is one in which no third rail losses occur, the steady-state heat source rate is equal to the rate of heat release from tunnel lighting only.

The initial conditions within the sample system were set equal to the outside ambient conditions as no data on the initial conditions within the system were provided. Therefore, the initial wall surface temperatures throughout the uncontrolled portion of the system were generally set equal to the outside ambient air dry-bulb temperature. As explained in Section 5.3 (Initial Conditions), the initial wall surface temperatures for the line segments within controlled zones were set equal to one degree Fahrenheit less than the design dry-bulb air temperature for the controlled zone. The initial dry-bulb and wet-bulb air temperatures for the uncontrolled portions of the system were set equal to the outside ambient dry-bulb and wet-bulb temperatures, respectively. Within the controlled zones, these temperatures were initialized at design conditions.

The calculations for the head loss coefficient between the station platform area and the mezzanine are shown in Figure 13.5. It is assumed that the mezzanine area and platform area are both plenums. The loss coefficient between the platform and mezzanine is then a square edge orifice loss between two plenums. The user must estimate the free area of a stairway opening based on the average number of patrons occupying the stairway at any given time and the amount of the total free area these patrons obstruct.

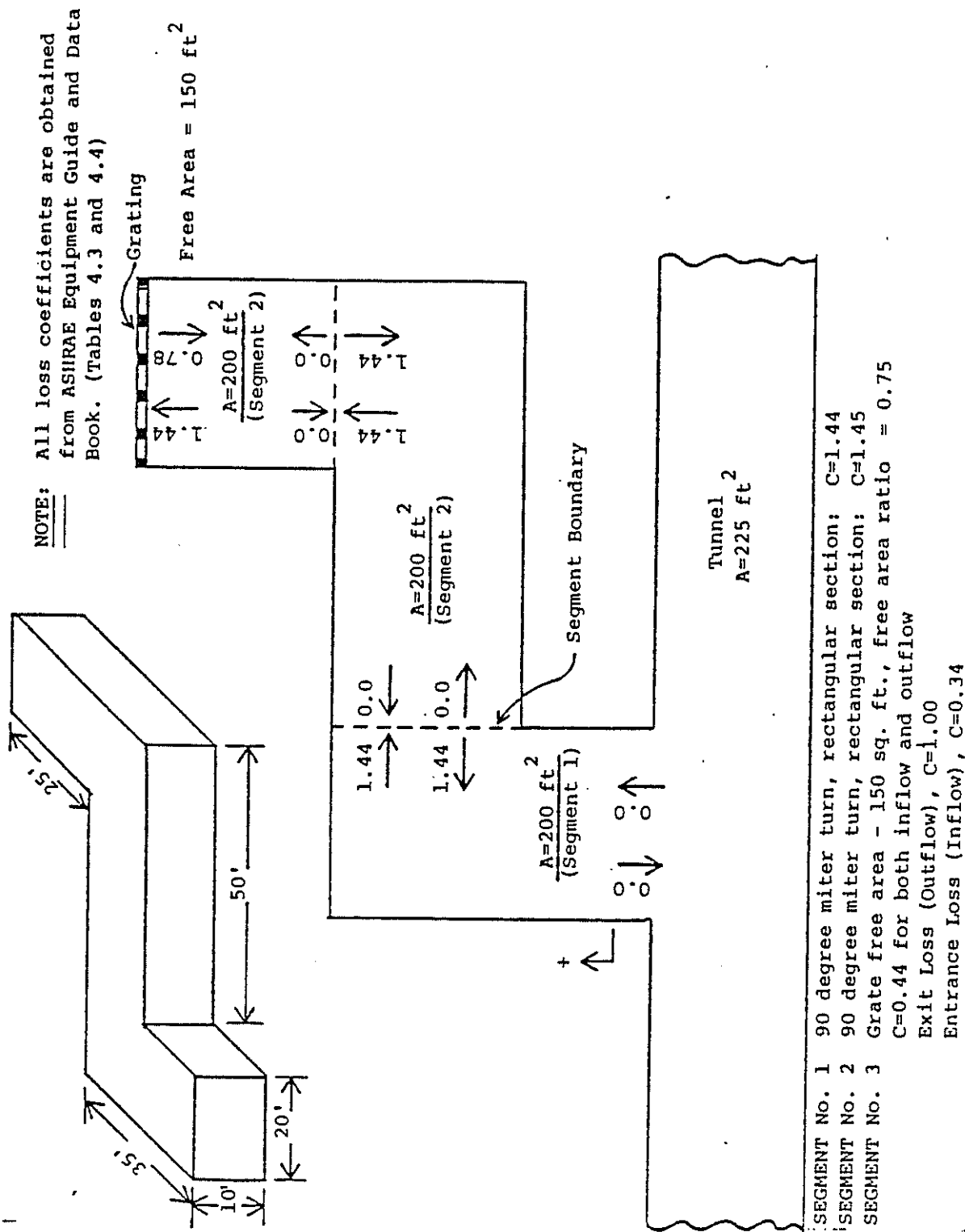
FIGURE 13-5 SAMPLE PROBLEM HEAD LOSS BETWEEN PLATFORM AREA AND MEZZANINE THROUGH STAIRWAY



13-4(A)

Figures 13.6 through 13.8 provide sketches of the vent shafts in the system. The head loss coefficients are calculated for both inflow and outflow in each segment of each vent shaft. The head loss coefficients for inflow in a vent shaft segment are often different from the loss coefficients for outflow in the same segment. This difference in loss coefficients for inflow and outflow is shown in Figure 13.7 at the boundary between Segment 1 and Segment 2.

The exhaust fan shaft located in the double-track tunnel at the east end of the system is shown in Figure 13.8. The loss coefficients were only calculated for the outflow (exhaust) direction of flow as this fan runs continuously in the outflow direction for the entire simulation (Fan Stopping/Windmilling Option 1.0). Therefore, the loss coefficients for the inflow direction were set equal to the loss coefficients for the outflow direction to avoid unnecessary calculations (a good approximation). This procedure is only valid if the Fan Stopping /Windmilling Option is 1.0. If the Fan Stopping/Windmilling Option is 2.0, the fan may possibly shut off and the simulation continue. When a fan shuts off within a vent shaft, both inflow and outflow will generally occur within the shaft as the fan is no longer forcing air to flow in one direction. Therefore, the loss coefficients for both inflow and outflow must be calculated for a fan shaft if the Fan Stopping /Windmilling Option is 2.0.

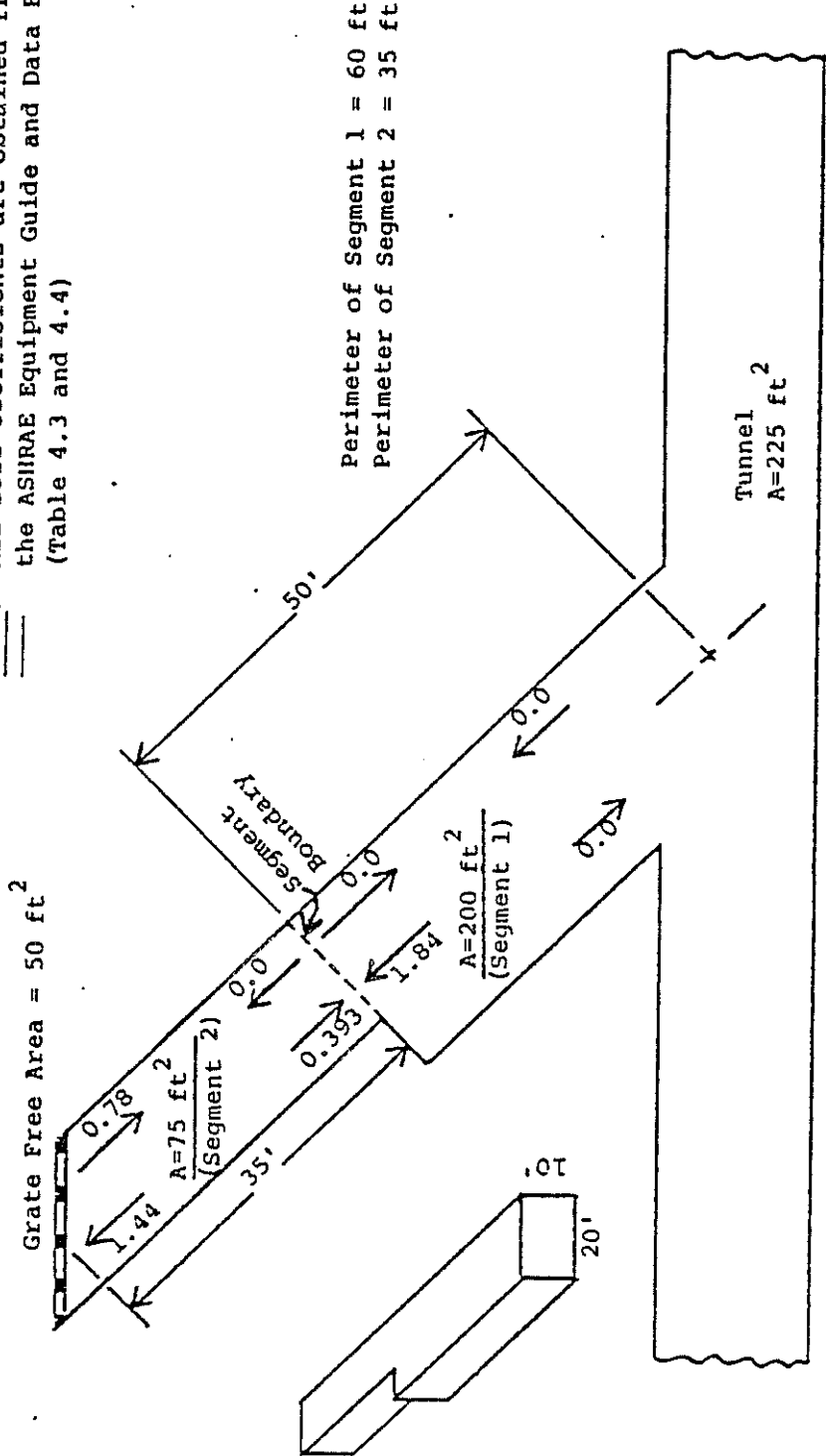


13-5(A)

SEGMENT NO. 1 90 degree miter turn, rectangular section: C=1.44
 SEGMENT NO. 2 90 degree miter turn, rectangular section: C=1.45
 SEGMENT NO. 3 Grate free area - 150 sq. ft., free area ratio = 0.75
 $C=0.44$ for both inflow and outflow
 Exit Loss (Outflow), $C=1.00$
 Entrance Loss (Inflow), $C=0.34$

FIGURE 13-6 SAMPLE PROBLEM #1 - VENT SHAFT HEAD LOSS CALCULATIONS FOR VENT AT 1600 FT - ROUTE 1

Note: All loss coefficients are obtained from the ASHRAE Equipment Guide and Data Book.
(Table 4.3 and 4.4)



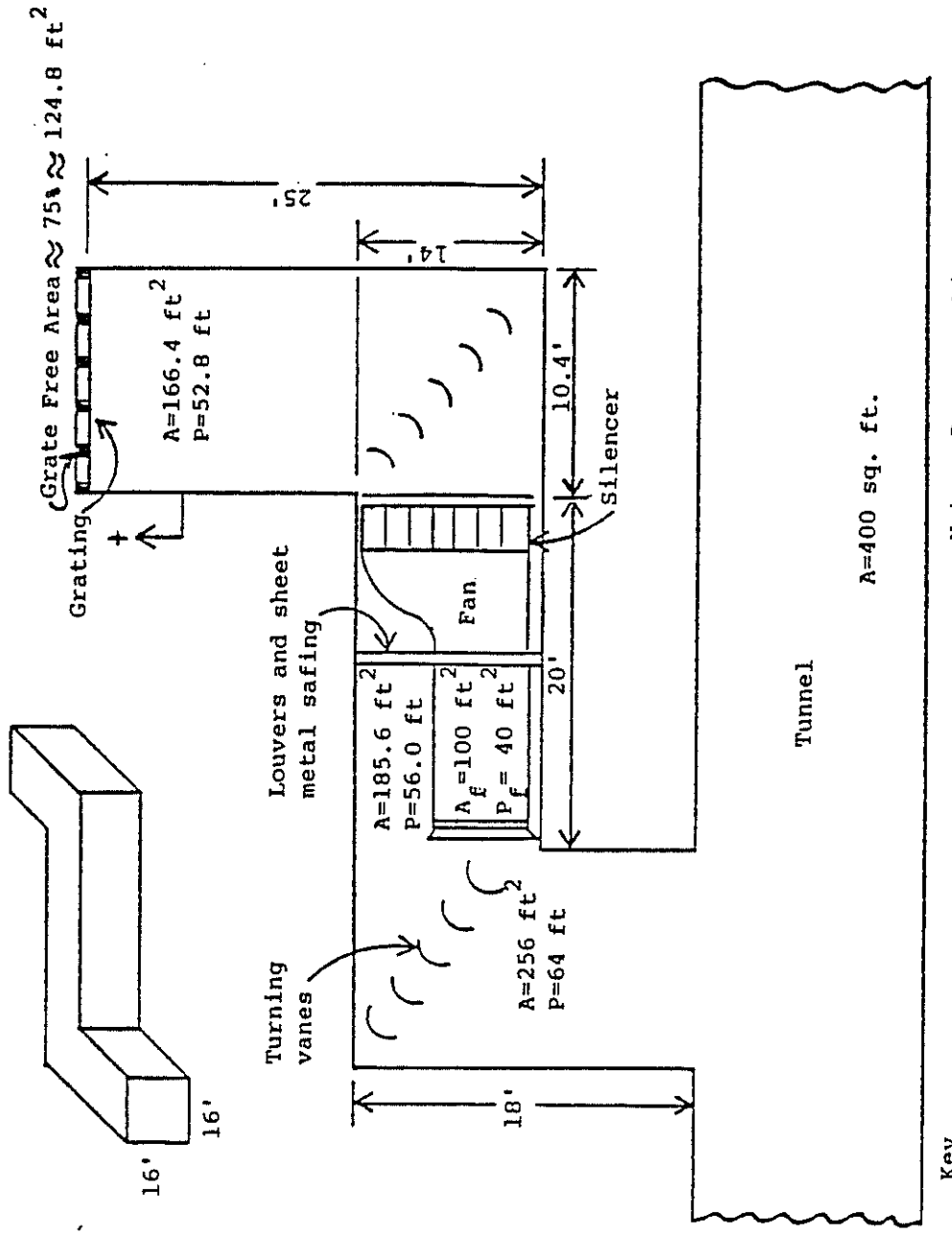
Segment #1. Abrupt Contraction:
(Forward End, Positive Flow) $A_2/A_1 = 0.375$ $C_2 = 0.259$

$$C_1 = 0.259 \quad \frac{200}{75} = 1.84$$

Segment #2. a. (Backward End, Negative Flow): Abrupt Expansion $A_1/A_2 = 0.375$ $C_1 = 0.393$

- b. Loss through Grating: Total Pressure loss through grating $\approx 0.0275 \text{ in. w.g.}$
@ 1,000 FPM therefore K through grating $= 0.44$ for both directions
Exit Loss = 1.00
Entrance Loss = 0.34

FIGURE 13-7 SAMPLE PROBLEM VENT SHAFT HEAD LOSS CALCULATIONS FOR VENT AT 1600 FPM - ROUTE 2



Key

- A = Area of Segment
- P = Perimeter of Segment
- A_f = Area of Fan Intake
- P_f = Perimeter of Fan Intake

Note:

Because this fan shaft operates continuously, in the exhaust (positive) direction, the loss coefficients for the inflow (negative) direction are never utilized and may therefore be set equal to the coefficients calculated for positive flow to avoid unnecessary calculations.

13-5(c)

FIGURE 13-8. SAMPLE PROBLEM TUNNEL EXHAUST FAN SHAFT 500 FT EAST OF THE STATION

1. From ASHRAE Equipment Guide And Data Book (Tables 3.3 and 3.4):

Segment 1: $A = 256 \text{ Sq. Ft.}$
 $P = 64 \text{ Sq. Ft.}$

Forward End:
(Positive and Negative)

a. Turning loss through turning vanes
Consider this as a miter with turning
vanes
Therefore $C \approx 0.225$

b. Abrupt contraction

$$A_1 = 256 \text{ Sq. Ft.} \quad A_2/A_1 = 0.391 \\ A_2 = 100 \text{ Sq. Ft.} \quad C_2 = 0.253$$

$$C_1 = (0.253) \left(\frac{256}{100} \right)^2 = 1.658$$

$$\boxed{\sum \text{SEGMENT 1} = 1.88}$$

Segment 2: $A = 100 \text{ Sq. Ft.}$
 $P = 40 \text{ Ft.}$

Forward End:
(Positive and Negative)

a. Loss through silencer - This depends
upon type of silencer installed.
Loss through silencer $\approx 0.15 \text{ in. w.g.}$
 $\times 22550 \text{ FPM}$

Reference This Loss to Fan Area and Fan Volume Flowrate:

$$\text{Area} = 100 \text{ Ft}^2 \quad \text{CFM} = 120,000 \text{ CFM}$$

$$0.15 = \Delta P = K \rho v^2 / 2g = (0.075) \left(\frac{120,000}{100 \times 60} \right)^2 \frac{(K)}{32.2 \times 5.202 \times 2} \quad \underline{\underline{K = 1.675}}$$

b. Turning loss through turning vanes
Consider this a miter turn with turning
vanes:
Therefore $C \approx 0.225$

c. Abrupt Expansion

$$A_1 = 100 \text{ Sq. Ft.} \quad A_1/A_2 = 0.601 \\ A_2 = 166.4 \text{ Sq. Ft.} \quad C_1 = 0.16$$

$$\boxed{\sum \text{SEGMENT 2} = 2.06}$$

FIGURE 13.8 CONTINUED

Segment 3: $A=166.4 \text{ ft}^2$
 $P=52.8$

Loss through grating:
Grate Free Area = 124.8 ft^2

Total pressure loss through grating = 0.0275 inches H_2O @ 1,000 FPM
therefore loss coefficient = 0.44 for both inflow and outflow.

Exit Loss = 1.00

Entrance Loss = 0.34

$$\sum \text{SEGMENT 3 out} = 1.44$$

$$\sum \text{SEGMENT 3 in} = 0.78$$

Sketch of the fan shaft with its equivalent areas and resulting loss coefficients for each segment

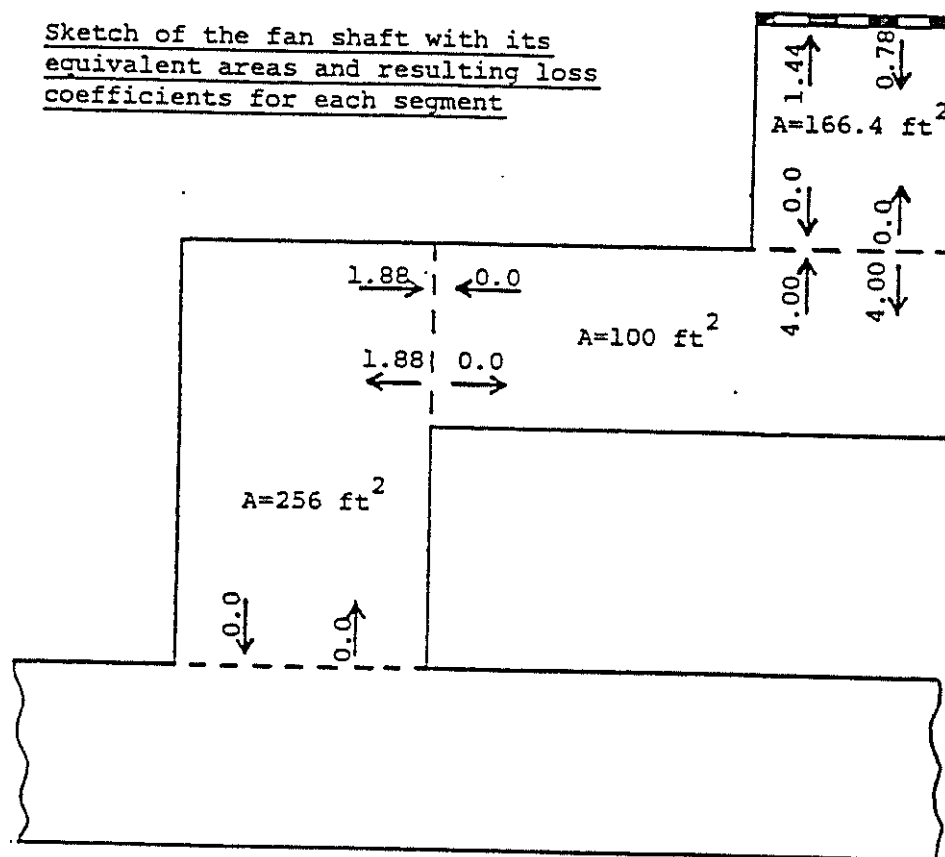


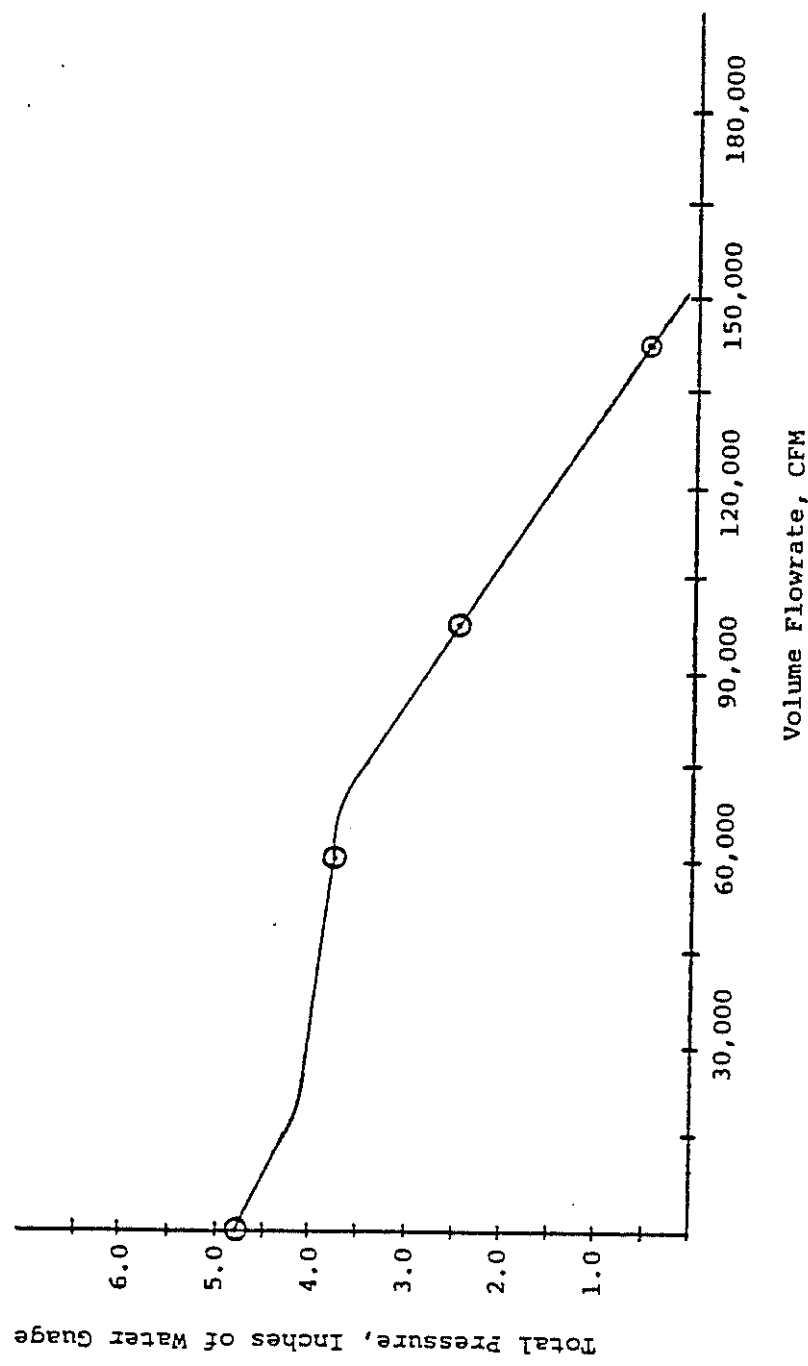
FIGURE 13-8 CONTINUED

13-5(E)

The aerodynamic type of each node is as follows:

<u>Node No.</u>	<u>Aerodynamic Type</u>
1	0 - straight-through junction or portal
2	0 - straight-through junction or portal
3	3 - "T" junction
4	4 - angled junction
5	5 - "Y" junction
6	7 - zero static pressure change junction
7	3 - "T" junction
8	7 - zero static pressure change junction
9	7 - zero static pressure change junction
10	3 - "T" junction
11	0 - straight-through junction or portal
50	0 - straight-through junction or portal
51	0 - straight-through junction or portal
52	0 - straight-through junction or portal
53	0 - straight-through junction or portal

The junction at Node 4 (see Figure 13.2) is a 45 degree angled junction. The SES program only allows the user to enter an angle of either 10, 20, or 30 degrees for junction angles. Therefore, when the junction angle is greater than 30 degrees, the user must choose whether to enter the junction as a 30 degree angled junction or as a 90 degree "T" junction. In this case, the 45 degree angled junction at Node 4 more closely resembles a 30 degree angled junction than a



① Point entered in input data

FIGURE 13-9. SAMPLE PROBLEM FAN PERFORMANCE CURVE FOR THE TUNNEL EXHAUST FAN

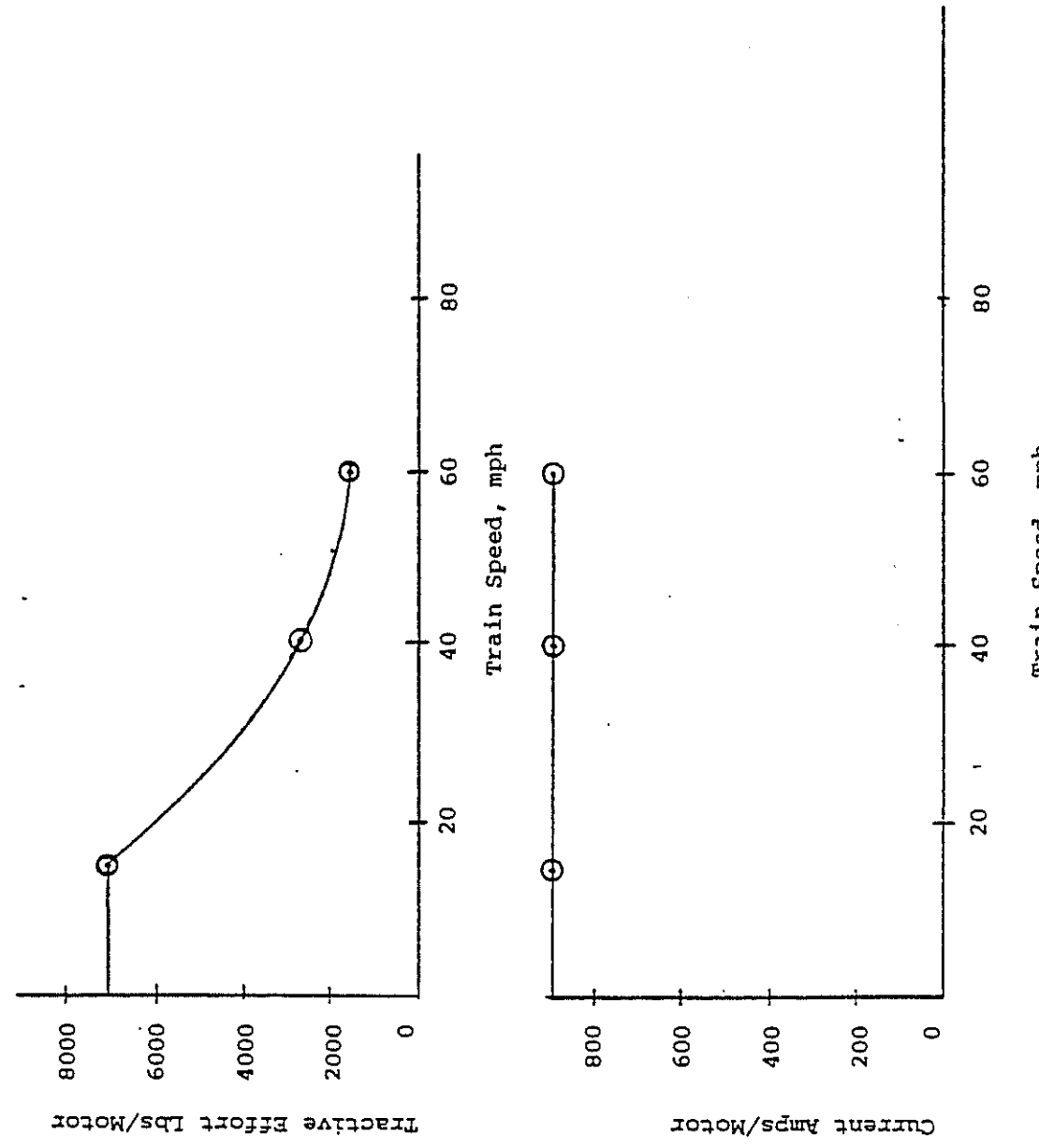
90 degree "T" junction, and was therefore entered as a 30 degree angled junction. The aerodynamic node types at the remaining junctions are basically self-evident and need no further explanation.

Figure 13.9 provides the fan curve for the exhaust fan mentioned above. The program requires the user to enter four points along this curve. These four points are spaced fairly evenly, with one of the points being where the volume flow rate is zero, and another of the points being where the total pressure rise across the fan is practically zero. The upper flow limit was set at 220,000 cfm to allow for a slight degree of windmilling when a train passes beneath the fan shaft. The lower flow limit was set at -2000 cfm for although it is intended for the fan to always operate in the outflow (exhaust) direction, it is possible that, depending on train, line segment and fan characteristics, air will be drawn into the system against the action of the fan. The simulation will terminate if the fan volume flow rate attempts to fall below -2000 cfm.

Data for the impulse fans (Form 7C) is taken from the manufacturer. The pressure efficiencies are calculated as described in Section 4.4, with the angle between the tunnel and outflow nozzle being 30° and 35° for Impulse Fan Types 1 and 2, respectively.

Figure 13.9 provides the tractive effort and motor current curve data used in the train performance subprogram. (Since both trains are chopper controlled the resistance speeds and external resistances on Form 9I are entered as zero.) These curves are interrelated with each other and must be entered in a specific manner. The tractive effort and current data must be entered for the same train speeds. The user must also remember that there is a constant internal resistance

Ⓐ Point entered in input data



13-7(A)

FIGURE 13-10. SAMPLE PROBLEM TRAIN PROPULSION MOTOR PERFORMANCE CURVES

that is used in the program calculations. This internal resistance is the third resistance entered on Form 9I. This internal resistance is not included in the entry of chopper efficiency. (It must also be taken into account when calculating the train heat rejection in kilowatts/train when using Train Performance Option 3).

Heat rejection from the subway vehicle (Form 9C) was calculated as per the method described in Appendix E.

The entries for percent of heat captured by the trackway exhaust system are based on the design of the vehicles in this system which have their resistor grids (Propulsion/Braking System Heat) located below the car, and their air conditioning condenser-compressors (Train Auxiliaries and Passenger Heat) located above. The sample system has only an underplatform exhaust, and no overtrack exhaust. Therefore certain percentages of the Propulsion/Braking System Heat will be reduced (40 percent and 20 percent for a stopped and moving train, respectively), since this heat is given off below the train. However none of the Train Auxiliaries and Passenger Heat will be captured by the trackway exhaust system, as this heat is released above the car, and as mentioned above, this system contains no overtrack exhaust.

Since this is not a fire simulation, the Stack Heights (Form 3A) were entered as zero. The actual stack height of a line segment should be entered only when a fire is being simulated.

The physical data for the train is not included as this information is very straight-forward and is most often supplied by the manufacturer. The actual train motor data entered is slightly different from the manufacturer's motor data supplied. As a result, the user may notice that the program adjusted the tractive effort curve data supplied in

Form 9G based on the adjusted vehicle data supplied in Form 9F. Many times the actual vehicle data will correspond to the manufacturer's data and no adjustment will be necessary. In the sample system two train types are simulated. Train Type One uses regenerative braking with an efficiency of 45%. Train Type Two uses flywheels (one per car) for on board energy storage. Other than these two differences, the two train types are identical.

Finally, all the input forms necessary to create a complete data set for the sample problems are provided herein.

13.2 Interpretation of Data Presented in Input Verification

The input verification prints all the data provided by the user as well as some additional information calculated by the program. The input verification prints the data in the same order in which it was entered. In other words, the input data verification printout corresponds exactly to the input forms used to enter the data in the SES program. The form numbers are printed in the right hand margin on each page of the input verification to enable the user to immediately identify at all times the exact portion of the input data being presented. The form numbers in the right hand margin help the user to establish a one to one correspondence between the input forms and the input verification.

One detail print is given at the completion of the SES input verification. This detail print provides the initial conditions of the system at the start of the simulation.

14. SYSTEM SIMULATIONS AND SENSITIVITY STUDIES

The preceding sections of this manual provide the information necessary to successfully apply the SES program in an evaluation of the subway environment to be expected for any specific geometrical arrangement and operational scheme. This section of the manual addresses the application of the SES program to a variety of hypothetical subway design and operational concepts. The results of these simulations supply the user with an added degree of insight regarding the aerodynamics and thermodynamics of these subway design concepts. Discussions of the sensitivity of simulation results to key SES program inputs are also presented.

The user is cautioned that the SES program results portrayed herein are not intended to supplant application of the SES program. However, together with the computational methods presented in Volume I, Part 3, these SES program-generated findings provide a valuable data base for formulating preliminary environmental control concepts and for developing cost-effective environment control strategies. Although the simulations described in the section were done using SES Version 1, the conclusions reached herein are applicable to SES Version 3 because the relevant mathematical models are not only phenomenologically identical, but in most cases provide the same numerical result.

These system simulations of subway airflows and temperatures encompass a variety of subway system geometries, environmental control features and train operations. Specific parameters considered include the following:

- o ventilation shaft flow impedance
- o number of ventilation shafts (ventilation shaft spacing)
- o blockage ratio
- o mechanical ventilation concepts
- o trackway exhaust systems and efficiencies
- o train headway and heat release
- o double-track tunnel versus parallel single-track tunnels
- o relative train situation during bi-directional operation
- o long-term heat sink behavior (with and without migrating groundwater condition)

- o station air conditioning with station design temperatures at and below ambient
- o emergency ventilation situations.

For the purpose of assessing the sensitivity of the subway environment to parametric variations, a base system configuration was defined which would provide reference values of the required airflows and temperatures. This base system, illustrated by Figure 14-1, comprises a series of five identical subsystems linked end to end. Train operations through the base system are illustrated by Figure 14-2. The maximum train speed achieved between stations is 60 mph, which is maintained for approximately 10 seconds of the station-to-station travel time. Also shown on Figure 14-2 are the train power dissipation and train heat rejection profiles. The peaks in the train power dissipation curve are, of course, due to the dissipation of the braking energy of the train. The substantial difference between this power dissipation and the corresponding train heat rejection is attributable to the thermal inertia of the dynamic braking resistor grids on board the train. For the trains used in these simulations, roughly 55 percent of the total train heat was rejected within the confines of the tunnel (4500 MBH) and 45 percent in the stations (3500 MBH). Of the total train heat, approximately 40 percent comes from the on-board air-conditioning system and auxiliaries, while 60 percent of the train heat is traceable to the propulsion system and braking losses.

Other quantitative details regarding the subway geometry and operations for each SES program-simulated system are presented in the appropriate following articles of this section. The results of the SES program-simulations are presented in a graphical, rather than a tabular format to aid understanding and interpretation.

14.1 BASE SYSTEM RESULTS

Results of the SES program Base System simulation are presented on Figure 14-3 in terms of average air-temperature distribution along the length of the five-station system. This is the average air temperature that would persist during a peak rush-hour operation with train headways of 120 seconds on each track. The tunnel temperatures average on the order of 15°F above the outside ambient, whereas the stations average on the order of 25°F above outside ambient with one notable exception: Station 3. In Station 3, the

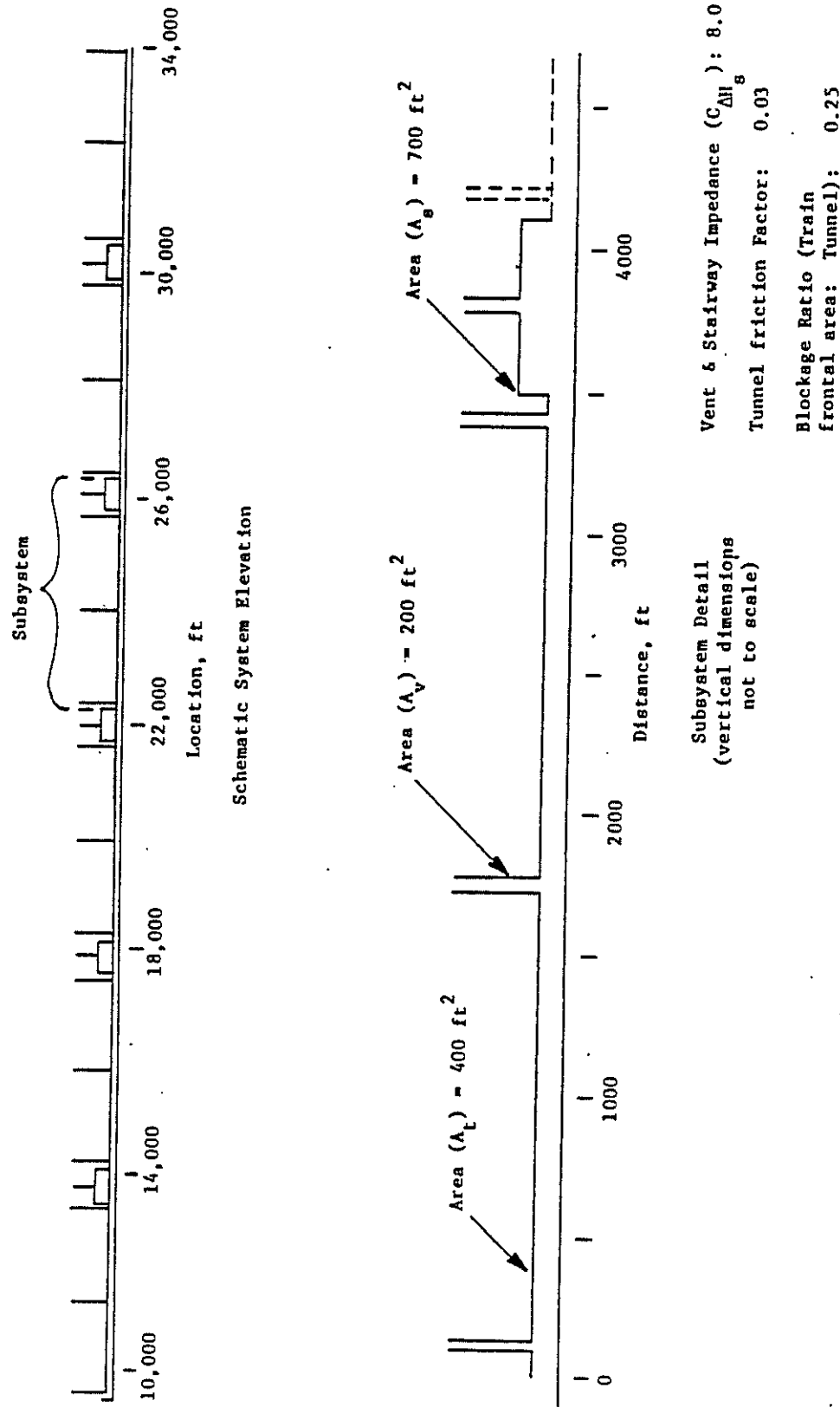


FIGURE 14-1. BASE SYSTEM GEOMETRY SCHEMATIC

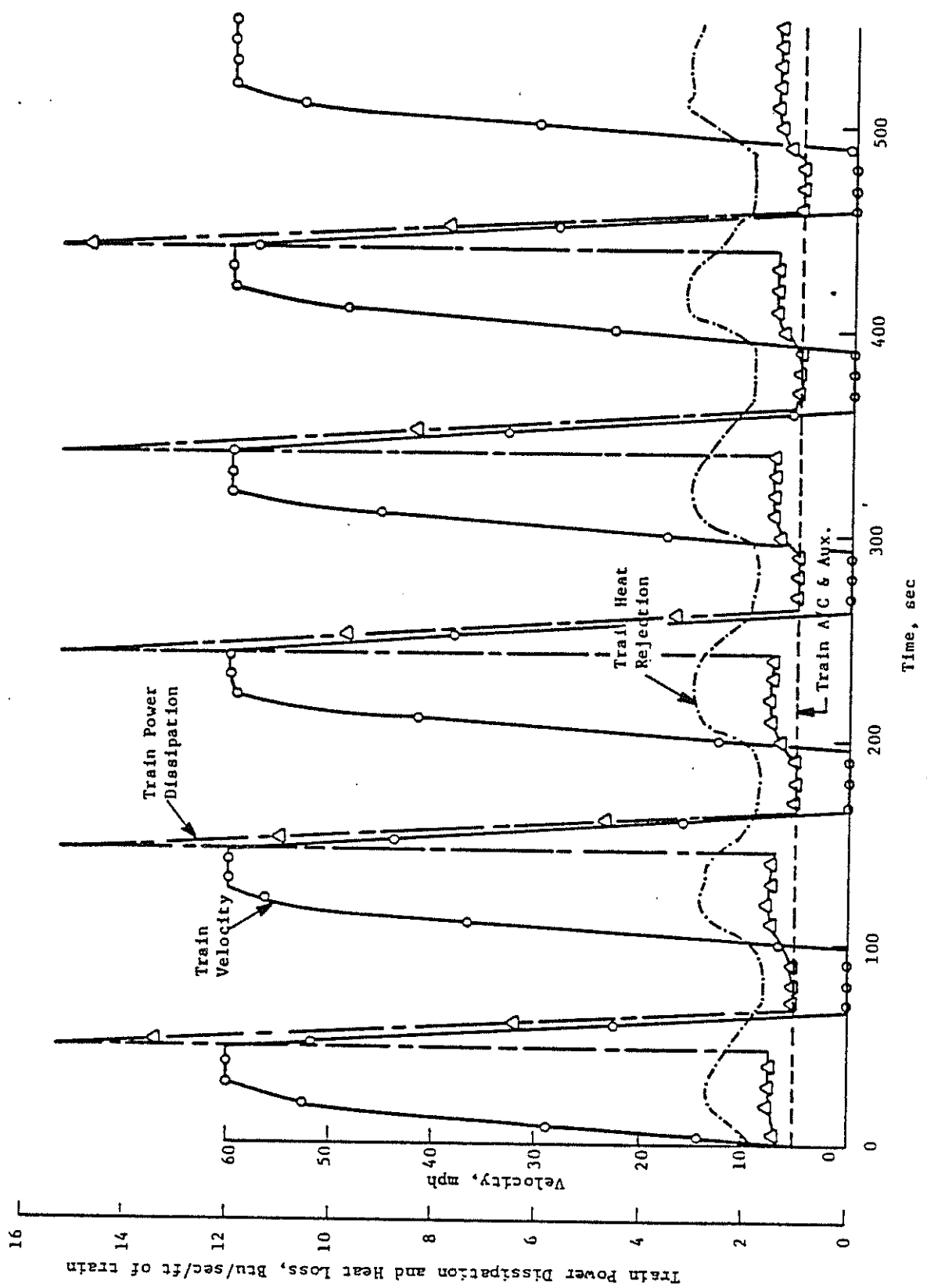
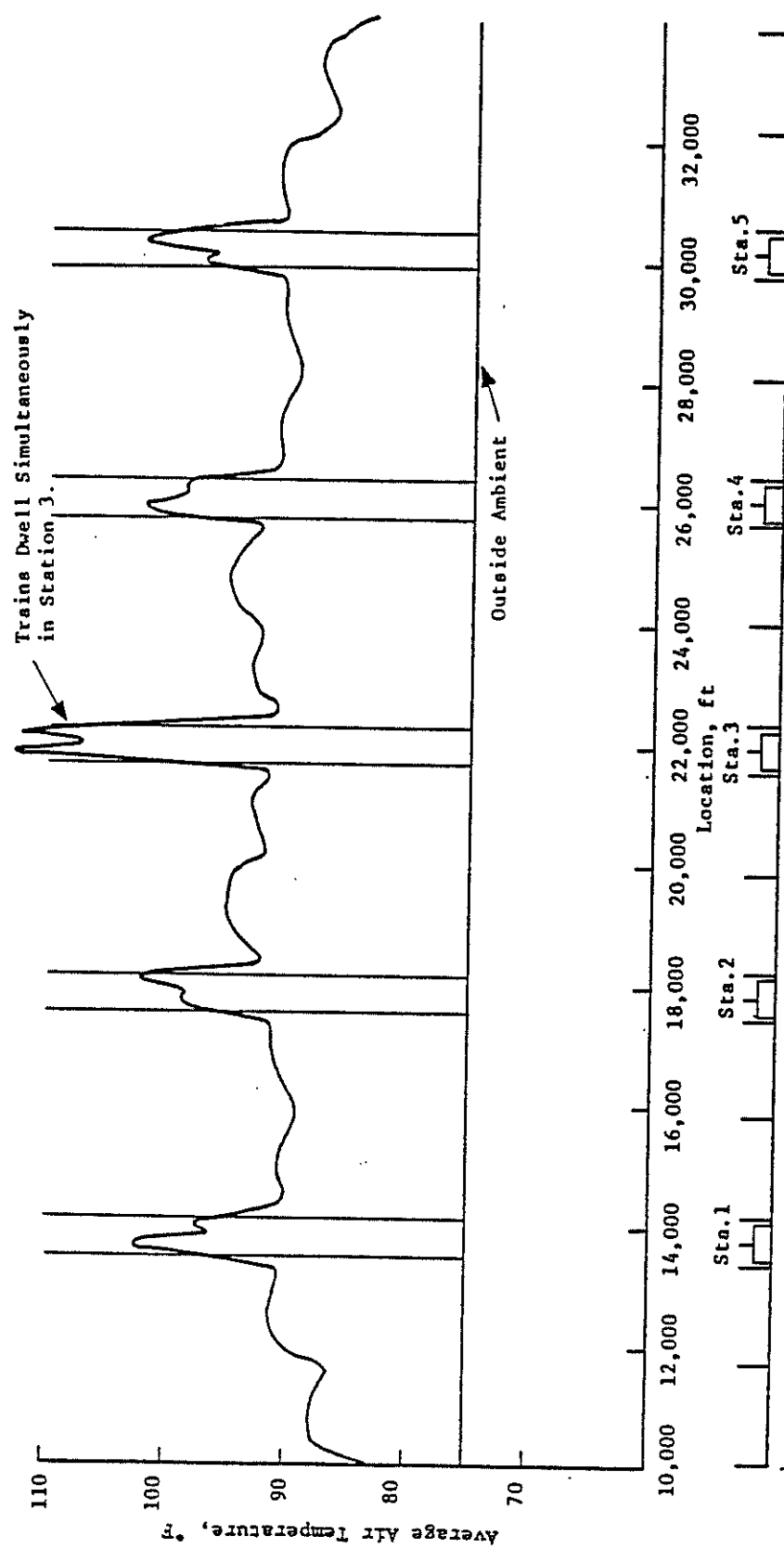


FIGURE 14-2. SYSTEM CONCEPT STUDIES: TRAIN OPERATION



14-5

FIGURE 14-3. SYSTEM TEMPERATURE DISTRIBUTION: RUN NO. DT-1
 $(N=4, \phi_v=0.03, \sigma=0.25)$

the average station temperature is approximately 35°F above outside the ambient. The one distinguishing feature of Station 3 regards train operation: the operation of trains on the two tracks of the double-track system is symmetrical relative to Station 3, since trains are dispatched from either end of the system at the same point in time and at the same distance from the center station. Only in Station 3 do the trains stop, dwell and depart simultaneously.

All of the stations in the system encounter the same number of trains per hour and have the same heat load from patrons and station lighting. Thus, the reason for the elevated temperature in Station 3 must be connected with the station ventilation rate created by the piston action of the trains. This is, in fact, the case and can be best illustrated by comparison of Figures 14-4 and 14-5, which illustrate the global station heat balances for Stations 2 and 3. Given the SES-computed net heat rate to the ventilation air in the station and the average ventilation rate, the average rise in station ventilation air temperature can be estimated readily. Further, given the SES-computed average temperature of the inflowing ventilation air, the average temperature of the air as it passes through the station can be calculated (calculations performed manually in this manner for illustrative purposes are generally within 1°F to 2°F of the average of the SES-computed subsegment temperature). In the case of Station 2, the average ventilation rate of the station is approximately 186,000 cfm at an average temperature of 88°F. Thus, the average air-temperature rise based on a net heat load of 2623 MBH is 13°F, resulting in an average station air temperature of 101°F (25°F above outside ambient).* In contrast, the ventilation rate for Station 3 was approximately 120,000 cfm, or 66,000 cfm less than for Station 2. This reduced ventilation rate results in an average station ventilation air-temperature rise of 19°F and an average station air temperature of 109°F.

*Note: The SES-computed heat exchange between the subway air and structures in SES program simulations presented in Section 14.1 through 14.10 is based on a structure surface temperature of 85°F. Detailed SES program computations of the long term behavior of the heat sink are presented in Sections 14.11 and 14.12

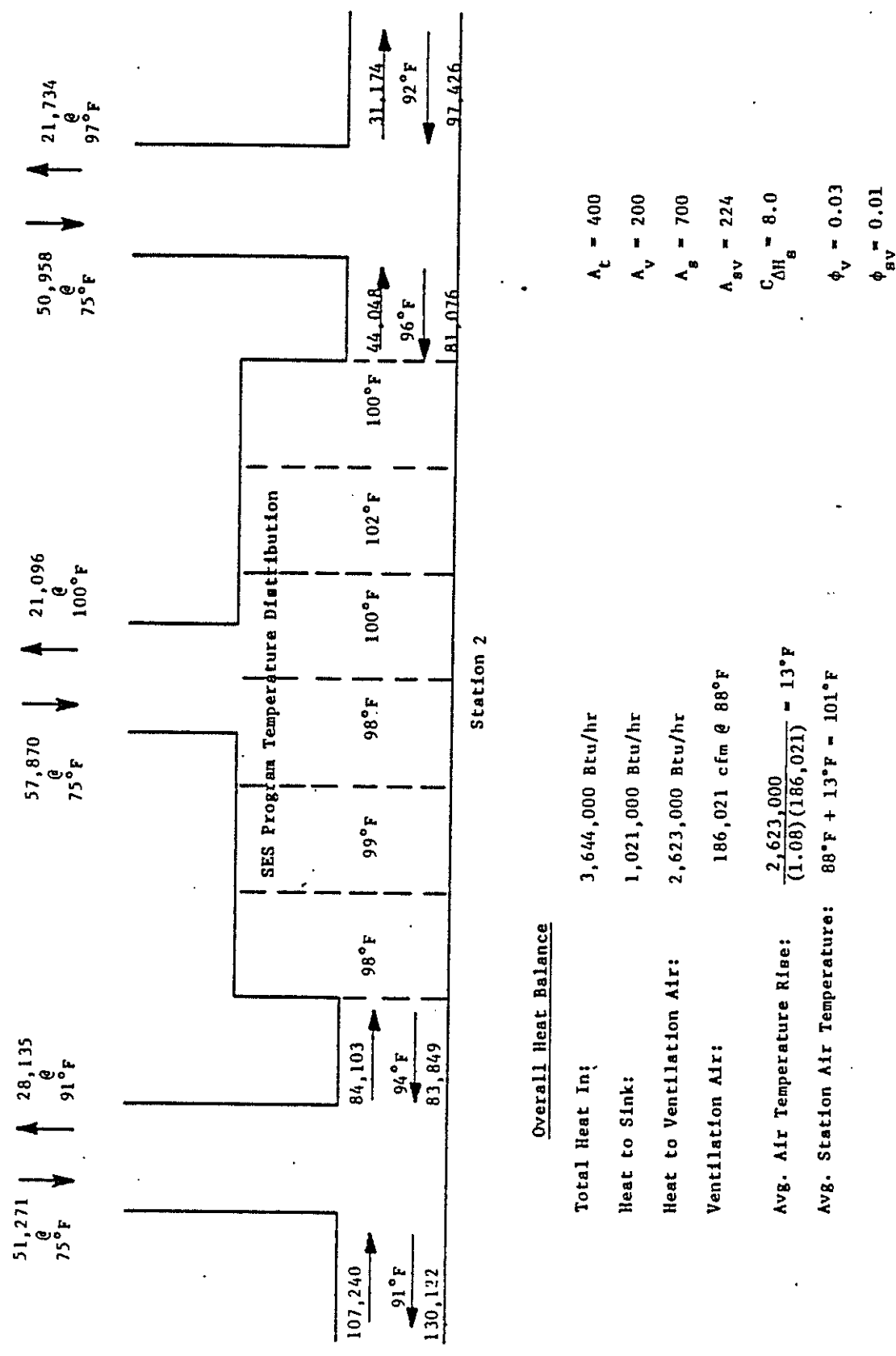


FIGURE 14-4. STATION HEAT BALANCE: RUN NO. DT-1, STATION 2

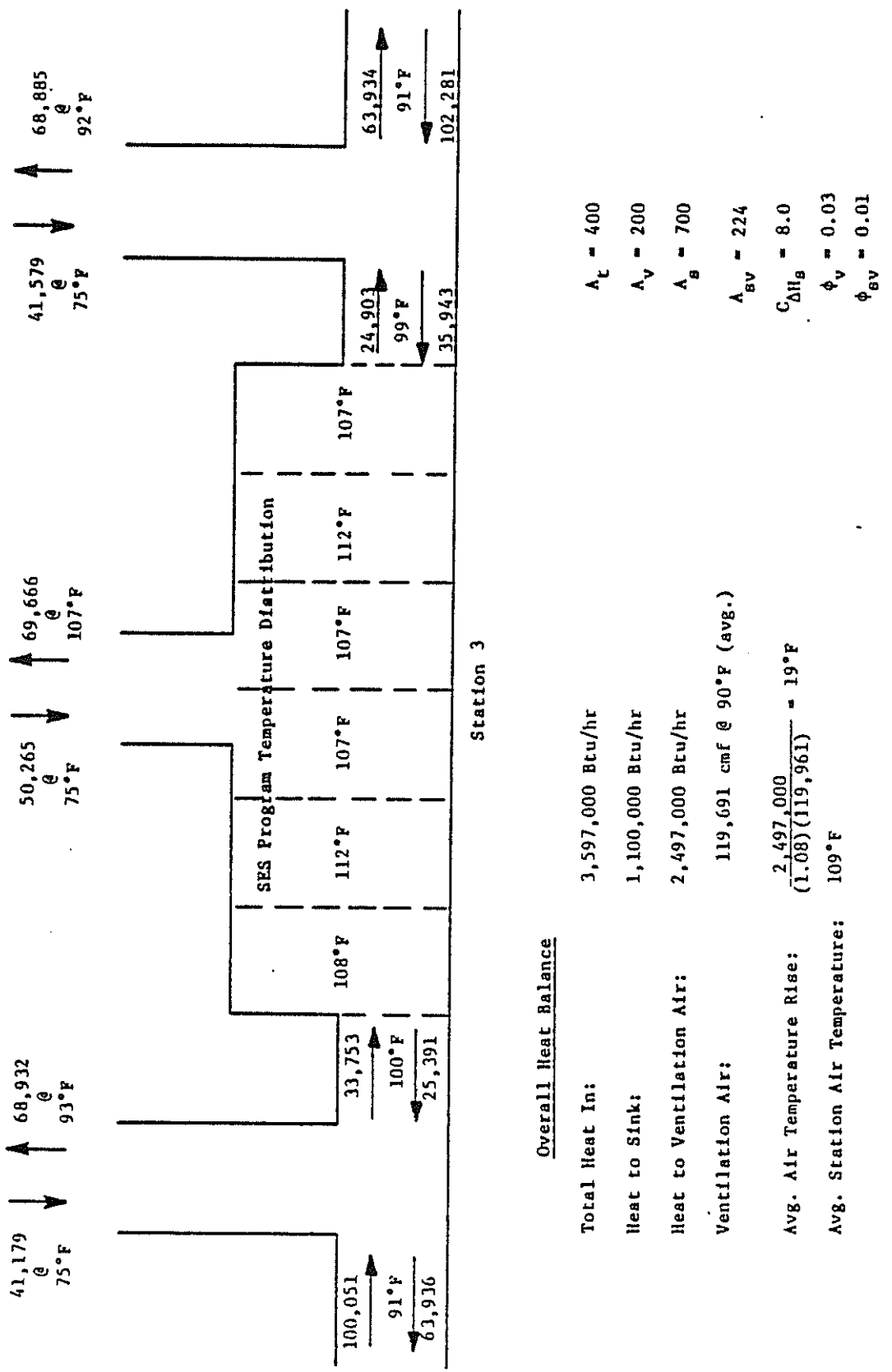


FIGURE 14-5. STATION HEAT BALANCE: RUN NO. DT-1, STATION 3

The reduced ventilation rate for Station 3 is a result of the relative operation of the trains on the two opposing routes. This effect of relative train situation on station ventilation is evidenced by Figure 14-6, which shows again an average air-temperature distribution through the base system but in this case with the train dispatching altered such that the simultaneous dwell occurs in Station 2 of the system. For this train operation, the peak temperature within the system occurs in Section 2.

The effect on station ventilation is more explicitly characterized by Figures 14-7 and 14-8. Figure 14-7 illustrates the flow in the tunnel and blast shaft adjacent to Station 2 for the case of symmetrical train operation within the subway (simultaneous dwell in Station 3). These flows are plotted in time-dependent fashion against a train situation diagram so that the interactive effects of trains operating on the two routes through the system can be examined. The fraction of tunnel airflow which actually serves to ventilate the station is, of course, the difference between the portrayed tunnel airflow rate and the shaft flow. When a train approaches the station on route 1, a large percentage of the tunnel air goes into the station with a relatively small amount (about 25 percent) being diverted into the blast shaft. Similarly, when a train departs the station on route 2, only a small percentage of the tunnel flow is made up by flow into the system through the blast shaft, the remainder again coming from the station. The important thing to note is that the train operation is such that the dwell times within Station 2 are shifted. When a train is dwelling in the station on route 1, the train on route 2 has already departed the station and is operating within the tunnel. Figure 14-8 portrays the same tunnel and blast-shaft flows but for train operation where both trains dwell simultaneously in Station 2. In this case, a larger percentage of the tunnel airflow must flow through the blast shaft. When trains approach the station simultaneously they must compete for the airflow through the blast shafts and through the station stairway. Similarly, when the trains depart the station, the only flow paths are the stairway and the blast shafts, and both trains are operating simultaneously to pull air through these passageways. As a consequence, there is little net flow of air through the station from one tunnel to the other and the station ventilation is reduced.

The implication of these findings is that in situations where trains approach, dwell, and depart a given subway station simultaneously, there is

Intentionally left blank?

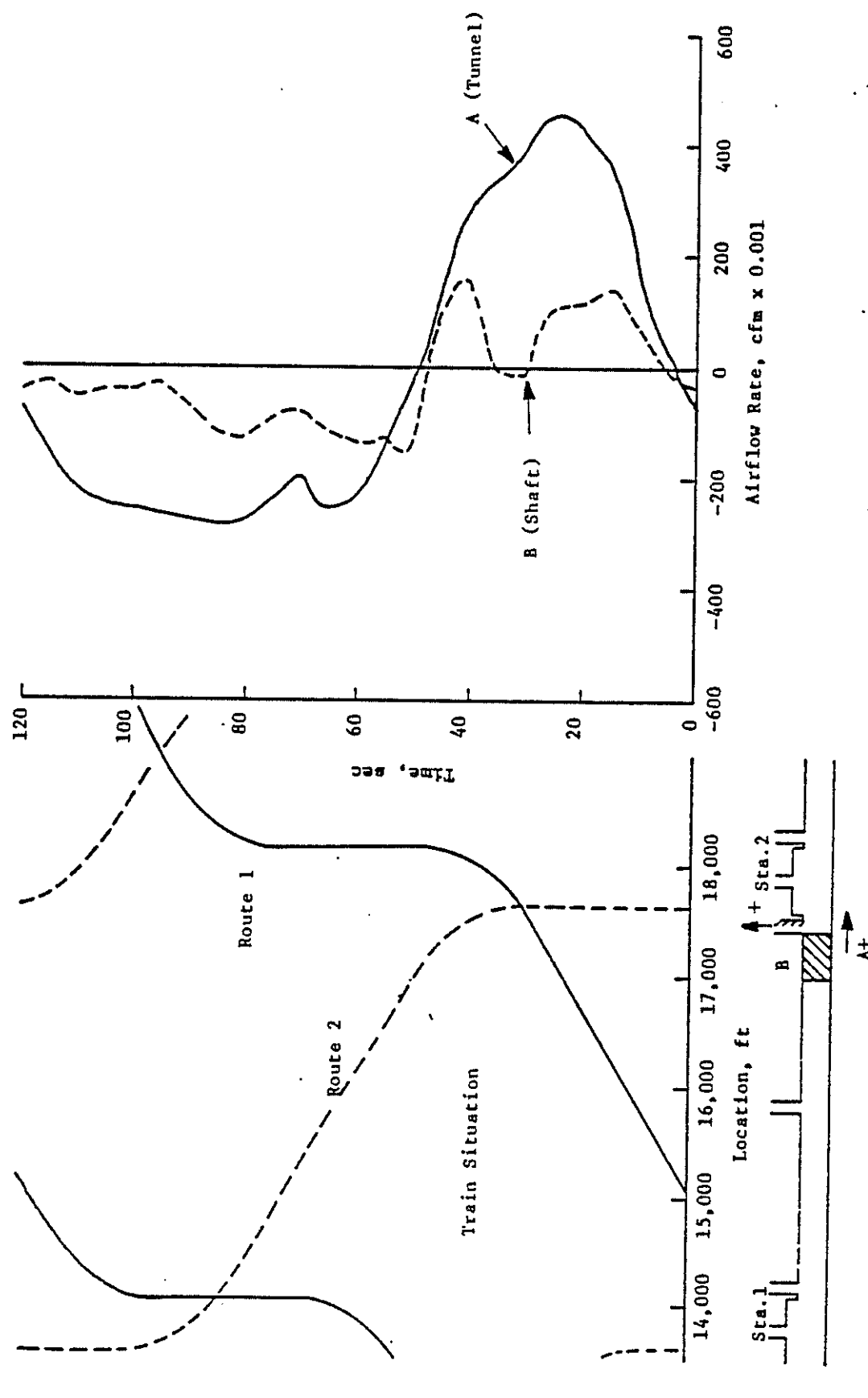


FIGURE 14-7. EFFECT OF RELATIVE TRAIN SITUATION ON VENTILATION SHAFT FLOW: RUN NO. DT-1

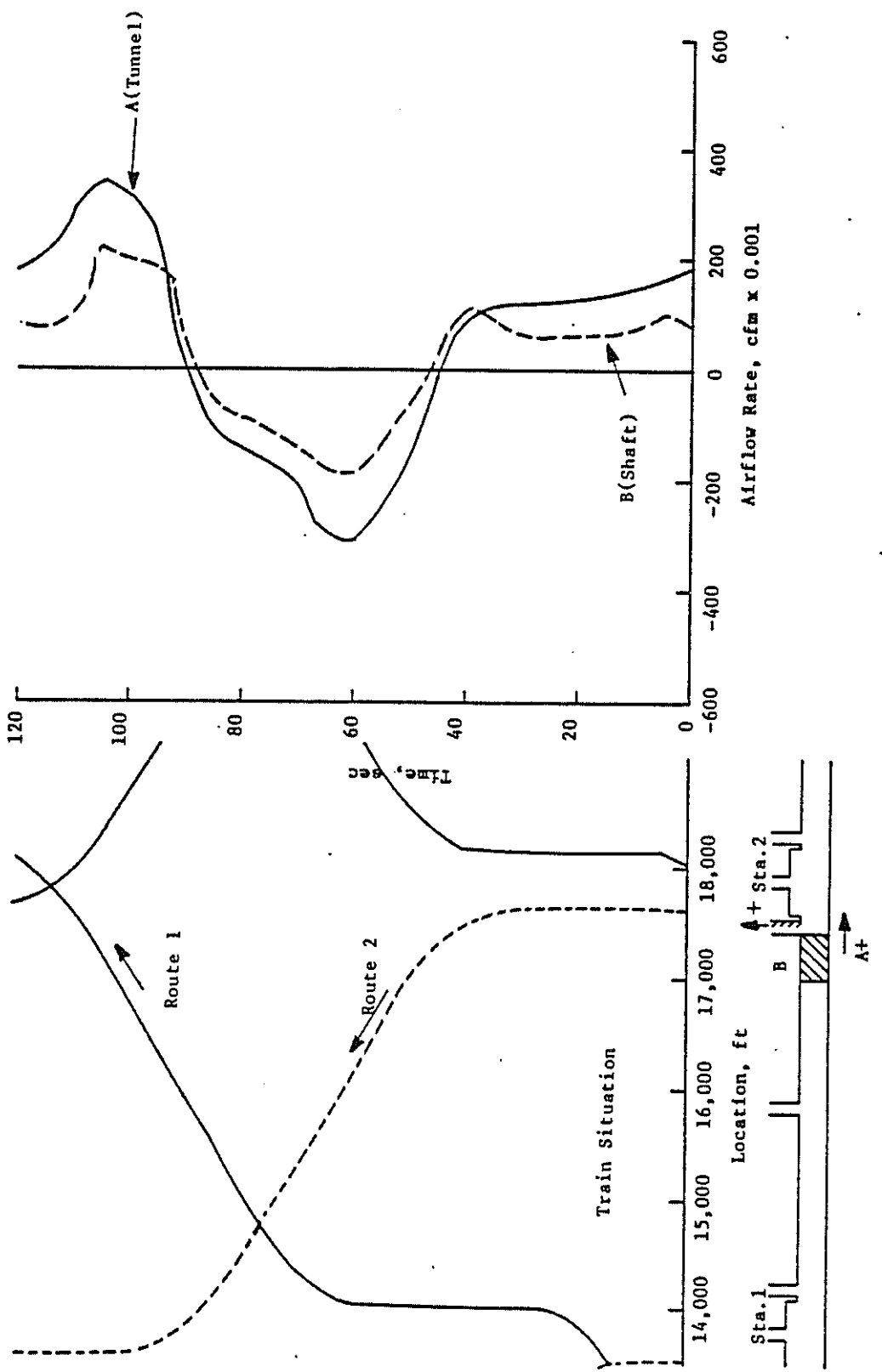


FIGURE 14-8. EFFECT OF RELATIVE TRAIN SITUATION ON VENTILATION SHAFT FLOW:
RUN NO. DT-2

a possibility of substantially reducing the ventilation rate for the station, since tunnel-to-tunnel flow-through is minimized (the same type of situation is encountered in underground terminal stations). The consequence is an elevation in station air temperature. On the other hand, the uniformity of the air-temperature results for the other stations of the Base System, including the train operations with simultaneous dwell in both Station 3 and Station 2, suggest that for train situations other than the simultaneous dwell case the station ventilation is not unduly sensitive to the relative train situation with respect to a given station.

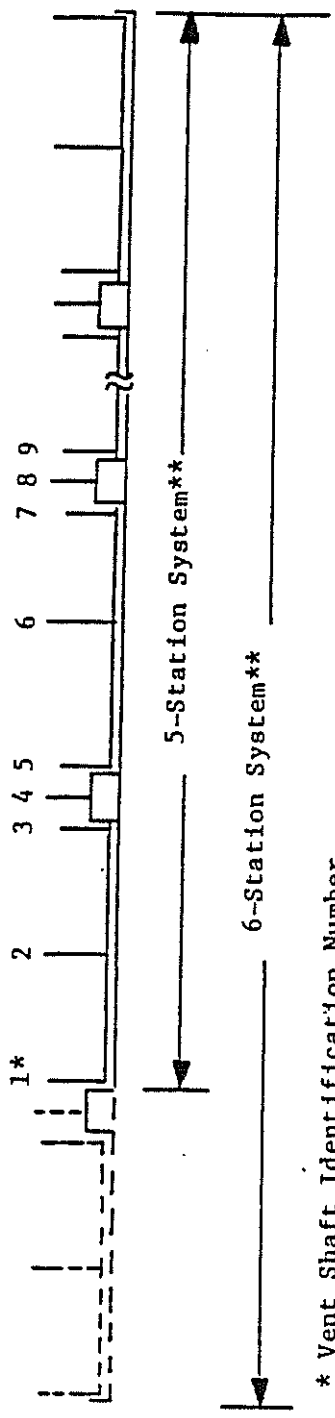
14.2 DOMAIN OF INFLUENCE

An accurate evaluation of airflows and temperatures in a specific region of interest within a subway must include the analysis of a somewhat larger portion of the system. The limits of this portion are denoted in the case of airflows as the Aerodynamic Domain of Influence (ADI), and in the case of air temperature as the Thermodynamic Domain of Influence (TDI). The importance of this concept is emphasized by its implications in an environmental analysis of part of a large subway, or perhaps an addition to an existing subway. The most economical approach would be to include in the analysis only the portion of the subway which influences results in the region of interest. The extent to which the analysis must include subway stations, tunnels and vent shafts adjacent to this region is dictated by the ADI and TDI (see Reference 1 for discussion of the ADI and TDI in systems with a single operational route).

For the double-track systems considered in this report, the ADI and TDI were evaluated by first simulating a six-station system, then a five-station system (the base system) with essentially the same train operations in the five stations common to both systems. This double-track system is illustrated by Figure 14-9. The ADI and TDI can then be ascertained by finding the location within the five-station system where the one station truncation ceases to affect the results.

Aerodynamics

The ADI was determined through a comparison between the average vent shaft flows at successive vents from the portal, the five-station double-track



* Vent Shaft Identification Number

** Relative train operation on the two routes maintained the same with respect to the 5-station system for both simulations.

FIGURE 14-9. SYSTEM SCHEMATICS FOR THE DOMAIN OF INFLUENCE STUDY

system and the corresponding vents of the six-station system (see Figure 14-9). Figure 14-10, which illustrates the results of this comparison, shows that the effect on vent-shaft flow of the system truncation is less than 10 percent at the fourth vent from the portal and is nil at the sixth vent. Stated another way, if the region of interest aerodynamically began at shaft number 4 and extended through the remainder of the system, then airflow calculation accuracy would suffer less than 10 percent in this region by simulating the five-station system even if the system were, in fact, six stations or more in length. This finding agrees reasonably well with Reference 1, which shows that, for single-track systems, the ADI included three vent shafts and the contiguous tunnels on either side of the region of interest. Although the results shown in Figure 14-10 are based on a single vent-shaft configuration ($A_v = A = 400 \text{ ft}^2$, $C_{\Delta H_s} = 8.0$, $\phi = 0.12$), the simplified theory presented in Reference 1 supports the application of a three vent-shaft ADI as an acceptable rule of thumb.

Thermodynamics

The TDI is a consequence of the tendency of the air temperature to cascade from station to station in an increasing fashion from the portals of a subway system. The cause of this cascading is an imbalance between heat inputs to the system and heat expelled from the vent shafts, absorbed by the sink, or removed by mechanical cooling systems. When such an imbalance exists, the excess heat is carried through the system by piston-effect airflow and the air becomes progressively hotter. In turn, the heat expelled through the vent shafts and transferred to the sink increases until a balance is achieved.

In systems with a single operational route, this cascading may progress several stations into the system from the entrance portal because of the positive flow-through ventilation effect of the unidirectional train operation. In contrast, the operation of trains on two routes in opposing directions substantially reduces this portal-to-portal flow-through ventilation of the system and reduces cascading (hence the TDI). Even with single-track, parallel tunnels, the tunnel-to-tunnel communication of airflow at stations acts to reduce the cascading effects (see Section 14.10).

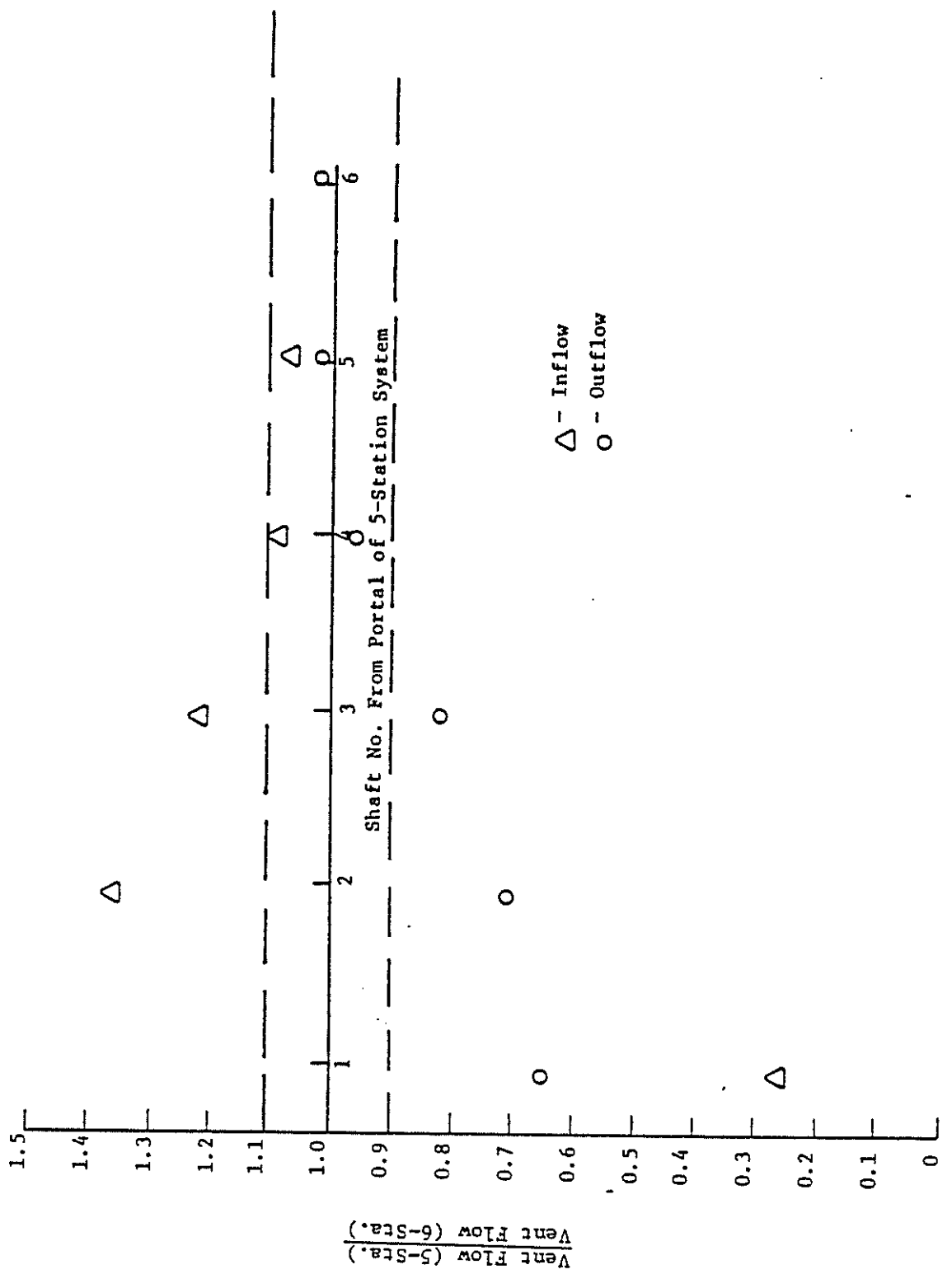


FIGURE 14-10. AERODYNAMIC DOMAIN OF INFLUENCE

For the five-station vs. six-station comparison, the TDI was evaluated through the average air-temperature distribution. Figure 14-11, which compares the average air-temperature distribution for the two systems, shows that the temperature cascading progresses only through the first station from the portal of the five-station system (it should be noted that a small temperature difference, on the order of 1°F (5 percent) of the station temperature rise above ambient in the stations, is caused by slight differences in the train heat rejection profile between the two SES program simulations). Thus, if the thermodynamic region of interest began with station two, accurate air-temperature results would be obtained by including only the adjacent station one and its contiguous tunnels.

There is a degree of correlation between the ADI and TDI for double-track systems which contrasts sharply with the single-track system observations of Reference 1. The reason is tied to the lack of portal-to-portal flow-through ventilation effect with bi-directional train operation. This is further evidenced by considering the average air-temperature differences between the tunnels and stations of the system. The ventilation resulting from unidirectional operation of trains on a single route produces a relatively homogeneous system air temperature, with Reference 1 results showing a station-tunnel temperature difference on the order of 5°F at most. The double-track average air-temperature results in this report for piston-action ventilated systems shows temperature differences between the tunnels and stations of 10°F and more.

14.3 VENTILATION SHAFT FLOW IMPEDANCE

As discussed herein, ventilation shaft impedance shall be taken as the impedance parameter, Φ , defined on Figure 14-12. This parameter includes the square of the ventilation shaft-to-tunnel area ratio as well as the flow impedance of a ventilation shaft in velocity heads and is, in fact, the parameter that dictates the flow behavior of the ventilation shaft. SES program simulations of the Base System were performed with a range of ventilation shaft impedances to evaluate the effect of this parameter on system ventilation and temperature distribution. The results of this study are reflected on Figure 14-12. This parameter is the ratio of average ventilation shaft flow for a given value of Φ to the ventilation shaft average flow

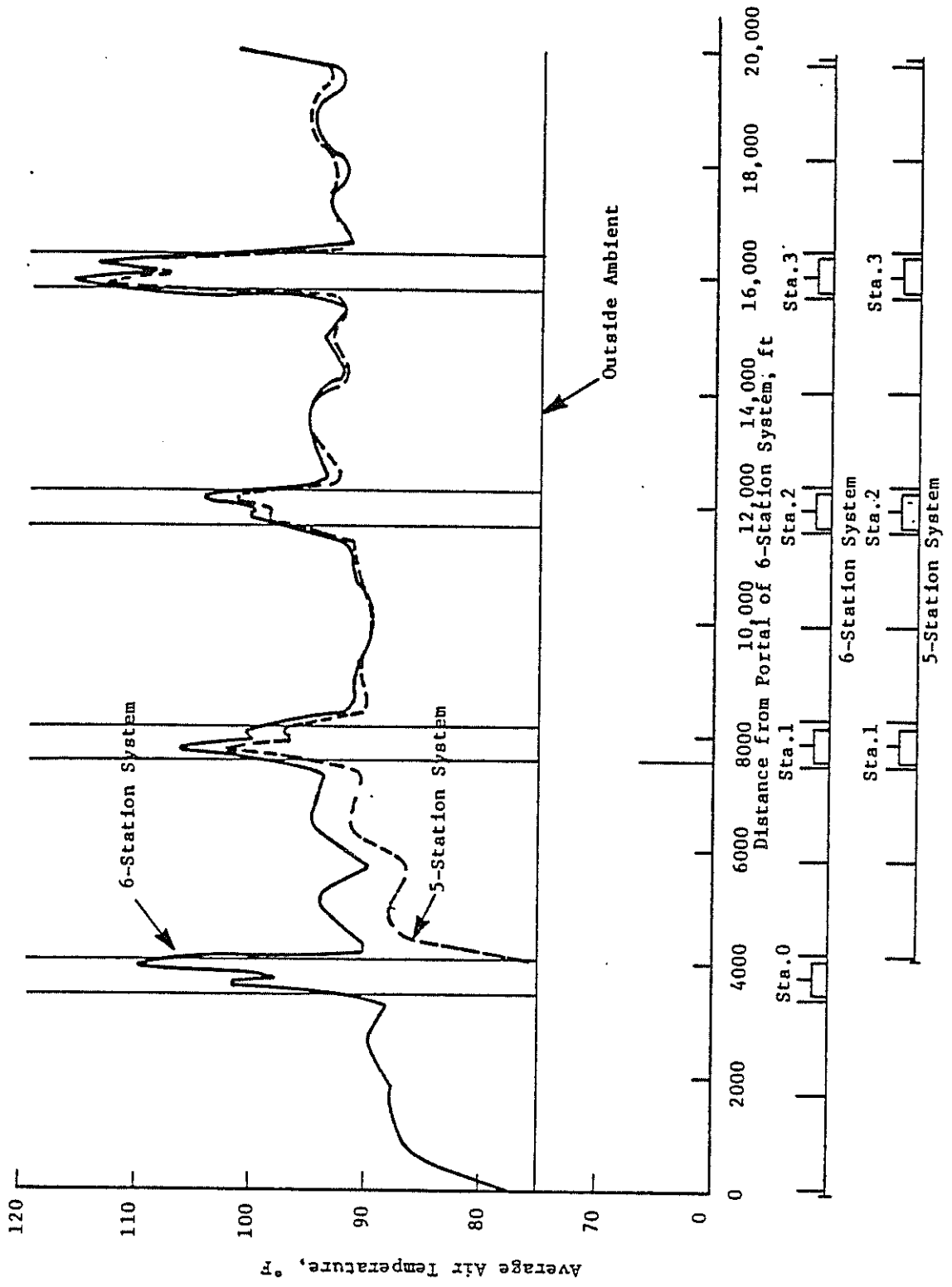


FIGURE 14-11. THERMODYNAMIC DOMAIN OF INFLUENCE

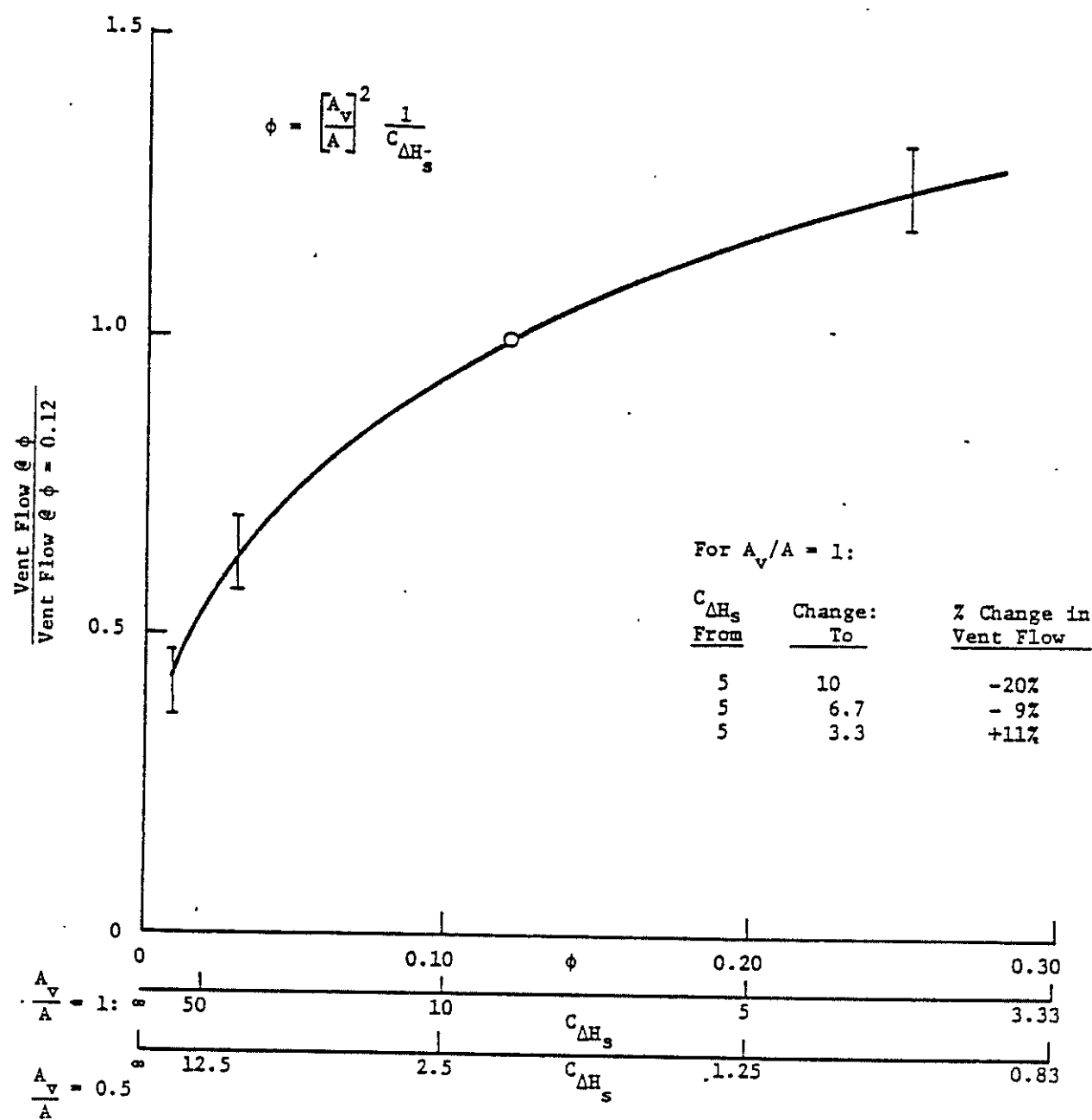


FIGURE 14-12. EFFECT OF IMPEDANCE ON AVERAGE VENTILATION SHAFT FLOW

resulting from a Φ value of 0.12. These vent flows are compared on a one-to-one basis, and since not all vent shafts are affected in an identical fashion, the result is a range shown by the vertical bars on the figure. The exception, of course, is the Base System reflected by the circled datum. A line has been faired through these results to portray the average effect of shaft impedance on the vent-shaft flow rate. The results are plotted both against Φ and against vent-shaft head-loss coefficient $C_{\Delta H_s}$ for specified area ratios to illustrate the possible trade-offs between vent-shaft flow impedance (configuration) and vent-shaft reference flow area. Note, for example, that for the situation with the vent-shaft area equal to the tunnel area, a ventilation shaft impedance value of 10 velocity heads will result in the same ventilation shaft performance as for a vent shaft with an area equal to half of the tunnel area and an impedance of 2.5 velocity heads. This sensitivity to vent-shaft area is attributable to the fact that Φ is proportional to the square of the vent-to-tunnel-area ratio. Also shown on Figure 14-12 is a portrayal of the sensitivity of vent-shaft behavior to the vent-shaft flow impedance for a given vent-shaft area, in this instance, equal to the tunnel area. In particular, it is worthwhile to note that an error in the evaluation of the vent-shaft flow impedance, $C_{\Delta H_s}$, on the order of 1.5 velocity heads, either side of an actual value of 5 velocity heads, will give rise to an error in vent-shaft flow on the order of 10 percent. Overall, the vent-shaft flow behavior as a function of impedance is as expected. That is, as the impedance parameter increases (head-loss coefficient decreases), the vent-shaft flow also increases. An increase in Φ from the reference value of 0.12 to a value of 0.25 results in an increase in average vent-shaft flow on the order of 25 percent.

However, a comparison of system temperatures shows some rather surprising results. Figures 14-13 (Run No. DT-4) and 14-14 (Run No. DT-5) are illustrations of average system temperature, with Figure 14-13 showing the temperatures for $\Phi = 0.01$ ($A_v = 113 \text{ ft}^2$) and Figure 14-14 showing results for the case where $\Phi = 0.25$ ($A_v = 575 \text{ ft}^2$). The ventilation shaft flow for Run No. DT-5 is on the order of 2.5 to 3 times greater than the flow associated with Run No. DT-4. As would be expected, the tunnel air temperatures associated with the higher ventilation shaft flows are about 5°F below the tunnel air temperatures associated with the low ventilation shaft flows. However, the station air temperature is not as predictable.

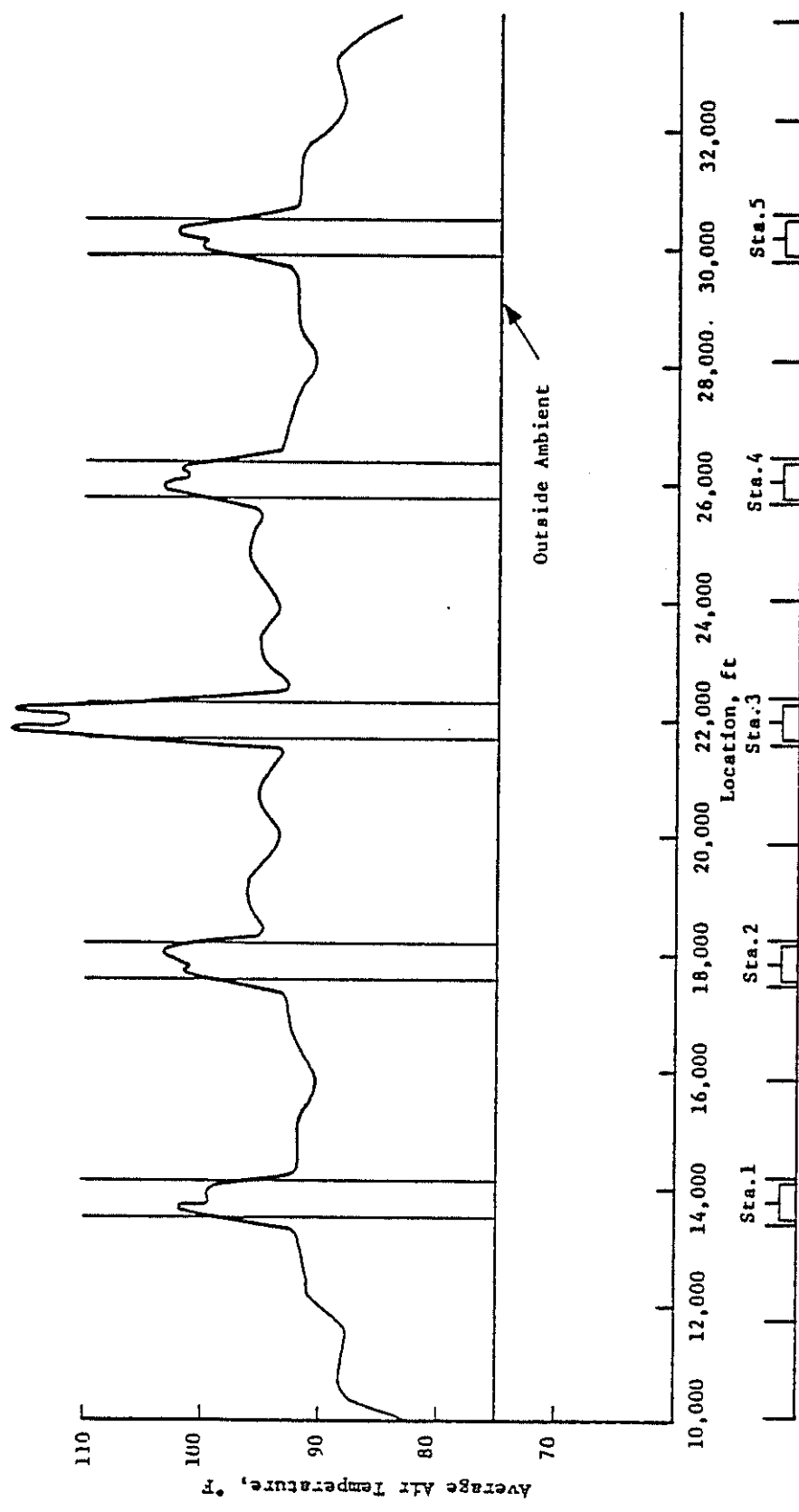


FIGURE 14-13. SYSTEM TEMPERATURE DISTRIBUTION: RUN NO. DT-4
 $(N=4, \phi_v=0.01, \sigma=0.25)$

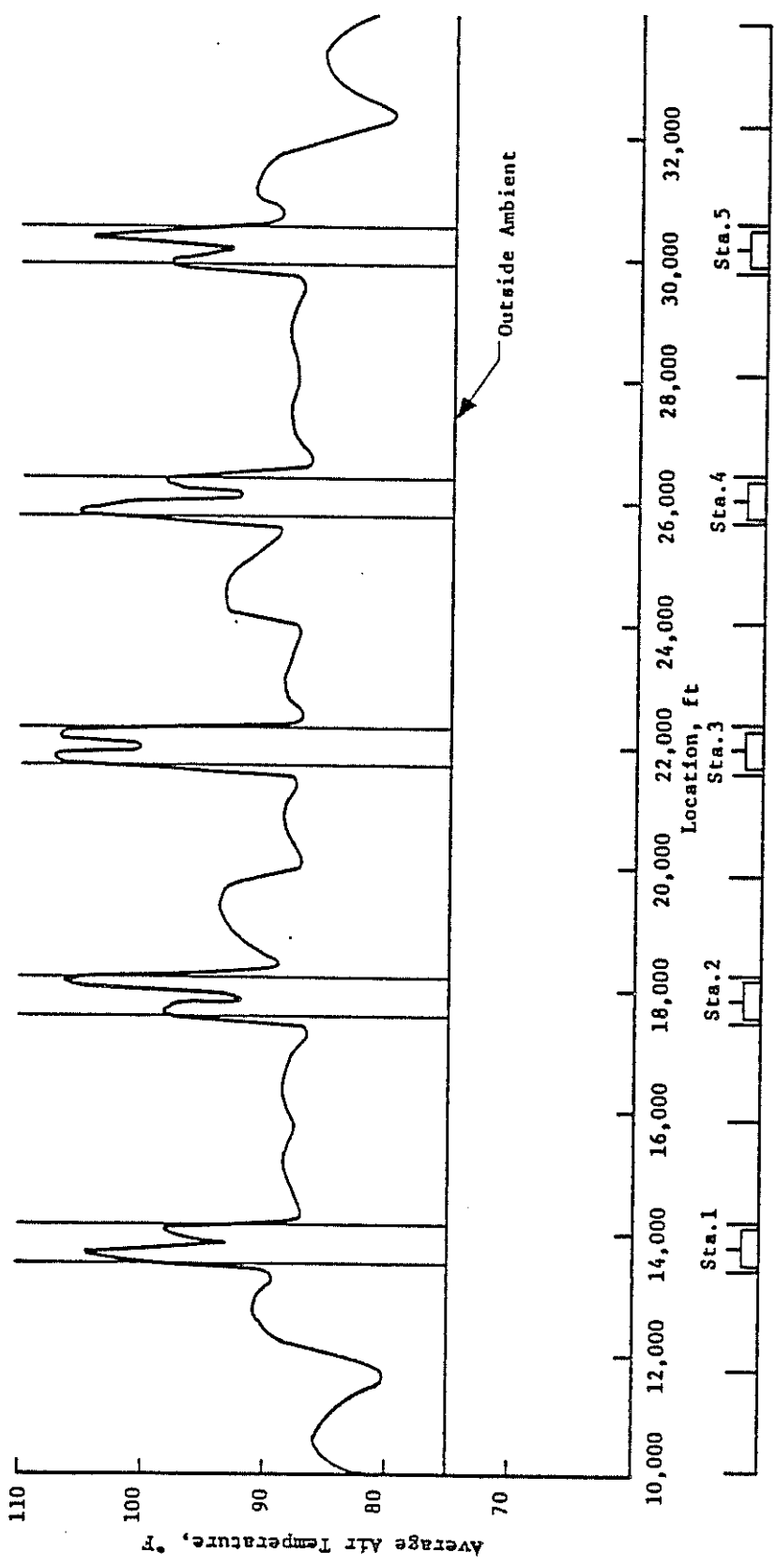


FIGURE 14-14. SYSTEM TEMPERATURE DISTRIBUTION: RUN NO. DT-5
(N=4, $\phi_v=0.25$, $\sigma=0.25$)

Considering Station 2 for example, the rather drastic five-fold increases in the area of ventilation shafts and stairways through the system resulted in a decrease in average station temperature of only 3°F from 102°F to 99°F. Note also that in the case of the system with larger ventilation shafts, the variation in air temperature along the length of the station platform was substantially more pronounced, with peak temperatures exceeding the station temperature associated with the smaller vent-shaft areas. Station heat balances illustrated in Figures 14-15 and 14-16 can again be used to ascertain the reason for this behavior. A comparison of these station heat balances shows that increasing the efficiency of the ventilation shafts has the effect of reducing the communication of air between the tunnels and the stations of the system. For example, the average flow rate into the station from the tunnel for Run No. DT-4 is on the order of 137,000 cfm, whereas for Run No. DT-5 this tunnel-to-station flow communication drops to approximately 81,000 cfm. Thus, although the temperature of the tunnel air for Run No. DT-5 is generally lower than for Run No. DT-4, this benefit in terms of station environment is to a large degree offset by the penalties in station ventilation. The greater variation in temperature along the length of the station can also be traced to the poorer circulation of tunnel air through the station. In particular, note the poorer circulation of air for Run No. DT-5 on the right-hand side of Station 2 as shown in Figure 14-16. This is a consequence of trains tending to pull more air through the station stairway and less air from the blast shafts contiguous to the station when departing.

The moral to be derived from these results is that simply decreasing the flow impedance of the ventilation shafts does not necessarily improve the environment of the subway station. The improvement in ventilation may be confined to the tunnels of the system, and there is a trade-off to be considered between a possible reduction in station ventilation and the reduction in the temperature of this ventilation air. This result further emphasizes the need for an integrated systems approach to the evaluation of subway environment and ways to improve the environment.

14.4 NUMBER AND SPACING OF VENT SHAFTS

SES program simulations of double-track systems with one, three and five tunnel vent shafts between stations were implemented to ascertain the impact

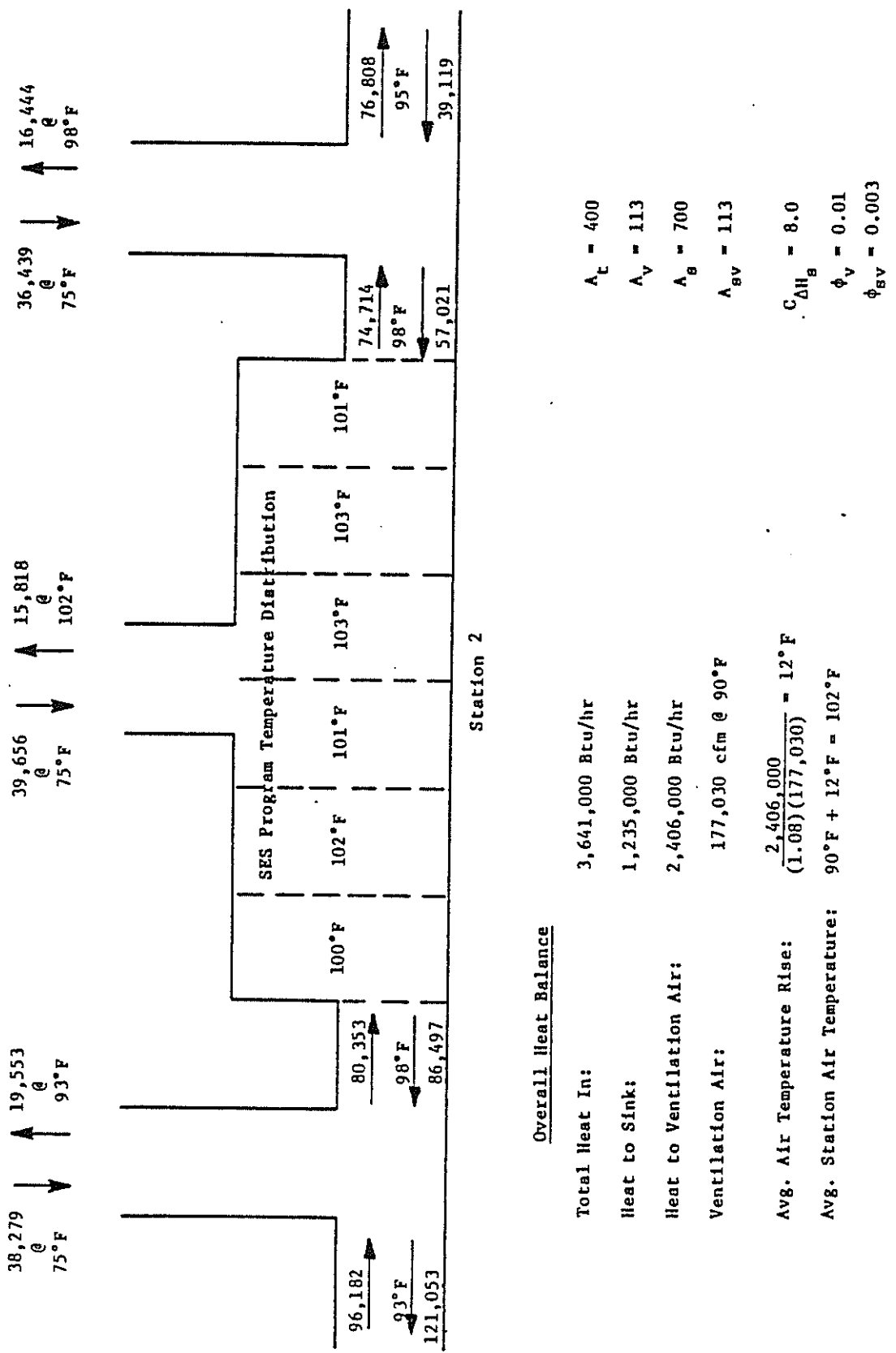
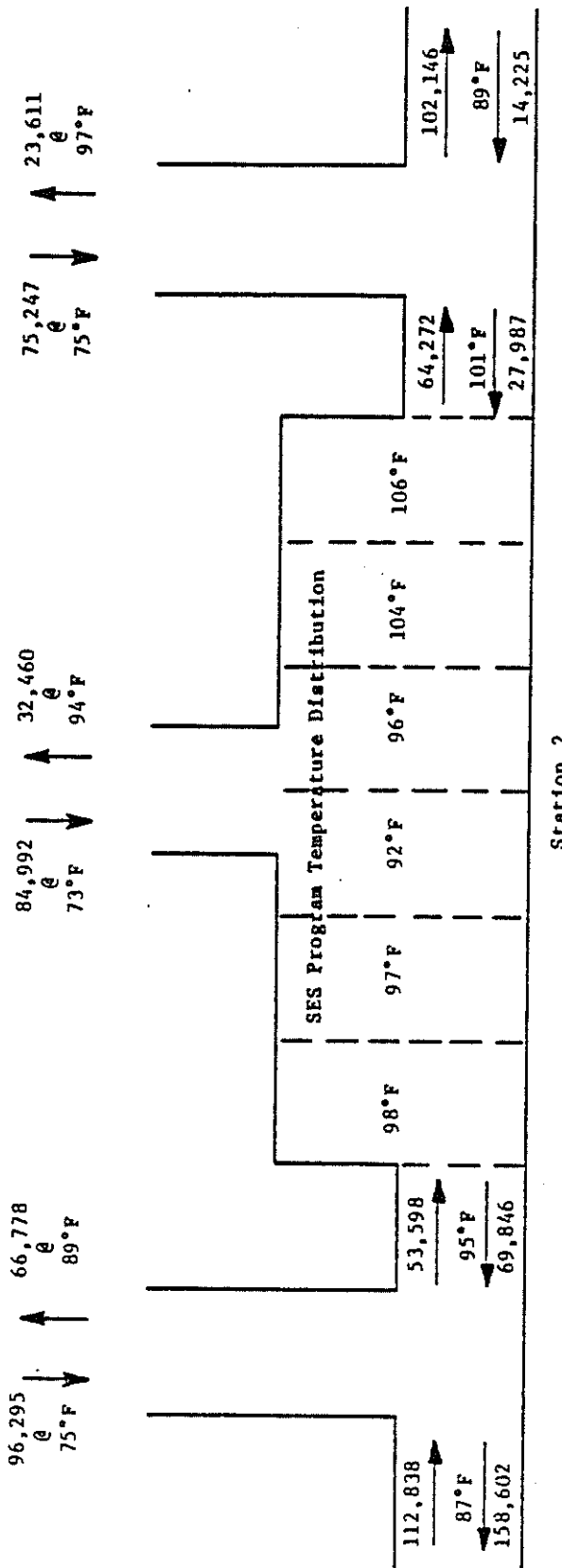


FIGURE 14-15. STATION HEAT BALANCE: RUN NO. DT-4, STATION 2



$A_t = 400$
$A_v = 575$
$A_s = 700$
$A_{sv} = 575$
$C_{All_s} = 8.0$
$\phi_v = 0.26$
$\phi_{vs} = 0.08$

FIGURE 14-16. STATION HEAT BALANCE: RUN NO. DT-5, STATION 2

on subway airflows and temperatures. Since the parameter N which identifies the number of shafts in a tunnel-station subsystem also includes by definition station stairways to the surface, the corresponding N values for these runs are 2(Run No. DT-6), 4(Run No. DT-7) and 6(Run No. DT-8).

The effect of the number of shafts on subsystem ventilation is illustrated by Figure 14-17. As would be expected, the ventilation rate increases with an increasing number of shafts. In fact, the relationship is almost linear: doubling the value of N from 2 to 4 results in a 50 percent increase in average subsystem ventilation, whereas tripling the value from 2 to 6 causes an increase of 100 percent in the ventilation rate.

As was noted with regard to the effects of vent-shaft impedance, however, the effect on air temperature of the increase in ventilation rate is not straightforward in this case either. Figures 14-18, 14-19, and 14-20, which depict average system temperature distribution for $N = 2, 4$ and 6 , respectively, show that as the number of shafts increases, the tunnel temperature decreases but the station temperature actually rises. This rise in the average station temperature is on the order of 3°F when N is increased from 2 to 4, and another 2°F when N goes from 4 to 6. Again, the station heat balance for Station 2 will be used to study the reason for this behavior. The station heat balance for the three cases, which is illustrated in Figures 14-21, 14-22 and 14-23, show that as N increases the air-flow through the stairways and tunnels into the station drops off significantly. In retrospect this would be expected: as more shafts are provided for tunnel ventilation, there is a tendency for a greater percentage of the piston-effect airflow to be processed up the shafts ahead of the train and down the shafts behind the train, rather than through the station. As a consequence, the increase in subsystem ventilation with increasing N shown by Figure 14-17 is confined to the tunnels for the systems evaluated. The potential benefit of added ventilation shafts then becomes a question of whether the decrease in station ventilation is more than offset by the lower temperature of the tunnel air entering the station. For the cases considered in this study, this was not the situation.

In summary, these results demonstrate the potential trade-off to be realized among N , tunnel air temperature, and station air temperature. Certainly, for $N = 1$ one could anticipate problems since a single vent would be relied upon to process all of the subsystem ventilation air. Also to be

considered is the question of air velocity. As the number of tunnel ventilation shafts decreases, station platform and stairway velocities increase both in magnitude and duration. The maximum stairway velocity increased from 630 fpm to 840 fpm in the systems simulated, a change of over 30 percent, when N was changed from 6 to 2.

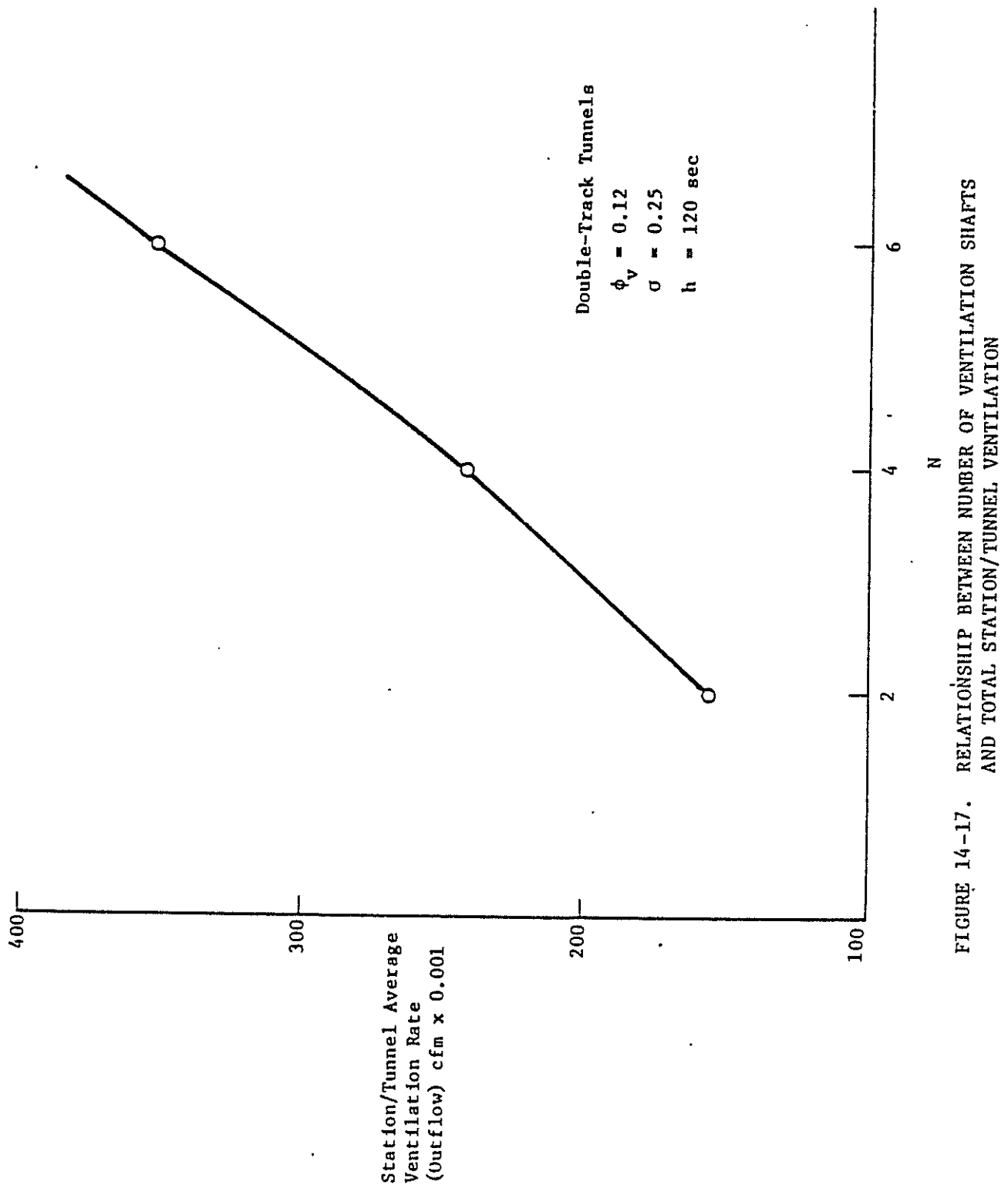


FIGURE 14-17. RELATIONSHIP BETWEEN NUMBER OF VENTILATION SHAFTS AND TOTAL STATION/TUNNEL VENTILATION

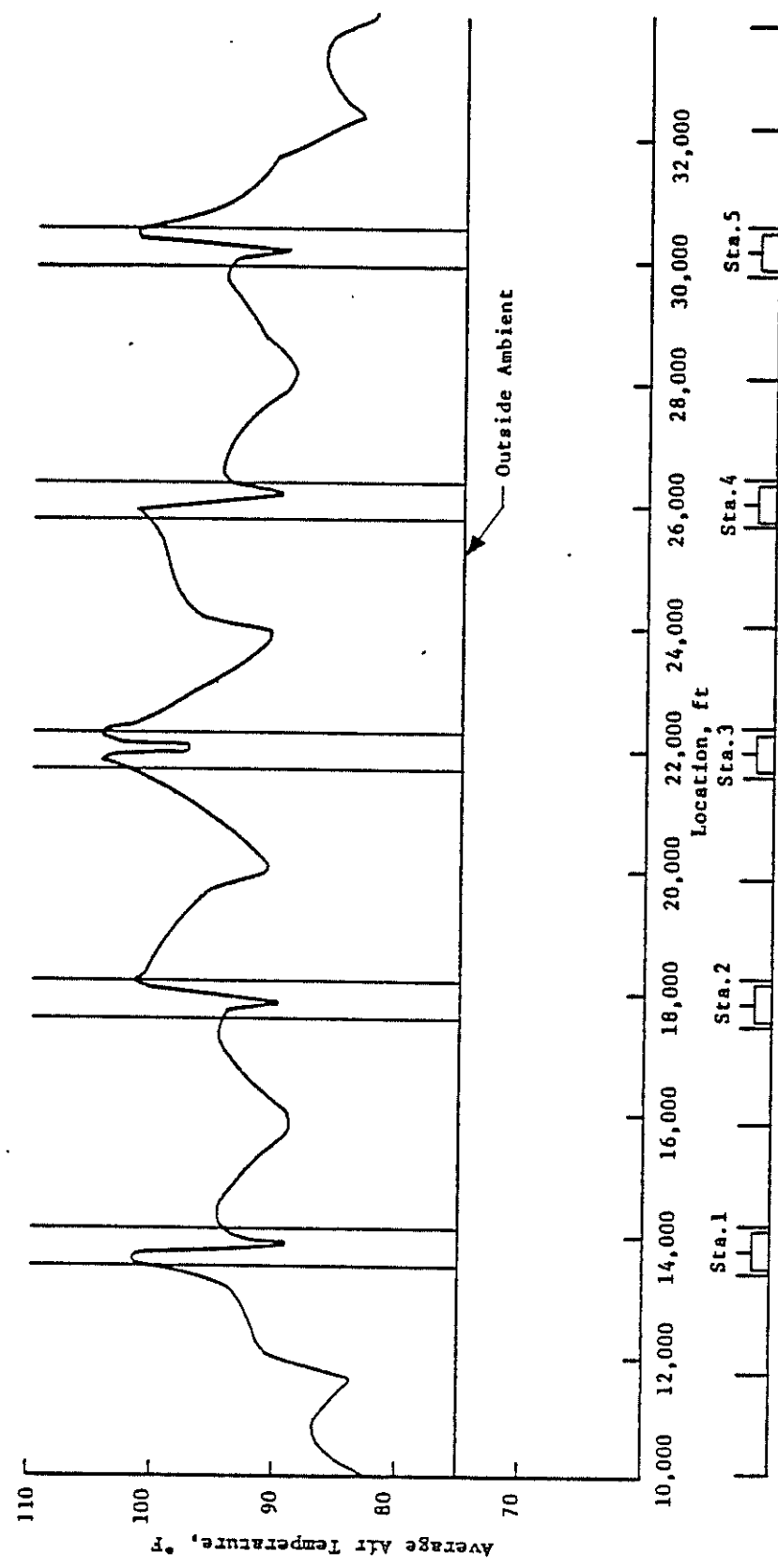


FIGURE 14-18. SYSTEM TEMPERATURE DISTRIBUTION: RUN NO. DT-6
(N=2, $\phi_v=0.12$, $\sigma=0.25$)

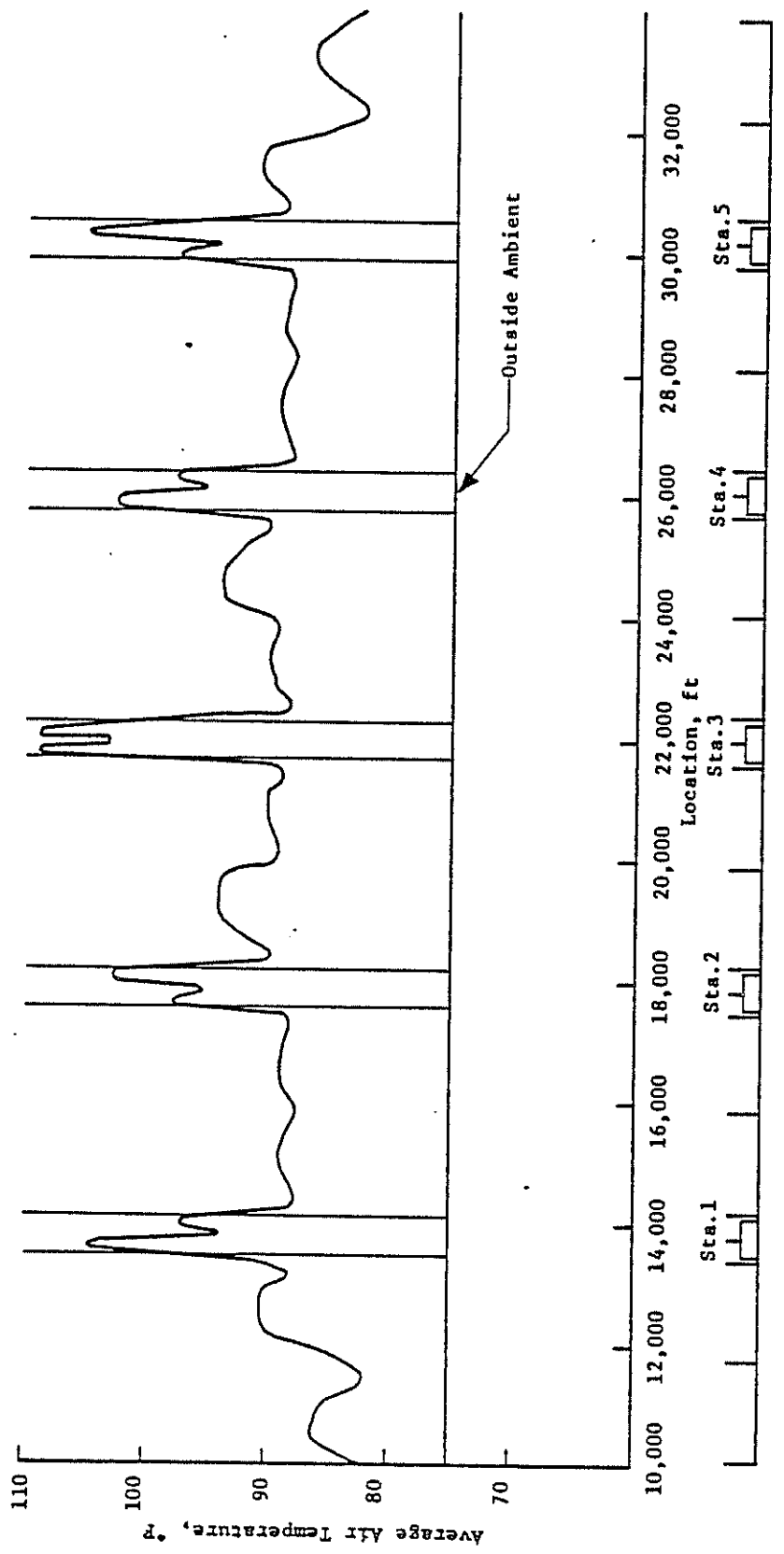


FIGURE 14-19. SYSTEM TEMPERATURE DISTRIBUTION: RUN NO. DT-7
(N=4, $\phi=0.12$, $\sigma=0.25$)

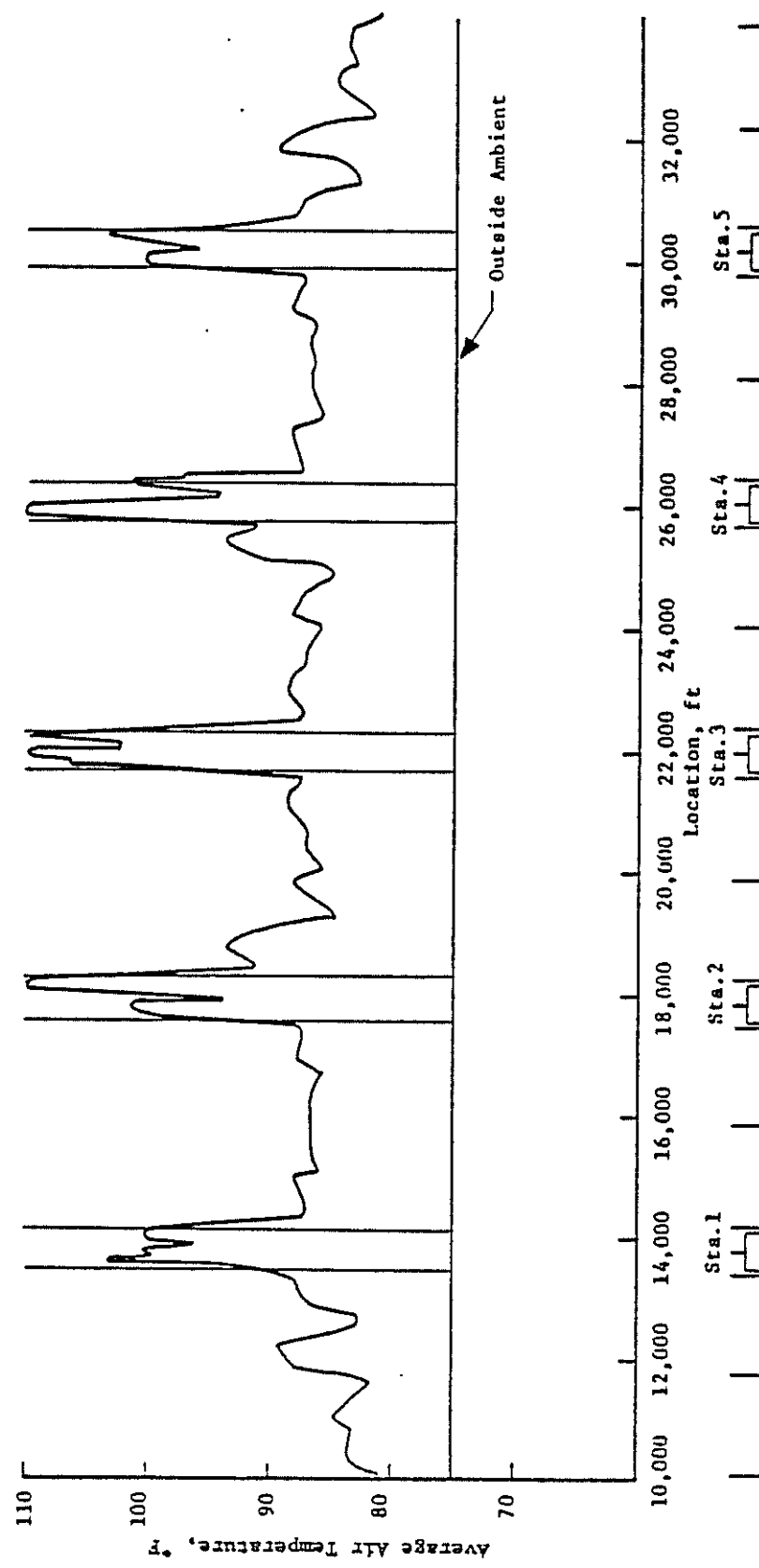
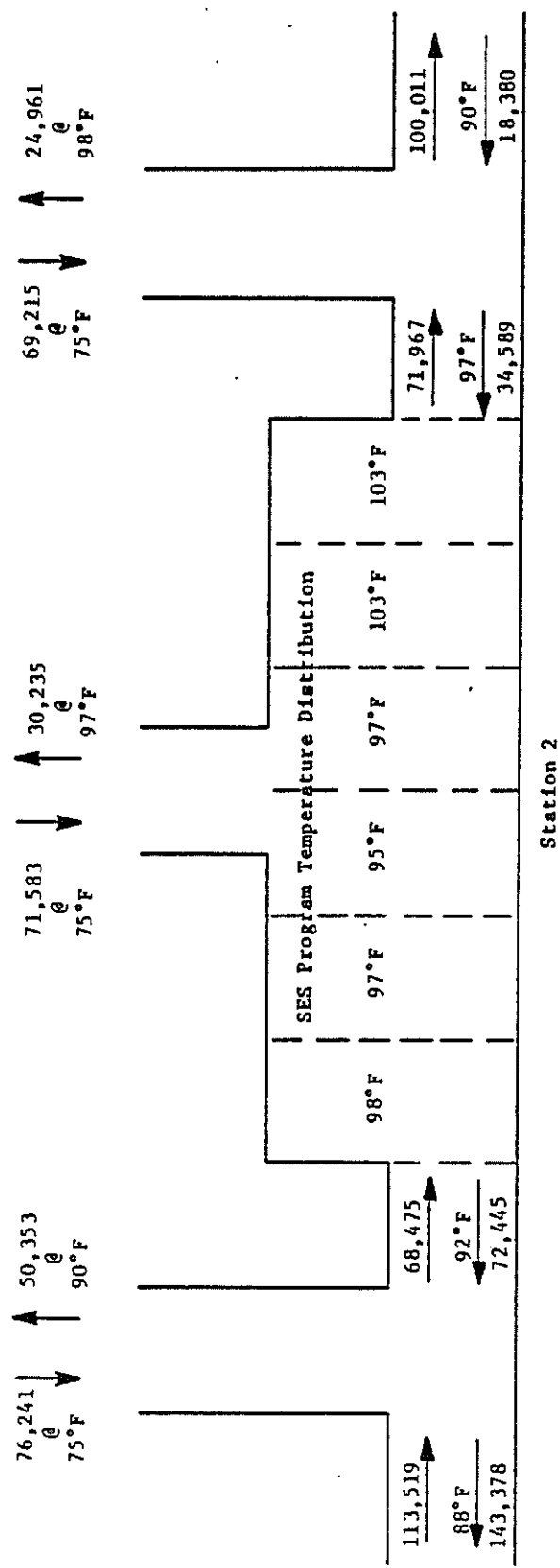


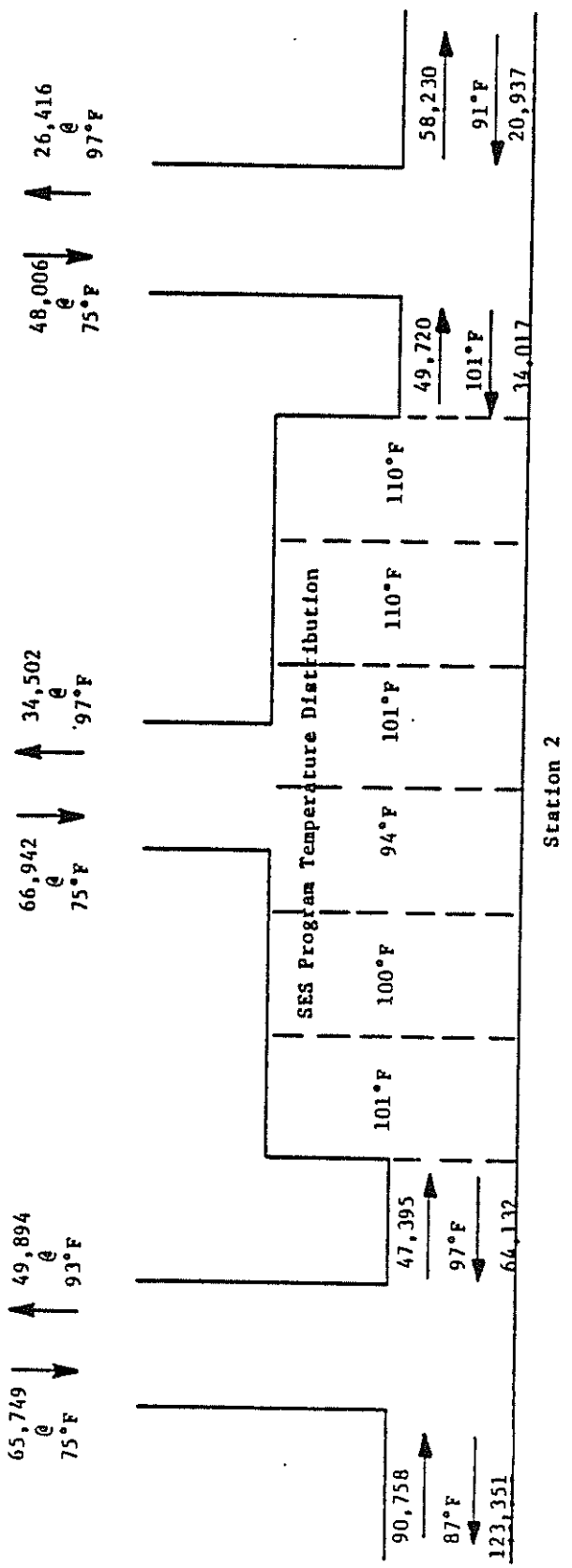
FIGURE 14-20. SYSTEM TEMPERATURE DISTRIBUTION: RUN NO. DT-8
 $(N=6, \phi_v=0.12, \sigma=0.25)$





$$\begin{aligned} A_t &= 400 \\ A_v &= 395 \\ A_s &= 700 \\ A_{sv} &= 395 \\ C_{AH_s} &= 8.0 \\ \phi_v &= 0.12 \\ \phi_{sv} &= 0.04 \end{aligned}$$

FIGURE 14-22. STATION HEAT BALANCE: RUN NO. DT-7, STATION 2



Overall Heat Balance

Total Heat In:	3,640,000 Btu/hr	$A_t = 400$
Heat to Sink:	899,000 Btu/hr	$A_v = 395$
Heat to Ventilation Air:	2,741,000 Btu/hr	$A_g = 700$
Ventilation Air:	148,354 cfm @ 85°F	$A_{sv} = 395$
Avg. Air Temperature Rise:	$\frac{2,741,000}{(1.08)(148,354)} = 17^\circ F$	$C_{AH_s} = 0.0$
Avg. Station Air Temperature:	102°F	$\phi_v = 0.12$
		$\phi_{sv} = 0.04$

FIGURE 14-23. STATION HEAT BALANCE: RUN NO. DT-8, STATION 2

14.5 BLOCKAGE RATIO

In addition to the base system tunnel blockage ratio of 25 percent, double-track systems with blockage ratios of 14 percent (Run No. DT-9) and 35 percent (Run No. DT-10), corresponding to tunnel cross-sectional areas of 715 ft^2 and 285 ft^2 , respectively, were simulated to evaluate the effect on environment. The ventilation shaft area was held constant for the three systems, thus the vent shaft impedance parameter, Φ , changed for each of the three cases.

The effect of blockage ratio on system ventilation is portrayed by Figure 14-24. To account for the Φ variation among the runs, the ventilation results are superimposed on Figure 14-12. As shown, for a given value of vent shaft Φ , the effect of blockage ratio on flow processed by the vent shaft is small. This may seem strange until one realizes that, to maintain the same value of Φ when the tunnel area is increased from 400 ft^2 to 785 ft^2 to cause a blockage ratio reduction from 25 percent to 14 percent, the vent shaft area must also be increased commensurately (from 400 ft^2 to 785 ft^2 for the case of $A_v/A = 1$). Thus, there is a potential trade-off in increasing the blockage ratio in a double-track, piston-effect ventilated system: for a given vent-shaft head-loss coefficient ($C_{\Delta H_s}$), essentially the same ventilation rates can be achieved with smaller vent shafts when the tunnel area is reduced.

Figures 14-25 and 14-26 illustrate the average system air temperature for Runs No. DT-9 and No. DT-10. As would be expected, a comparison of these results with systems having the same Φ value but a blockage ratio of 25 percent (Run No. DT-1, Figure 14-3, and Run No. DT-5, Figure 14-14, respectively) shows that systems with different blockage ratios, but the same ventilation rate and distribution, will demonstrate approximately the same thermal behavior.

14.6 TRAIN OPERATIONS

14.6.1 Headway

Results presented to this point have portrayed the environment in piston-effect ventilated systems with a high utilization factor (10-car trains at top speeds of 60 mph and headways of 120 seconds on both tracks). This situation does not occur presently in existing transit systems, but represents anticipated future operations in many systems. Therefore, it is difficult to

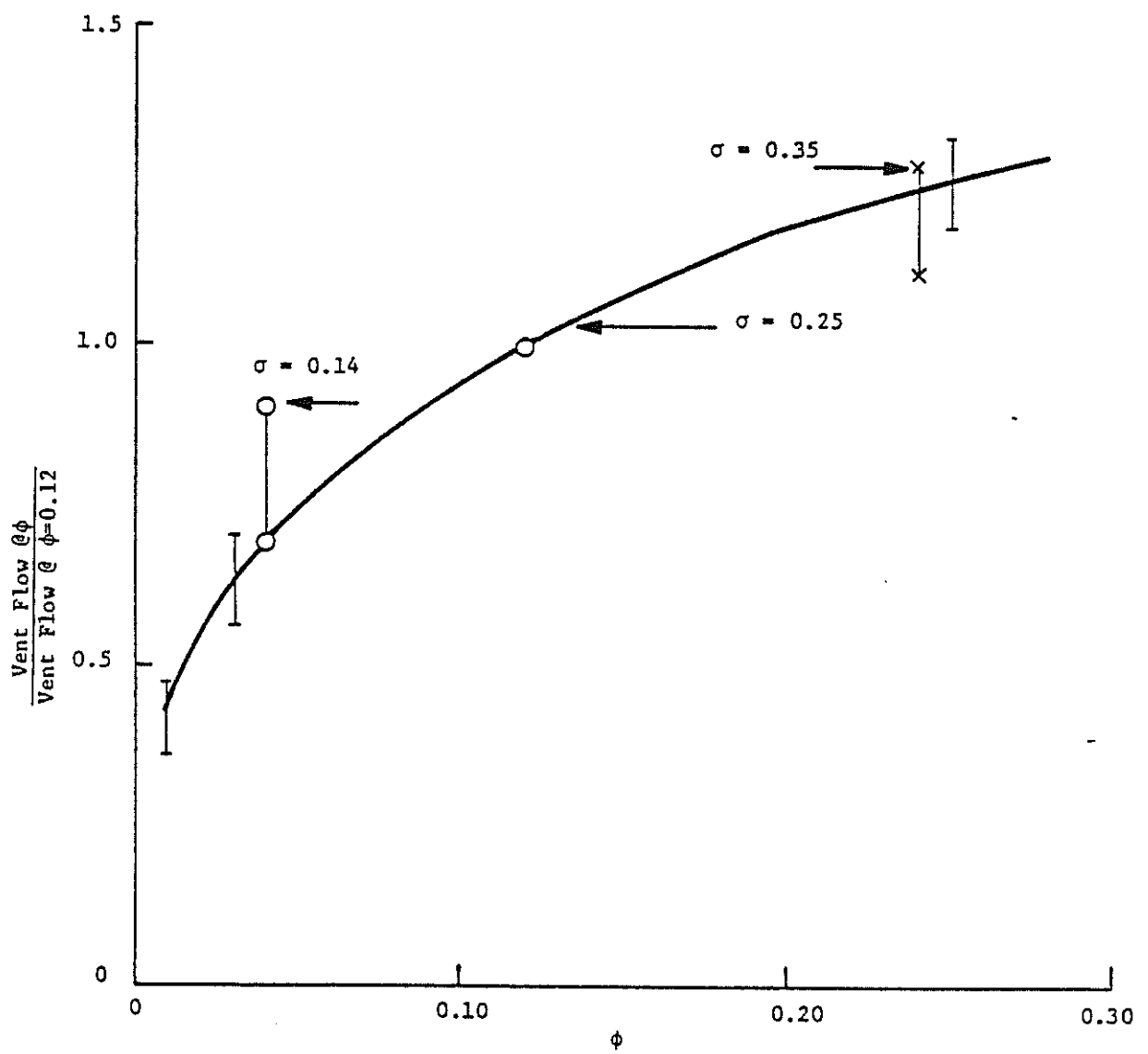


FIGURE 14-24. EFFECT OF BLOCKAGE RATIO ON AVERAGE VENTILATION SHAFT FLOW

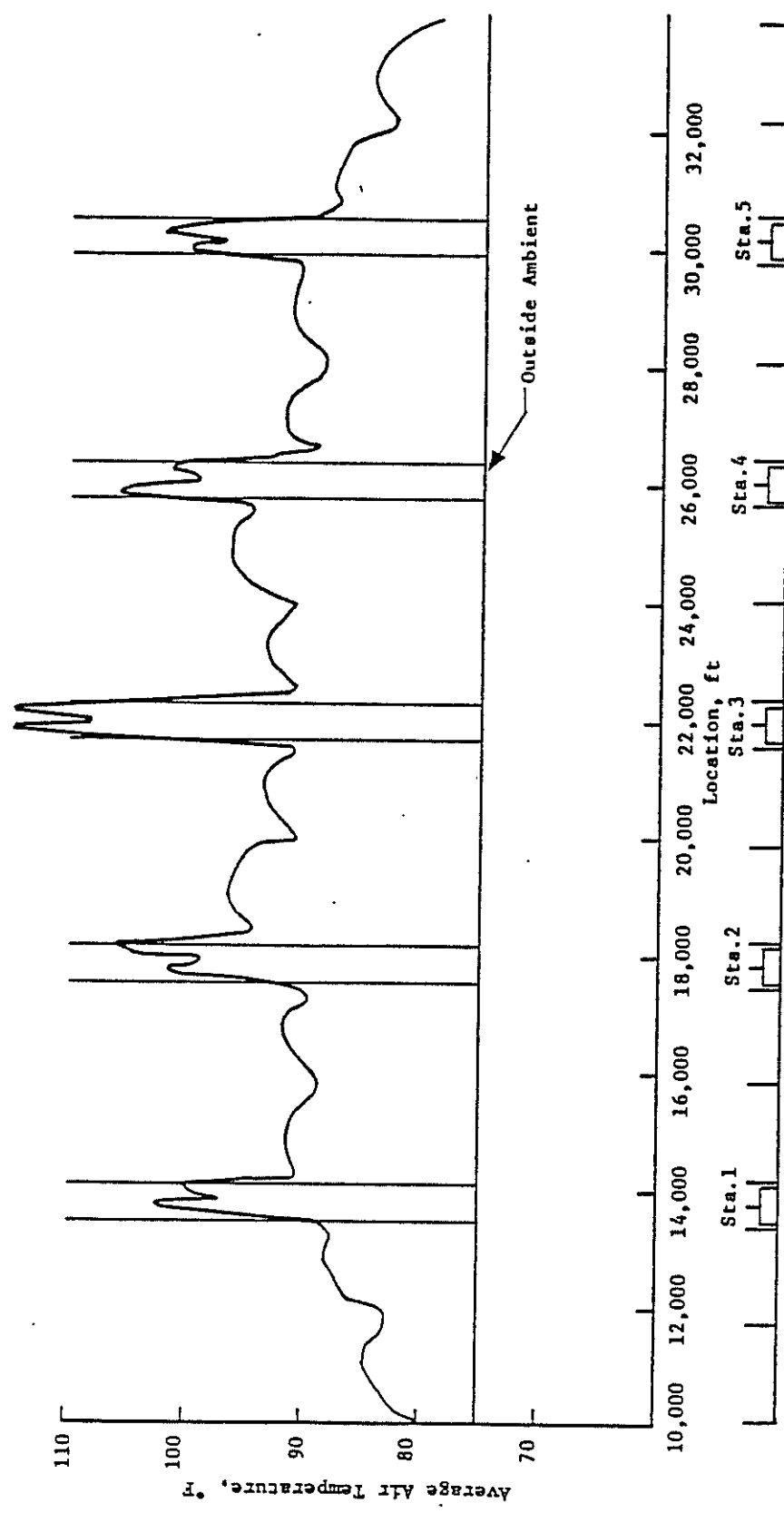


FIGURE 14-25. SYSTEM TEMPERATURE DISTRIBUTION: RUN NO. DT-9
 $(N=4, \phi_v = 0.04, \sigma = 0.14)$

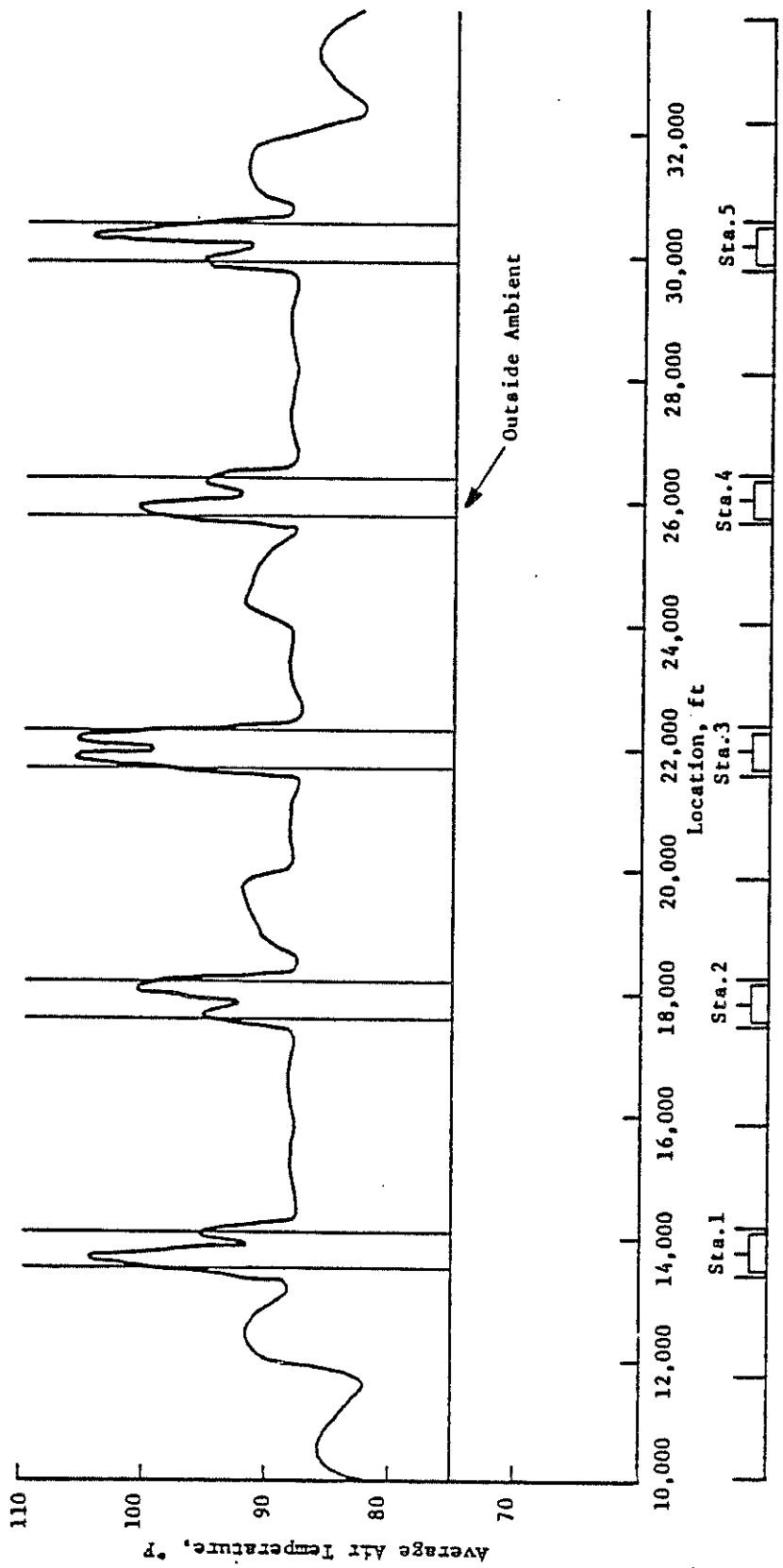


FIGURE 14-26. SYSTEM TEMPERATURE DISTRIBUTION: RUN NO. DT-10
(N=4, $\phi_v=0.24$, $\sigma=0.35$)

relate current operating experience to the high subway-to-ambient temperature differences reflected in the results.

The differences between the reported SES program findings and operating experience can be reconciled in two ways. First, the results herein can be adjusted in an approximate fashion for a more direct comparison with a given operating system. The basic adjustment regards system heat load and its impact on the subway/ambient temperature difference. For example, if a given double-track transit system has train peak speeds of 50 mph rather than 60 mph and headways of 3 minutes rather than 2 minutes, then the subway heat load will be roughly $(50/60)^2$ (2/3), or 46 percent, of the heat load associated with the results in this report. (Such factors as station dwell time, vehicle air-conditioning heat rejection, and the change in running time between stations because of the reduced operating speed also affect the system heat load.) As an approximation, the subway ventilation can be taken as directly proportional to the headway. In the present example, this means that the ventilation in this hypothetical system is about 67 percent of the ventilation associated with the results of other systems discussed in this report. Thus, from the standpoint of a simple, approximate heat balance, the temperature difference for the example system is about 70 percent of the values presented herein. For the base system, this translates into temperature differences of about 10°F between tunnel and ambient and 17°F between station and ambient.

The above approximation is conservative in the sense of overestimating the impact of headway variation on subway ventilation. This is demonstrated by the second approach, namely, an actual SES program simulation of other system geometries and/or operational parameters. Consider the system geometry of Run No. DT-7 (Figure 14-19: $\Phi_v = 0.12$, $\sigma = 0.25$, $h = 120$ seconds) but with train operation at a headway of 360 seconds. The simplified rationale would suggest that, with the same maximum train speed between stations, the two-thirds reduction in heat load due to the headway increase would be offset by a commensurate reduction in ventilation. In fact, the SES program simulation shows nearly a two-thirds reduction in the subway/ambient temperature difference as shown in Figure 14-27 (Run No. DT-11). A study of the ventilation results associated with this SES program simulation shows that, with the increased headway, the counteracting effect of opposing train operation is lessened substantially and the inertial die-down of the piston-effect airflow

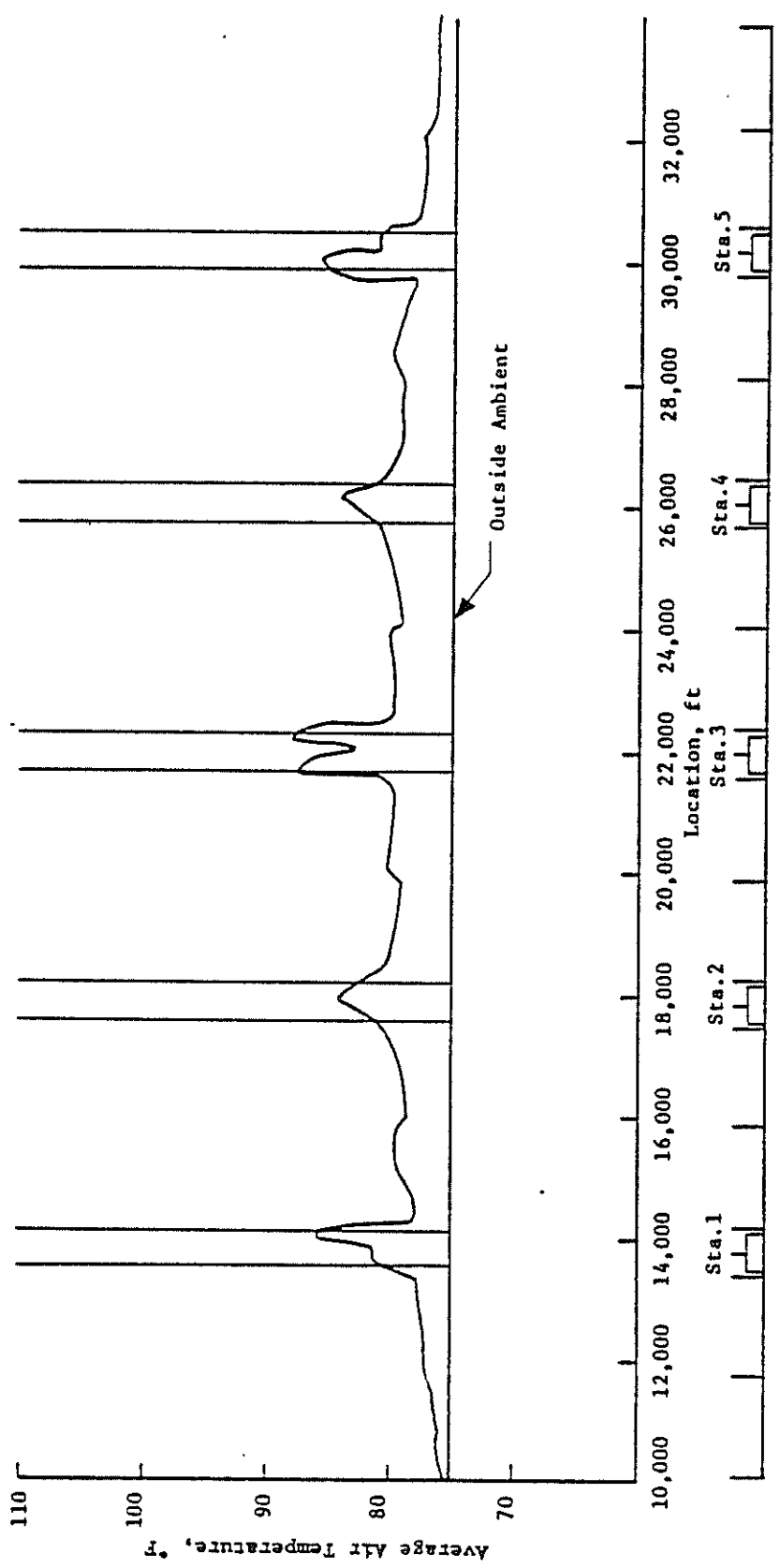


FIGURE 14-27. SYSTEM TEMPERATURE DISTRIBUTION: RUN NO. DT-11
 $(N=4, \phi_v=0.12, \sigma=0.25, h=360 \text{ sec})$

between successive trains becomes increasingly important. (Remember: an almost imperceptible tunnel air velocity of 100 fpm in a 400 ft² tunnel cross section provides a ventilation of 40,000 cfm.)

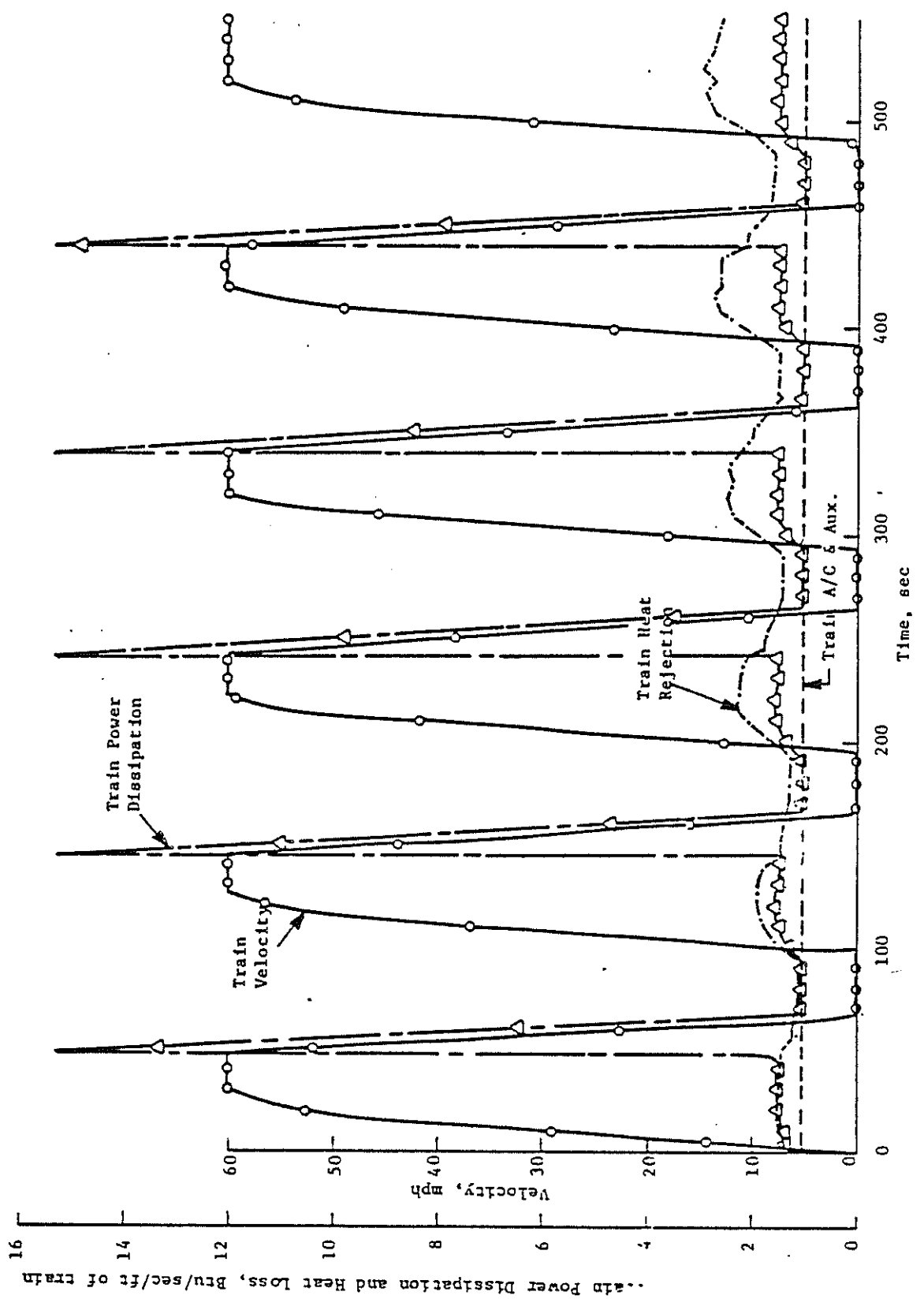
This finding has a twofold impact: (1) it demonstrates a basic caution to be observed in trying to extrapolate the results portrayed in this chapter on subway environment over too broad a range; and (2) it should suggest to transit agencies with currently acceptable environments that substantial future increases in system patronage may cause a serious deterioration in the environmental conditions.

14.6.2 Train Heat Release

Another factor materially affecting the subway heat load is the heat release rate from trains traversing the system. As described in Section 14.1, the total train heat release in these simulations comprises approximately 40 percent from vehicle air conditioning and auxiliaries and 60 percent from the propulsion system, braking energy dissipation, and mechanical losses. Of these heat sources, one is dependent on the history of train operation prior to entering the system: the heat release from the braking resistor grids. In the simulations to this point, the braking resistors were operating near thermal equilibrium throughout the system. The heat released during each travel-dwell cycle is approximately the same as the braking energy dissipated to the resistors of all the trains dispatched into the simulated system during one travel-dwell cycle. The resistors were assumed to have been heated to 600°F during several station stops outside the portion of the system being simulated. If, on the other hand, the braking resistors were initially at ambient conditions prior to system entry, only a small fraction of the braking energy would be dissipated as heat to tunnel and station air during the first station stop, the remainder going to heat the resistor grid mass. The braking heat release would increase on successive station stops as the resistor grids heated toward the condition where the temperature-dependent heat release during a travel-dwell cycle balanced against the braking energy dissipation.

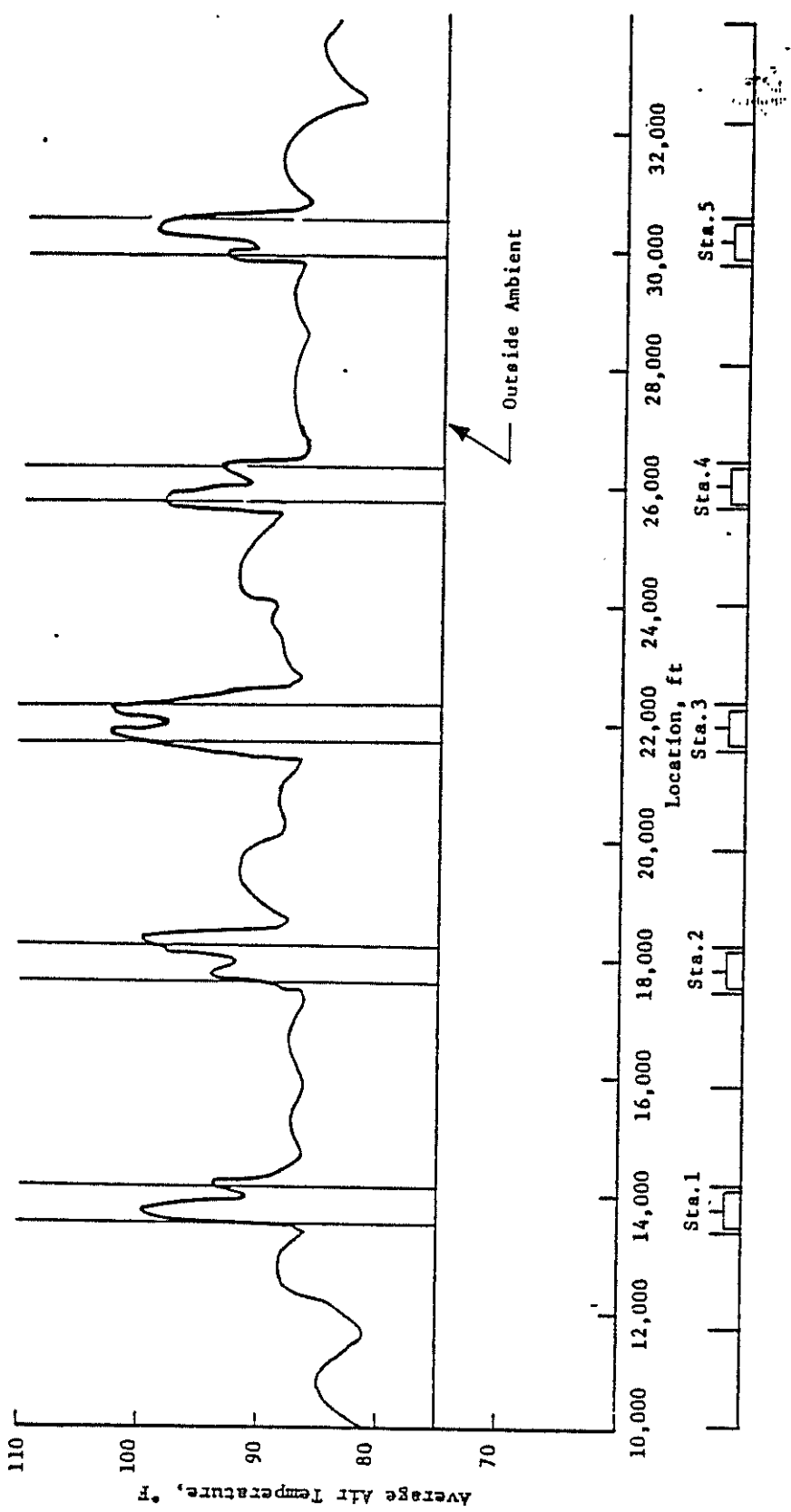
A SES program simulation (Run No. DT-12) was undertaken to demonstrate this behavior and the effect on system environment. The results in terms of train operation and heat release are shown on Figure 14-28 which depicts the

FIGURE 14-28. CASCADING OF BRAKING RESISTOR HEAT RELEASE: RUN NO. DT-12



velocity, power dissipation and heat rejection as a function of time for a train traversing the simulated system. The increase in train heat rejection from stop to stop through the system represents the SES-calculated buildup in the grid's thermal energy. Comparing with Figure 14-2, which illustrates the thermal equilibrium operations case, it is noted that the braking resistors are approaching thermal equilibrium as the train reaches the last station of the system. It is important to remember that bi-directional train operation acts to offset the heat-load reduction somewhat; i.e., the first station stop on one route of the system represents the fifth stop on the opposing route.

The system geometry used for this simulation was identical to the geometry for Run No. DT-7. System temperature distribution and station heat balance results should thus be compared with Run No. DT-7 calculations to ascertain the effect of the altered braking resistor heat release profile. Figure 14-29 represents the system average temperature distribution for Run No. DT-12. A comparison with Run No. DT-7 temperature findings (see Figure 14-19) shows temperatures on the order of 1°F to 3°F cooler in the tunnels and 5°F cooler in the stations. The effect on system heat load is better depicted by the Station 2 heat balance shown on Figure 14-30. Comparing with Run No. DT-7 (see Figure 14-22), the average heat load in the station is approximately 20 percent lower because of the reduced heat rejection rate from the braking resistors. Since the piston action ventilation is the same as the Run No. DT-7 simulation, the result is a decrease of 20 percent in the average rise of the station ventilation air temperature from 15°F for Run No. DT-7 to 12°F for Run No. DT-12. This decrease, together with the 2°F cooler average temperature of the inflowing ventilation air, results in an overall decrease of 5°F in station temperature as a consequence of the thermal inertia of the braking resistors. In terms of the temperature difference between Station 2 and outside ambient, the 26°F value for Run No. DT-7 was reduced by approximately 20 percent to 21°F for Run No. DT-12. This also explains the relatively lower difference in the tunnel temperatures for the two simulations. The tunnel air temperature in Run No. DT-7 averaged about 13°F above outside ambient between Stations 1 and 2, while Run No. DT-12 results show tunnel temperatures in this region about 11°F above the outside ambient. Again, the temperature results correlate with an overall reduction of about 20 percent in tunnel heat gain.



14-44

FIGURE 14-29. SYSTEM TEMPERATURE DISTRIBUTION: RUN NO. DR-12
(N=4, $\phi=0.12$, $\sigma=0.25$)

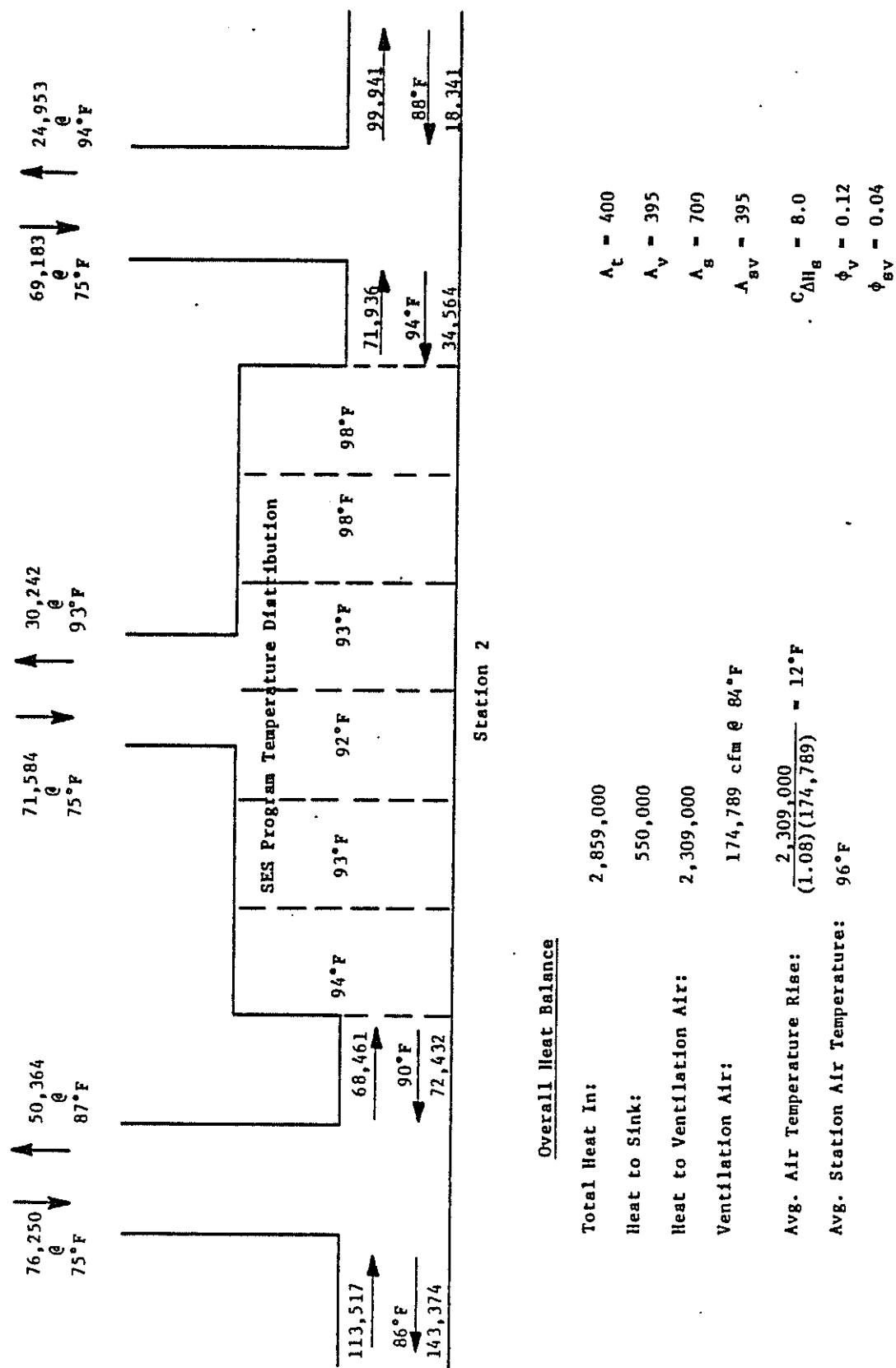


FIGURE 14-30. STATION HEAT BALANCE: RUN NO. DT-12, STATION 2

Similar correlations can be made in cases where other contributors to total train heat are reduced or removed. Since train air conditioning and auxiliaries comprise about 40 percent of the train heat release for the equilibrium braking resistor thermal condition, this heat source is responsible for about 40 percent of the subway temperature rise above outside ambient in Run No. DT-7. In a system operation with fewer passengers per car and/or no vehicle air conditioning, this heat load may be on the order of one-fourth the value used in the SES program simulations (271,000 Btu/hr per car), in which case the average rise of system air temperature would be about 70 percent of Run No. DT-7 (18°F in Station 2, for example).

In summary, the objective of this section is to emphasize that the heat loads and temperatures encountered in any system are dependent on the operational features peculiar to that particular system. This relates not only to the headway of operation which affects both airflows and heat loads as discussed in the previous section, but to the operation of trains in regions beyond the system being analyzed as well.

14.7 MECHANICAL VENTILATION

As the preceding piston-action ventilation results suggest, the ventilation created by the movement of trains through a system may not provide for adequate control of subway temperatures. This situation suggests consideration be given to supplementing the piston-action ventilation with mechanical systems.

To explore the potential benefits to be gained from mechanical ventilation systems, the SES program was used to simulate the System Geometry associated with Run No. DT-7 (Figure 14-19), but with 200,000 cfm exhaust fans located in the mid-tunnel shaft between each of the stations. The results, in terms of the system temperature distribution, are shown by Figure 14-31 (Run No. DT-13). The mechanical ventilation system had the effect of decreasing station temperature on the order of 5°F below Run No. DT-7; a disappointing result in view of the large capacity of the installed fans. An overall heat balance for Station 2, illustrated in Figure 14-32, provides a clue as to the reason for this behavior: recalling that the average station ventilation without the fans was about 175,000 cfm (see Figure 14-22), the mid-tunnel

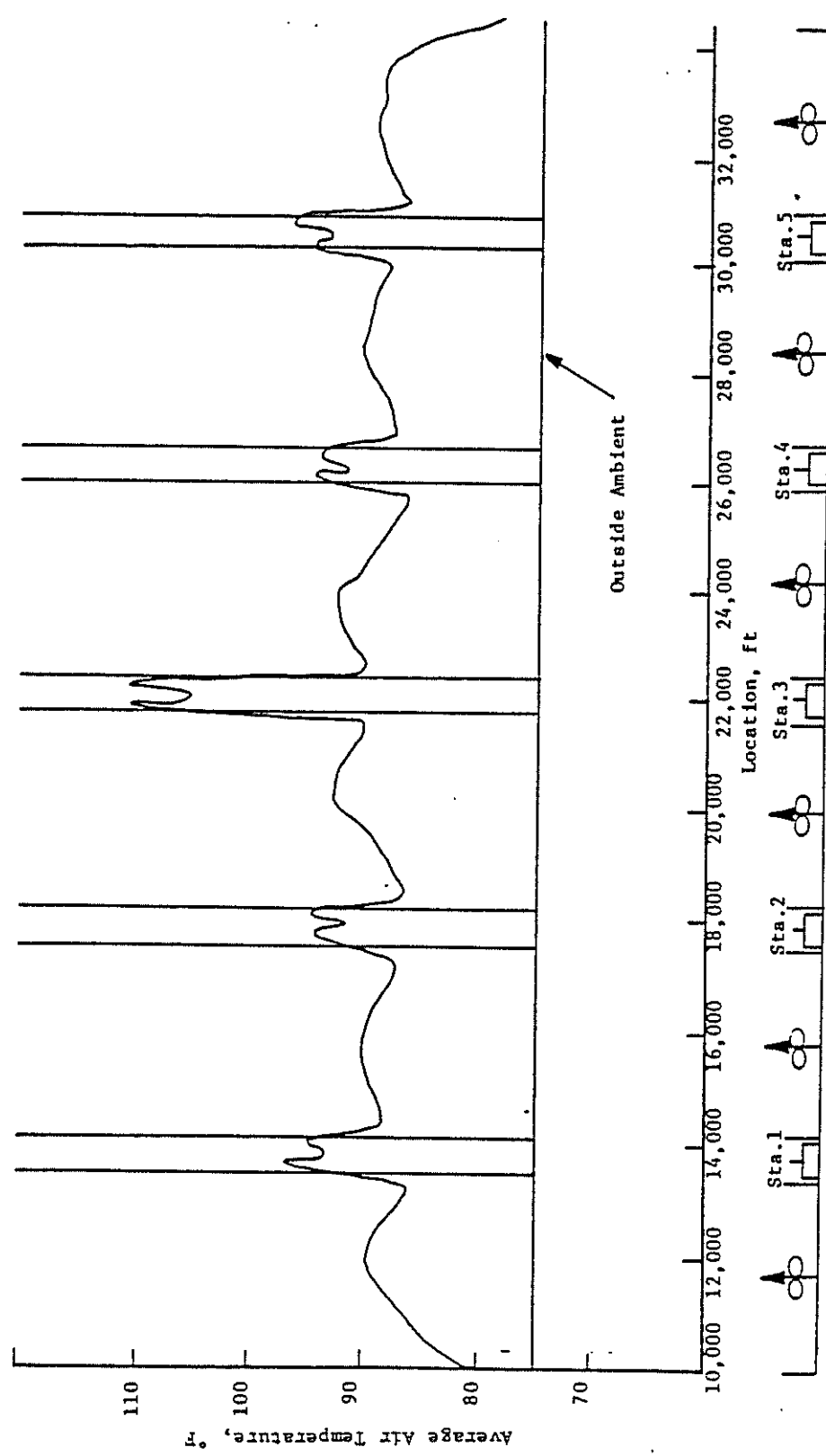


FIGURE 14-31. SYSTEM TEMPERATURE DISTRIBUTION: RUN NO. DT-13
(N=4, Mid-Tunnel Exhaust of 200,000 cfm)

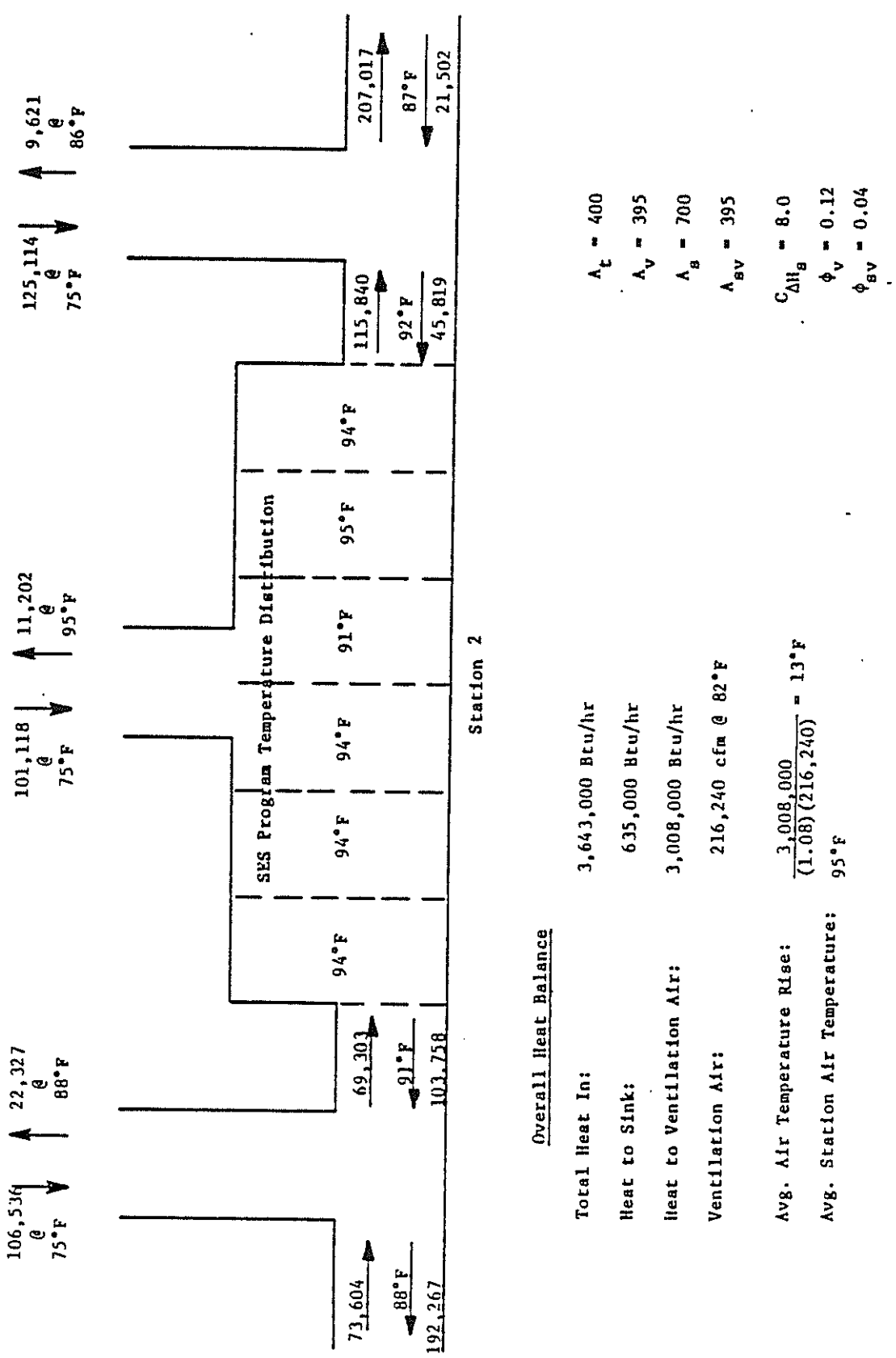


FIGURE 14-32. STATION HEAT BALANCE: RUN NO. DT-13, STATION 2

fans increased the station ventilation by only 23 percent, to 216,000 cfm. Comparison of Figure 14-31 and Figure 14-19 shows another interesting point: even with the mid-tunnel fans, the station temperatures still average 5°F to 15°F hotter than the tunnels. These observations suggest that a substantial fraction of the air exhausted by the fans is coming through the blast shafts adjacent to the stations. The result is a well ventilated tunnel, with little of the potential benefits of the fans being realized by the stations.

A second SES program mechanical ventilation simulation was conceived with the objective of enhancing station ventilation by removing the adjacent blast shafts. The results of this simulation run, illustrated by Figure 14-33 (Run No. DT-14), contrast dramatically with both the previously described mechanical ventilation results (see Figure 14-31) and the piston-action ventilated system (see Figure 14-19). With this system configuration, the ventilation air exhausted at mid-tunnel must come through the station entranceways, sweeping the station heat into the tunnels. The result is a reversal in the relationship between tunnel and station air temperatures, with the stations averaging 5°F to 10°F cooler than the tunnels. The longitudinal station temperature profile illustrated by Figure 14-33 is a consequence of the station entranceway location. Outside air is drawn through this entrance at the center of the station; thus, the station temperature is lowest at this location and increases toward the ends of the station as the ventilation air picks up additional heat.

A Station 2 heat balance further demonstrates the increased station ventilation brought about by the removal of the blast shafts. As Figure 14-34 shows, the average station ventilation rate has been increased to approximately 318,000 cfm, an 82 percent increase over the piston-action ventilated system and a 47 percent jump over the mechanically ventilated system with station blast shafts. The 88°F average temperature of Station 2 is 7°F below the station temperature of Run No. DT-13 and about 12°F below Station 2 in the Run No. DT-7 simulation.

As the number of ventilation shafts, fan shafts, and entranceways is reduced, the potential for undesirable air velocities in these areas increases and should be carefully evaluated during system design. In the present case, removal of the blast shafts contiguous to the station resulted in a 75 percent increase in maximum inflowing velocity through the 395 ft² net free area entranceway (from 665 fpm to 1160 fpm).

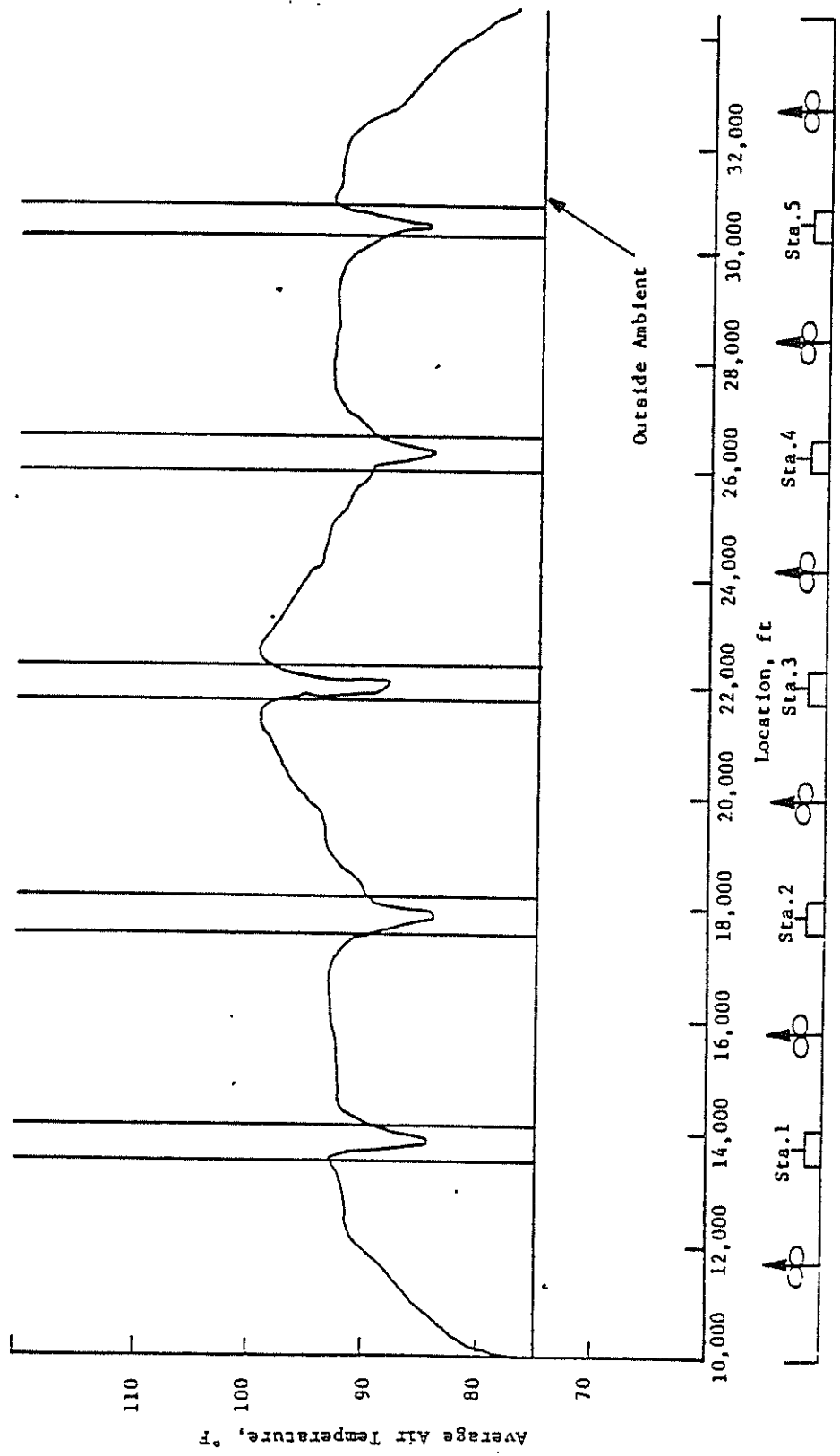


FIGURE 14-33. SYSTEM TEMPERATURE DISTRIBUTION: RUN NO. DT-14
(N=2, Mid-tunnel exhaust of 200,000 cfm)

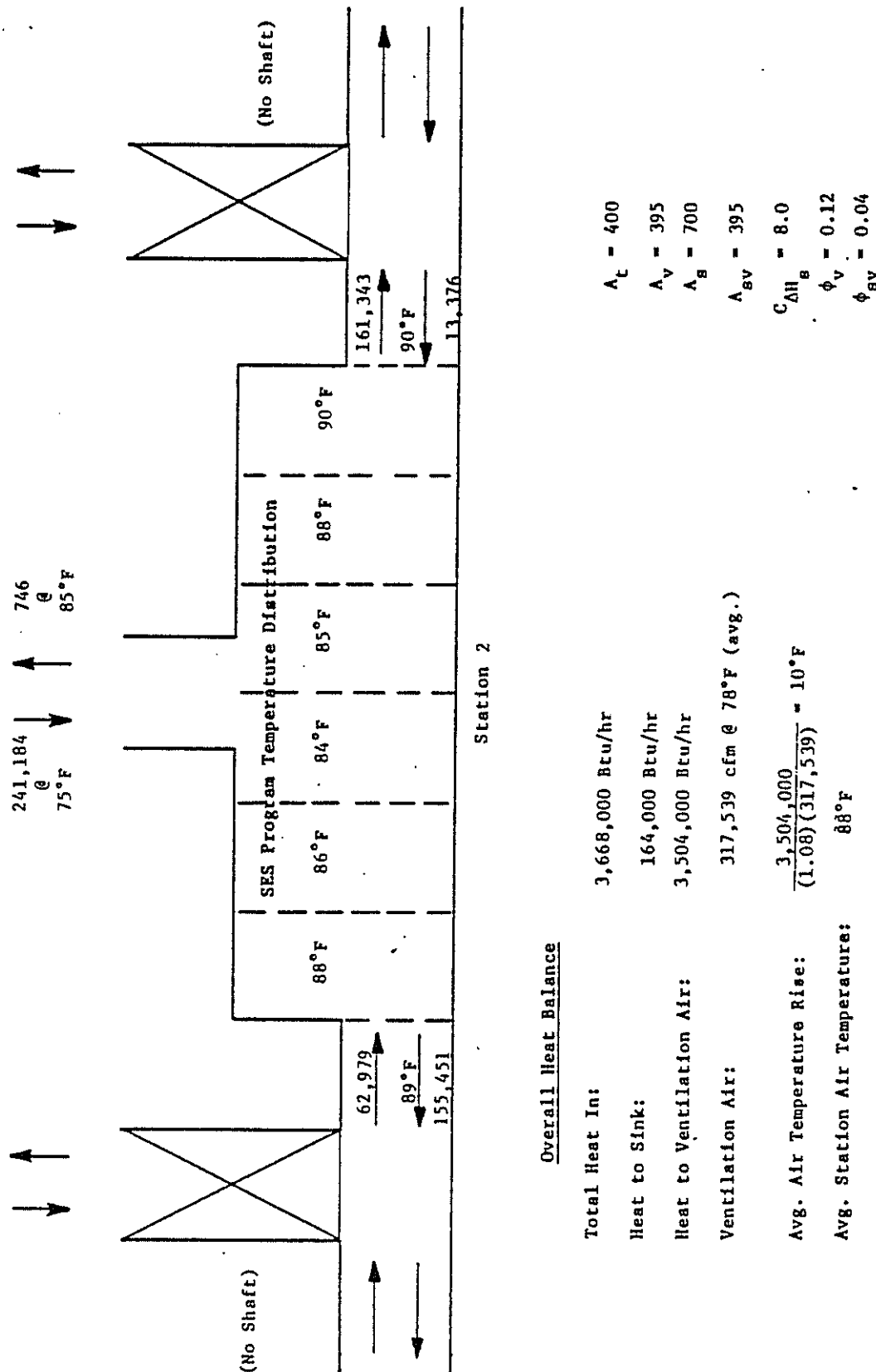


FIGURE 14-34. STATION HEAT BALANCE: RUN NO. DT-14, STATION 2

As a general conclusion, these SES program results show that the use of mechanical systems to supplement subway ventilation has significant potential. To maximize the benefit to be derived from such systems, careful consideration must be given to the overall ventilation strategy with a view toward assuring that the stations benefit from the supplemental ventilation.

14.8 TRACKWAY EXHAUST SYSTEM

A popular mechanical system for reducing subway heat loads is the trackway exhaust system (TES). This concept entails the siting of a number of air intakes beneath the platform and/or above the trackway along the length of the station for the purpose of sweeping air heated by under and/or above car components (braking resistors, air conditioning condensers, etc.) from beneath and/or above trains within the station. The basic exhaust system may be enhanced by a make-up air supply system also located above the trackway and/or below the platform for the purpose of further promoting this sweeping action.

Transit agencies in the U.S. currently using a TES include Atlanta (MARTA) and Washington, D.C. (WMATA). Such systems are also being designed for Baltimore (MTA), New York (NYCTA), and Buffalo (NFTA).

Agencies with operational TES report varying degrees of success. The Metro in Mexico City originally reported disappointing results with its system. The exhaust capacity per trackway was on the order of 60,000 cfm, but the original installation made no provision for adjusting the intake air distribution along the platform length. In fact, as originally installed, measurements showed the underplatform exhaust flow to be severely localized in the vicinity of the fan duct connection. Following a retrofit program to correct this situation, station temperature measurements in retrofitted stations suggested significant improvement.

The Japanese have undertaken one-fifth scale model studies of TES augmented by combination air curtain and over-the-train supply systems. Although not totally conclusive in terms of the expected behavior of a full-scale system, the tests suggest that efficiencies on the order of 90 percent extraction of the heat released by a train dwelling in the station may be achieved. However, these tests correspond to a full-scale supply/exhaust system capacity

of about 170,000 cfm per trackway. Based on these scale model results, actual supply/exhaust systems in the Tokyo subway were constructed.

As a part of the Subway Environmental Research Project, the Associated Engineers developed a simplified model of TES behavior for the purpose of making order-of-magnitude estimates of exhaust capacity requirements in the absence of definitive performance data on an actual system. The model is based on the premise that, as a train dwells in a station, an effective TES must provide for at least one air change in the volume beneath the train. For a train that completely occupies a 600 ft station, this volume is about 18,000 ft³ (assuming a 10 ft car width and an average clearance of 3 ft between the trackway and undercar equipment). Thus, if the dwell time in the station is set at 15 seconds, the TES would require a capacity of approximately 72,000 cfm per trackway to meet the air change criterion, with no allowance for "short-circuiting" of air through the gap between the platform and the train.

Finally full-scale tests conducted in the Toronto Subway System have led to the development of empirical equations for TES efficiencies based on air volume flow rate per unit length of station, and number of air changes per effective dwell time. For further information it is suggested that the user consult Volume 1 of this handbook (Principles and Applications) Pages 3-54 through 3-58.

A series of three SES program studies were implemented to shed further light on the potential benefits and problems of the TES concept. These simulations focused on the questions of the maximum potential benefit that may be realized from a TES in terms of station temperatures; implications of an exhaust-only system in terms of overall system aerodynamics and thermodynamics; and the sensitivity of certain assumptions regarding TES efficiency.

The SES program requires five specific inputs to simulate the thermodynamic performance of a TES. Four of these inputs involve the efficiency of the TES to capture heat from various sources and at different operating modes. The fifth input is the maximum train speed at which the TES operates. The moving efficiencies are applied only when a train is below the prescribed speed, and only to that part of the train that is actually in the station at an instant during deceleration or acceleration.

The overall system geometry and train operations for the TES simulations are identical to those used for Run No. DT-7 (see Figures 14-19 and 14-22).

Thus, the effect of the TES can be measured against the results of this simulation.

Run No. DT-15 employed assumed TES efficiencies of 90 percent during dwell and 90 percent while moving in the station below 40 mph for both types of heat sources (the user is cautioned that these efficiencies are in excess of those determined by testing, and are used only for the purposes of comparison). The simulation assumed a combination supply/exhaust system with no net effect on station aerodynamics. The results, in terms of system temperature distribution, are shown by Figure 14-35. A comparison with Run No. DT-7 results on Figure 14-19 shows the dramatic potential of an effective TES: although the tunnels are only slightly cooler, the stations are on the order of 10°F to 15°F cooler. The reason for this behavior is better illustrated through a comparison of station heat balances: Figures 14-36 and 14-22 show the ventilation of Station 2 to be approximately the same, as would be expected. However, the TES reduced the total sensible heat release in the station by about 85 percent, from 3642 MBH to 528 MBH, resulting in a much lower station air temperature rise.

An examination of the implications of an exhaust-only TES on overall subway environment was undertaken with Run No. DT-16. This simulation employed the same efficiency values as Run No. DT-15, but also included the aerodynamic simulation of a total station exhaust capacity of 200,000 cfm. The results of this simulation are presented by Figure 14-37 in terms of system temperature distribution. A comparison with Figure 14-35 shows the overall effect of the 200,000 cfm station exhaust to be a general reduction in station and tunnel temperatures on the order of 1°F to 2°F. This result is to be expected for this particular subway environmental control concept, since the overall effect of the exhaust system is the introduction of additional, cool outside air into the system. The station heat balance on Figure 14-38 further illustrates this concept. The combination of piston-action and exhaust fans introduces 260,000 cfm of ventilation air into the station, an increase or more than 50 percent over piston action alone (see Figure 14-36). The flow path by which this air reaches the station is largely influenced by the interaction with the train piston-action. In this simulation, the additional airflow in Station 2 came largely from the station blast shafts, but inflow from the tunnel to the station was also boosted.

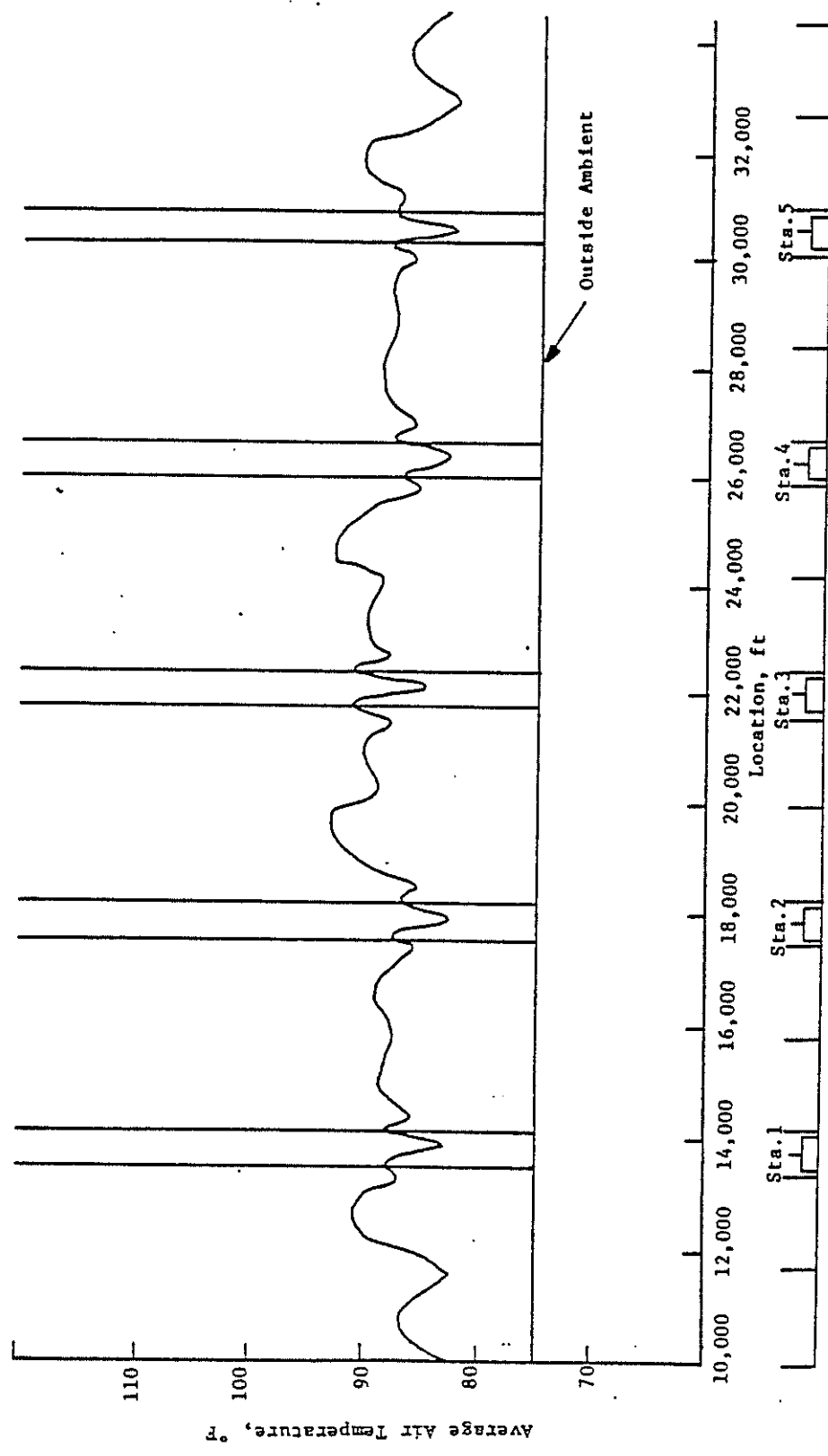


FIGURE 14-35. SYSTEM TEMPERATURE DISTRIBUTION: RUN NO. DT-15
(TRACKWAY EXHAUST, EFFICIENCIES OF 90% FOR
EFFICIENCY INPUTS)

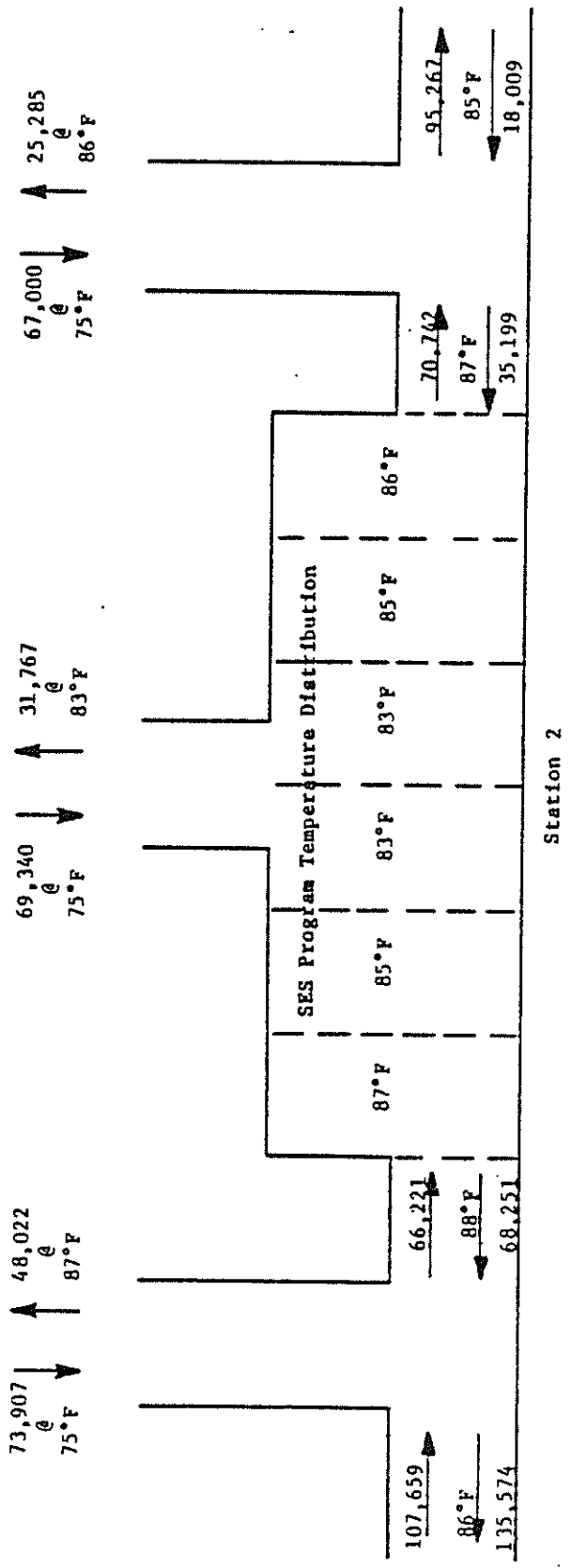


FIGURE 14-36. STATION HEAT BALANCE: RUN NO. DT-15, STATION 2

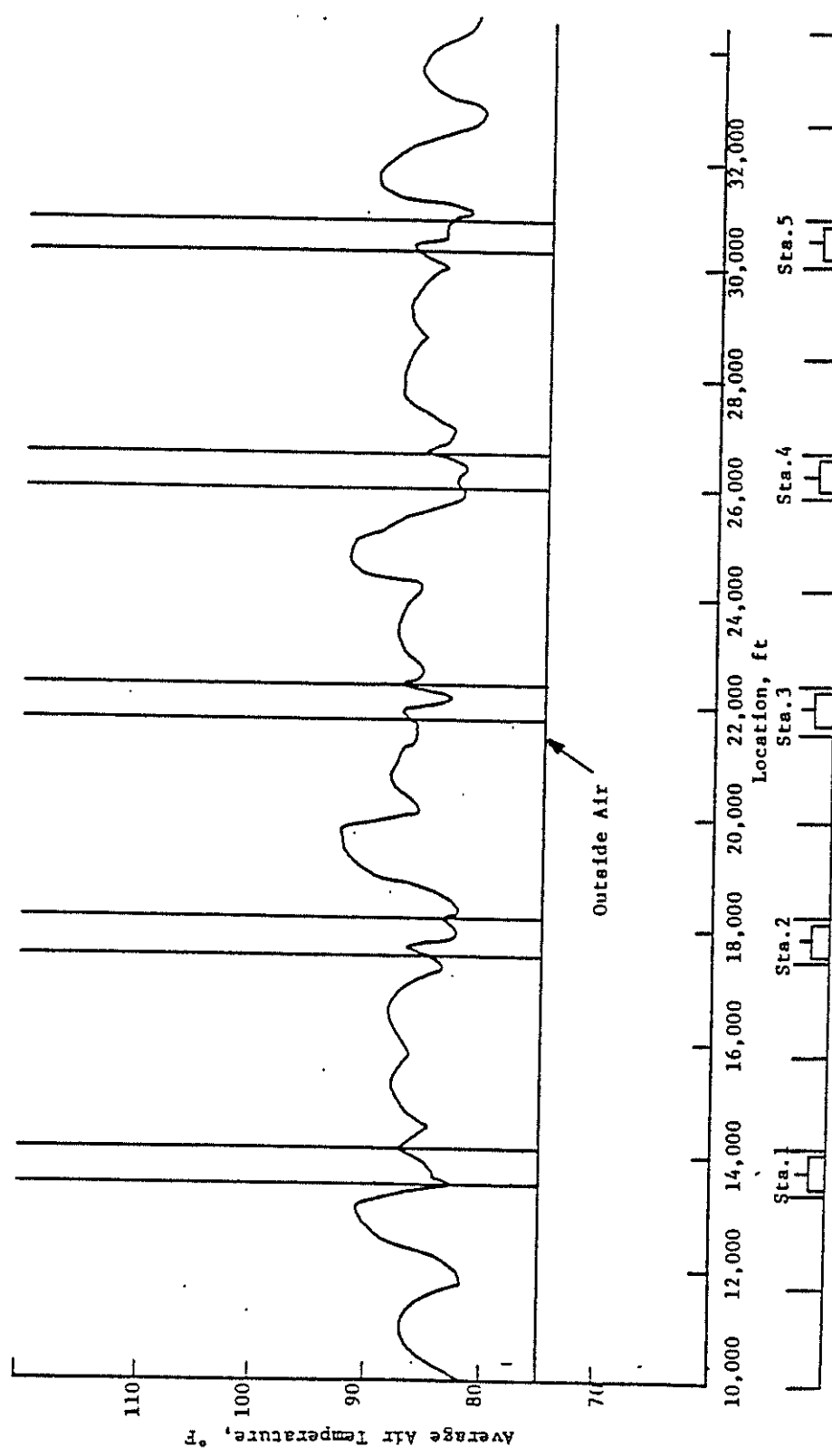


FIGURE 14-37. SYSTEM TEMPERATURE DISTRIBUTION: RUN NO. DT-16
(TRACKWAY EXHAUST SYSTEM, NO MAKE-UP AIR)

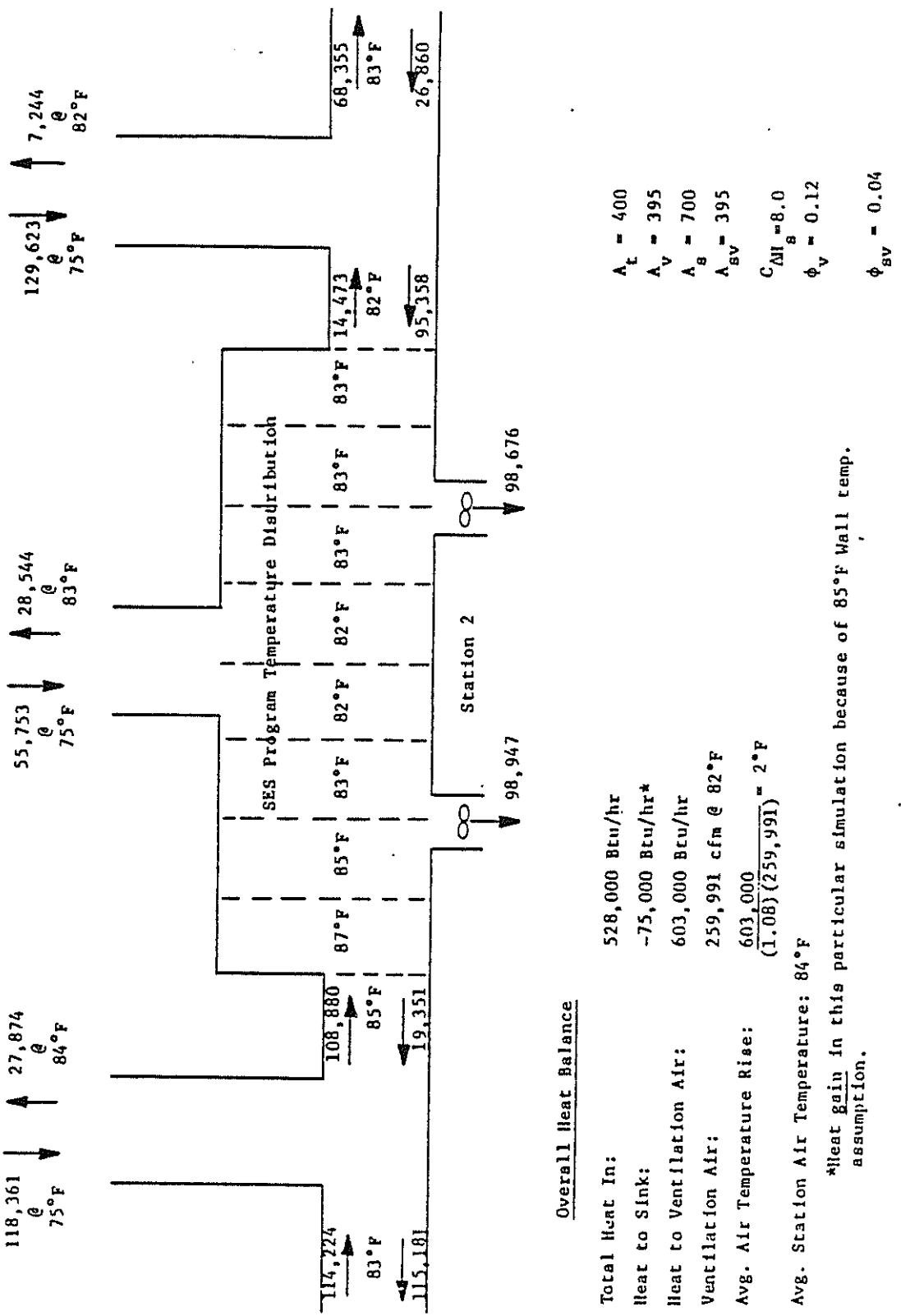


FIGURE 14-38. STATION HEAT BALANCE: RUN NO. DT-16, STATION 2

It should be noted that for environmental control strategies where tunnel temperatures and/or outside ambient temperature exceed station temperature, the TES exhaust-only scheme could have the unwanted effect of introducing warmer air into the station. In general, however, the benefits to be derived from the heat extraction by the system and the added ventilation air in a station without mechanical cooling would be expected to outweigh this detracting possibility.

The sensitivity of station environment to the assumed value of moving efficiency was explored with Run No. DT-17. This run was the same in all respects to Run No. DT-15, with the single exception that the moving efficiencies for both types of heat source were reduced from 90 percent to 30 percent. The result was station temperatures averaging about 5°F hotter than the 90 percent efficiencies case, as shown in Figure 14-39, although these temperatures were 5°F to 10°F cooler than Run No. DT-7 with no TES. Table 14-1 suggests the reason for this sensitivity: with 90 percent efficiencies the station sensible load was reduced by 85 percent, whereas with 30 percent moving efficiencies the sensible load was reduced by about 55 percent. This reflects the fact that of the total train heat released within the confines of the station, on the order of 40 percent occurs while the train is moving.

Taken as a whole, the SES program's TES simulations demonstrate the significant potential benefit to be realized by its inclusion in an environmental control strategy. The results also emphasize the need for definite data regarding actual performance so that these systems can be designed with confidence. The demonstrated sensitivity to such parameters as the moving efficiency indicates that any performance data must be broad in scope, addressing train operations as well as system design.

14.9 FOUR-TRACK OPERATION

A SES program simulation of a system containing four operational train routes, Run No. DT-18, provided additional insight into subway aerodynamics and thermodynamics. Although the tunnel and station cross-sections were enlarged to 800 ft², respectively, to accommodate the additional tracks, the overall ventilation concept and vent shaft impedance parameter, Φ , were the same as for Run No. DT-7. The results of Section 14.6 show that, for the same

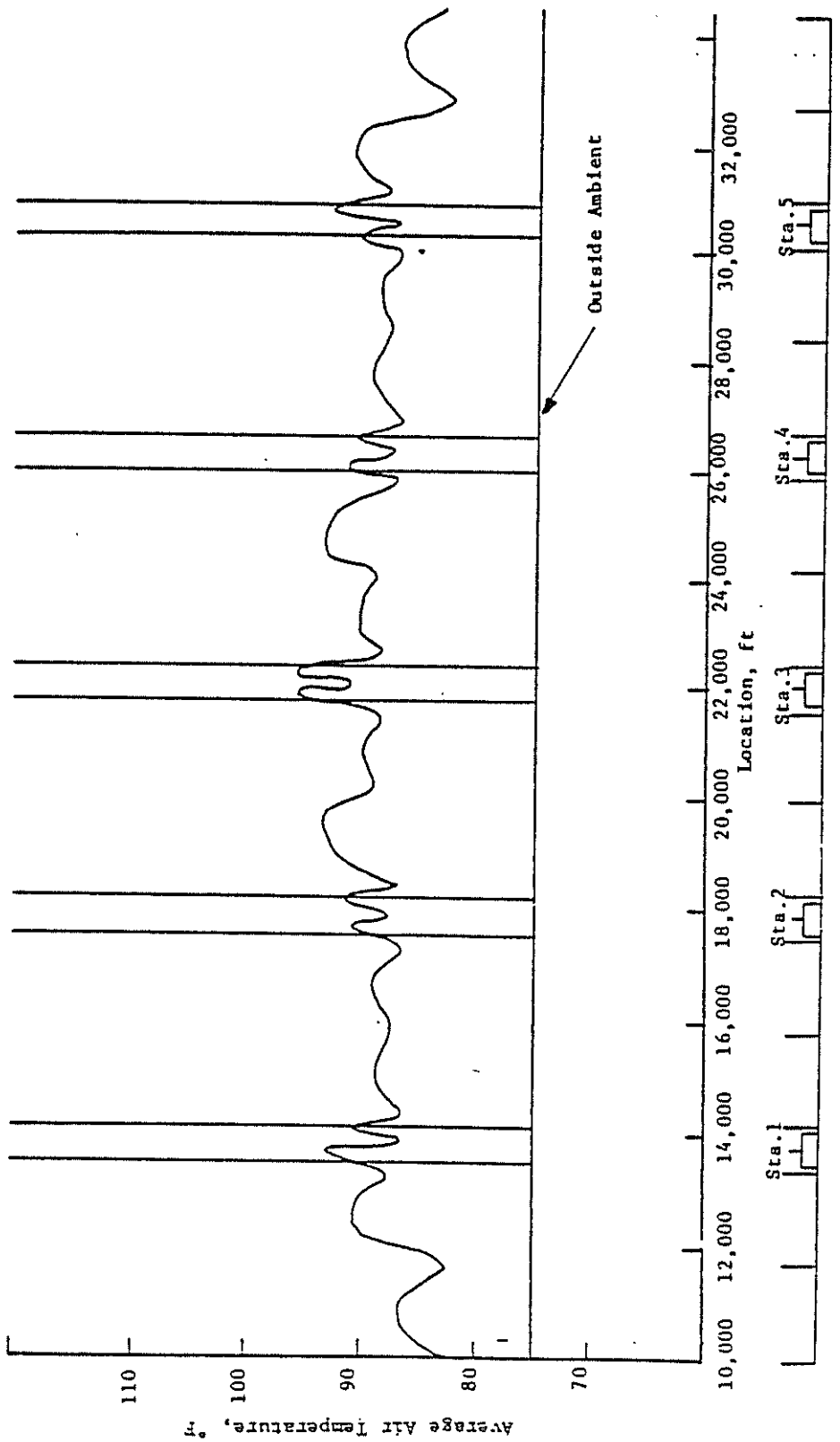


FIGURE 14-39. SYSTEM TEMPERATURE DISTRIBUTION: RUN NO. DT-17
(TRACKWAY EXHAUST SYSTEM, EFFICIENCIES = 90%
STOPPED, 30% MOVING)

TABLE 14-1. IMPACT OF TES ON STATION HEAT LOAD

SENSIBLE HEAT LOAD (MBH)			
STATION 2			
<u>System</u>	<u>Platform</u>	<u>Train</u>	<u>Total</u>
<u>DT-7</u> (No TES)	105	3537	3642
<u>DT-17</u> (TES; 30% efficient below 40 mph, 90% efficient during dwell)	105	1408	1513
<u>DT-15</u> (TES; 90% efficient below 40 mph 90% efficient during dwell)	105	423	528

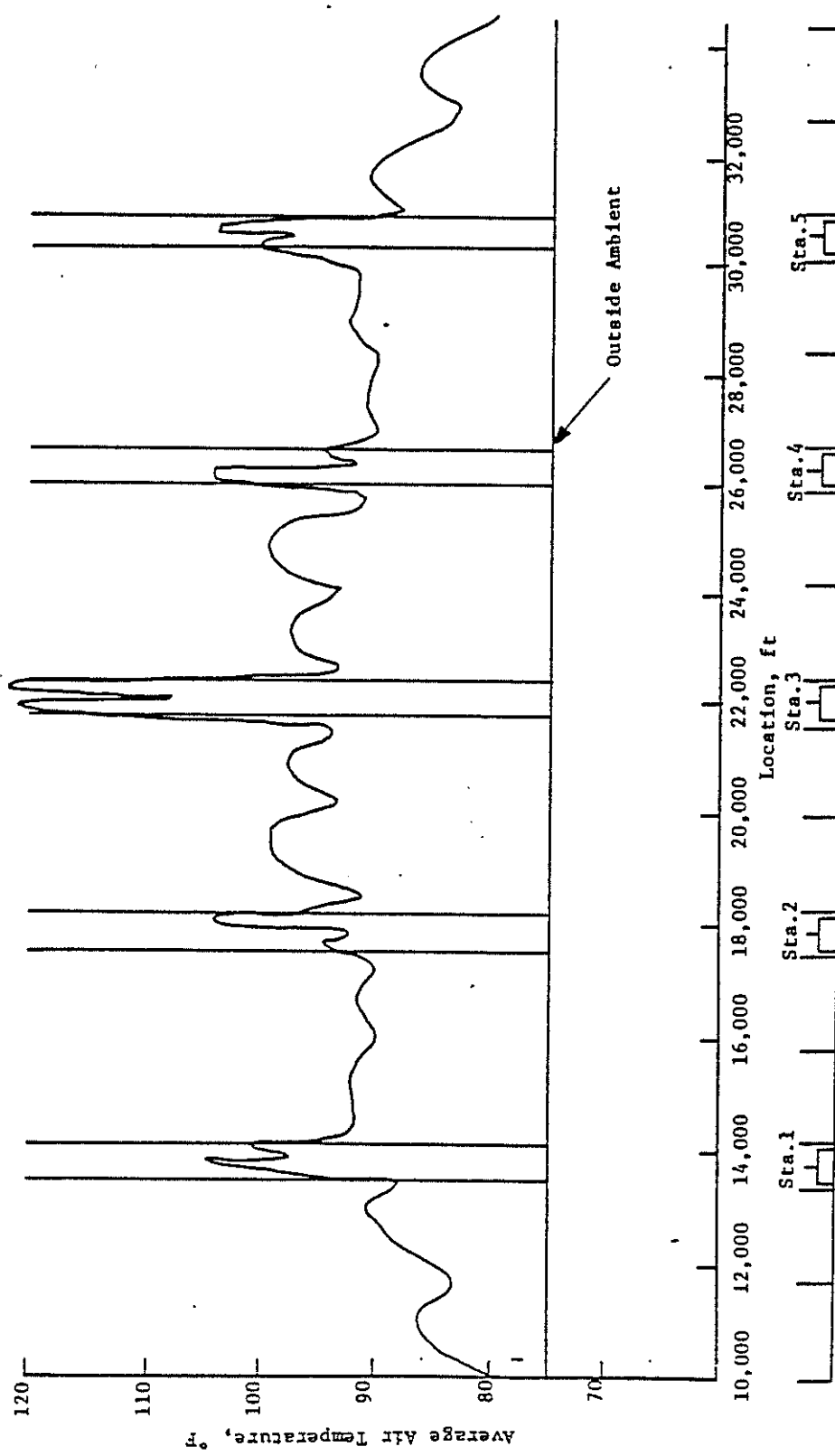
train operation, similar airflows and temperatures would prevail within the subway; thus, the effect of the additional train routes can be determined through direct comparison with Run No. DT-7 results.

Train operation on two routes of the four-track system were the same as for Run No. DT-7, representing local service. The two additional routes were express routes, with stops at Stations 1, 3 and 5. Maximum train speed on all routes was 60 mph, and the headway on each of the routes was 120 seconds.

The effect on system temperature of the additional train routes, shown by Figure 14-40, is at first glance surprising. Comparing with Run No. DT-7, the air temperature in the local stop stations (2 and 4) is actually about 2°F less than the two-track system results. The heat balance for Station 2, illustrated by Figure 14-41, shows the reason. Although the average temperature of the ventilation air entering the station is about 3°F hotter in the four-track simulation, the passing of express trains through the station boosts the average ventilation rate by almost 85 percent while increasing the station sensible heat load by only about 15 percent. As a consequence, the rise in ventilation air temperature in Station 2 of the four-track system is about 5°F less than in the two-track system.

SES-calculated temperatures in the express stop stations (1, 3 and 5) and in all the tunnels for Run No. DT-18 generally range from 2°F to 5°F hotter than the two-route simulation, suggesting that the additional heat load is to a large degree offset by the added ventilation produced by the combination of express and local train operations. The exception to this observation is Station 3, where both express and local trains dwell simultaneously on their respective routes. In this station, temperatures range 8°F to 9°F hotter for the four-route simulation.

The time dependent airflows in one of the tunnels and blast shafts of the four-track system are shown on Figure 14-42. These flows are accompanied by a schematic train situation diagram portraying train operation on each of the four tracks, to enable a cause-and-effect interpretation of the airflows. As an illustration, consider the abrupt positive peak (outflow) in blast-shaft flow occurring at the reference time of about 15 seconds. In the interval between 0 and 12 seconds, air was being drawn into the system behind the local train on route 3 which had just departed Station 2. Meanwhile, the express train on route 4, en route from Station 3 to 1, approached the



14-63

FIGURE 14-40. SYSTEM TEMPERATURE DISTRIBUTION: RUN NO. DT-18
(FOUR-TRACK OPERATION, EXPRESS STOPS AT STATIONS
1, 3, & 5)

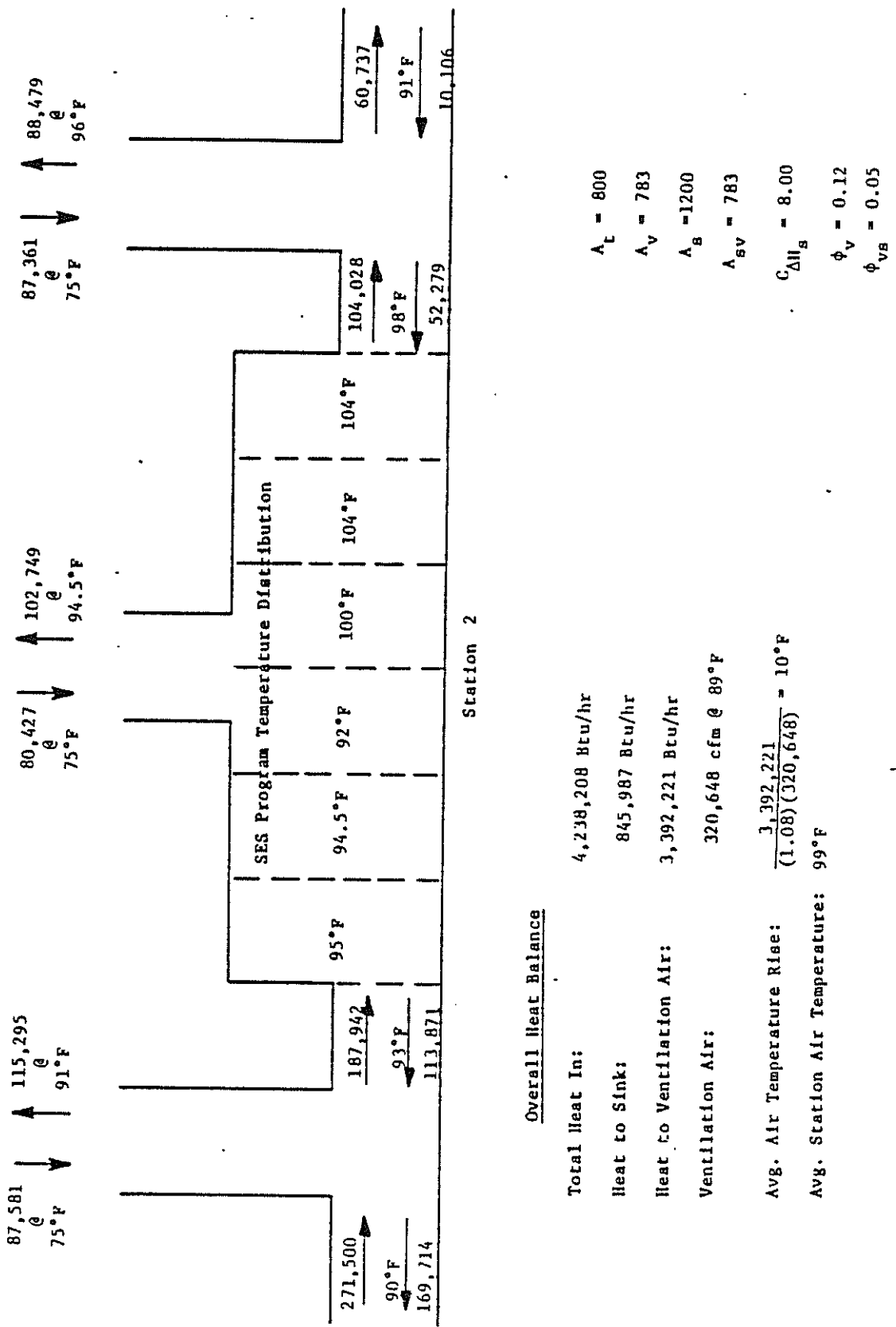
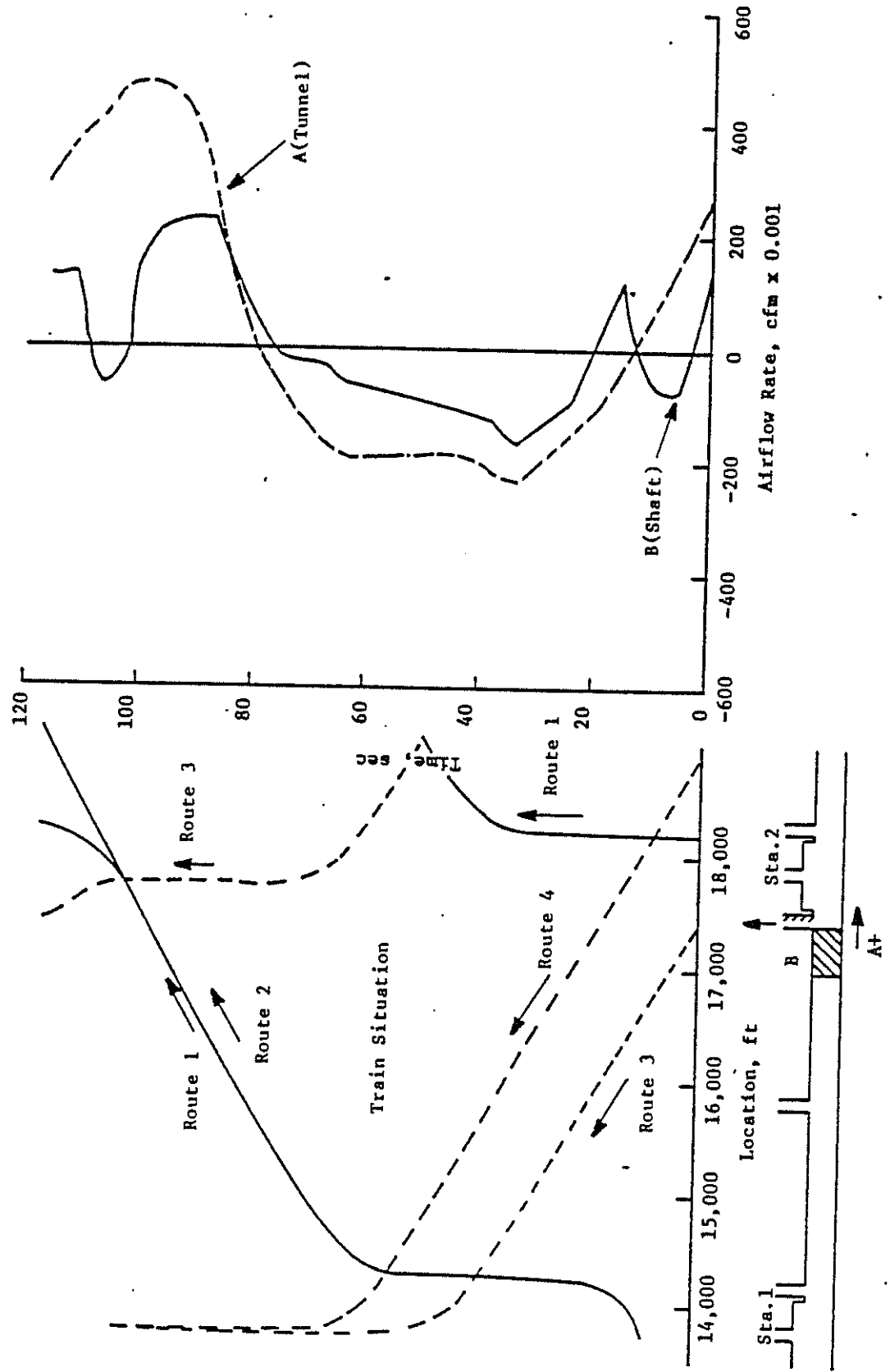


FIGURE 14-41. STATION HEAT BALANCE: RUN NO. DT-18, STATION 2



14-65

FIGURE 14-42. EFFECT OF RELATIVE TRAIN SITUATION ON VENTILATION SHAFT FLOW:
RUN NO. DT-18

shaft creating a greater piston-action flow than that in the tunnel occupied by the local train. The result was a shift in blast-shaft flow direction, peaking just as the front of the express train reached the shaft and once again shifting direction as the express train passed.

In summary, the conclusion of greatest significance to be drawn from Run No. DT-18 is the observation that the effect of the additional heat release to the system by the two additional train routes is to be largely offset by the increase in system ventilation. This should not be interpreted as a general rule, but as an additional caution to be considered in the extrapolation of the results of a given system analysis.

14.10 TWIN-TUNNEL SYSTEMS

The SES program simulations of systems comprising parallel, single-track tunnels between stations considered the same station spacing and train operations as the double-track tunnel systems, thus enabling comparisons of results for the different tunnel configurations. These twin-tunnel simulations focused on piston-action ventilation, and the parameter varied was the number of vent shafts between stations. The system geometry was symmetrical in each simulation: each tunnel ventilation shaft had a companion shaft connected to the adjacent tunnel. The purpose of these simulations was a study of the basic behavior of subway aerodynamics and thermodynamics, rather than the development of a viable environmental control concept.

The first twin-tunnel simulation to be discussed is identified as Run No. DT-19. The ventilation scheme comprised three shafts in each of the tunnels ($\Phi = 0.12$) and the station stairway ($\Phi = 0.01$). The tunnel blockage ratio was 0.50. For consistency with the double-track notation, the number of shafts in a tunnel-station subsystem, N , is four in this case (adjacent shafts in the parallel tunnels are counted as one shaft for comparative purposes). This simulation corresponds closely to double-track Run No. DT-7, the total tunnel area and total shaft area being the same in each case. The one departure from commonality is the station stairway: the stairway cross section corresponds to the area of a single ventilation shaft in both simulations, thus the twin-tunnel system stairway area (196 ft^2 ; $\Phi = 0.01$) is half the stairway area in the double-track system (395 ft^2 ; $\Phi = 0.04$).

The results of Run No. DT-19 are presented in terms of the average system temperature distribution by Figure 14-43. Note that tunnel temperature is plotted separately for each of the twin-tunnels. A comparison with corresponding double-track results (see Figure 14-19) shows that the twin tunnels are generally on the order of 2°F to 3°F cooler, but that the average station temperature is only about 1°F cooler in the twin tunnel system. Choosing Station 2 for a closer examination, the station heat balance, illustrated by Figure 14-44, suggests the reason for this behavior. The approach tunnel airflows average over 200,000 cfm, but only about 20 percent to 30 percent of this flow enters this particular station, the remainder being drawn over to the adjacent departure tunnel without picking up a share of the station sensible heat load. The actual station ventilation of 153,000 cfm is close to the 175,000 cfm observed in the double-track simulation (a significant percentage of the difference in ventilation is probably attributable to the smaller stairway area in the twin-tunnel simulation).

The phenomenon of the recirculation of air between approach and departure tunnels deserves further discussion because of its importance in terms of station environment. Based on limited scale model studies (Ref. 2) and field observations, the degree of recirculation would be expected to correlate with relative train operation in the parallel tunnels. When the adjacent tunnels are occupied by trains simultaneously for a significant percentage of the time a train requires to traverse the tunnel, the degree of recirculation at the station portals should be high. Conversely, when the adjacent tunnels are alternately occupied by trains, the degree of recirculation should be low.

Both situations are encountered in the SES program twin-tunnel simulation, as Figure 14-45 illustrates. Recalling that the headway on each route is 120 seconds, Figure 14-45 shows the duration that each tunnel of the system is occupied by a train both with respect to the 120 seconds reference time and with respect to the adjacent tunnel. Note that each tunnel between stations is occupied by a train for 60 seconds out of 120 seconds. The fact that each tunnel is occupied by a train for 50 percent of the time because of the short headway operation is sufficient reason to expect recirculation to be of some significance. With respect to the degree of recirculation, Section 2 and 3 will be used for comparative purposes. Note that the adjacent tunnels

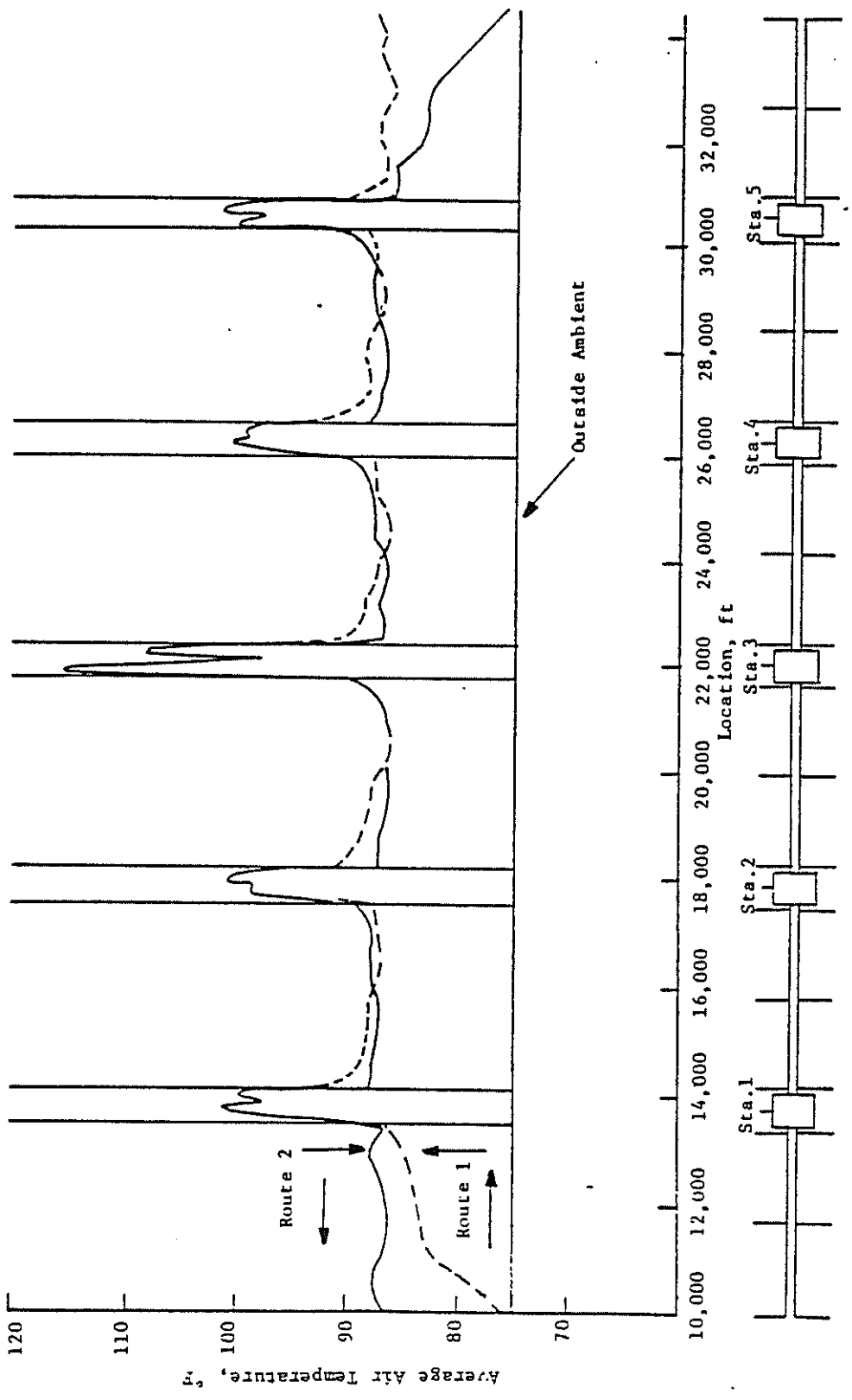


FIGURE 14-43. SYSTEM TEMPERATURE DISTRIBUTION: RUN NO. DT-19
(TWIN TUNNELS, N=4, $\phi_v=0.12$, $\sigma=0.50$)

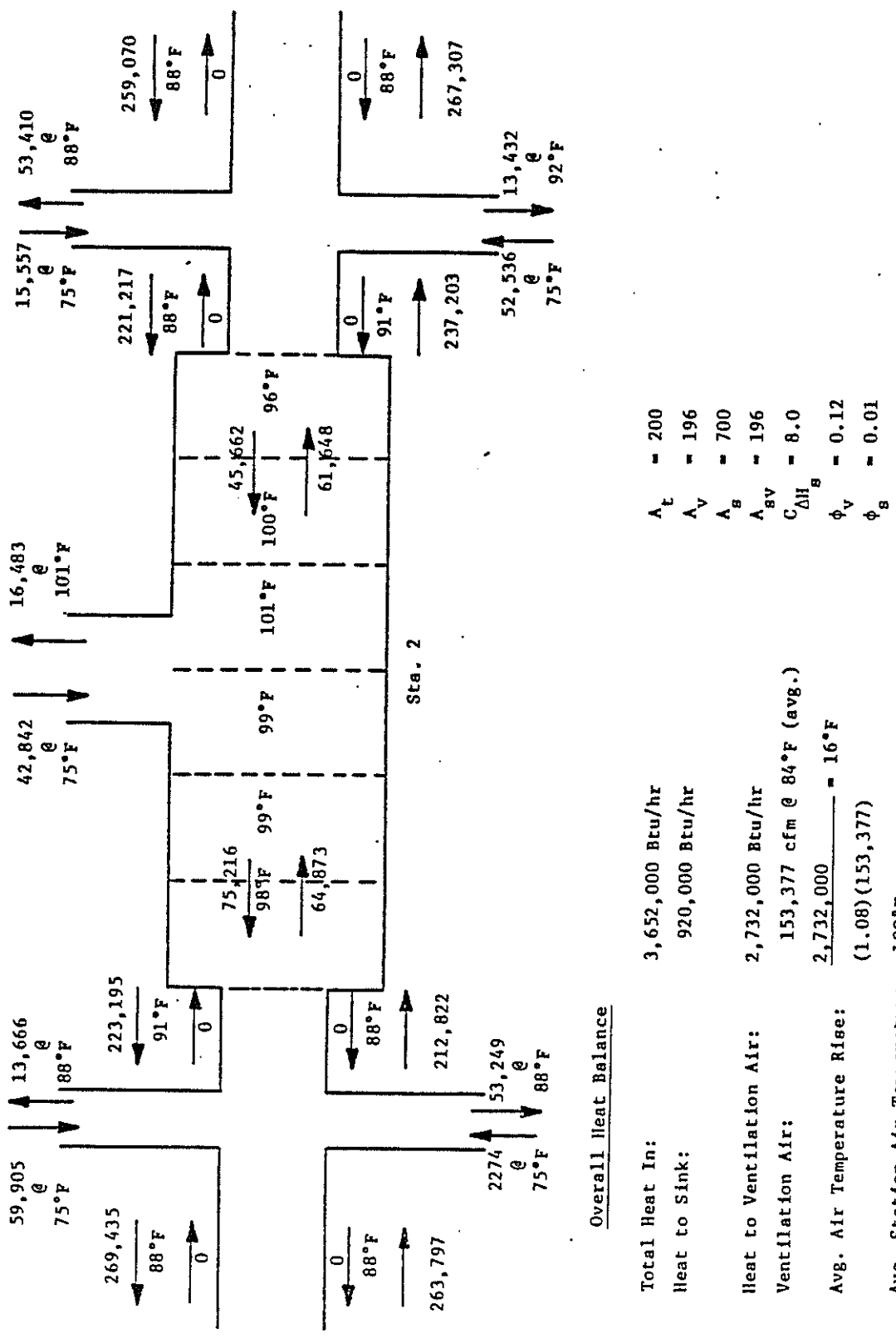
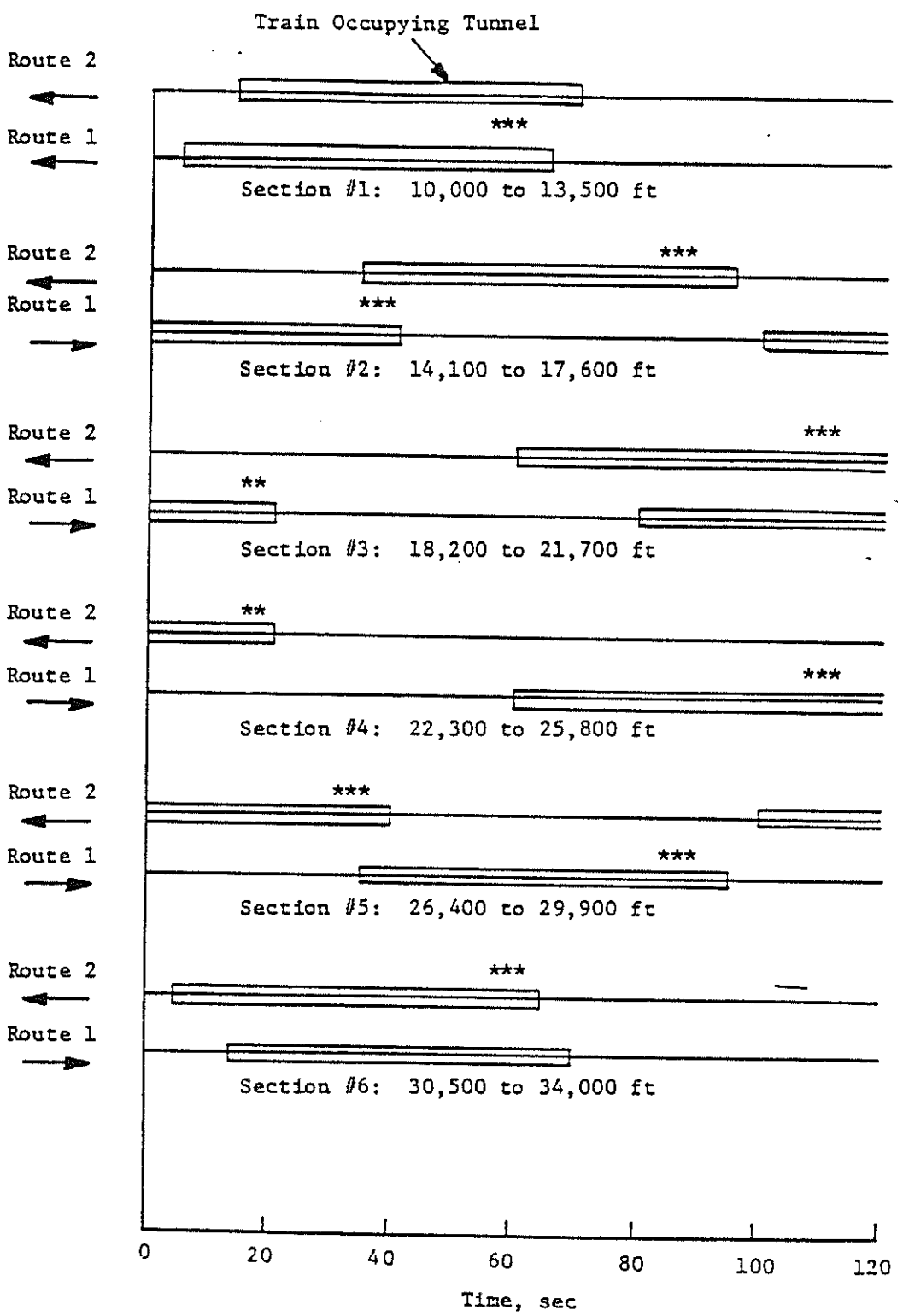


FIGURE 14-44. STATION HEAT BALANCE: RUN NO. DT-19, STATION 2



*Deceleration into station

FIGURE 14-45. SCHEMATIC OF BI-DIRECTIONAL TRAIN OPERATION

identified as Section 2 are occupied simultaneously for only 5 seconds of the 60-second station-to-station run time, whereas the tunnels of Section 3 are occupied simultaneously for 40 seconds. The degree of recirculation between the tunnels in each of the sections is shown by Figures 14-46 and 14-47. The figures portray the time dependent flows in the approach tunnel adjacent to the station, as related to train situation (the simultaneous operation of trains in other sections of the system will have some effect on recirculation, but will be ignored in this discussion). The amount of approach tunnel air drawn into the departure tunnel at any instant in time is the difference between the approach tunnel flow and the station flow. As Figure 14-46 indicates, a large percentage of the piston-action flow generated by the train approaching Station 2 on route 1 (from 0 to 40 seconds on the reference time scale) is processed through the station. Shortly before this train stops in the station a train departs the station on route 2. The negative station airflow during the interval from 40 seconds to 120 seconds indicates that the piston-action air drawn into the departure tunnel comprises a mixture of approach tunnel air (the die-down airflow behind the route 1 train) and station air drawn through the stairway and the tunnels at the opposite end of the station.

Sharply contrasting results are shown for the Station 3 portal of tunnel Section 3 (see Figure 14-47). The approach tunnel airflow for this case is of the same order of magnitude as for the previous one. However, as the low station flows suggest, the bulk of the approaching airflow is drawn into the departure tunnel. Only when the train on route 2 begins braking for the next station stop does the approach tunnel flow provide positive station ventilation (110 seconds to 120 seconds and 0~(120) seconds to 20~(140) seconds).

The relationship between single-track and double-track piston-action airflows in terms of station ventilation is further explored by Figures 14-48 and 14-49 which compare the time-dependent station flow contiguous to the tunnel portal in Station 2 and 3, respectively, for twin-tunnel Run No. DT-19 and double-track tunnel Run No. DT-7. These comparisons show that although substantial temporal differences exist, the net station ventilation effect is sensibly the same in both simulations. This observation suggests that the lower tunnel temperatures resulting from better tunnel ventilation in twin-tunnel systems may be the more significant attribute of this system ventilation scheme.

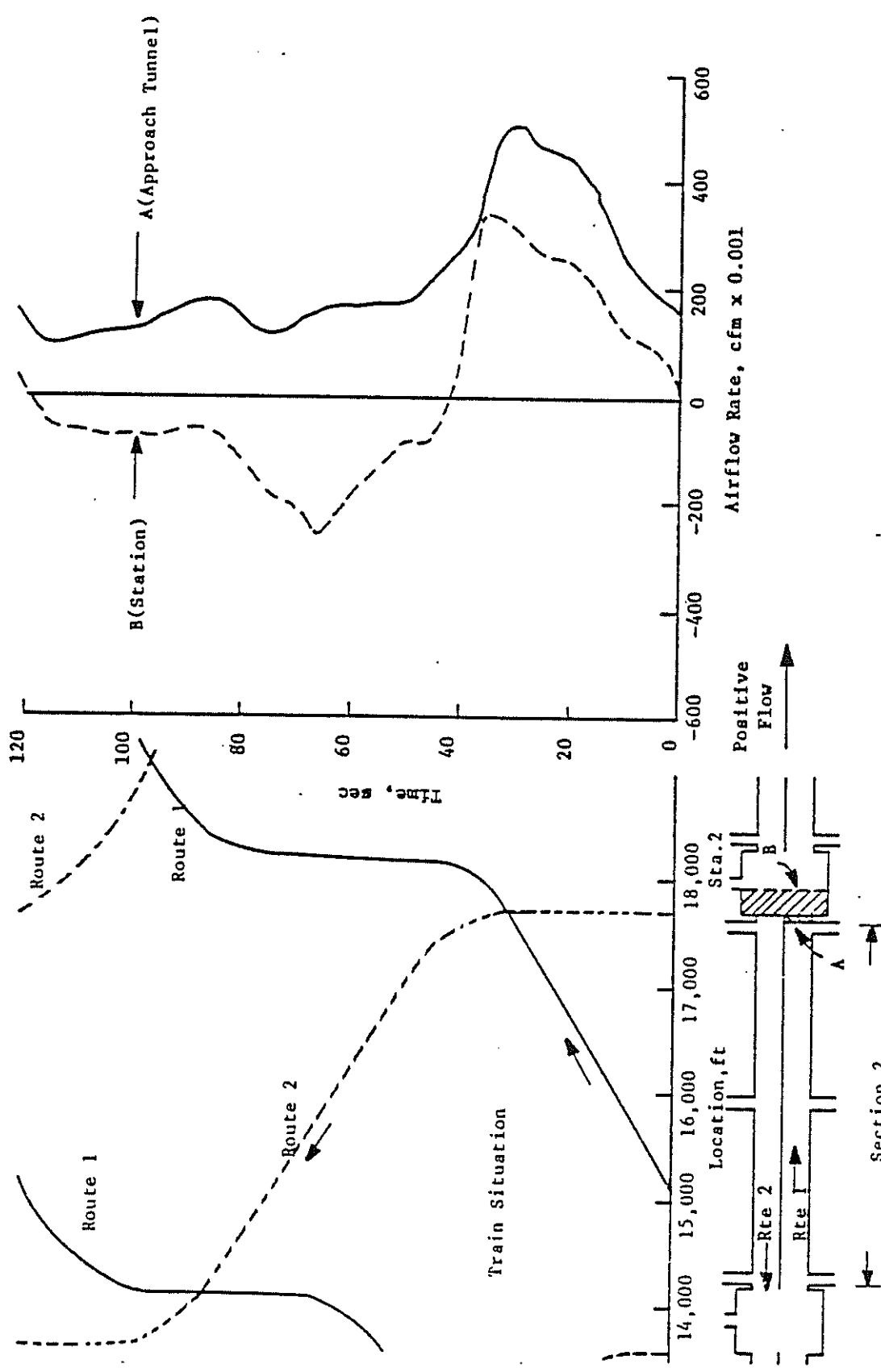


FIGURE 14-46. FLOW RECIRCULATION BETWEEN TWIN TUNNELS: RUN NO. DT-19, STATION 2

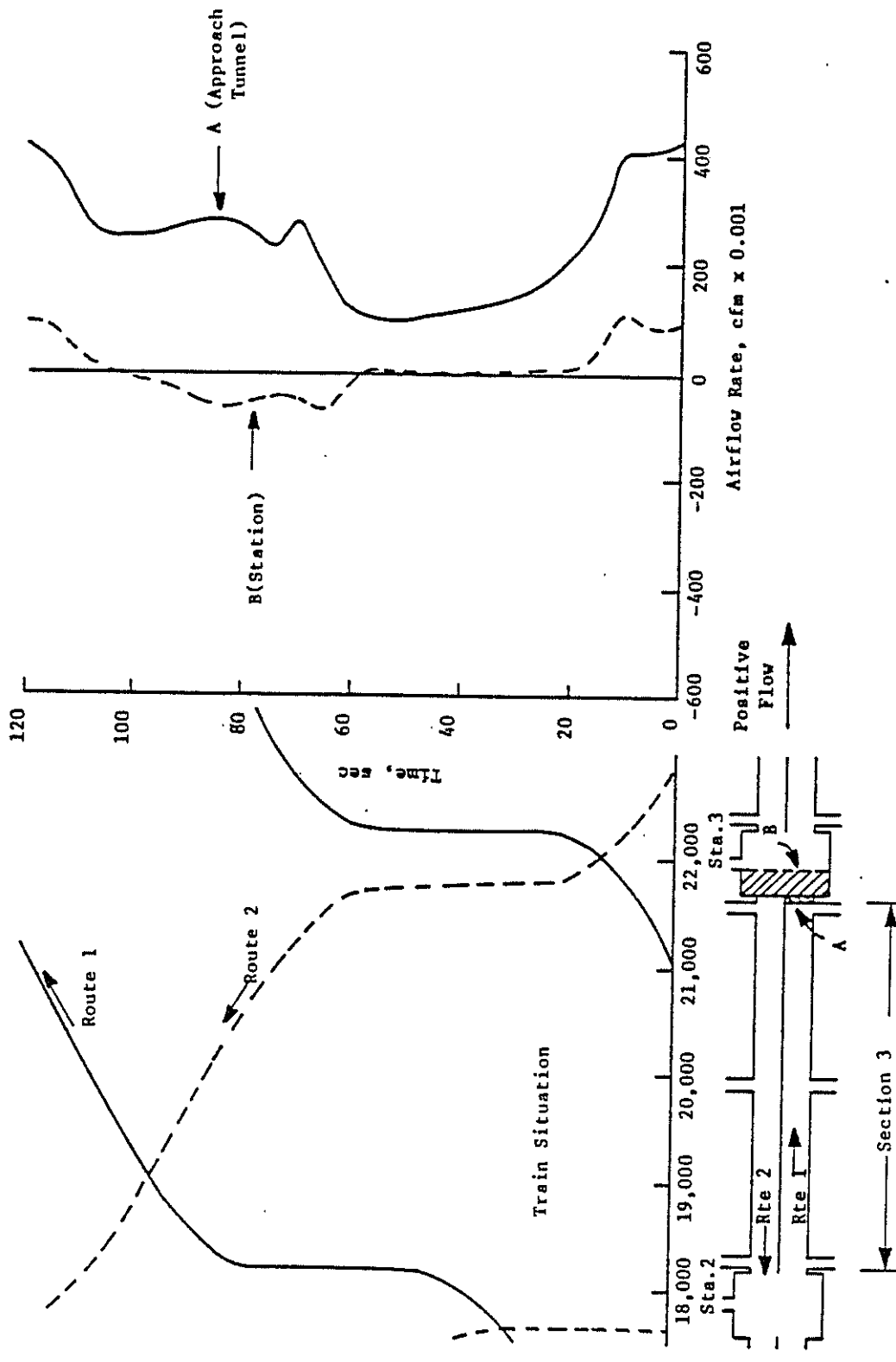
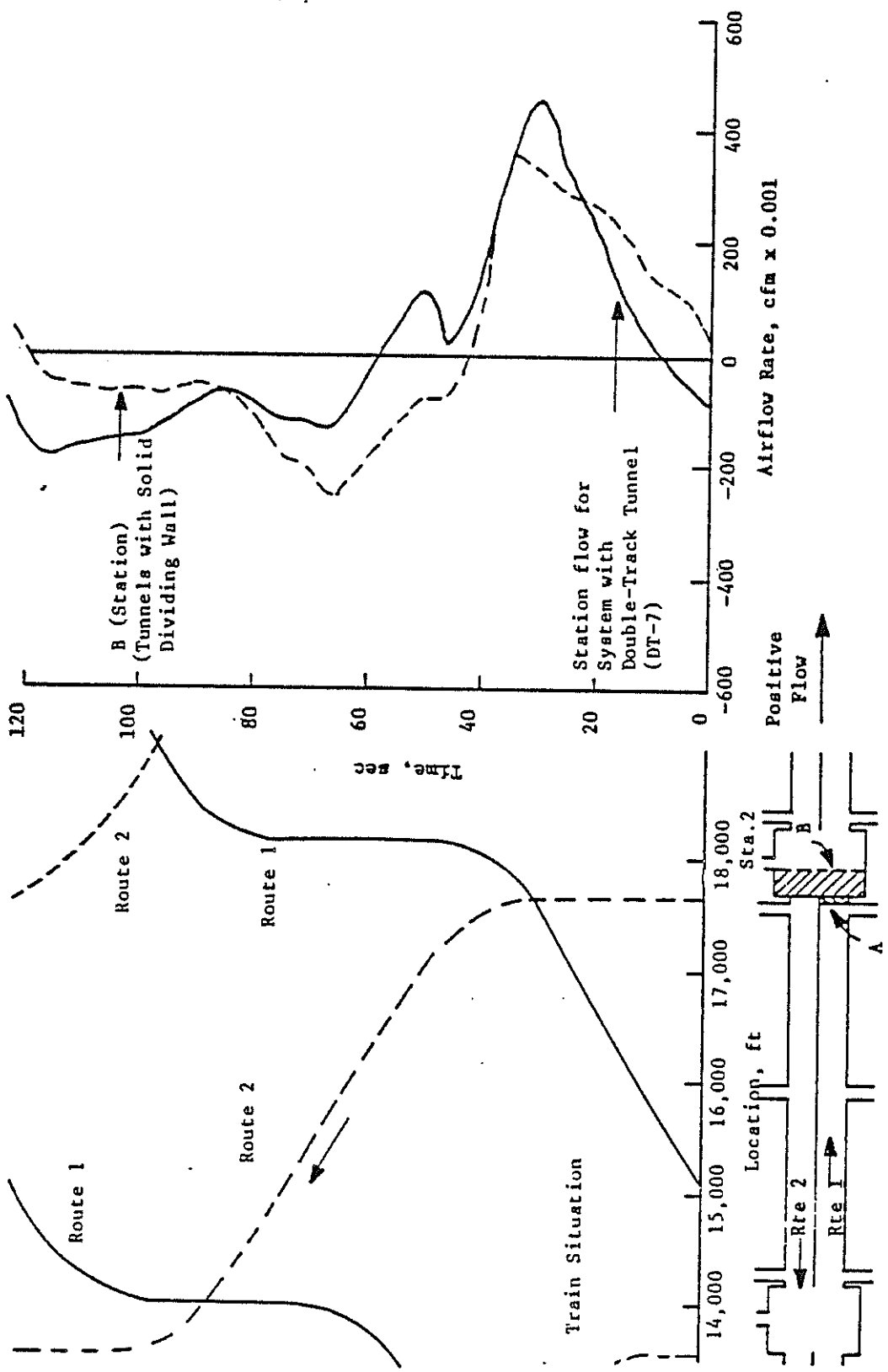


FIGURE 14-47. FLOW RECIRCULATION BETWEEN TWIN TUNNELS: RUN NO. DT-19, STATION 3



14-74

FIGURE 14-48. COMPARISON OF STATION 2 VENTILATION:
RUN NO. DT-19 (TWIN TUNNEL) AND RUN NO.
DT-7 (DOUBLE TRACK TUNNEL)

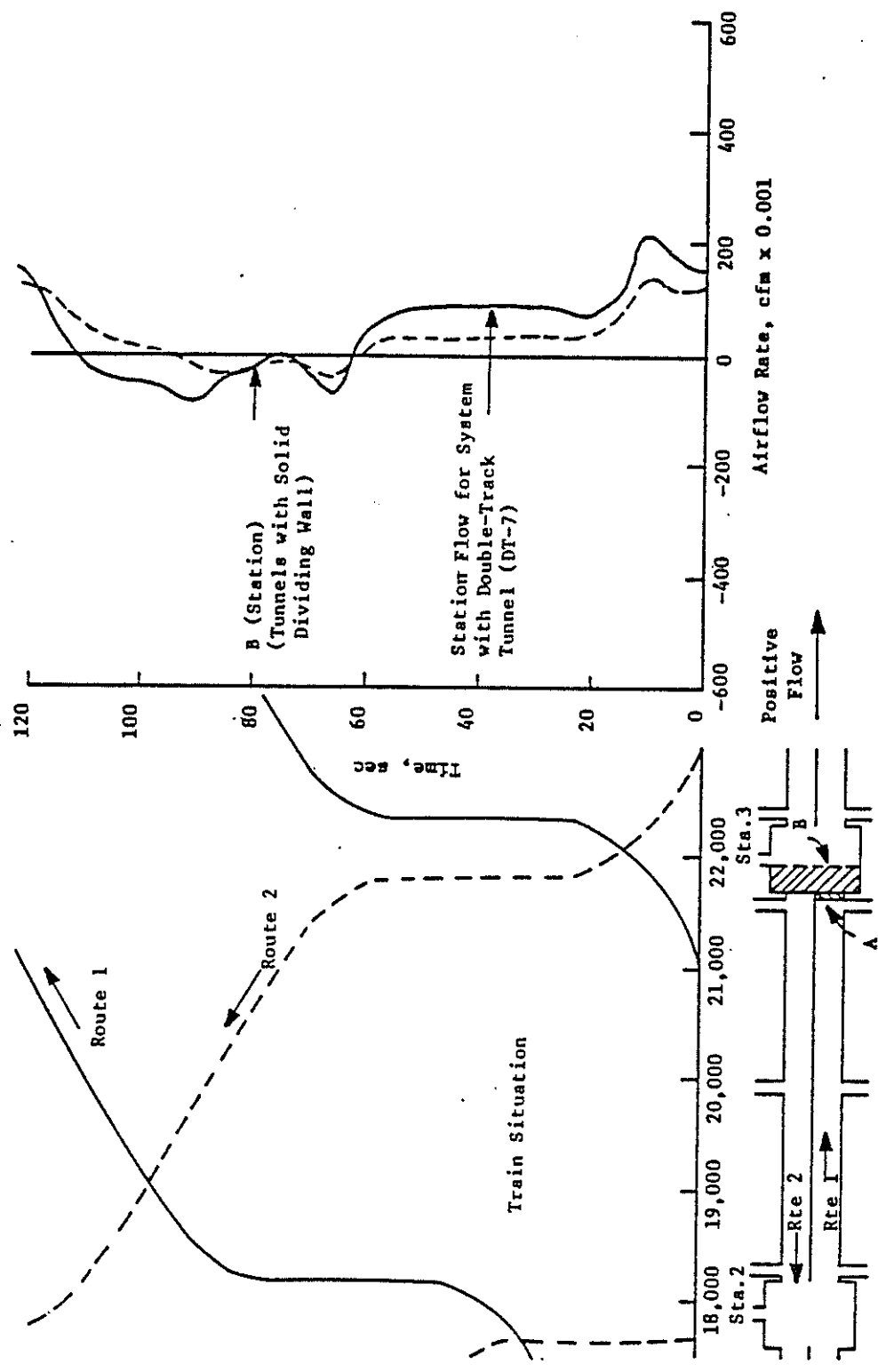


FIGURE 14-49. COMPARISON OF STATION 3 VENTILATION:
RUN NO. DT-19 (TWIN TUNNEL) AND RUN NO.
DT-7 (DOUBLE TRACK TUNNEL)

The twin-tunnel system shown schematically on Figure 14-50 (Run No. DT-20) was simulated to explore the effect of an increase in the number of ventilation shafts ($N = 6$). As was found for the corresponding double-track tunnel simulation (see Figure 14-20, Run No. DT-8) the added ventilation shafts acted to improve tunnel ventilation, causing tunnel temperature reduction on the order of 1°F to 2°F , but at the expense of station environment where temperatures increased by about 1°F . A Station 2 sensible-heat balance, illustrated by Figure 14-51, shows that the decrease in the temperature of ventilation air emanating from the tunnels was more than offset by the reduced ventilation rate and consequent station temperature rise.

The twin-tunnel, piston-action ventilation simulations have shown the flow recirculation between adjacent tunnels at station portals to be a significant phenomenon in terms of station environment. Although the train aerodynamic interactions occurred indirectly across the station-tunnel portals, the SES-computed, average ventilation airflow into the stations was close to that achieved in double-track systems where the trains interacted directly. The positive piston-action ventilation achieved in each of the twin tunnels provided for lower tunnel temperatures which ultimately benefited the station environment, albeit at the expense of higher platform air velocities near the station-tunnel portals.

14.11 HEAT SINK EFFECTS

The term heat sink refers to the heat transfer between the air in the subway tunnels, stations and vent shafts and the underground structure. Although this transfer of heat may be either to or from the subway air depending on the time of day and month of the year, the description as a "heat sink" has gained acceptance since attention focuses on it when the subway air is relatively hotter than the surface of the surrounding structure. The heat transfer rate is dependent on this air-wall temperature differential as well as flow-dependent convective heat-transfer coefficient, with heat transferring to the structure and surrounding earth (the sink) when the air is hotter than the structures' surfaces.

For heat-sink computations in the short term, dynamic SES program simulation, the program uses an internally computed, time-varient

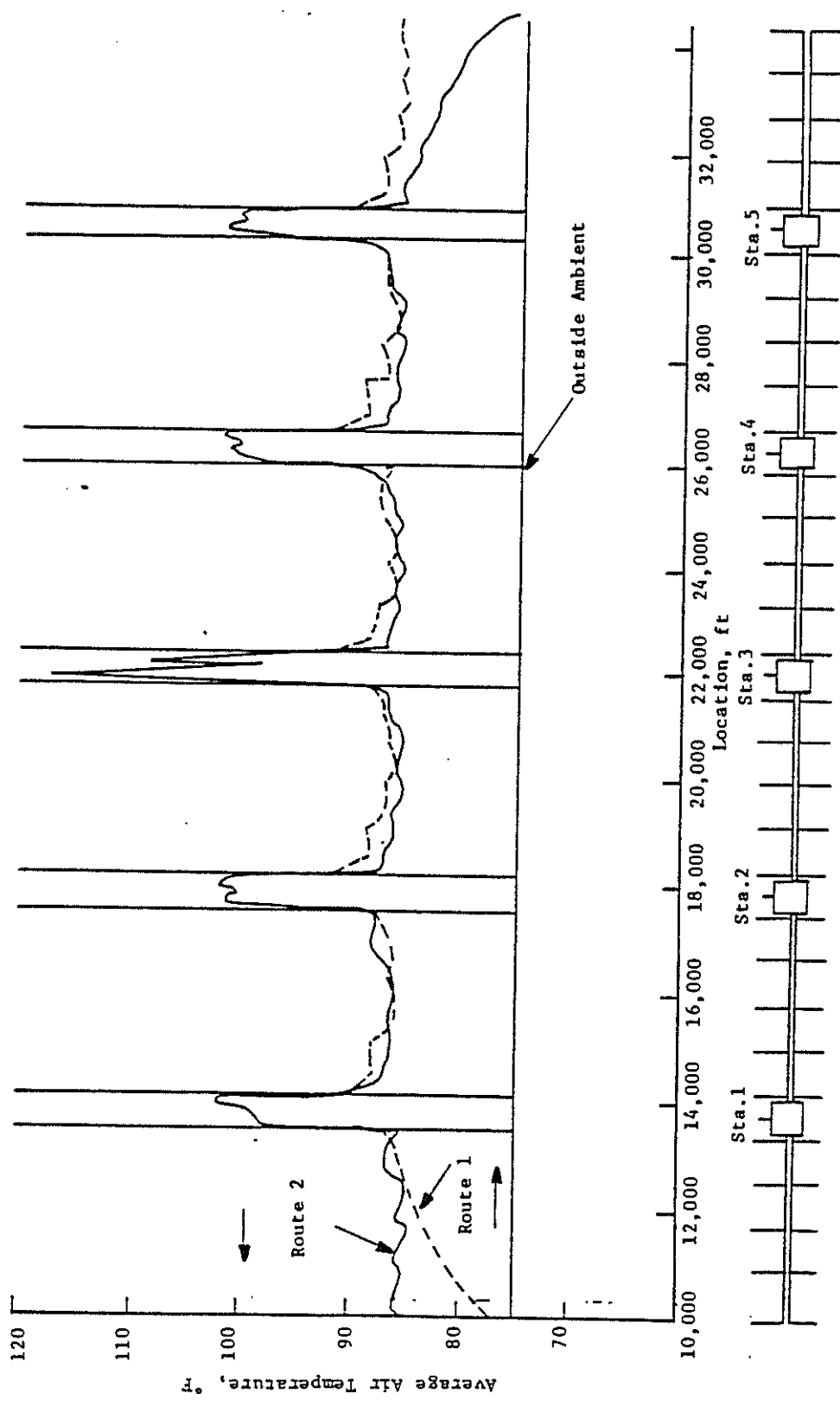


FIGURE 14-50. SYSTEM TEMPERATURE DISTRIBUTION: RUN NO. DT-20
(TWIN TUNNELS, N=6, $\phi_v = 0.12$, $\sigma = 0.5$)

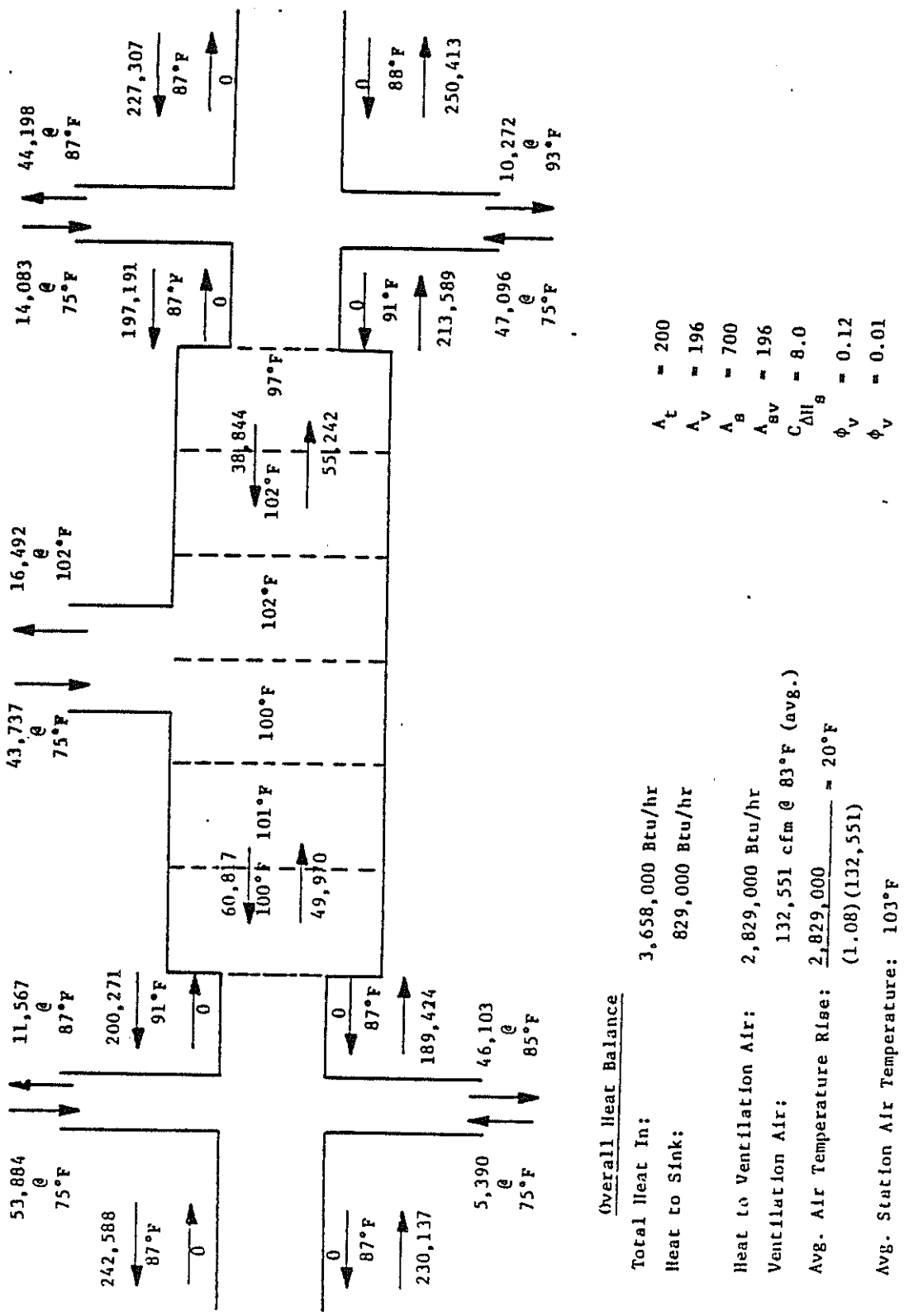
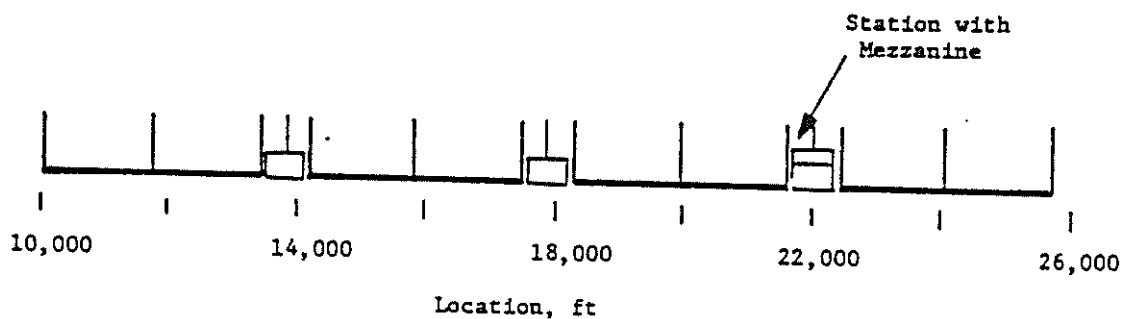


FIGURE 14-51. STATION HEAT BALANCE: RUN NO. DT-20, STATION 2

heat-transfer coefficient and the instantaneous difference in temperature between the air and the wall surface at discrete locations throughout the system. The singular parameter in this SES program heat sink computation requiring further analysis than is provided in the short-term simulation is the structure surface temperature. This surface temperature is dependent on the conduction of heat within the structure and the soil surrounding the subway and thus is influenced by the thermal properties of materials in these regions. Other parameters of importance in the determination of the heat sink behavior include the airflows and heat loads within the subway, the daily and yearly variations in ambient temperature, and the temperature of the earth far removed from the underground structure (the "deep-sink" temperature). The evaluation of the appropriate wall-surface temperature for a short-term SES program simulation at a specified time of the day and year, accounting for the interactive phenomena which influence this temperature, is the function of the heat sink subprogram described in Reference 3. The analysis used in this subprogram has been validated with field measurements from the Toronto Transit Commission subway system (Ref. 4).

A new system geometry was established to study the SES-program predicted heat sink behavior in greater detail. This system, described schematically on Figure 14-52, comprises three underground stations, one of which has a full mezzanine with access to the platform at each end of the station. Train operations on each route are the same as depicted by Figure 14-2, with near-simultaneous train dwell in Stations 1 and 3. The thermal parameters used in the analysis are shown on Figure 14-52. The dynamic SES program simulation corresponds to evening rush-hour operations when the outside ambient dry bulb temperature is 90°F.

Results of the SES program heat sink simulation of the system depicted by Figure 14-52 (Run No. DT-21) are shown on Figure 14-53, in terms of the system air temperature and wall-surface temperature distributions during the evening rush hour. Not shown are the estimated daily ranges of these parameters: the tabular SES program output shows wall-surface temperature in this particular system to vary on the order of 3°F during the day, while air temperature varies about 10°F in the interior of the system (compared with the 20°F daily variation in outside temperature). Of particular interest in the illustrated temperatures is the behavior of the wall-surface temperature in relation to the average air temperature. The wall-surface temperature



General Geometry

Tunnel Area: 400 ft^2
 Station Area: 700 ft^2
 Vent Area: 395 ft^2
 Stairway Area: 395 ft^2
 Vent/Stairway Impedance: 8.0

Thermal Parameters

Wall Thickness:	2.0 ft
Wall Conductivity:	0.7 Btu/ $\text{ft}\cdot\text{hr}\cdot{}^\circ\text{F}$
Wall Diffusivity:	$0.025 \text{ ft}^2/\text{hr}$
Soil Conductivity:	1.33 Btu/ $\text{ft}\cdot\text{hr}\cdot{}^\circ\text{F}$
Soil Diffusivity:	$0.03 \text{ ft}^2/\text{hr}$
Deep Sink Temperature:	60°F

Mezzanine Station Geometry

Station length: 600 ft
 Platform stair locations:
 100 ft from either end of platform
 Stairway to surface: Midstation
 Flow Area of platform stairs: 100 ft^2
 Flow Area of Stair to Surface: 395 ft^2

Ambient Conditions

Evening Rush Hour:	$900^\circ\text{F db}, 750^\circ\text{F wb}$
Morning Condition:	$800^\circ\text{F db}, 700^\circ\text{F wb}$
Annual Amplitude:	$200^\circ\text{F } 11.1^\circ\text{C}$

Even - $32.2^\circ\text{C DB}, 23.9^\circ\text{WB}, 55\% \text{RH}$
 Morn - $26.7^\circ\text{C DB}, 21.1^\circ\text{WB}, 60\% \text{RH}$

FIGURE 14-52. SYSTEM SCHEMATIC AND PARAMETERS FOR HEAT SINK STUDY (RUN DT-21)

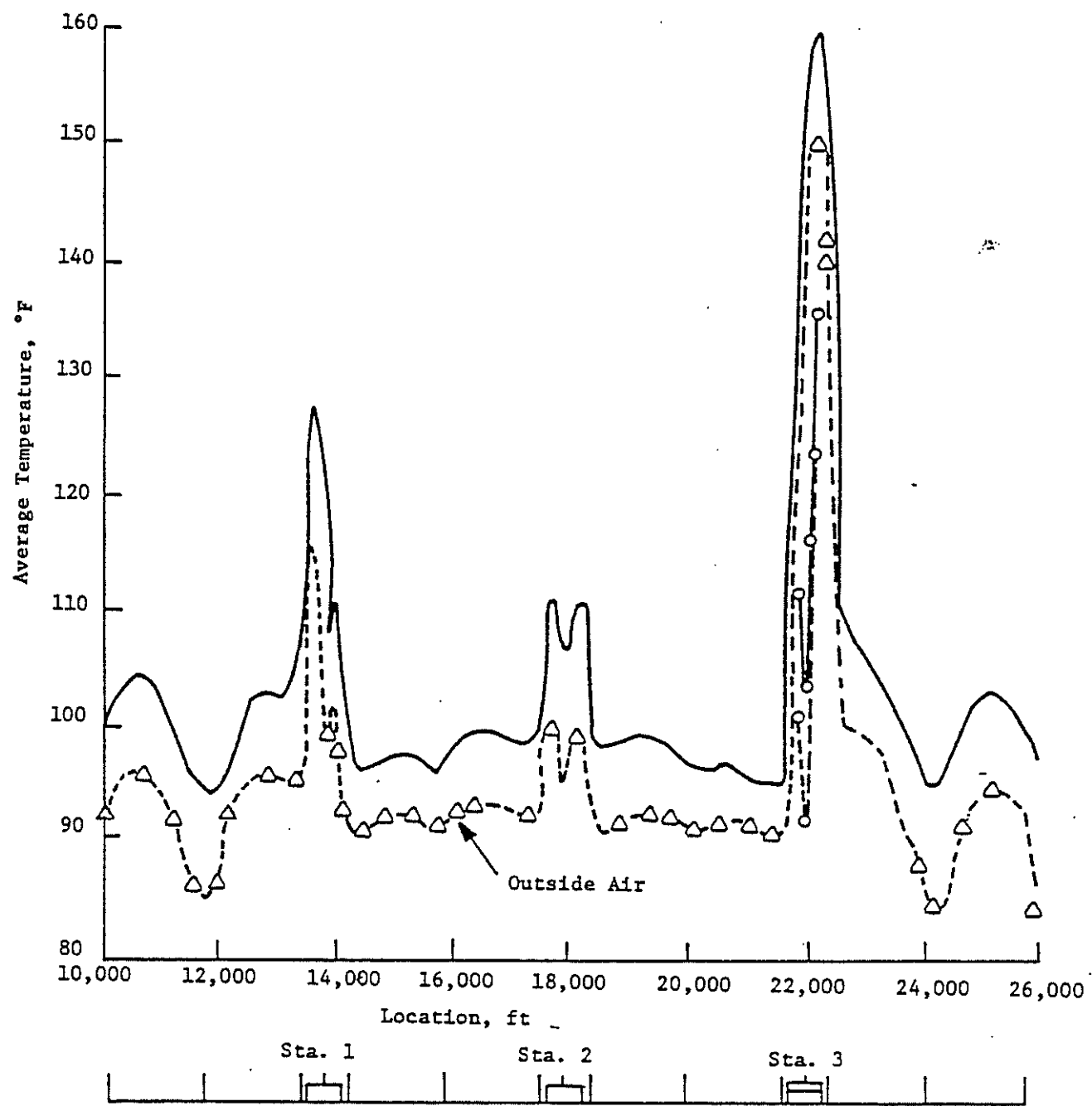


FIGURE 14-53. SYSTEM TEMPERATURE DISTRIBUTION RUN NO. DT-21
(HEAT SINK)

varies along the system length, maintaining an almost uniform differential of from 6°F with respect to the average air temperature during the evening rush hour (in this simulation, the heat-transfer coefficient was such that the heat transfer in the tunnels averaged from 8 to 10 Btu/hr ft²). This further confirms the findings of earlier studies; namely, that the behavior of the heat sink is influenced to a large degree by the subway heat load, ventilation, and outside ambient conditions, the deep sink temperature generally being of secondary importance.

Another striking feature of Figure 14-53 is the temperature extremes predicted for the station with the mezzanine. Close examination of the temperature plot shows these temperatures to exist along the platform between the two stairways to the messanine. Figure 14-54 shows the reason for this behavior. This figure illustrates, as a function of time, the train situation on both routes and the volumetric airflow rate at three locations: (1) in the tunnel and station between the blast shaft and the mezzanine stairway and (2) in the mezzanine on both sides of the stairway to the surface. At any instant in time, the platform flow is the difference between the tunnel flow and the mezzanine flow at the end of the station. As the results show, for almost two-thirds of the time (from 40 to 120 seconds) the platform is poorly ventilated, and most of the airflow is processed through the mezzanine area. In fact, the average platform ventilation is only about 80,000 cfm, or about one-half of the ventilation in the corresponding non-mezzanine station, and the majority of the station heat load occurs in this area. The particular combination of station geometry and train operations admittedly exaggerates the extreme platform temperatures. The absence of a mid-station mezzanine stairway decreases the flow of ventilating air along the platform, and the near-symmetrical operation of the trains on opposing routes nullifies the tunnel-to-tunnel flow-through ventilation. In actual operations, the probability of a repeated simultaneous dwell of trains on each route is remote. Nevertheless, the results are indicative of a piston-action ventilation problem which could arise in similar station/mezzanine configurations.

The earlier generalization regarding the secondary importance of the deep-sink temperature holds true for subways in soil or rock strata whose thermal properties fall within the normally encountered range. There is a circumstance, however, when the deep-sink temperature can have a first order effect on the air-structure heat transfer. This occurs when there is a

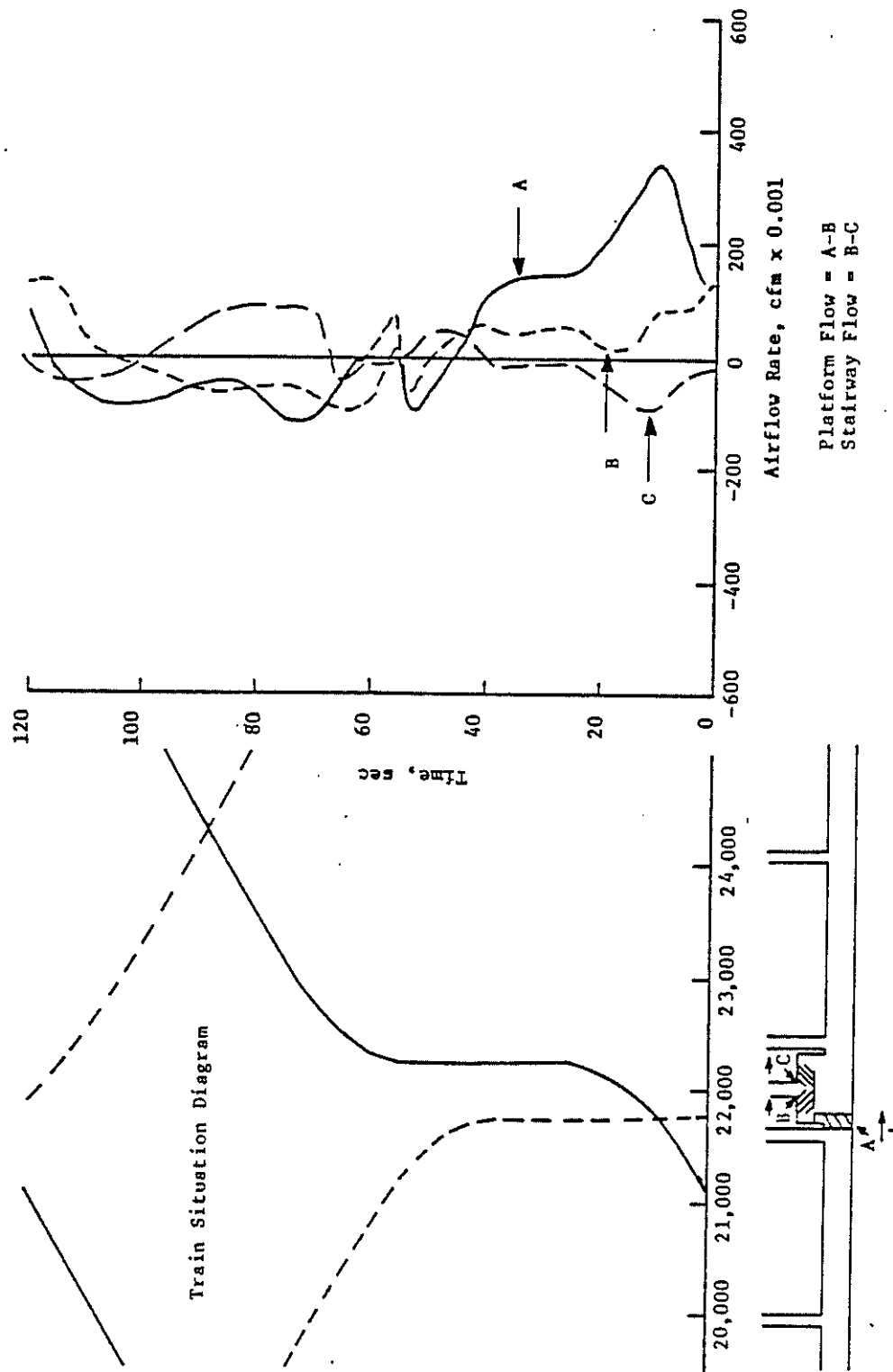


FIGURE 14-54. AIRFLOW IN STATION WITH MEZZANINE

migrating ground water condition normal to the longitudinal axis of the subway tunnels. This is obvious from consideration of a limiting case: if the subway were surrounded by free-flowing water, the outer surface of the structure would be very close to the water temperature and would be essentially unaffected by daily and annual fluctuations in ambient temperature. An approximate method of accounting for the convective transport of heat from a subway tunnel by migrating ground water has been developed by the Viennese (Ref. 5). This approximation is simply a means of computing an "effective" thermal conductivity of the soil as a function of migrating ground-water velocity and thermal diffusivity, and thus is applicable in the SES program heat sink computations. A SES program simulation was the same in all respects to Run No. DT-21 except for the soil thermal conductivity implemented to explore this phenomenon. For this simulation (Run No. DT-22), the soil conductivity was entered as 17.3 Btu/ft/hr/F (a 13-fold increase over Run No. DT-28) as determined by the Viennese methodology, corresponding to a migrating ground water velocity normal to the tunnel of 0.052 ft/hr (460 ft/yr). The results, in terms of average air and wall-surface temperature distributions, are shown by Figure 14-55. The wall surfaces ranged from 10°F to 15°F cooler as a consequence of the migrating ground water condition, with corresponding reductions in air temperature on the order of 5°F to 10°F, the air-wall temperature difference, and hence the wall-heat transfer rate, increased on the order of 50 percent.

A twin-tunnel system similar in geometry and train operations to the double-track system depicted on Figure 14-52 was developed to study the effect of separated tunnels on the heat sink. Conceptually, this system can be visualized as the double-track system with a solid wall separating each of the tunnels and ventilation shafts into two identical halves. The results of this simulation are presented by Figure 14-56 in terms of the average air and wall-surface temperature distribution in each tunnel and station of the system. Comparing with the double-track tunnel results (see Figure 14-53), there are three significant observations. First, the air temperature is lower in the parallel twin tunnels (particularly in the tunnels terminating at a portal). This is indicative of the positive tunnel ventilation achieved in the twin tunnels as opposed to the back and forth movement of tunnel air and correspondingly poorer tunnel ventilation in the double-track tunnel.

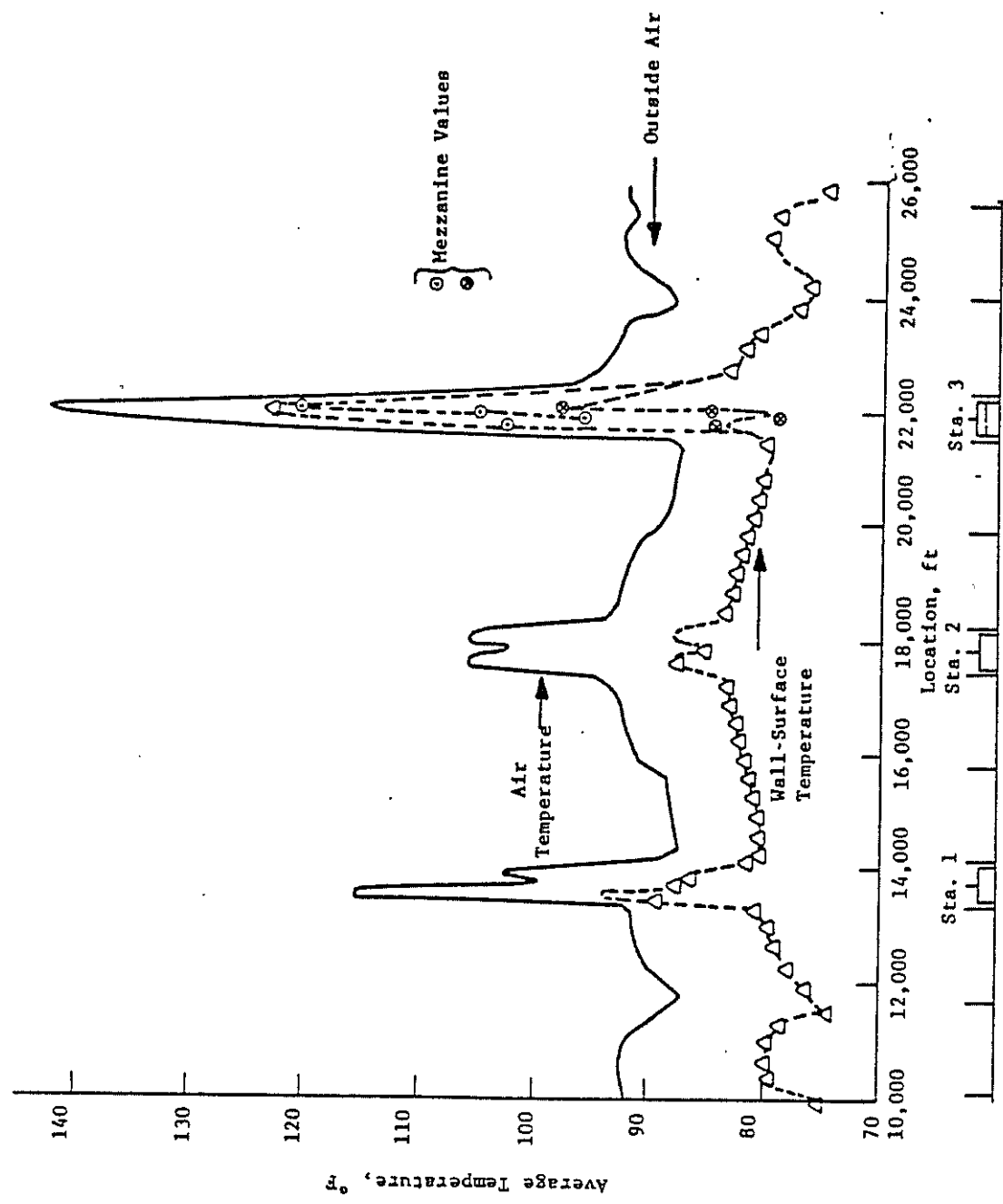


FIGURE 14-55. SYSTEM TEMPERATURE DISTRIBUTION: RUN NO. DT-22
(HEAT SINK WITH MIGRATING GROUND WATER)

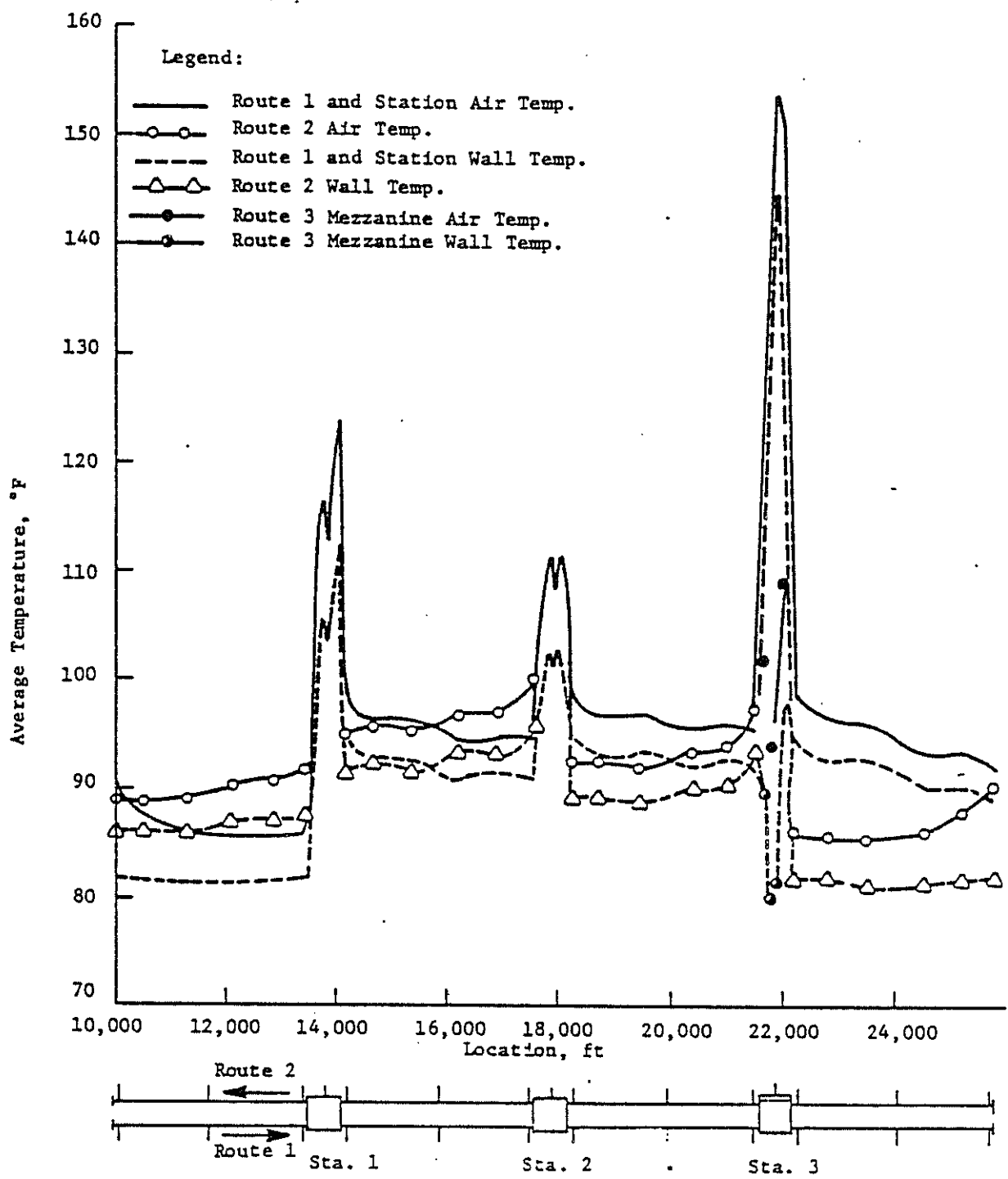


FIGURE 14-56. SYSTEM TEMPERATURE DISTRIBUTION: RUN NO. DT-23
(HEAT SINK IN TWIN-TUNNEL SYSTEM)

Second, the station air temperature is only slightly cooler in the twin-tunnel system. An examination of the temperature profiles shows the reason for this behavior. Considering the tunnels between Station 1 and the portal, the air drawn into the system from the outside ambient by trains operating on route 1 is cooled by the heat sink from 90°F to about 85°F by the time it reaches the station. However, because of the short headway operation, the recirculation of this cooled air to the adjacent, outbound tunnel (route 2) described in Section 14.10 is such as to permit only a fraction of this cool air to flow into the station, the remainder flowing across to the outbound tunnel. From a temperature viewpoint, this is evidenced by the relatively cooler air near the station in the outbound tunnel: if all of the air drawn into the outbound tunnel were from the station, the temperature of this air would be close to the station air temperature. Instead, the air temperature at this location is between the station temperature and inbound tunnel temperature, indicating that the source of this air is actually a mixture of station air and inbound tunnel air. The same rationale can be applied to the other parallel tunnels in the system.

The third observation of interest regards the air-wall temperature difference. With the exception of the inbound tunnels at the ends of the system where daily variations in outside ambient temperature have a greater effect on the thermal inertia of the heat sink, the air-wall temperature difference is almost uniform along the system length. This behavior was also observed in the double-track simulation results, the only difference being the magnitude of the temperature differential: in the twin-tunnel system, the wall-surface temperature averages about 3°F to 4°F below the air temperature during evening rush hour, or about half the differential observed in the double-track tunnel system. This reduced differential is attributable to, and to a large degree offset by, the higher convective heat-transfer coefficient averaged about twice the double-track tunnel value, resulting in approximately the same heat transfer rate in the tunnels of from 8 to 10 Btu/hr-ft² during evening rush hour. There is, of course, the advantage of the greater surface area and proportionally greater heat transfer per foot of tunnel system in the twin-tunnel configuration (the effect of the adjacent tunnels is taken into account in the computation of the average wall-surface temperatures).

14.12 MECHANICALLY COOLED STATIONS

The SES program has the capability of estimating the mechanical cooling load required to maintain the stations of a subway system at predetermined temperature and humidity levels for specified times of the day and levels of system utilization. The computed loads relate directly to the heat gains and losses attributable to the geometry and operations of the subway and do not reflect any added cooling coil load that may result as a consequence of designs requiring outside make-up air. This additional load can be readily ascertained by straightforward application of a psychrometric chart.

Depending upon the design, operation and capacity, a mechanical cooling system may introduce a significant quantity of air into the station. The net inflow, if on the same order of magnitude as the piston-action and/or tunnel fan ventilation, will have an effect on system aerodynamics which should be included in the SES program simulation. This is accomplished by actually including the fans and the ducts in the SES-simulated station geometry. Only the net inflow need to be considered: if all the coil make-up air is drawn from the station environment, offsetting the supply air, there is no net flow to affect the global system aerodynamics addressed by the SES program simulation. The relative merits of the use of various percentages of outside air across the cooling coils is beyond the scope of this report. Suffice to say that there are several reasons that an engineer may opt to use at least a partial outside air make-up system, ranging from the use of positive supply air to reduce the amount of relatively hotter air flowing into the stations from tunnels and stairways, to systems where additional outside air may be required to satisfy local codes concerning air change rate criteria for stations.

The double-track tunnel system described by Figure 14-52 of the previous section was used for a SES program simulation which included the station mechanical cooling load option (Run No. DT-24). For this particular simulation, the station design temperature was 80°F db (dry bulb). The station design value was maintained throughout the day, so that during the morning rush the station was at outside air temperature while during the evening rush the station was 10°F below outside ambient.

The average air and wall-surface temperatures prevailing throughout the system during the evening rush hour are shown by Figure 14-57. Although the

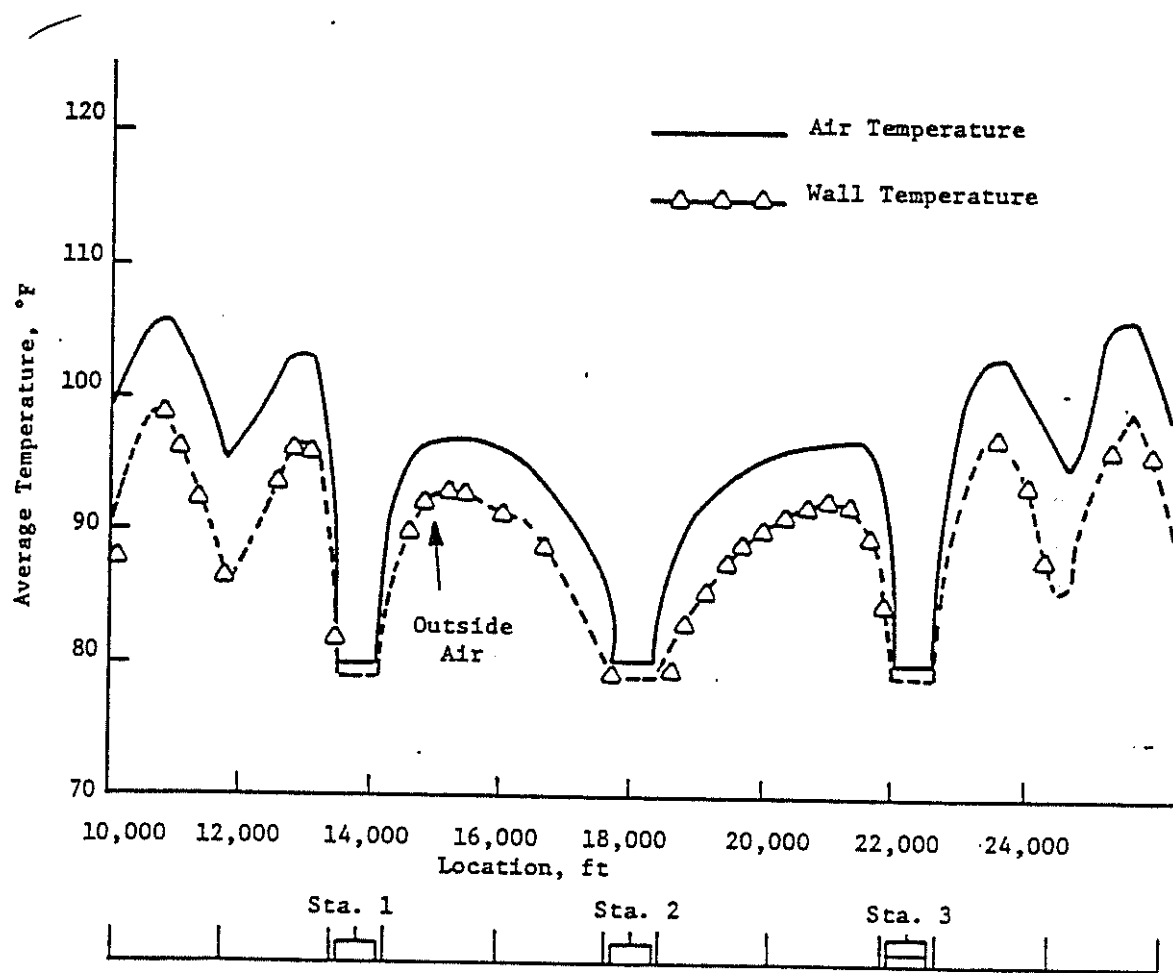


FIGURE 14-57. SYSTEM TEMPERATURE DISTRIBUTION: RUN DT-24
(MECHANICALLY COOLED STATIONS, DESIGN = 80°F)

station air is being maintained at 80°F, the tunnels are generally almost as hot as in the system without air-conditioned stations (see Figure 14-53). The principle reason for this behavior is the low exchange of tunnel and station air. This resulted in poor station ventilation and high station temperatures in the non-air-conditioned system, but in the present case little of the cool station air is carried into the tunnels. In terms of station cooling load this behavior is desirable, since the hot tunnel air entering the station in this case represents a part of the total load.

Another interesting aspect of the results is the behavior of the wall-surface temperature. The air-wall temperature difference in the stations is only about 1°F. This small value is a consequence of the constant air temperature maintained throughout the day by the mechanical cooling equipment. Such operation tends to negate the thermal inertia effect caused by daily variations in subway air temperature and thus reduces the effectiveness of the sink in areas of the system where the environment is maintained at uniform temperature.

The station mechanical cooling loads for each of the three stations of the system are shown in Table 14-2. The load is shown for each subsegment of a station (one-sixth the total station length) and is broken down into the individual components representing heat released by trains while in the station (Q_t), the steady-state platform load from patrons, lighting, etc., (Q_p), and the heat transfer to the sink within the confines of the station (Q_s). A word of explanation is in order concerning the presence of convective loads in those subsegments which are not adjacent to a tunnel or the stairway. These small loads are a consequence of the fluctuation of air temperature in the station about the design value as computed during the dynamic SES program simulation. A positive load in one of these interior subsegements means that, on the average, the air flowing into the subsegment from the adjacent subsegments was at a temperature slightly higher than the design value (and vice-versa for a negative load value). This convective "carry-over" of heat from one subsegment to the next is caused by the time-dependent behavior of the heat loads and airflows as influenced by train operations within the system.

Considering Station 2 for discussion purposes, the percentage contribution to the station heat load of the various heat sources is as follows:

TABLE 14-2. STATION SENSIBLE COOLING LOAD ESTIMATE: RUN NO. DT-24

Q_t :	478	590	600	600	591	489
Q_p :	18	18	18	18	18	18
Q_a :	275	41	190	186	146	1021
Q_s :	<u>-7</u>	<u>-7</u>	<u>-7</u>	<u>-11</u>	<u>-10</u>	<u>-9</u>
Q_c :	764	642	801	793	745	1519

Station 1 - Total Sensible Load: 5264 MBH (439 tons)

Q_t :	494	603	614	614	602	488
Q_p :	18	18	18	18	18	18
Q_a :	313	12	296	288	12	308
Q_s :	<u>-10</u>	<u>-10</u>	<u>-10</u>	<u>-10</u>	<u>-10</u>	<u>-10</u>
Q_c :	815	623	918	910	622	804

Station 2 - Total Sensible Load: 4692 MBH (391 tons)

Q_p :	-	9	9	9	9	-
Q_a :	-	-80	208	171	-19	-
Q_s :	<u>-</u>	<u>-3</u>	<u>-3</u>	<u>-3</u>	<u>-3</u>	<u>-</u>
Q_c :	-	-74	214	177	-13	-
Q_t :	499	603	613	612	602	488
Q_p :	12	12	12	12	12	12
Q_a :	898	170	64	36	-21	360
Q_s :	<u>-9</u>	<u>-6</u>	<u>-6</u>	<u>-6</u>	<u>-6</u>	<u>-6</u>
Q_c :	1400	779	673	654	587	852

Station 3 - Total Sensible Load: 5249 MBH (437 tons)

Note: All Q Values in MBH.

Q_t :	3415 MBH	72%
Q_p :	108 MBH	2%
Q_a :	<u>1229 MBH</u>	26%
Total:	4752 MBH	100%
Q_s :	<u>- 60 MBH</u>	

Net Cooling Load: 4692 MBH (391 tons)

The overall convective load, Q_a , is split roughly 53 percent to 47 percent between inflowing air from the tunnels and the stairway, respectively. The small amount of heat extracted by the heat sink (about 1 percent of the gross station load) is a result of the previously discussed diminished thermal inertia effects.

The distribution percentage of the various sources of station heat can be used in establishing strategies to reduce the station cooling load. In the present case, for example, it is obvious that there is more to be gained from a system which reduces the train heat release in the station than from a system designed to reduce the convective inflow from the tunnels.

A SES program simulation of the same system, but with an operating Trackway Exhaust System (TES) (Run No. DT-25), was undertaken to explore the potential benefit in terms of station cooling load. The assumed TES efficiencies for both types of heat sources were 50 percent when the train was moving at a speed of less than 30 mph within the station, and 75 percent when the train was dwelling in the station (see Section 14.8 for a discussion of TES efficiencies). The system and operations were the same as the previous case in all other respects. As would be expected, the system temperature distribution as shown in Figure 14-58 is essentially identical to the previous results. However, the station sensible load balance, shown in Table 14-3, illustrates the effect of the underplatform exhaust. Again considering Station 2, the sensible load breaks down as follows:

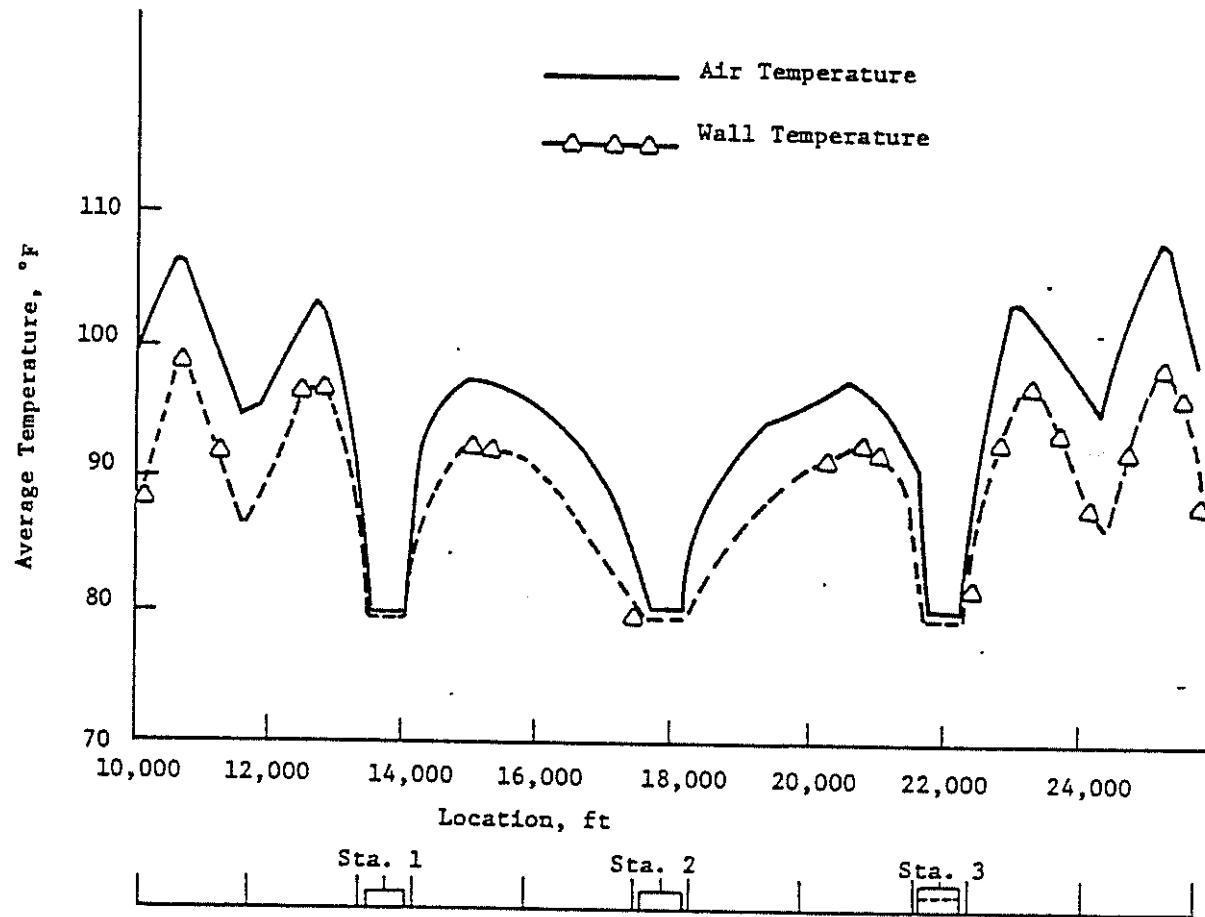


FIGURE 14-58. SYSTEM TEMPERATURE DISTRIBUTION: RUN DT-25
(TRACKWAY EXHAUST SYSTEM; DESIGN = 80°F)

TABLE 14-3. STATION SENSIBLE COOLING LOAD ESTIMATE: RUN NO. DT-25

Q_t :	222	246	242	240	244	223
Q_p :	18	18	18	18	18	18
Q_a :	284	6	149	220	109	1024
Q_s :	-7	-7	-7	-11	-10	-9
Q_c :	517	263	402	467	361	1276

Station 1 - Total Sensible Load: 3286 MBH (274 tons)

Q_t :	226	250	247	247	250	223
Q_p :	18	18	18	18	18	18
Q_a :	321	31	289	284	32	317
Q_s :	-10	-10	-10	-10	-10	-10
Q_p :	555	289	544	539	290	548

Station 2 - Total Sensible Load: 2765 MBH (230 tons)

Q_p :	-	9	9	9	9	-
Q_a :	-	-55	205	167	4	-
Q_s :	-	-3	-3	-3	-3	-
Q_c :	-	-49	211	173	10	-
Q_t :	226	249	245	247	251	226
Q_p :	12	12	12	12	12	12
Q_a :	920	117	-7	-11	-11	333
Q_s :	-9	-6	-6	-6	-6	-8
Q_c :	1149	372	244	242	246	563

Station 3 - Total Sensible Load: 3161 MBH (263 tons)

Note: All Q Values in MBH.

Q_t :	1443 MBH	51%
Q_p :	108 MBH	4%
Q_a :	<u>1274 MBH</u>	45%
Total:	2825 MBH	100%
Q_s :	<u>- 60 MBH</u>	

Net Cooling Load: 2765 MBH (230 tons)

The convective load, Q_a , platform load Q_p , and heat to the sink, Q_s , are about the same in magnitude as in the previous simulation. However, the TES exhaust served to reduce the total train heat release within the station approximately 58 percent, from 3415 MBH to 1443 MBH, resulting in a reduction of about 40 percent in the net station cooling load. Although the caution regarding the actual performance of TES must be observed, these results do emphasize the potential to be realized.

SES program simulation Run No. DT-26 was implemented to explore the effect of an alternative subway system ventilation scheme on station cooling load. The system and operations analyzed were the same as Run No. DT-24 except for the number and location of tunnel ventilation shafts. The three vent shafts between stations in Run No. DT-24 were replaced by a single, mid-tunnel exhaust fan shaft with a capacity of 200,000 cfm. The system air and wall-surface average temperature distributions during the evening rush hour are shown by Figure 14-59. The tunnel air temperatures range from about 3°F to 14°F cooler, depending upon location within the system, because the exhaust fan shafts draw cooled air into the tunnels from the stations. One exception to this behavior is the tunnel section between the exhaust fan and the station at both ends of the system. Being contiguous to a portal, this exhaust shaft pulls a large percentage of the air from the portals and actually decreases the amount of tunnel/station air exchange. The result is higher average air temperatures.

The impact of the exhaust shaft ventilation scheme on station sensible cooling load is shown in Table 14-4. Considering Station 2 for comparative purposes, the sensible load breaks down as follows:



TABLE 14-4. STATION SENSIBLE COOLING LOAD ESTIMATE: RUN NO. DT-26

Q_t :	481	592	603	603	593	491
Q_p :	18	18	18	18	18	18
Q_a :	132	1	166	982	476	318
Q_s :	-8	-8	-8	-13	-12	-11
Q_c :	623	603	779	1590	1075	816

Station 1 - Total Sensible Load: 5486 MBH (457 tons)

Q_t :	496	606	618	618	605	490
Q_p :	18	18	18	18	18	18
Q_a :	282	126	876	803	76	232
Q_s :	-16	-17	-16	-16	-16	-15
Q_c :	780	733	1496	1423	683	725

Station 2 - Total Sensible Load: 5840 MBH (486 tons)

Q_p :	-	9	9	9	9	-
Q_a :	-	88	518	572	75	-
Q_s :	-	-4	-4	-4	-4	-
Q_c :	-	93	523	577	80	-
Q_t :	500	604	614	614	603	490
Q_p :	12	12	12	12	12	12
Q_a :	274	132	49	-45	-26	199
Q_s :	-11	-6	-6	-6	-6	-8
Q_c :	775	742	669	575	583	693

Station 3 - Total Sensible Load: 5310 MBH (443 tons)

Note: All Q Values in MBH.

Q_t :	3433 MBH	58%
Q_p :	108 MBH	2%
Q_a :	<u>2395 MBH</u>	40%
Total:	5936 MBH	100%
Q_s :	<u>- 96 MBH</u>	

Net Cooling Load: 5840 MBH (487 tons)

This ventilation configuration results in a 25 percent increase in the sensible cooling load of Station 2, compared with the Run No. DT-24, Station 2 load of 391 tons (note that Stations 1 and 3 were affected to a smaller degree, with increases of 4 percent and 1 percent, respectively). This is chiefly attributable to the exhaust fan shaft between the station and the portal acting to reduce the tunnel/station air exchange). The heat-load breakdown shows the reason for the increase: the convective part of the sensible load, Q_a , increased from 1229 MBH (DT-24) to 2395 MBH. The convective load splits roughly 30 percent to 70 percent between inflowing air from the tunnels and the stairway, respectively, showing that the source of the additional convective load is the air drawn through the stairway into the station by the mid-tunnel exhaust fans. It is also of interest to note the higher heat transfer to the sink in the present case. Although still only about 2 percent of the total station load, the higher heat-transfer coefficient resulting from the higher air velocities within the station acted to increase the heat transfer to the sink by about 50 percent.

Run No. DT-27 was formulated to explore the effects of an alternative station-design temperature criterion and mechanical cooling system operation on station cooling load. The system and train operations described for Run No. DT-24 were used for this study, and the station dry-bulb design temperature was changed to 90°F during evening rush and 80°F during morning rush (in other words, the station design temperature varied throughout the day to match outside ambient conditions). The system average air and wall-surface temperature during evening rush hour are shown by Figure 14-60. Even though the station temperature is 10°F higher than Run No. DT-24, the tunnel air temperature in this case are generally within 1°F to 2°F of the Run No. DT-24 results. The reason for this is two-fold: first, the relatively small exchange of air between tunnel and station reduces the

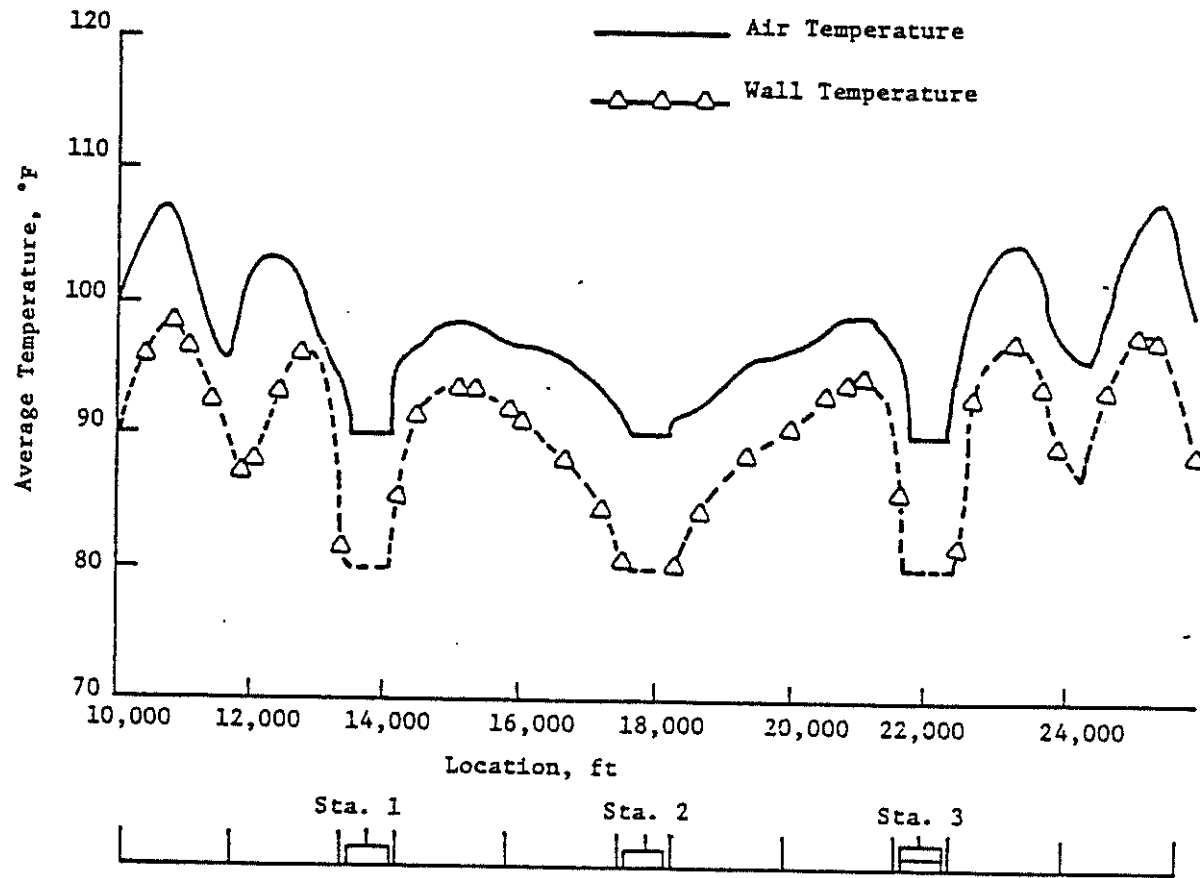


FIGURE 14-60. SYSTEM TEMPERATURE DISTRIBUTION: RUN NO. DT-27
(DESIGN: 80F A.M., 90F P.M.)

sensitivity of tunnel conditions to station temperature; and second, the daily swing in station air temperature acts to enhance the thermal inertia effect of the heat sink both within the tunnels and stations. In fact, whereas the maintenance of a constant air temperature in the station through the day results in an air-wall temperature difference in the station of about 1°F, this difference increases to about 10°F during evening rush hour when the station air temperature varies through the day with an amplitude of $\pm 10^{\circ}\text{F}$ about the average value of 80°F (morning rush).

The station sensible heat balance is shown on Table 14-5. The breakdown of the Station 2 cooling load is as follows:

$$Q_t: 3399 \text{ MBH}$$

$$Q_p: 108 \text{ MBH}$$

$$Q_a: -132 \text{ MBH}$$

$$\text{Total: } 3375 \text{ MBH}$$

$$Q_s: -556 \text{ MBH}$$

$$\text{Net Cooling Load: } 2819 \text{ MBH (235 tons)}$$

Increasing the station evening rush-hour design temperature by 10°F and causing the temperature to vary with a daily cycle reduced the evening rush-hour cooling load from the Run No. DT-24 value of 391 tons to 235 tons, a 40 percent reduction. The negative sign on the small convective heat-load term means that, on the average, air flowing into the station was slightly below the 90°F design temperature. Note that the heat transfer to the sink within the station, Q_s , has increased almost 10 times compared with the Run No. DT-24 results. This effect is ascribed to the previously discussed enhancement of the thermal inertia effect. As a consequence, the heat sink becomes a significant factor in the station sensible heat load, extracting about 16 percent of the total station heat in this particular instance.

This run demonstrates that a significant decrease in the station mechanical cooling requirement can be achieved at the expense of a higher design temperature. It follows that the relationship between outside ambient and station design is a sensitive parameter in determining station cooling loads. The results also suggest that the thermal inertia effect of the heat sink can be substantially enhanced by causing the station air temperature to vary

TABLE 14-5. STATION SENSIBLE COOLING LOAD ESTIMATE: RUN NO. DT-27

Q_t :	483	594	604	604	595	488
Q_p :	18	18	18	18	18	18
Q_a :	110	50	36	-255	36	492
Q_s :	-61	-65	-65	-98	-90	-81
Q_c :	550	597	593	269	559	917

Station 1 - Total Sensible Load: 3485 MBH (290 tons)

Q_t :	489	599	611	610	599	491
Q_p :	18	18	18	18	18	18
Q_a :	25	-68	-19	-22	-70	22
Q_s :	-90	-94	-94	-94	-94	-90
Q_c :	442	455	516	512	453	441

Station 2 - Total Sensible Load: 2819 MBH (235 tons)

Q_p :	-	9	9	9	9	-
Q_a :	-	-46	-45	-35	-21	-
Q_s :	-	-63	-62	-48	-36	-
Q_c :	-	-63	-62	-48	-36	-
Q_t :	487	591	604	604	594	483
Q_p :	12	12	12	12	12	12
Q_a :	427	93	85	57	-27	183
Q_s :	-77	-46	-49	-51	-54	-73
Q_c :	849	650	652	622	525	605

Station 3 - Total Sensible Load 3694 MBH (308 tons)

Note: All Q Values in MBH.

through a daily cycle.. It must be remembered, however, that the achievement to similar heat sink behavior for Run No. DT-24 would require cooling the station to 70°F during morning rush hour. In such a case, it could well occur that the morning rush hour would represent the peak station cooling load, since the heat sink is ineffectual at this time of day,. the outside air-station design temperature difference is the same as evening rush, and the train heat load may be approximately the same. The actual benefit to be derived from the enhancement of station heat sink by purposely varying station design temperature through the day with mechanical cooling equipment should be determined by an economic trade-off analysis comparing the increased 24-hr cooling system energy demand with the possible reduction in peak load.

Station mechanical cooling loads in a system comprised of parallel, twin tunnels were evaluated with SES program simulation Run No. DT-28. Conceptually, the system can be visualized by imagining a solid dividing wall to be placed along each of the tunnels of the DT-32 configuration, splitting each of the tunnels and ventilation shafts into two identical halves. System operations and station design conditions are otherwise the same as Run No. DT-24.

The results of this simulation are shown by Figure 14-61 in terms of the system average air and wall-surface temperature distributions. The most marked contrast between these results and Run No. DT-24 (see Figure 14-57) are the tunnel air temperatures. Tunnel air in the twin-tunnel system is consistently below outside ambient and ranges 10°F to 20°F below Run No. DT-24 calculations. The tunnel-station configuration in the twin-tunnel simulation is such that all of the air flowing into a station on inbound tracks including that which flows into an adjacent, outbound tunnel, is cooled to the design condition. It follows that all of the air leaving the station is also at station design. This differs from the double-track tunnel airflow behavior of Run No. DT-24, where the direct interaction of the trains creates a bi-directional air flow and reduced the tunnel/station air exchange.

The breakdown of the sensible cooling load for Station 2, shown in Table 14-6, is as follows:

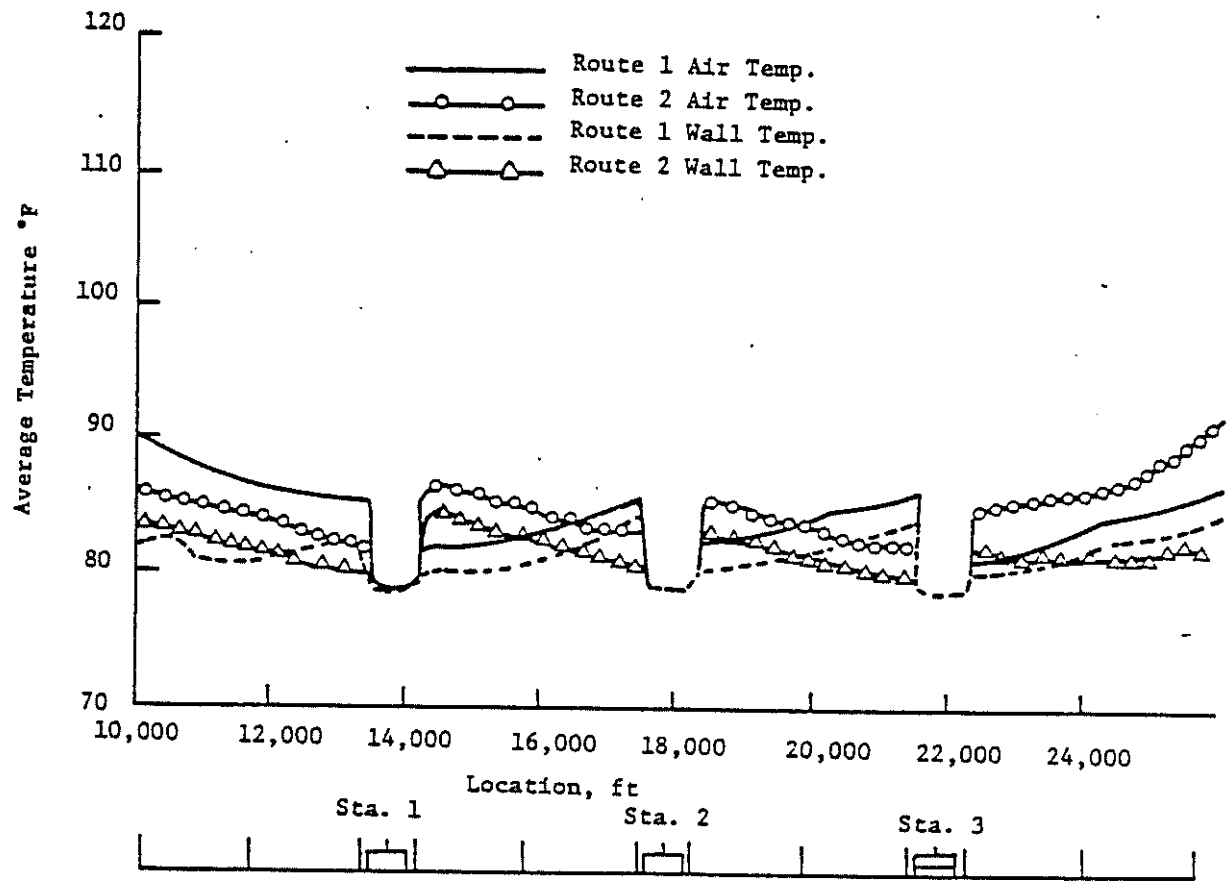


FIGURE 14-61. SYSTEM TEMPERATURE DISTRIBUTION: RUN NO. DT-28
(SINGLE-TRACK TUNNELS; DESIGN = 80°F)

TABLE 14-6. STATION SENSIBLE COOLING LOAD ESTIMATE: RUN NO. DT-28

Q_t :	480	692	603	602	593	489
Q_p :	18	18	18	18	18	18
Q_a :	1217	-25	201	254	90	1685
Q_s :	-7	-7	-7	-7	-6	-5
Q_c :	1708	578	815	867	695	2187

Station 1 - Total Sensible Load: 6850 MBH (571 tons)

Q_t :	494	603	614	614	603	488
Q_p :	18	18	18	18	18	18
Q_a :	1005	-40	71	75	-19	993
Q_s :	-11	-12	-12	-12	-12	-11
Q_c :	1506	569	691	695	590	1488

Station 2 - Total Sensible Load: 5539 MBH (462 tons)

Q_p :	-	9	9	9	9	-
Q_a :	-	-54	214	162	-20	-
Q_s :	-	-2	-2	-2	-2	-
Q_c :	-	-49	219	169	-13	-
Q_t :	499	604	614	614	604	489
Q_p :	12	12	12	12	12	12
Q_a :	1574	93	85	40	-59	1218
Q_s :	-5	-4	-5	-5	-5	-8
Q_c :	2080	705	706	661	552	1711

Station 3 - Total Sensible Load: 6415 MBH (535 tons)

Note: All Q Values in MBH.

Q_t :	3416 MBH	61%
Q_p :	108 MBH	2%
Q_a :	<u>2085 MBH</u>	<u>37%</u>
Total:	5609 MBH	100%
Q_s :	<u>- 70 MBH</u>	

Net Cooling Load: 5539 (462 tons)

The station sensible load for this twin-tunnel system is 18 percent greater than the corresponding double-track tunnel system (Run No. DT-28). Compared with Run No. DT-24, the twin-tunnel configuration shows an increase of 70 percent in the convective load, Q_a , of the air entering the station (1229 MBH vs. 2085 MBH). Of this convective load, approximately 95 percent comes from the approach tunnels, thereby reflecting the greatly increased tunnel-to-station inflow.

There may be instances where a separated twin-tunnel system is mandated for such reasons as emergency egress, structural considerations, or a greater tunnel ventilation than can be achieved with a double-track configuration. In such cases, it is of use to recall the discussion of Section 14.10 regarding the recirculation phenomenon between adjacent inbound and outbound tracks. For a given circumstance of relative train operation, it was demonstrated that the net inflow penetrating deeply into the station was almost the same for both the twin-tunnel and double-track configurations. It follows that if the recirculation from the inbound tunnel to the outbound tunnel could be effected outside the cooled station environment, the convective load in the twin-tunnel system would be reduced to a value near that associated with the double-track station convective load, albeit at the expense of somewhat hotter tunnels.

REFERENCES

1. Parsons, Brinchkerhoff, Quade & Douglas, Inc., "Single-Track System Concepts Study," Associated Engineers Report No. UMTS-DC-MTD-7-72-19, 1972.
2. Developmental Sciences Inc. - Aerospace Technology Division, "Subway Aerodynamic and Thermodynamic Test (SAT) Facility - Double-Track Aerodynamics," Technical Report No. UMTA-DC-MTD-7-72-17, 1972.
3. Parsons, Brinckerhoff, Quade & Douglas, Inc., "A Model for the Prediction of Long Term Heat Sink Effects on Subway Thermal Environment," Associated Engineers Report No. UMTA-DC-MTD-7-72-22, 1972.
4. Parsons, Brinckerhoff, Quade & Douglas, Inc. "SES Heat Conduction Model Validation," Associated Engineers Report No. UMTA-DC-06-0010-73-5, 1974.
5. Vienna Office of Public Works, Council Department 32, "Vienna Underground Railway, Part 2 - Investigation of the Thermodynamic Problems of the Underground Railway," Report No. MA 32-UB/13/69, May 1970.

15. FIELD VALIDATION

The SES program assumes a significant responsibility in the sense that the decisions derived from its application to the design process will guide future expenditures of millions of dollars on environmental control systems. This responsibility dictates the evaluation of any uncertainties in the mathematical models which comprise the program.

Although the simulations described in this section were done using SES Version 1, the conclusions reached herein are applicable to SES Version 3 because the relevant mathematical models are not only phenomenologically identical, but in most cases provide the same numerical result.

Confirmation of the basic mathematical models was achieved through comparisons with scale model tests (Ref. 1 and 2), with controlled full-scale field tests conducted at the Bay Area Rapid Transit (BART) District's Berkeley Hills Tunnel (Ref. 3), and with long-term temperature measurements in the Toronto subway (Ref. 4). Final confirmation of the SES program required a comprehensive field testing program in an operating subway system, the Montreal METRO.

The purpose of the Montreal METRO full-scale field validation tests was to directly validate the SES program for use as a design tool, and to validate by inference many of the related analytical techniques developed during the Subway Environmental Research Project. High standards were established for the analytical techniques developed as a part of the project, and the comparison of the SES program against these standards is provided in the body of this section. Much of the discussion of the results revolves around the cause of small discrepancies between the measurements and the SES program predictions. Such meticulous checking of the SES program is necessary in order to verify the mathematical modeling techniques and concepts used in the SES program, and to further develop and refine the SES mathematical models by identifying the sources of, and correcting, any discrepancies that arise between the measurements and the SES program predictions. From a designer's standpoint, the magnitude of the discrepancies encountered and discussed in this section are for the most part virtually insignificant due to the fact that the discrepancies not caused by input related errors (e.g., a wrong vent shaft cross-sectional area or train speed-time profile) are generally within the bounds of experimental

uncertainty. Within the limits of experimental precision, the SES program has been shown to predict accurately the airflow, air temperature and humidity, train performance, fan performance, and vent shaft performance in an operating subway. In other words, the SES program can be used as a design tool for predicting the environment within a given subway. In other words, the SES program can be used as a design tool for predicting the environment within a given subway system with a high level of confidence. The specific conclusions reached during the METRO full-scale field validation tests are as follows:

1. The near-field aerodynamic theory has been confirmed by measuring the static pressure in the tunnel to obtain the pressure signature of the passing train. The average discrepancy between field measurements and theoretical predictions was on the order of 6 percent, which is within the range of experimental uncertainty. The full-scale pressure signatures are similar to those measured in the Berkeley Hills Tunnel Tests and are amenable to straightforward analytical treatment as used in the SES program.
2. By using an effective train skin-friction coefficient of 0.023 to account for the combined effect of skin friction and bogie-form drag, the requirement for precise bogie measurements is eliminated. This value of the effective skin-friction coefficient has been validated over a wide range of blockage ratios and train configurations through the tests undertaken at the Berkeley Hills Tunnel as well as in the METRO.
3. The simplified model to predict subway air-pressure transients on board passing trains by hand computation has been verified and determined to be suitable for preliminary design calculations. The process of this simplified model can be used with confidence to estimate the effects of train speed, blockage ratio, and frictional roughness on the pressure transients.
4. The far-field aerodynamic theories relating to airflow ahead of and behind the train, tunnel friction factor, non-steady flow characteristics, multiple train operation, and the flow split at "T" and "Y" type junctions have been confirmed. The SES program can accurately predict the airflows induced by both single and multiple bi-directional train operations and fans, including the inertial effects caused by accelerating large volumes of air. With regard to the

non-steady air flows, it appears that the inertial effects are dominant when compared with the acoustic or sonic effects.

5. The METRO tests have validated the computer program as a design tool to predict the flow, temperature, and humidity of air throughout a multiple-track subway system. The validation of the SES program as a whole implicitly validates within engineering accuracy the component theories, formulations and scale model tests comprising the SES program. Furthermore, the SES program can be used as a reference to validate subsequent, simplified computational procedures.
6. The validation process also provided valuable information regarding the proper application of the SES program. In particular, the need was demonstrated for simulating more than one circumstance of relative, bi-directional train operations in a multi-track subway when making use of the SES heat sink subprogram. This is required to obtain average ventilation computations throughout the subway which are representative of the long-term behavior. These computations are required by the heat sink model for accurately predicting long-term heat sink effects.

15.1 TEST DESCRIPTION

The full-scale field test validation process consisted of a series of field measurements, a corresponding series of SES program simulations, and a direct comparison of measured and predicted transient airflows, temperatures and humidities. The SES program validation tests were specifically tailored to address the following aerodynamic uncertainties:

1. Near-Field Aerodynamics. The BART tests (Ref. 3) provided near-field data in the form of pressure signatures for a BART train operating in a 0.43 blockage ratio tunnel. The agreement between measurement and theory was good, but the comparison emphasized the importance of accurate near-field calculations and the influence of vehicle geometry and roughness. Therefore, an additional data point for another vehicle at another blockage ratio was required for a more complete validation of the theory.
2. Multi-Junction Flow. To test the multi-junction theory employed by the SES program, tests were required to evaluate the flow split

for difference ventilation shaft and intersecting tunnel configurations. In particular, multi-junctions with small momentum transfer (90-degree "T"-junction) and larger momentum transfer ("Y"-junction) were to be tested for a variety of piston-effect flow situations. As an obvious consequence of these tests, the subject of piston-action flow in double-track tunnels with bi-directional train operation was also addressed.

In addition to the above tests, there were overall system validation tests. The overall system validation tests were much broader in scope than the above described tests which addressed only specific components of the total system aerodynamics. The overall system validation required simultaneous measurements of airflow, temperature and humidity over a length of subway encompassing several stations. These measurements were required at intervals throughout the daily cycle of operations, with particular emphasis on rush-hour conditions.

A portion of the Montreal METRO was selected as the site for the full-scale field validation tests (see Figure 15-1). This particular portion of the METRO permitted examination of a maximum number of uncertainties with a minimum of instrumentation.

The instrumentation for the Montreal METRO tests comprised air velocity, temperature, humidity and pressure sensors located as shown in Figure 15-2. Instrument sites A,B,C,E and H had sensors both in the station and in the tunnel adjacent to the station approximately 150 feet from the tunnel-station junction (see Reference 5 for a detailed description of each instrument site). Each field test did not require data to be taken at each of the instrument sites shown in Figure 15-2. Figures 15-3 through 15-6 show the various instrumentation used during the calibration, near-field, multi-junction and system tests, respectively. Figures 15-7 through 15-9 provide illustrations of typical stations, tunnels, and ventilation shafts within the METRO system. Illustrations of the actual instrumentation sites are provided in Reference 5.

All of the field measurements were undertaken by KLD Associates, Inc., under contract with the Associated Engineers. Train velocities were recorded by the Associated Engineers using METRO-provided transducers. Each of the measurements was recorded continuously during a test, with time coordination accomplished via telephone and public address communication with the METRO's Central Control.

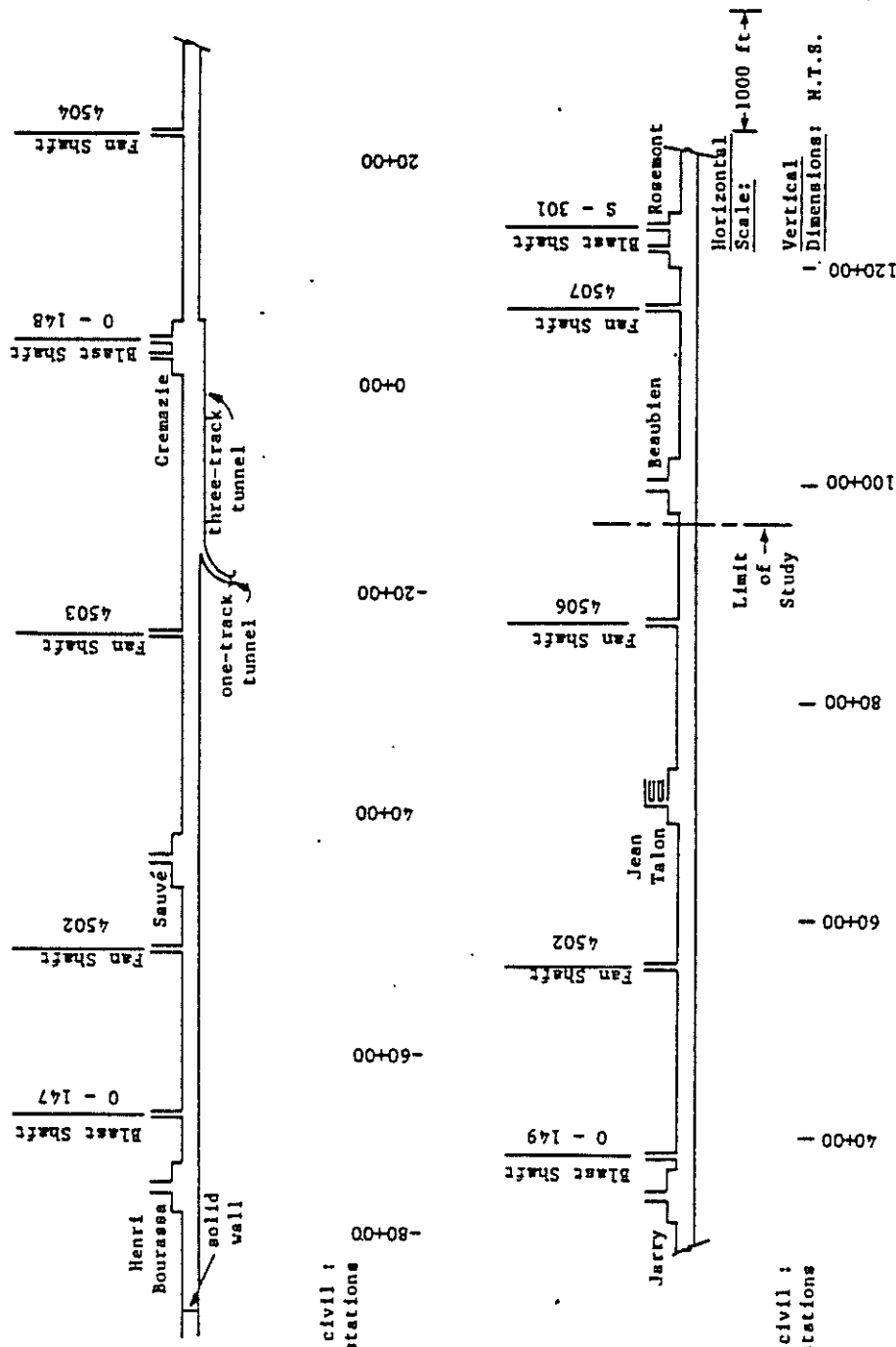


FIGURE 15-1. SCHEMATIC PLAN OF PORTION OF MONTREAL METRO LINE NO. 2 USED IN THE FIELD VALIDATION TESTS

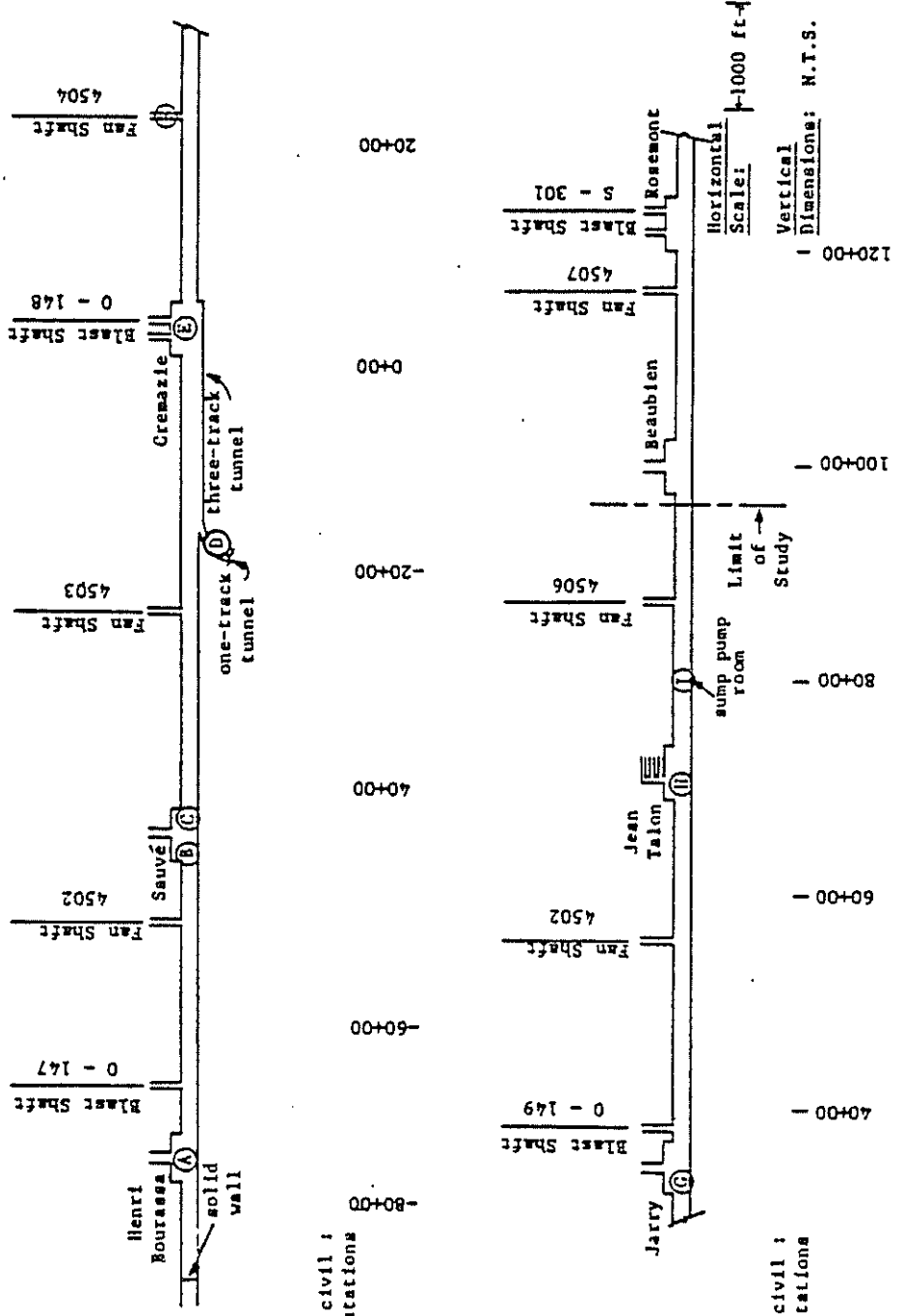
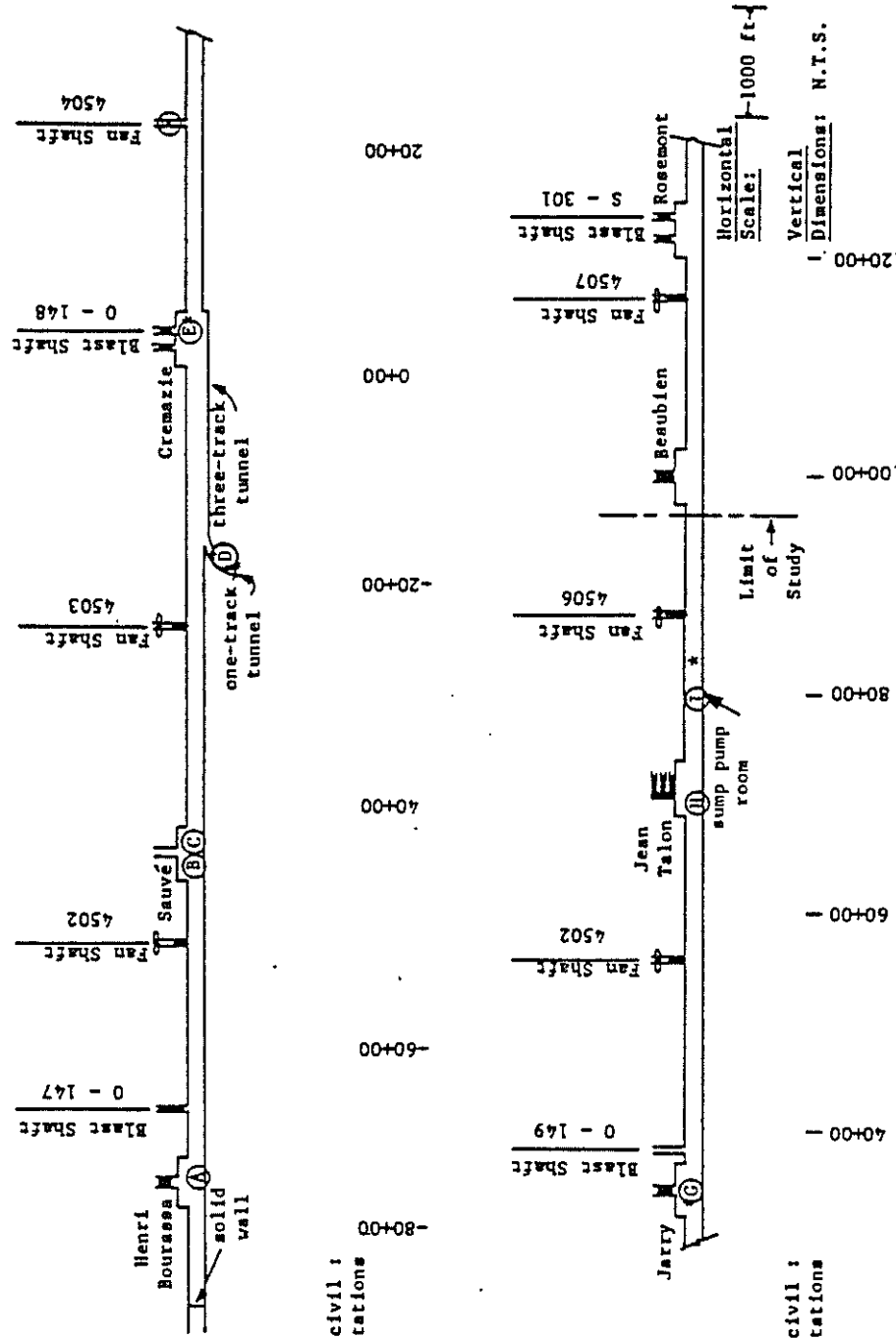


FIGURE 15-2. INSTRUMENTATION SITE LOCATIONS IN MONTREAL METRO TEST SECTION

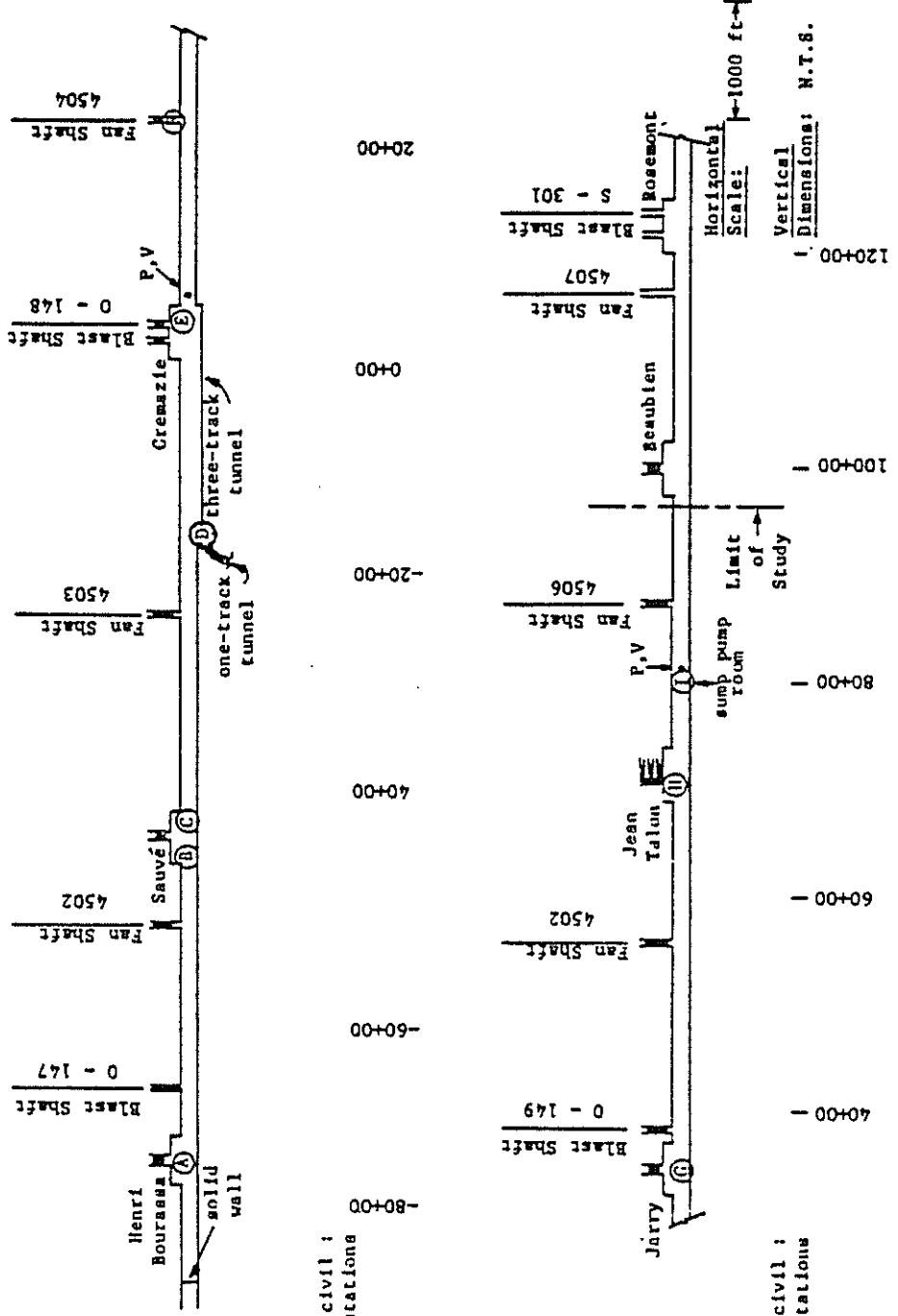
1. Open Shaft or Stairway 2. Closed Shaft or Stairway
 3. Except as noted, all tunnels are double-track 4. Instrumentation site identification



Notes:

1. Open Shaft or Stairway
2. Closed Shaft or Stairway
3. Except as noted, all tunnels are double-track
4. Instrumentation Site Identification
5. Fan Shaft Operating in Direction Indicated
5. * Test Section Areas where Velocity Profiles were Obtained

FIGURE 15-3. FULL-SCALE VALIDATION CALIBRATION TESTS (NO TRAINS OPERATING) TEST SERIES N-00Y



Notes:

1. [Open Shaft or Stairway]
2. [Closed Shaft or Stairway]
3. Except as noted, all tunnels are double-track
4. ⓘ Instrumentation Site Identification
5. [Shaft or Tunnel that is Open for Certain Tests, closed for others]
6. P: Static Pressure Measurement.
7. V: Air Velocity Measurement

FIGURE 15-4. INSTRUMENTATION FOR FULL-SCALE NEAR FIELD VALIDATION TESTS - TEST SERIES M-1YX

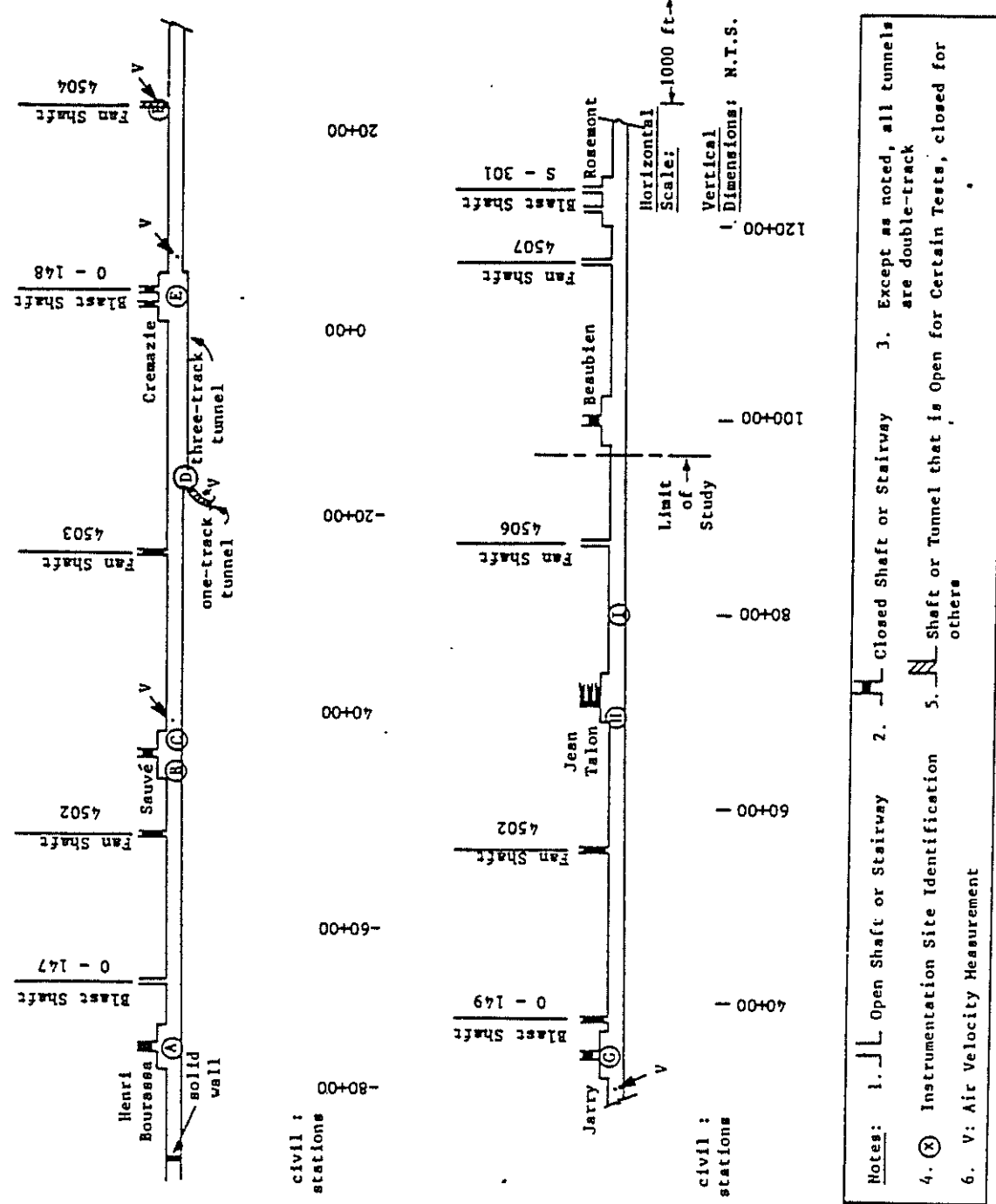
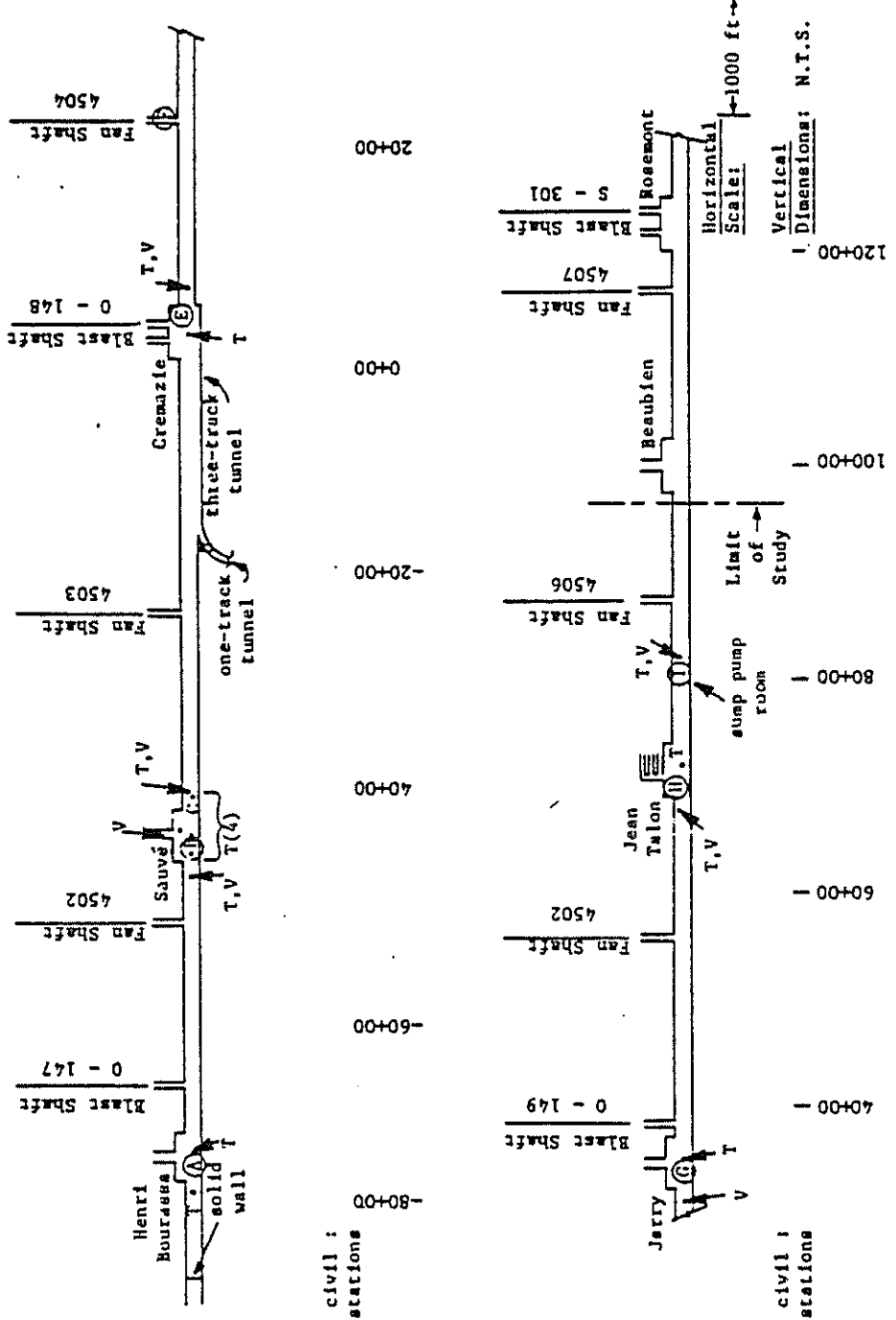
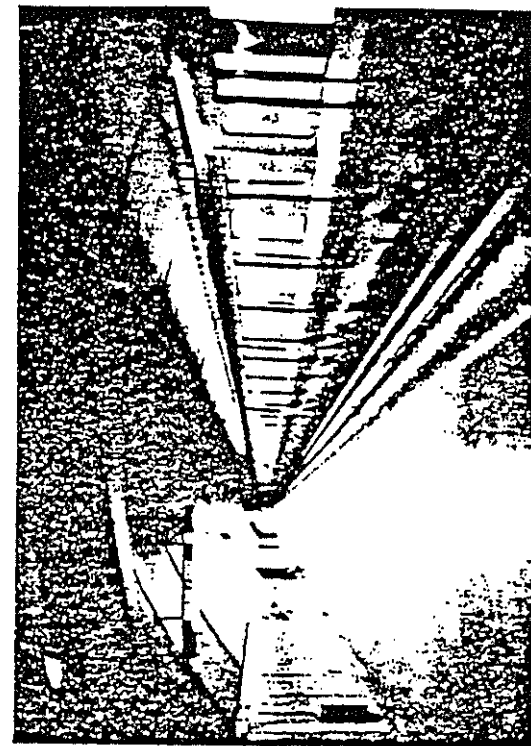


FIGURE 15-5. INSTRUMENTATION FOR FULL-SCALE MULTI-JUNCTION AND TUNNEL-FLOW TESTS - TEST SERIES M-2XX

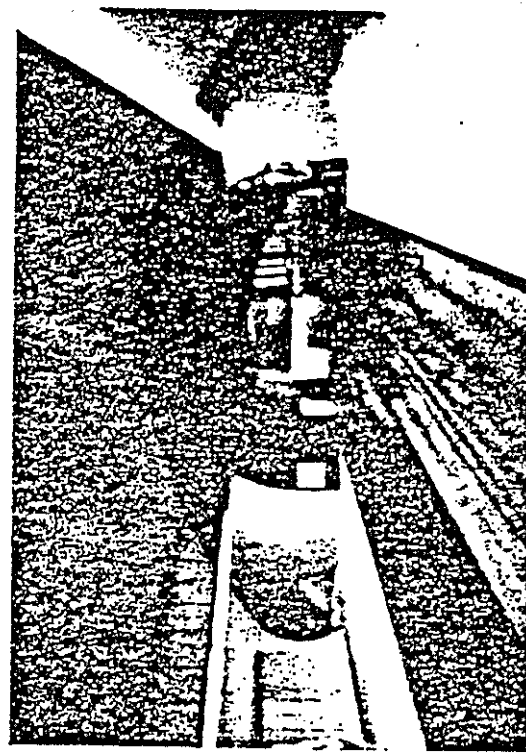


Notes: 1. Open Shaft or Stairway 2. Except as noted, all tunnels are double-track
 3. All blast shafts, doors, and fan shafts as per normal service 4. (X) Instrumentation Site Identification
 5. T: Air Temperature Measurement 6. V: Air Velocity Measurement

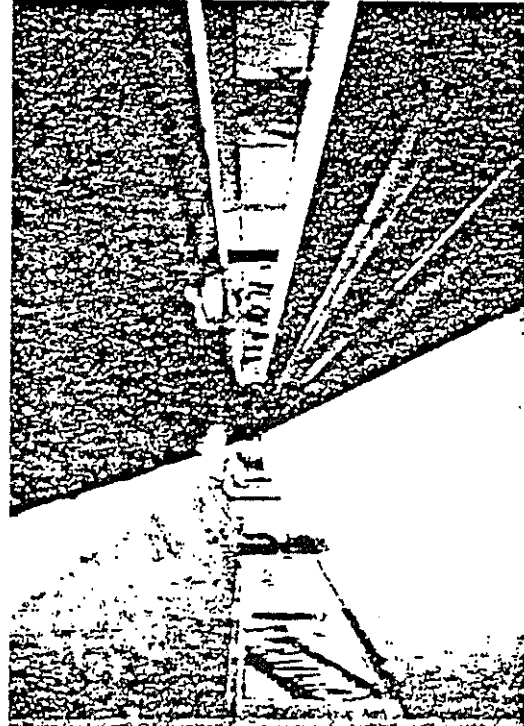
FIGURE 15-6. INSTRUMENTATION FOR FULL-SCALE SYSTEMS TESTS - TEST SERIES M-30X



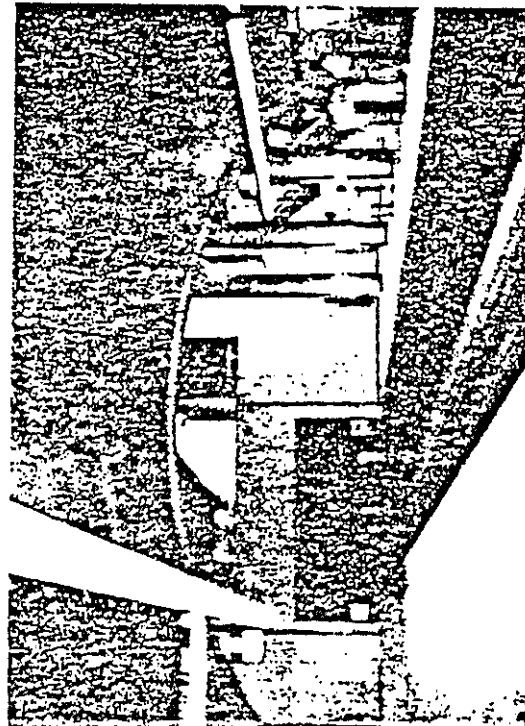
B: Lengthwise View of a Sta. with a Dwelling Train



D: Platform View of a Train Entering a Sta. from a Tunnel



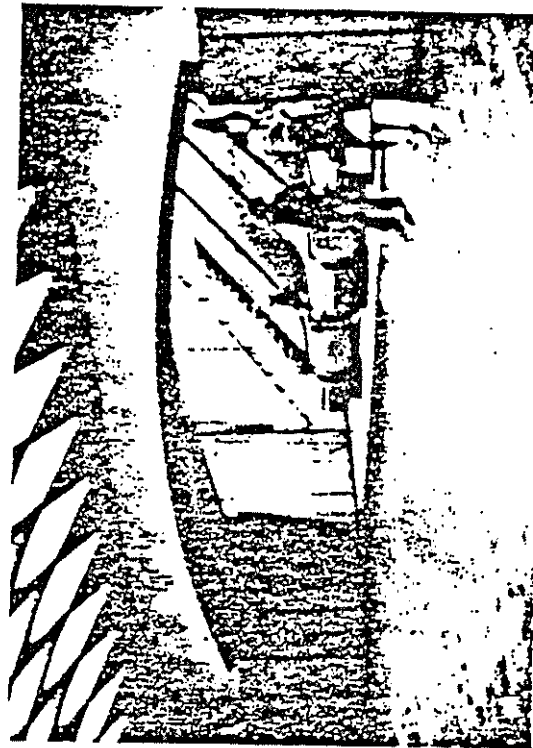
A: Lengthwise View of a Sta. (Hezz. Crosswalk in Backgd.)



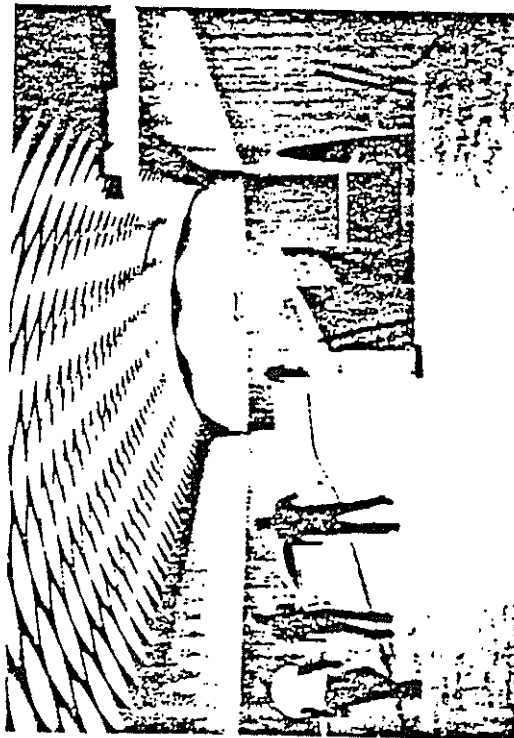
C. View of the Opening to the Plat. area from the Plat. area

FIGURE 15-7. ILLUSTRATIONS OF TYPICAL STATION AND TUNNEL GEOMETRY IN THE METRO

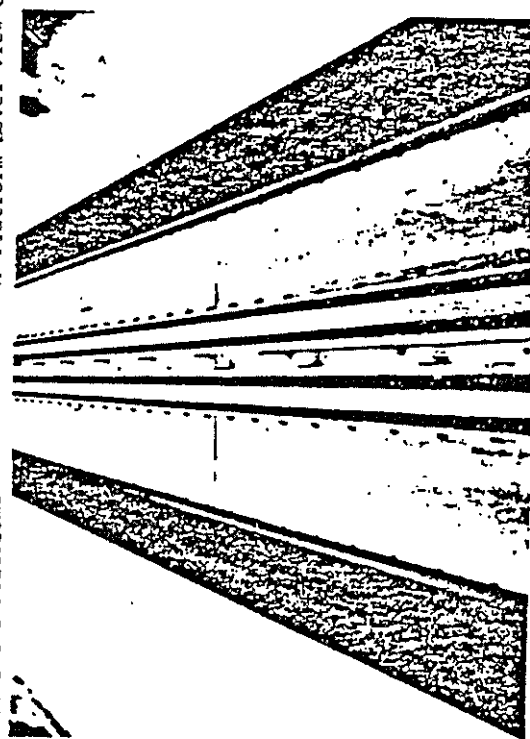




A: Mezz. View of Escalators leading to the Mezz.



B: Mezz. View of a Crosswalk over the Platforms



C: View of the Trackways from a Mezz. Crosswalk

FIGURE 15-9. ILLUSTRATIONS OF TYPICAL MEZZANINE AND TRACKWAY GEOMETRY IN THE METRO

A matrix of
data in the val
junction and sys
In addition to
plemented using
stations for pur
instrument site

The calibrat
representation
SES program compu
accomplished in
these comparisons
drawings and othe

Test No.
M-131
M-132
M-193
M-194
M-195

*Y = Car
X = Test

All tes
Rosemon

TABLE 15-2. TEST SERIES M-2YX*

MULTI-JUNCTION TESTS			
Test No..	One Track Tunnel Status	F.S. 4504 Status (fan off)	Trains in Operation
M-211	closed	open	1, SB
M-212	open	closed	1, NB
M-213	open	closed	1, SB
M-214	open	open	1, NB
M-215	open	open	1, SB
M-226	open	open	2
M-227	open	closed	2

SB: Southbound (toward Rosemont)

NB: Northbound (toward Henri-Bourassa)

*Y = No. of trains in operation

X = Test No.

All trains are 9 cars in length.

Trains' speed for all tests is 45 mph.

TABLE 15-3. TEST SERIES M-30X

SYSTEM TESTS		
Test No.	Time of Day	Remarks
M-301	Weekday Morning Rush Hour	All recorders on low speed* for 45 min., higher speed during 15 min. peak.
M-302	Noon	Low speed 1 hour recording.
M-303	Weekday Evening Rush Hour	See M-301.
M-304	10 P.M.	See M-302.
M-305	Weekday Morning Rush Hour, Second Day	See M-301.
M-306	Noon, Second Day	See M-302.
M-307	Weekday Evening Rush Hour, Second Day	See M-301.
M-308	10 P.M., Second Day	See M-302.

One temperature probe at site C-St and the temperature probe at site C-TL should be capable of 24 hr. continuous recording.

*Low speed: 1-2 in./min.

15.2 NEAR-FIELD AERODYNAMICS

Near-field aerodynamics is defined as the behavior of the airflow in the immediate vicinity of a train. Its importance is twofold: first, as the motivating force causing the far-field piston-effect airflow; and second, from a standpoint of the aerodynamic drag exerted on the train. Considerable effort has been devoted to this subject during the Transit Development Corporation's Subway Environmental Research Project, the result being a theoretical treatment of the near field which is in good agreement with both scale model tests (Ref. 1 and 3) and full-scale field tests (Ref. 2). As explained previously, an additional full-scale data point for different vehicles at a different blockage ratio was desired to complete the near-field validation effort. This additional data point was obtained in the full scale Montreal METRO field validation tests.

Near-field aerodynamic behavior commonly has been characterized by the pressure signature of the train; that is, the variation in static pressure along the train length caused by the flow-area contraction at the front of the train viscous forces in the annulus, and the flow-area expansion at the rear. In terms of data reduction and analysis, the simplest situation exists at steady-state, where the train speed and far-field air velocity are constant. In this case, a single, tunnel-mounted static-pressure transducer provides sufficient information to evaluate the near field.

Five test runs were conducted for the near-field validation. Each test train maintained constant speed within the tunnel after accelerating from Rosemont station northbound towards Henri-Bourassa Station (see Figure 15-4 and Table 15-1). It was intended for all openings in the test section to have been closed off in order to create a "zero-flow" condition for these tests. A tunnel with zero-flow conditions would maximize the magnitude of the pressure signatures obtained and thereby increase the resolution of the measurements. In addition, corrections must be made to the pressure signature when zero-flow conditions do not exist and only one wayside pressure transducer is used to record the signature. This is due to the fact that when the pressure measurement is made at a single axial station, the far-field tunnel pressure distribution changes during the passage of the train (Ref. 6). The measured signature drag must be corrected as follows:

$$C_{D_{\text{actual}}} = C_{D_{\text{measured}}} - f_t \frac{l}{d} \frac{\beta^2}{\sigma} \quad (\text{Ref. 6})$$

where:

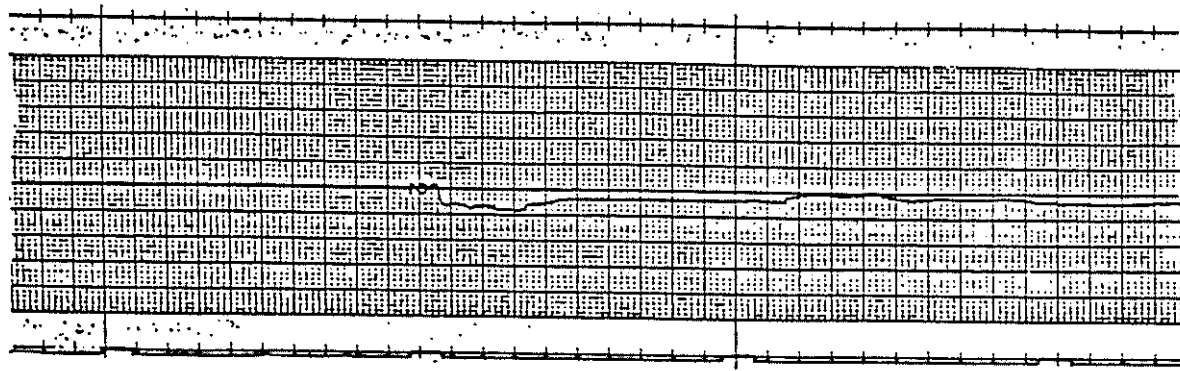
- $C_{D_{\text{actual}}}$ = the corrected drag coefficient
- $C_{D_{\text{measured}}}$ = the measured drag coefficient
- f_t = the tunnel friction factor
- l = the train length, ft
- d = the train hydraulic diameter, ft
- β = instantaneous air velocity/instantaneous train velocity
- σ = train cross-sectional area/tunnel cross sectional area

When there is no far-field tunnel flow, β equals zero and there is no correction to be made. It was discovered during the progress of these tests that the test section could not be completely sealed due to leaking dampers in various shafts and doors that did not completely seal the entranceways to the stations, and a relatively small tunnel flow occurred during the near-field tests as a result of these leaks (see Figure 15-7 through 15-9).

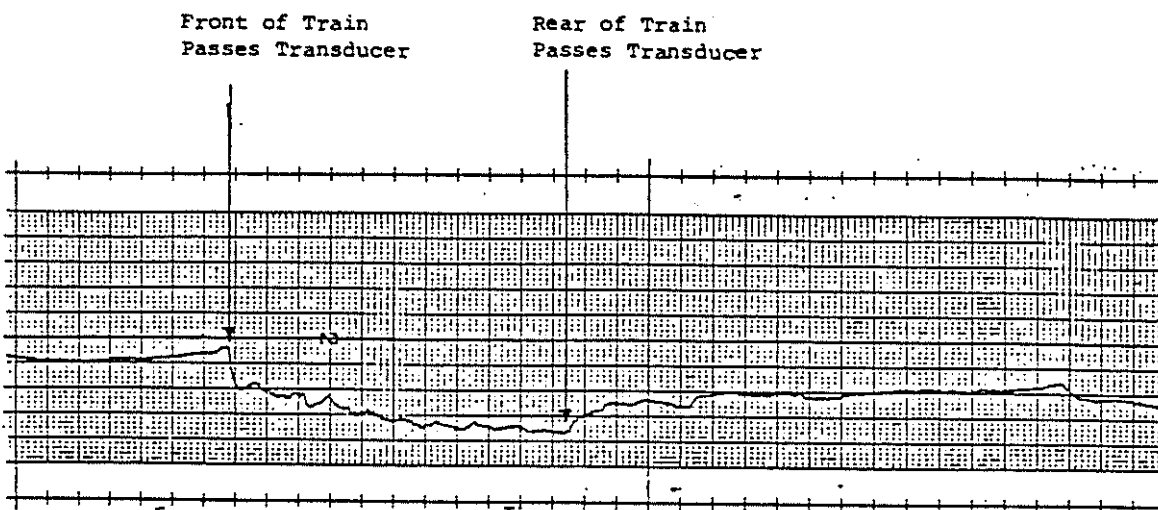
However, these far-field tunnel flows that occurred in the M-1YX tests were relatively low in comparison with the train speeds, and the effect the above correction had upon the measured pressure signatures was insignificant. The fact that the system could not be completely sealed as planned did not materially affect the near-field validation tests or results. It simply meant that the magnitudes of the pressure signatures were slightly less than maximum.

By the time the test train reached the transducer at instrumentation site I both the train speed and piston-effect airflow were very nearly steady-state. The actual static pressure measurements for tests M-131 and M-194 at site I are shown in Figure 15-10.

As the front of the train passes the transducer an abrupt pressure drop occurs due to the contraction and acceleration of the flow. The pressure continues to drop because of tunnel and train friction as the train passes,



Pressure Signature at Site I - Test M-191



Pressure Signature at Site I - Test M-194

FIGURE 15-10. SAMPLE STATIC PRESSURE MEASUREMENTS OBTAINED IN THE MONTREAL FULL SCALE FIELD VALIDATION TESTS

then abruptly increases when the rear of the train reaches the transducer and the annular flow experiences a sudden expansion and deceleration. After the train passage the pressure maintains a constant value, in these cases below ambient, as a result of the steady-flow pressure drop between Rosemont Station and the transducer.

These pressure signatures can be used to infer the drag coefficient for the train through the following steady-state relationship:

$$C_D = \frac{\Delta p}{1/2 \rho U_v^2 \sigma g_c} - f_t \left(\frac{\sigma - \beta}{1 - \sigma} \right)^2 \frac{l}{d \sqrt{\sigma}}$$

where:

Δp = net static pressure change as a consequence of train passage, lb-f/ft²

U_v = train velocity, ft/sec

σ = blockage ratio (0.254)

f_t = tunnel friction factor (0.03)

β = ratio of tunnel air velocity to train speed

l = train length, ft

d = train hydraulic diameter (9.17 ft)

Applying this relation to both the test measurements and to the pressure calculations using the near-field theory provides the following comparison:

Test	Measured C_D	Theoretical C_D	% Difference
M-131	1.827	1.734	-5.6
M-132	2.252	2.025	-10.0
M-193	2.993	2.993	0.0
M-194	2.486	2.713	+8.4
M-195	3.588	3.323	-7.4

A graphical representation of these results is given in Figures 15-11 through 15-15.

From these results it appears that the near-field theory predicts within 10 percent accuracy the drag on both three-car and nine-car trains at speeds up to 45 mph. A more detailed examination shows that the near-field theory tends to slightly underpredict the drag on the three-car trains. This

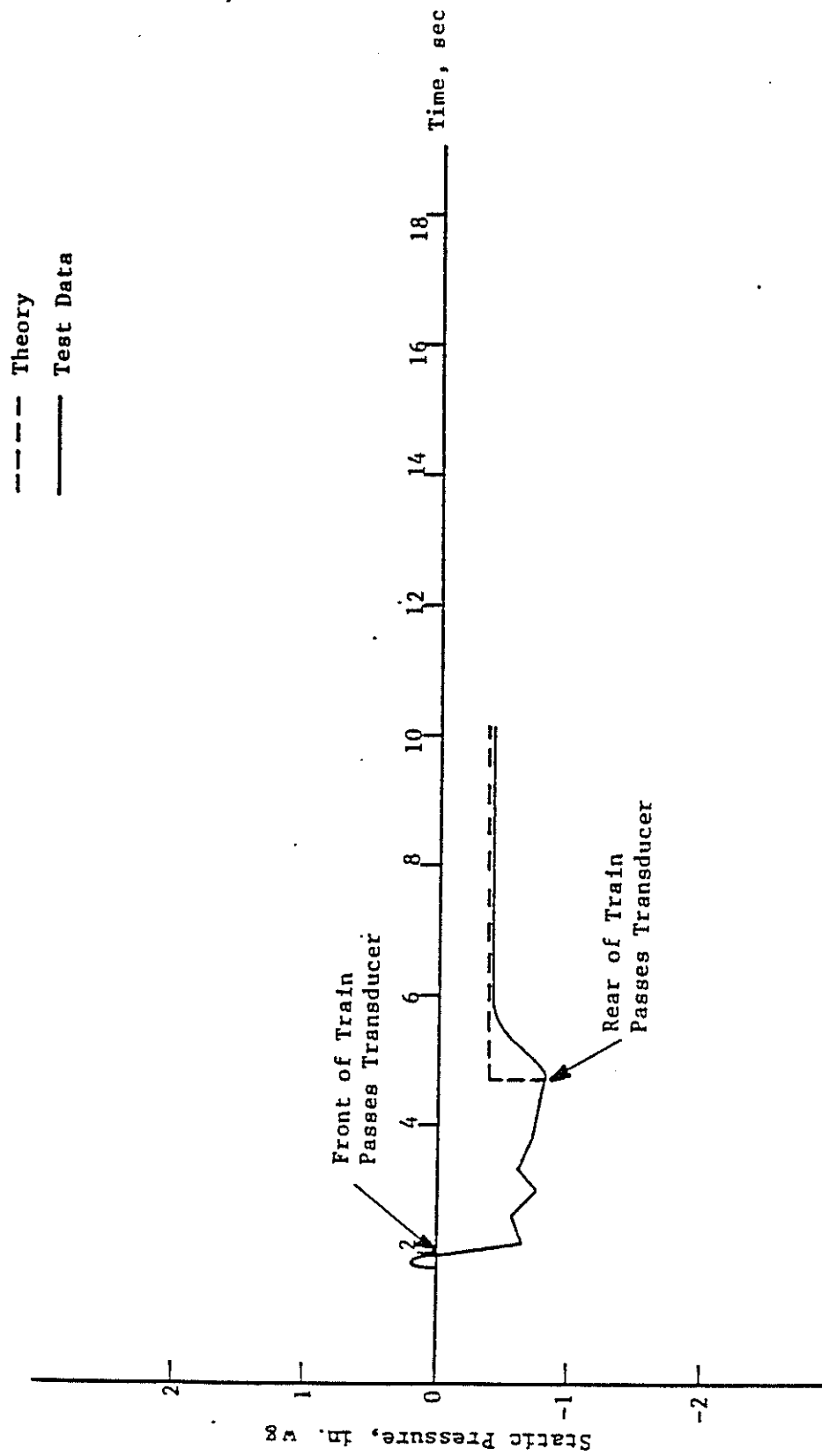


FIGURE 15-11. COMPARISON OF MEASURED AND PREDICTED NEAR-FIELD PRESSURE SIGNATURES: TEST H-131

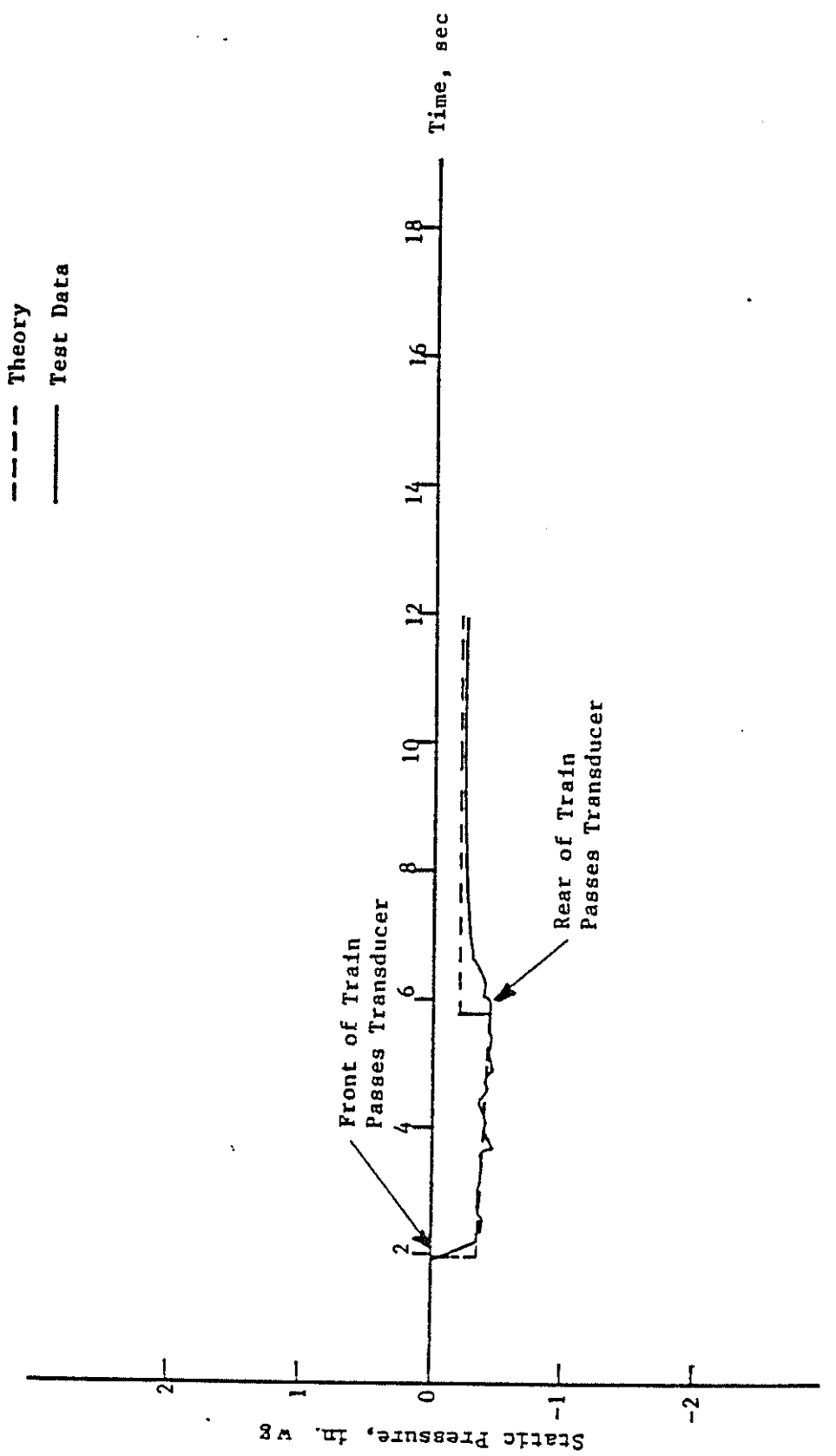


FIGURE 15-12. COMPARISON OF MEASURED AND PREDICTED NEAR-FIELD PRESSURE SIGNATURES: TEST M-132

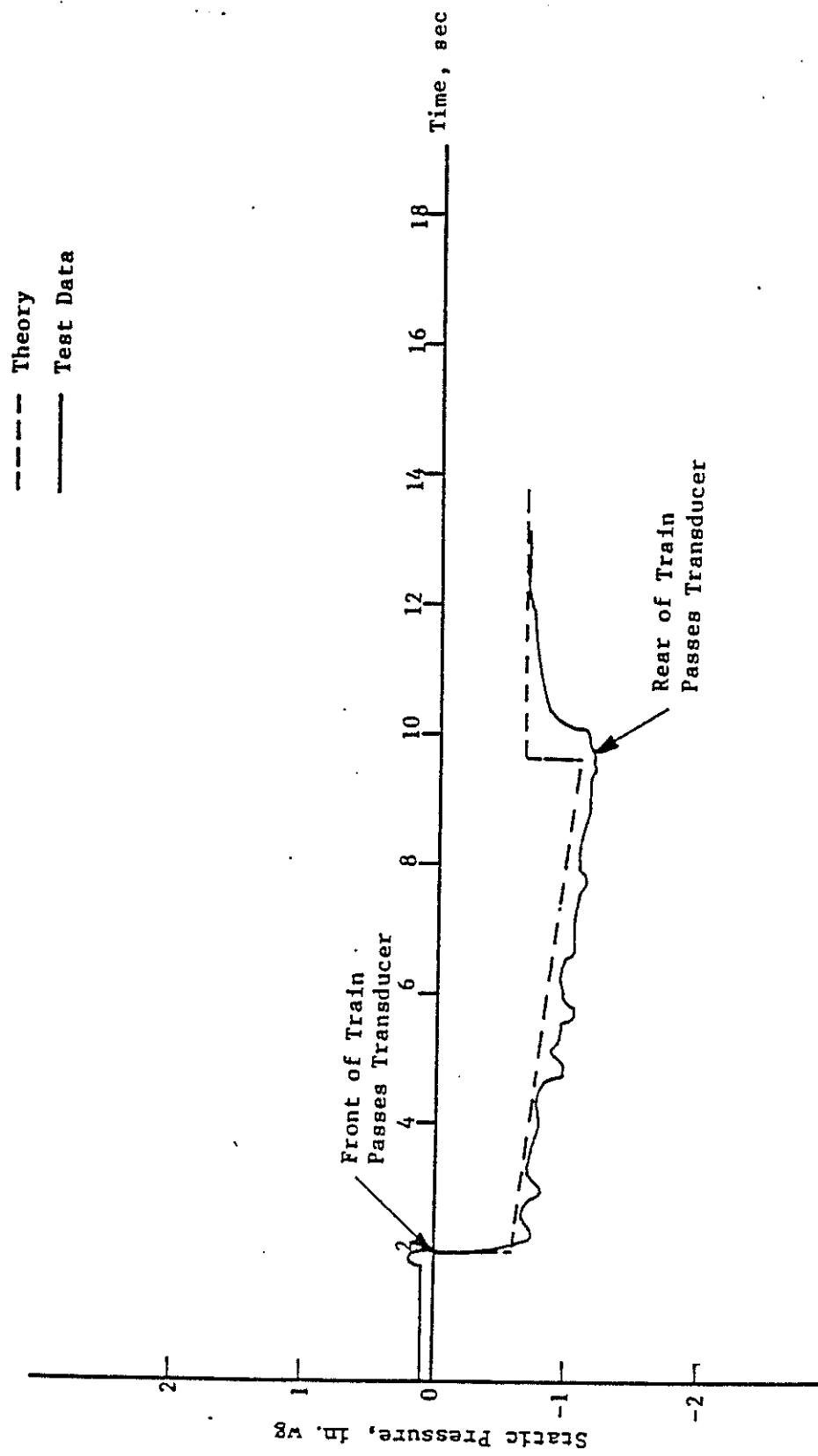


FIGURE 15-13. COMPARISON OF MEASURED AND PREDICTED NEAR-FIELD
PRESSURE SIGNATURES: TEST H-193

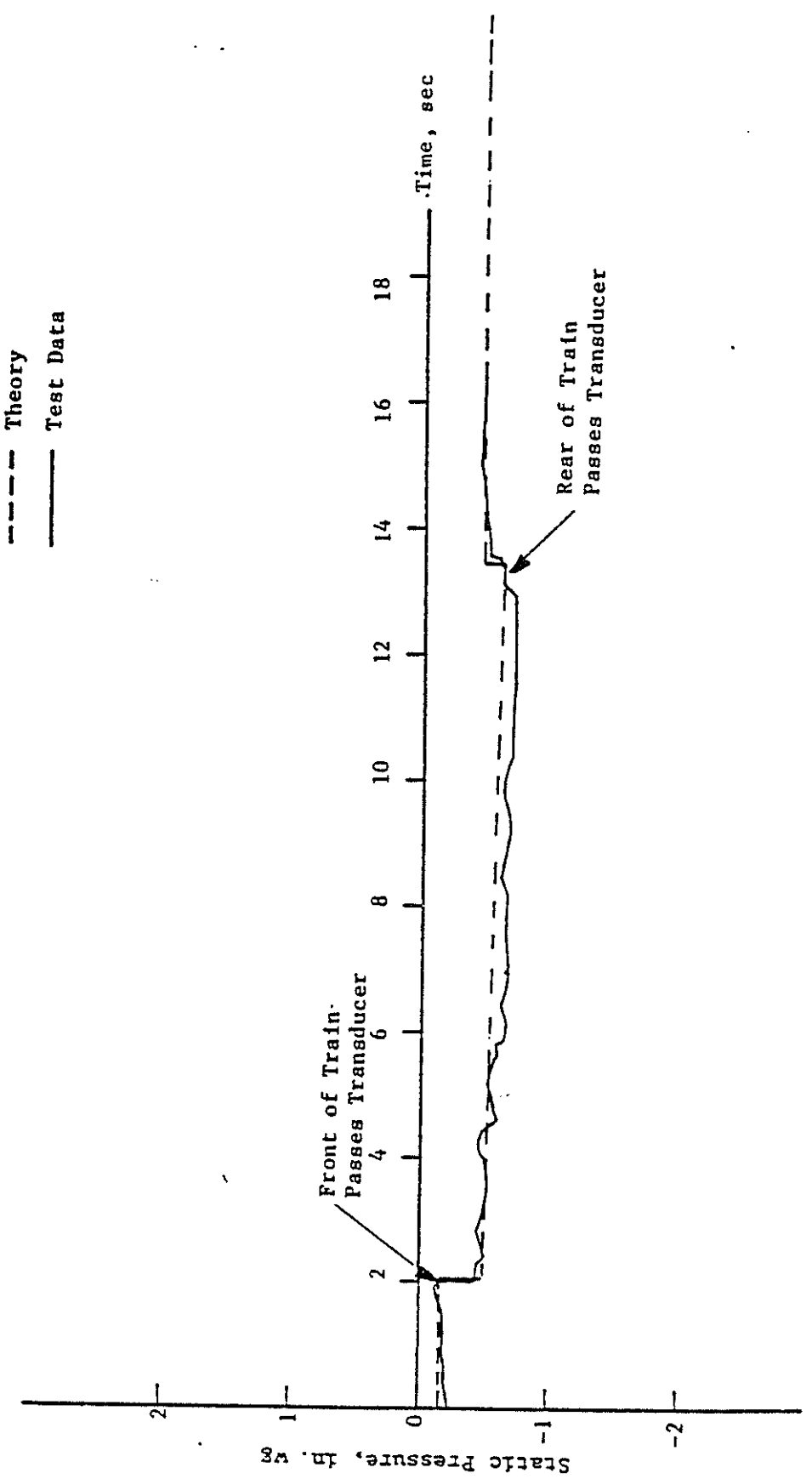


FIGURE 15-14. COMPARISON OF MEASURED AND PREDICTED NEAR-FIELD PRESSURE SIGNATURES: TEST M-194

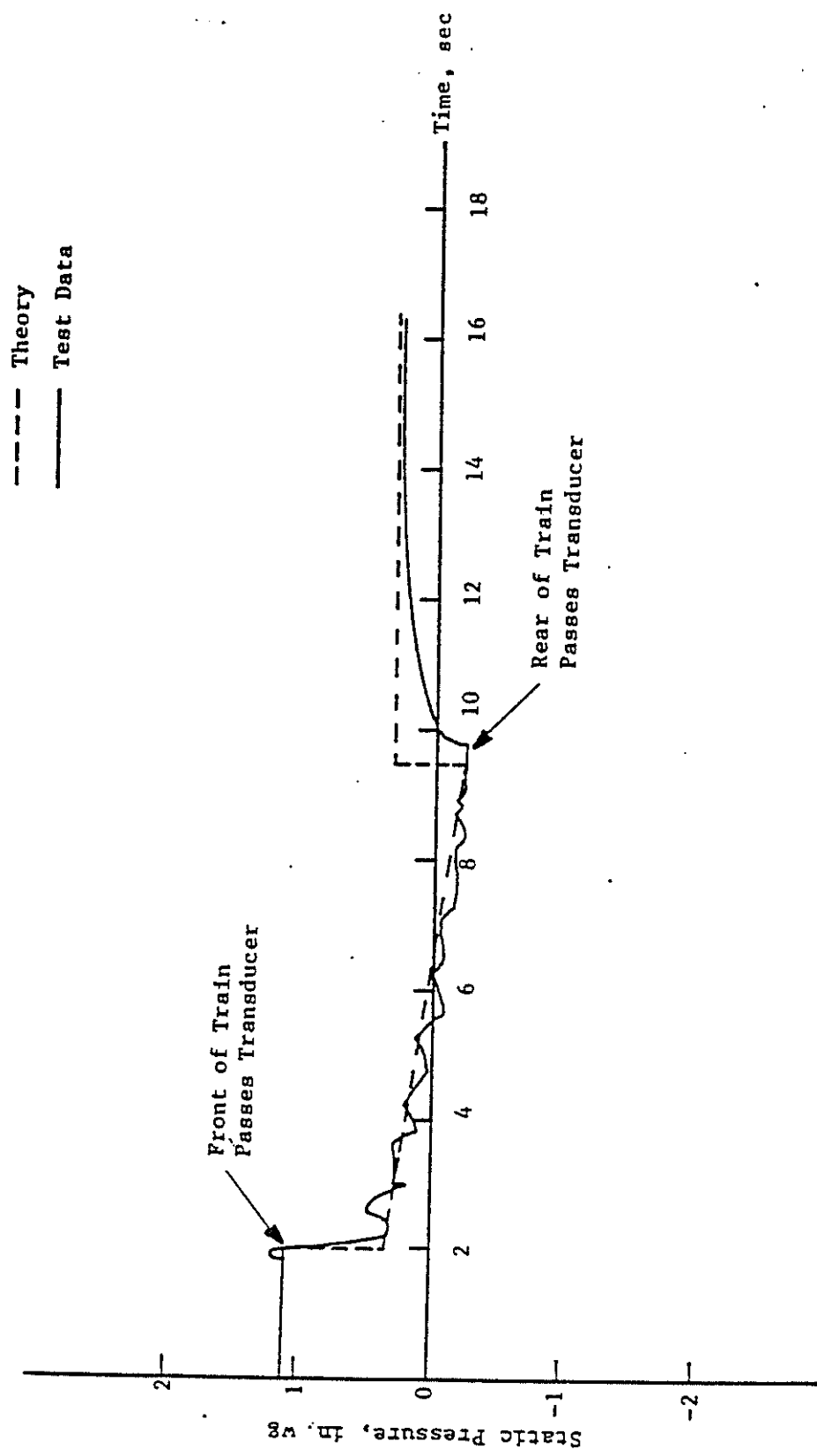


FIGURE 15-15. COMPARISON OF MEASURED AND PREDICTED NEAR-FIELD PRESSURE SIGNATURES: RUN M-195

observation was similarly made for the two-car trains in the Berkeley Hills Tunnel tests (Ref. 2). The results of the nine-car tests provide measured drag coefficients that are within -8.4, 0.0, and +7.4 percent of the theoretical drag coefficients. The six-car trains in the Berkeley Hills Tunnel tests gave measured results within +3.0 percent of the theoretical results.

Because of the smaller blockage ratio, lower speeds and the inability to achieve zero-flow conditions, the expected magnitudes of the pressure signatures in the METRO tests were approximately one quarter of the pressure signatures obtained in the Berkeley Hills Tunnel. Consequently, experimental error in the instrumentation system was proportionately greater. As can be seen in Figure 15-10, the thickness of the ink line on the scale provided by the recorder at site I in test M-131 is equivalent to approximately 10 percent of the total measured pressure drop between the front and the rear of the train, or 5 percent of full scale. Therefore, the agreement and consistency between theory and measurement is quite good when the inherent errors in obtaining the data are taken into consideration.

The results of these comparisons show the near-field aerodynamic theory developed during the Transit Development Corporation's Subway Environment Research Project to be more than adequate for computations of piston-effect air flow and train aerodynamic drag. The theory has now been tested during four separate testing programs (Ref. 1, 2, and 3), and the results of all four have deemed the near-field aerodynamic theory to be well within the desired accuracy objectives of the SES program.

It was observed during all four of the validation testing programs that the accuracy of the near-field theory is sensitive to the value used for the cross-sectional areas of the wheel bogies which affects form drag in the annulus. It is very difficult to determine the exact cross-sectional area of a wheel bogie from scale drawings of a train. A 10 percent error in measuring the cross-sectional area of the Montreal trains' wheel bogies (equivalent to a 1.2 percent error in the total cross-sectional area of the train) results in a 10 percent error in the near-field drag calculations. It was found in both the BART and METRO full-scale field tests that a value of 0.023 for the "effective" skin-friction coefficient for the entire train (car-surface, frictional drag, plus wheel-bogie form drag) gave excellent agreement between theory and measurement. This observation is particularly significant in view of the substantial differences in configuration between the BART and METRO

cars. Therefore, if the cross-sectional area of a train's wheel bogies has not been determined exactly, it is recommended that this value of 0.023 be used for the skin-friction coefficient for the entire train in order to circumvent the potential error inherent in determining the bogie cross-sectional area from scale drawings.

15.3 ONBOARD PRESSURE TRANSIENTS - *not for St 1*

Tests M-226 and M-227 were designed to validate the aerodynamic subprogram of the SES program for multiple-(two) train operations. However, since the Montreal METRO is basically a two-track subway with no dividing wall, these tests offered an excellent opportunity to validate the simplified models of Reference 7 for pressure transients associated with the passage of two trains travelling in opposite directions.

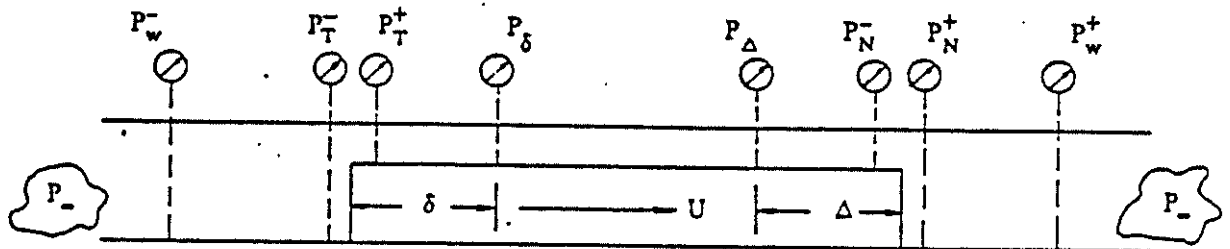
In preparation for Tests M-226 and M-227, wayside pressure instruments, used during the near-field aerodynamics tests (M-1YX series), were removed from their tunnel sites and used for on-board pressure measurements. Only one train was fitted with on-board static pressure transducers. One transducer was placed inside the lead car, just behind the front cab. The second pressure transducer was placed inside the trailing car, just ahead of the rear cab. Power (110V/AC) for strip-chart recorders was obtained using portable inverters, provided by MUCTC.

Both test trains were instrumented with continuous speed-time recorders. Time synchronization of the various instruments was accomplished by voice using the METRO communications system and by visual observation of significant events.

In Reference 4, non-dimensional coefficients are used as an intermediate step in the calculation of subway air-pressure changes. These coefficients are defined by Table 15-4. In Table 15-4, the symbol P denotes static pressure, absolute. Combinations of superscripts and subscripts on P are used to denote points of pressure measurement. The symbol C is used to denote pressure coefficients. A unique pressure coefficient is defined for each pressure measurement location. The units of P, ρ and U must be selected so that the resulting pressure coefficient is non-dimensional.

From Table 15-4 it is clear that, given the quantity $0.5\rho U^2$ and the appropriate pressure coefficient C, the pressure rise ($P - P_\infty$) at that location

TABLE 15-4. DEFINITION OF PRESSURE COEFFICIENTS



$$C_T^- = (P_T^- - P_\infty) / \frac{1}{2} \rho U^2$$

$$C_T^+ = (P_T^+ - P_\infty) / \frac{1}{2} \rho U^2$$

$$C_\delta = (P_\delta - P_\infty) / \frac{1}{2} \rho U^2$$

$$C_w^- = (P_w^- - P_\infty) / \frac{1}{2} \rho U^2$$

$$C_N^+ = (P_N^+ - P_\infty) / \frac{1}{2} \rho U^2$$

$$C_N^- = (P_N^- - P_\infty) / \frac{1}{2} \rho U^2$$

$$C_\Delta = (P_\Delta - P_\infty) / \frac{1}{2} \rho U^2$$

$$C_w^+ = (P_w^+ - P_\infty) / \frac{1}{2} \rho U^2$$

may be calculated.

For a standard air weight density of 0.075 lb/ft^3 , the quantity $0.5\rho U^2$ can be determined from

$$\frac{1}{2} \rho U^2 = 3.1 \left(\frac{U}{80} \right)^2 \text{ in. wg} \quad (1)$$

where U is expressed in MPH.

The simplified models for determining air pressure transients from passing trains (Ref. 7) are shown in Table 15-5 in terms of pressure coefficients. Two trains, each having speed U , length l , cross-sectional area a , hydraulic diameter d , and frictional coefficient f_t , approach from opposite directions and pass in an undivided double-track tunnel. It is assumed that the tunnel area A , hydraulic diameter D , and frictional coefficient f , are uniform in the neighborhood of the passing location.

In developing the process equations of Table 15-5, it is assumed that tunnel-air velocity in the far field is equal to zero. This causes the solution of the problem to become symmetrical, so that pressures at corresponding locations on both trains are equal. Further, it is assumed that air-pressure changes due to the passage of two trains can be described satisfactorily using one-dimensional, incompressible flow theory.

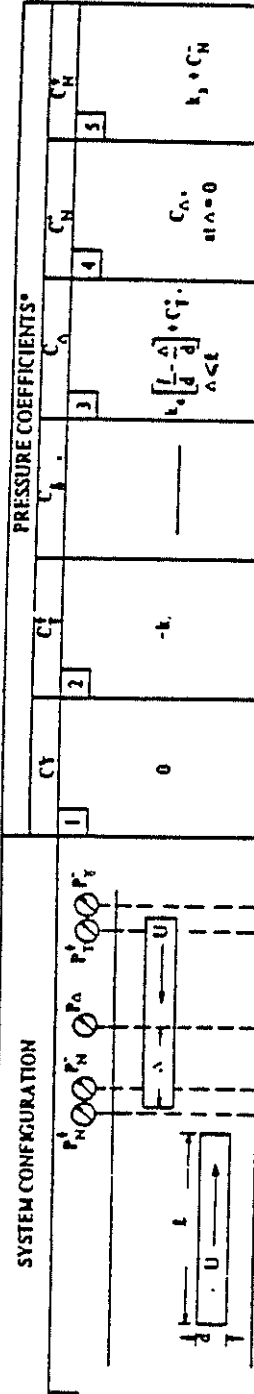
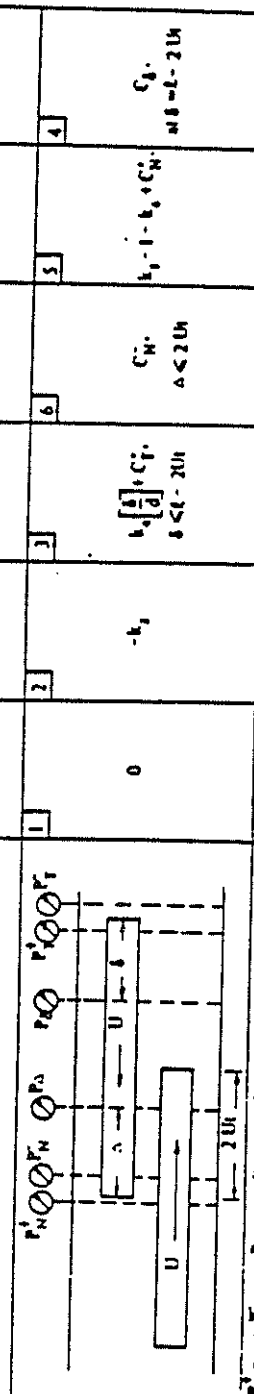
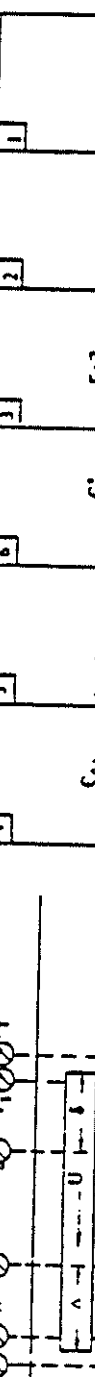
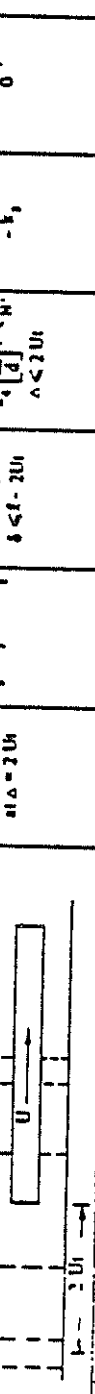
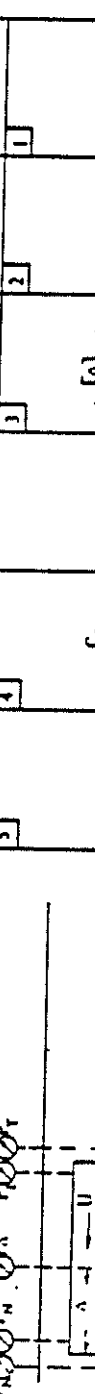
As shown in Table 15-5, the problem of train passage can be conveniently divided into four basic configurations. A set of pressure coefficient equations is given for each configuration. In general, the order of solution for the pressure coefficients is important, and is different for each system configuration. The required solution order of the pressure coefficients for each configuration is given by the "boxed" arabic numbers (e.g., the solution order for configuration III is $C_N^+, C_N^-, C_\Delta, C_T^-, C_T^+$ and C_δ).

Reference 7 proposes that pressure waves generated by the passage of trains will not be a design factor for train speeds up to 80 mph and blockage ratios up to 0.3.

The basic constraints for field validation implied by Table 15-5 are:

1. Both trains are identical.
2. The speeds of both trains are equal.
3. The tunnel geometry over a distance l encompassing both sides of the point in the tunnel where the noses of the trains meet is uniform.

TABLE 15-5. TRAIN PASSAGE PRESSURE TRANSIENTS PROCESS EQUATIONS

SYSTEM CONFIGURATION	PRESSURE COEFFICIENTS*					
	C_V	C_I^1	C_I^2	C_H	C_H	C_H
I 	0	- k_1	—	$k_1 \left[\frac{1}{d} - \frac{\alpha}{d} \right] + C_I^1$	C_H	$k_1 + C_H$
II 	0	- k_1	$k_1 \left[\frac{A}{d} + C_I^1 \right]$	C_H	$k_1 + k_2 + C_H$	$k_1 + C_H$
III 	0	- k_1	$k_1 \left[\frac{A}{d} + C_I^1 \right]$	C_H	$k_1 + k_2 + C_H$	$k_1 + C_H$
IV 	0	- k_1	$k_1 \left[\frac{A}{d} + C_I^1 \right]$	C_H	$k_1 + k_2 + C_H$	$k_1 + C_H$
V 	0	- k_1	$k_1 \left[\frac{A}{d} + C_I^1 \right]$	C_H	$k_1 + k_2 + C_H$	$k_1 + C_H$
VI 	0	- k_1	$k_1 \left[\frac{A}{d} + C_I^1 \right]$	C_H	$k_1 + k_2 + C_H$	$k_1 + C_H$

* Trains identical, $\alpha = a/A$, $k_N = 0.1 \circ (1-\alpha)^2$, $k_F = \alpha^2$, $k_A = [1/d]^2$, $k_1 = k_2 = k_N + k_F + k_A$, $k_1 \cdot [1/d]^2$ $\ln(\alpha t + \sigma d)$, $k_1 \cdot [1/d]^2$ $\ln(1 + k_N t + k_F t + k_A t)$, $k_1 = 0.1 \left(\frac{a}{d} \right)^2 k_1$.

These test constraints were approximately satisfied by starting a southbound nine-car train from Henri Bourassa Station and northbound nine-car train from Beaubien Station simultaneously and running the trains at a nominal speed of 45 mph. This scheme, devised through pre-test planning, allowed the trains to meet and pass completely in the section of tunnel between Cremazie Station and fan shaft 4504. This section of tunnel, about 1699 ft in length, has uniform aerodynamic properties with no ventilation shafts.

15.3.1 Theoretical Calculations

From structural drawings and the near-field aerodynamic tests, train parameters were established as:

$$\begin{aligned} l &= 500 \text{ ft} & a &= 86 \text{ ft}^2 \\ d &= 9.17 \text{ ft} & f_t &= 0.023 \end{aligned}$$

Similarly, relevant tunnel parameters were given as:

$$\begin{aligned} A &= 338 \text{ ft}^2 & f &= 0.0267 \\ D &= 19.1 \text{ ft} \end{aligned}$$

Following the procedure given in Table 15-5.

$$\sigma = 86 \text{ ft}^2 / 338 \text{ ft}^2 = 0.254$$

$$\frac{l}{d} = \frac{500 \text{ ft}}{9.17 \text{ ft}} = 54.53$$

$$k_N^- = (0.3)(0.254)(1-0.254)^2 = 0.0424$$

$$k_T^- = (0.254)^2 = 0.0645$$

$$k_1 = \left[\frac{1}{1-0.254} \right]^2 = 1.796$$

$$k_2 = (1.796)(1-0.0645) - 1 = 0.680$$

$$k_3 = (1.796)(1+0.0424) - 1 = 0.872$$

$$k_4 = \left[\frac{1}{1-0.254} \right]^3 [(0.254)^{5/2}(0.0267) + (0.254)(0.023)] = 0.0162$$

$$k_5 = \left[\frac{1-2(0.254)}{1-0.254} \right]^2 = 0.435$$

$$k_6 = (0.3) \left[\frac{0.254}{1-0.254} \right] (0.435) = 0.047$$

$$k_7 = \left[\frac{0.254}{1-0.254} \right]^2 = 0.116$$

Continuing the procedure given in Table 15-5, the solution for pressure coefficients C_T^- , C_T^+ , C_N^- , and C_N^+ gives

Approaching trains:

$$C_T^- = 0.0$$

$$C_T^+ = -0.680$$

$$C_N^- = (0.0162)(54.53) - 0.680 = 0.203$$

$$C_N^+ = 0.872 + 0.203 = 1.075$$

Just after the nose of one train passes the nose of the other train:

$$C_T^- = 0.0$$

$$C_T^+ = -0.680$$

$$C_N^+ = (0.0162)(54.53-0.0) - (0.680) = 0.203$$

$$C_N^- = (0.435) - 1 - (0.044) + (0.203) = -0.406$$

Just before the nose of one train reaches the tail of the other train:

$$C_T^- = 0.0$$

$$C_T^+ = -0.680$$

$$C_N^+ = -0.680$$

$$C_N^- = 0.435 - 1 - 0.044 - 0.680 = -1.289$$

Just after the nose of one train passes the tail of the other train:

$$C_N^+ = 0.0$$

$$C_N^- = -0.872$$

$$C_T^- = -0.872$$

$$C_T^+ = 0.435 + 0.116 - 1 - 0.872 = -1.321$$

Just before the tail of one train reaches the tail of the other train:

$$C_N^+ = 0.0$$

$$C_N^- = -0.872$$

$$C_T^- = -(0.0162)(54.53) - 0.872 = -1.755$$

$$C_T^+ = 0.435 + 0.116 - 1 - 1.755 = -2.204$$

After the trains have passed:

$$C_N^+ = 0.0$$

$$C_N^- = -0.872$$

$$C_T^+ = -(0.0162)(54.53) - 0.872 = -1.755$$

$$C_T^- = 0.680 - 1.755 = -1.075$$

15.3.2 Performance of Models

For comparison of the models shown in Table 15-5 with field-test results, it was assumed that pressure inside the lead car is approximately equal to P_N^- . Similarly, it was assumed that pressure inside the rear car is represented by P_T^+ . These simplifications imply that pressure changes occurring in the annular space around a train at a given location are transmitted undiminished to the car interior at that location. The validity of these approximations is to a large degree dependent on the net free area of openings (ventilation ducts, cracks, etc.) allowing passage of small quantities of air between the interior and exterior of the cars. Car ventilation fans were shut down during the tests to avoid extraneous effects.

Air temperature inside the subway during tests M-226 and M-227 was on the order of 70°F. For simplicity, it was assumed that atmospheric conditions within the subway were approximately standard.

Test M-226. For test M-226, the train dispatched southbound from Henri Bourassa Station contained the on-board pressure instrumentation. Use of measured train speed-time profiles with static pressure records, marked with significant events, enabled a reasonably accurate map of train position-time-static pressures to be reconstructed for analysis. Such a map is shown in Figure 15-16.

Figure 15-16 was formulated by enlarging, tracing, and synchronizing original strip chart data. This figure shows static pressure inside the lead and rear cars of the southbound train between the time that the train enters Cremazie Station until it passes fan shaft 4504 (site F). These results include pressure transients occurring as the northbound and southbound trains pass (about 143 seconds to 150 seconds after train start).

Examination of Figure 15-16 leads to the following general conclusions;

1. The most predominant on-board pressure transients arise during passage of the trains. On-board pressure transients of secondary significance are caused by the train passing fixed discontinuities, such as changes in tunnel cross-section and openings to the outside.
2. Pressure waves are not a significant phenomenon. In fact, from Figure 15-16, it is difficult to positively identify any wave effects.

A detailed comparison of measured and predicted on-board pressure transients during train passage is shown in Figure 15-17. The field test results shown in Figure 15-17 represent a further enlargement of the data shown in Figure 15-16 to concentrate on the phenomena of interest.

From the train speed-time profiles, the speed of the southbound train was about 47 mph during passage. Similarly, the speed of the northbound trains was estimated as 45.5 mpg. The average train speed U is then

$$U = \frac{47 + 45.5}{2} = 46.25 \text{ mph}$$

Using the average train speed with equation (1),

$$\frac{1}{2}\rho U^2 = 3.1 \left(\frac{46.25}{80}\right)^2 = 1.036 \text{ in. wg}$$

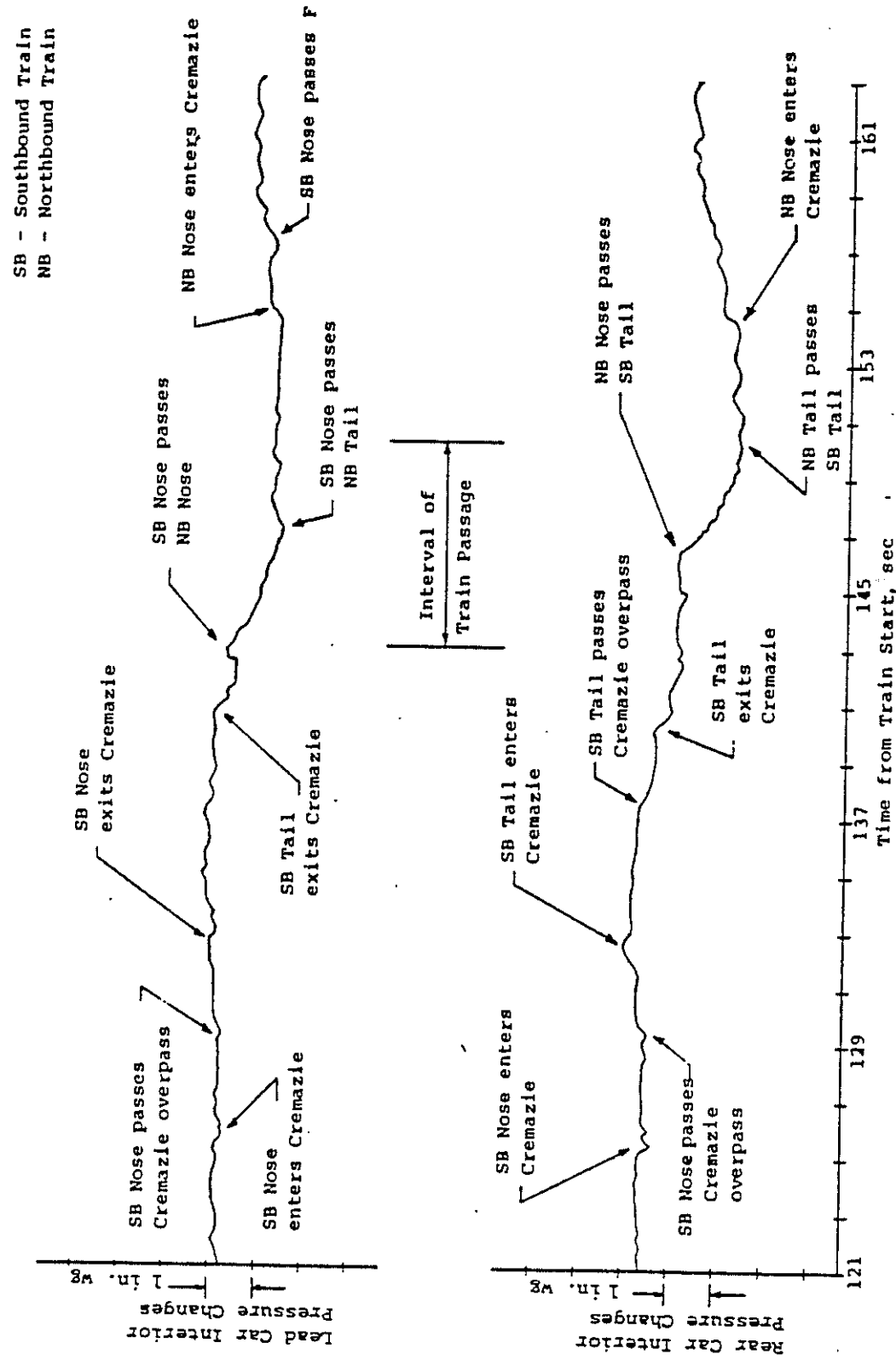


FIGURE 15-16. PRESSURE TRANSIENTS ONBOARD SOUTHBOUND TRAIN - TEST M-226

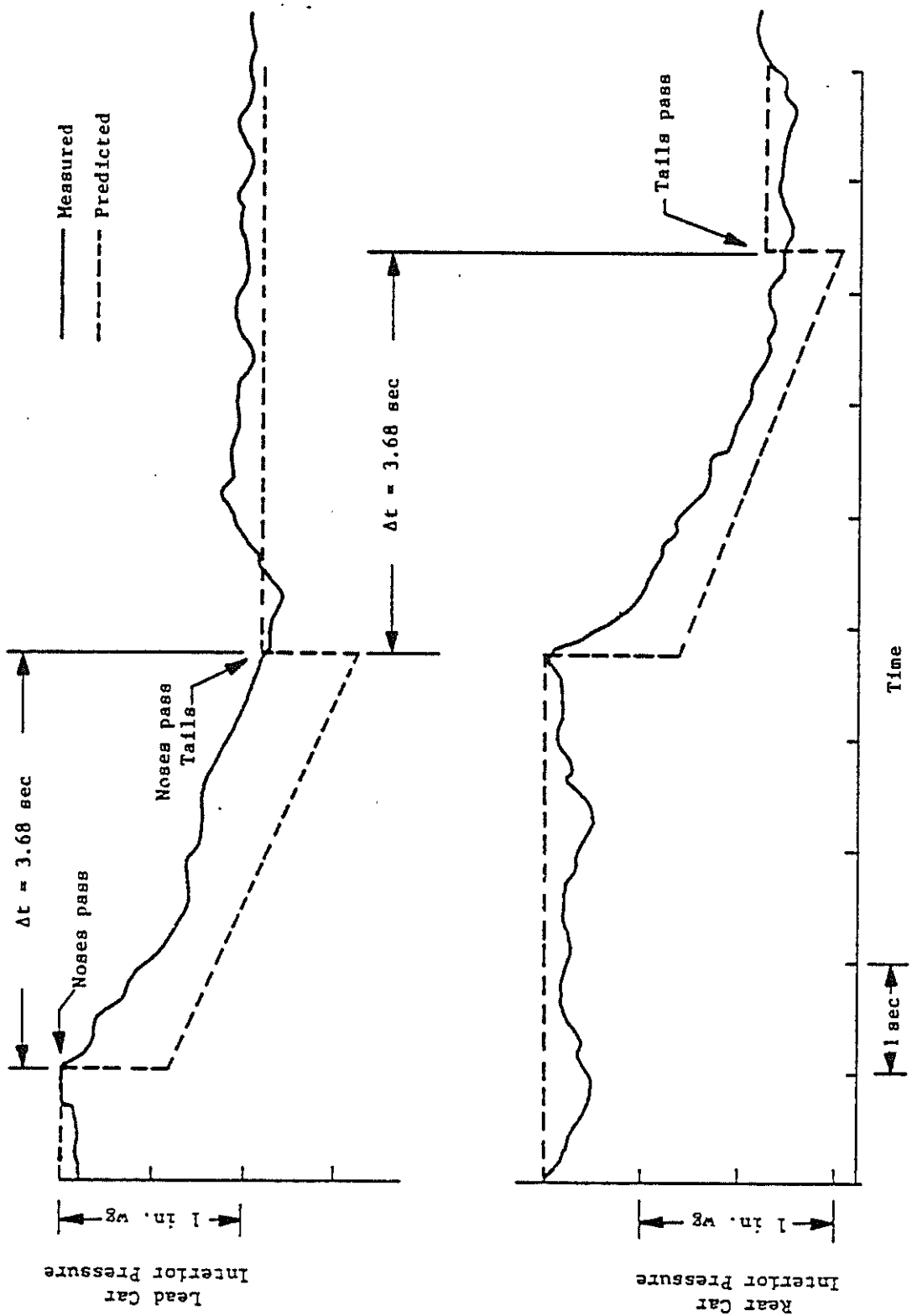


FIGURE 15-17. COMPARISON OF MEASURED AND PREDICTED RESULTS FOR PASSING TRAINS - TEST M-226

In Figure 15-17, the phenomena of particular interest are the pressure changes that occur as the trains pass rather than levels of absolute pressure that exist before, during and after this event. Therefore, differences in pressure coefficients play an important role. Using Table 15-5 and the pressure coefficients developed earlier, the predicted pressure change occurring in the lead cars as the train noses pass is simply given by the difference in C_N just before and after nose passage, times $1/2\rho U^2$, or

$$(1.036 \text{ in.wg})(-0.406 - 0.203) = -0.631 \text{ in.wg}$$

Table 15-5 predicts that the pressure change occurring in the lead car as the nose of one train closes on the tail of the second train will be linear. In this case, the magnitude of the pressure change is given by

$$(1.036 \text{ in.wg})(-1.289 + 0.406) = -0.915 \text{ in.wg}$$

The duration of this linear pressure change is simply

$$\Delta t = \frac{\lambda}{2U} = \frac{500 \text{ ft}}{(2)(46.25 \text{ mph})(1.47 \text{ fps/mph})} = 3.68 \text{ sec}$$

The remainder of the predicted pressure changes in the lead and trailing cars for Figure 15-17 were developed in a similar manner.

Finally, since pressure changes are of primary interest, the predicted pressure in the lead car just before the trains meet has been set equal to the measured pressure in Figure 15-17 to facilitate comparison.

Figure 15-17 shows that the overall changes in pressure and linear rates of pressure change inside the southbound train are predicted reasonably well by the simplified models.

The most notable discrepancy between measured and predicted results in Figure 15-17 is associated with the abrupt changes in pressure predicted by the simplified models when the train noses pass, when the nose of one train passes the tail of the second train, and when the train tails pass. The causes of this discrepancy are thought to arise from:

1. Attenuation of pressure changes by the car body.
2. A short-term breakdown of the one-dimensional flow assumption as the trains transition between the configurations shown in Table 15-5.
3. Failure of the process equations to account for the limited amount of compression of air which does occur during extremely rapid pressure changes.

Unfortunately, it is not possible to determine the exact cause(s) of the observed discrepancy based upon the limited instrumentation employed for the test.

Test M-227. For Test M-227, the train with on-board pressure instrumentation was dispatched northbound from Beaubien Station.

From train speed-time profiles, the speed of the northbound train was about 46 mph during train passage. Similarly, the speed of the southbound trains was about 44 mph. Therefore, average train speed was 45 mph. Assuming standard ambient conditions within the subway and using techniques similar to those applied previously, a detailed comparison of measured and predicted pressure changes was performed and this comparison is shown in Figure 15-18.

Generally, comments made in association with Figure 15-17 are applicable to Figure 15-18, except that for Figure 15-18 the comparison between measured and predicted results is somewhat more favorable.

Conclusions. In spite of discrepancies noted in the discussion of Figures 15-17 and 15-18, it is considered that the process equations of Table 15-5 are suitable for preliminary design calculations. In this context, the process equations of Table 15-5 can be used with confidence to estimate the effects of train speed, blockage ratio, and frictional roughness on pressure transients arising from passing trains.

15.4 MULTI-JUNCTION AND TUNNEL FLOW AERODYNAMICS

The aerodynamic behavior in the far field, that is, the piston-effect tunnel airflow, is directly influenced by the near-field train-induced pressures. Tests were performed specifically to validate the far-field mathematical model in the Berkeley Hills Tunnel Tests (Ref. 2). As explained previously, the METRO tests specifically addressed the piston-action airflow behavior at "Y" and "T" multi-junctions. These multi-junction tests implicitly addressed the far-field theory for both single and bi-directional train operations, since the multi-junction mathematical model requires the far-field piston-action tunnel flows at the junction.

It is important to note that these multi-junction and tunnel-flow tests were performed in order to check the accuracy of the SES program in predicting the overall flow split at "Y" and "T" junctions. The predominant influences on the flow split at a junction are usually the tunnel-wall friction ($\delta LV^2/2D$)

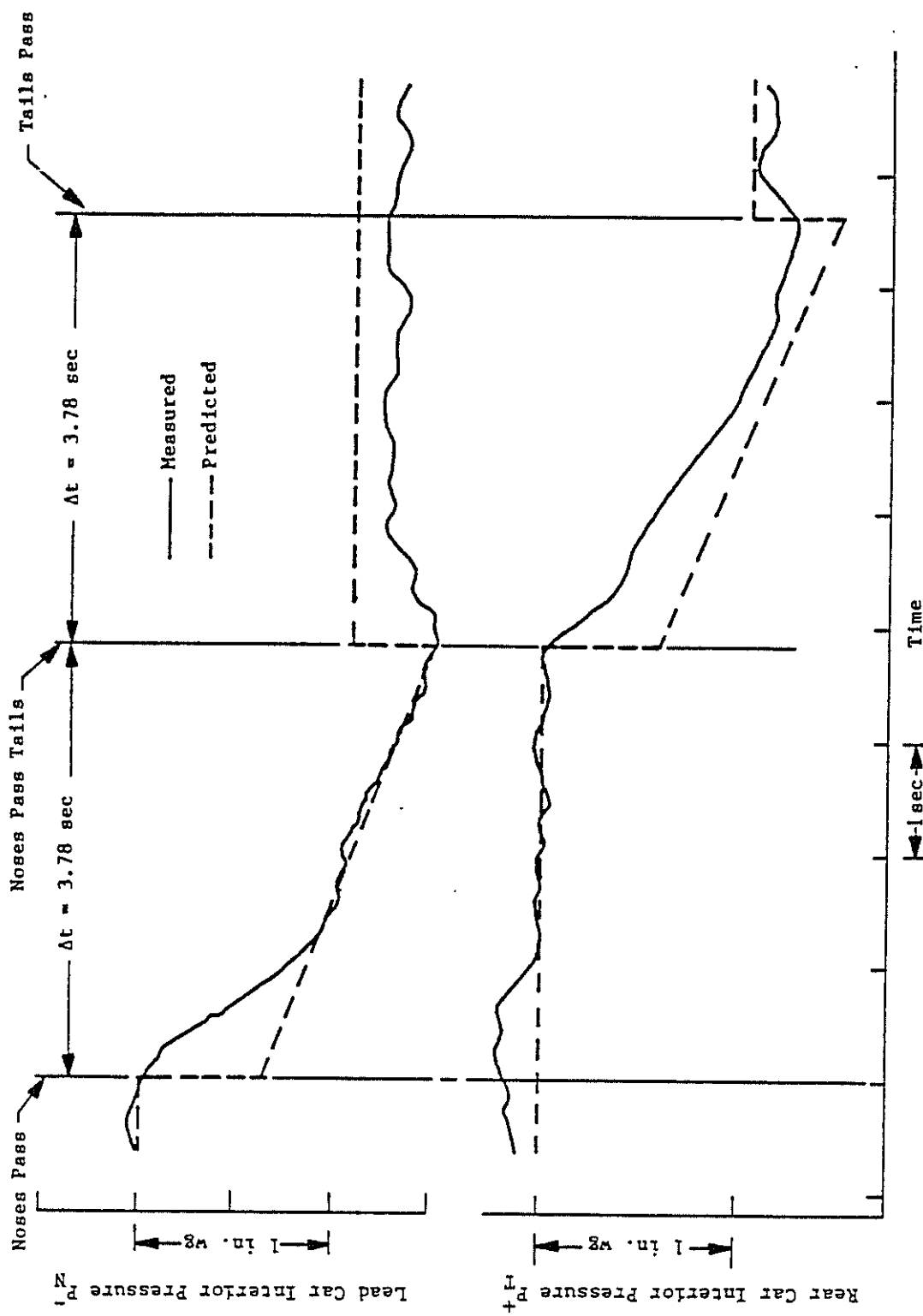


FIGURE 15-18. COMPARISON OF MEASURED AND PREDICTED RESULTS FOR PASSING TRAINS MONTREAL VALIDATION FIELD TESTS - TEST M-227

and geometry-dependent, "minor" ($KV^2/2$) head losses in the tunnel segments forming the junction, and if there is a vent shaft at the junction, the head-loss coefficient of the vent shaft. In addition, the inertia of the airflows in the various tunnels and/or ventilation shafts forming the multi-junction also have a large influence on the overall split of the unsteady flow at the multi-junction. The accuracy of the SES-computed multi-junction flow-split computations is further enhanced by the "multi-junction theory" of Reference 8. This theory addresses the flow losses due to turning or expanding flow at the junction. Since these losses are usually small in comparison with tunnel-friction losses and vent-shaft head-loss coefficients, this theory often results in a fine tuning of the computed flow splits.

The "T" junction examined was the junction of the tunnel between Cremazie and Jarry Stations and fan shaft 4504 at site F (see Figure 15-5). The "Y" junction examined was the junction of the single-track tunnel leading to the workshops and the tunnel between Sauvé and Cremazie Stations at site D (see Figure 15-5).

Seven test runs were conducted for the multi-junction field validation (see Table 15-2). There were five one-train tests (M-211 through M-215) and two two-train tests (M-226 and M-227). Each test train maintained constant speed within the tunnel after accelerating from either Beaubien Station northbound: (tests M-212, M-214, M-226 and M-227); or Henri Bourassa Station southbound tests: (M-211, M-213, M-215, M-226 and M-227).

As shown in Figure 15-5, various shafts and station entrance-ways were closed in order to channel a greater volume of airflow toward the junction being examined in each particular test.

Prior to undertaking the task of comparing the test findings with the SES program calculations, it was necessary first to ascertain the meaning of the point-velocity measurements in terms of the bulk-fluid velocity computed by the SES program. [Velocity traverses conducted under steady-state conditions with fan-induced airflows indicated that at the transducer locations at sites C, E, F and G the flow velocities were representative of the actual bulk flows (see Figure 15-19). Thus the measured velocity was taken as representative of this bulk-flow velocity.]

The velocity profile is, of course, distorted when unsteady flow conditions exist. During acceleration of the air, inertial forces play a

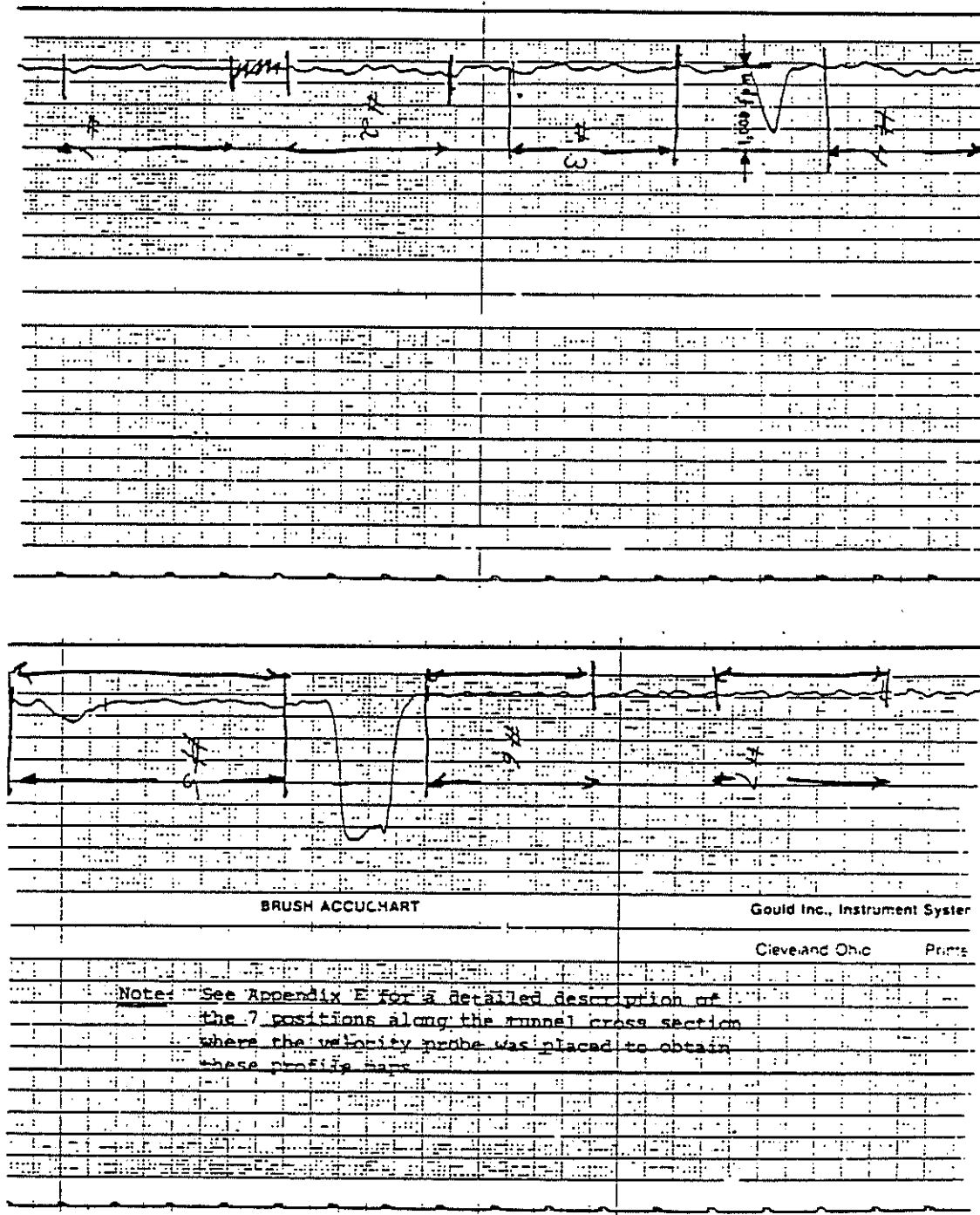


FIGURE 15-19. VELOCITY PROFILE MAP FOR BOTH FORWARD AND REVERSE FLOW FOR TEST M-001 AT INSTRUMENT SITE G

a relatively larger role than viscous forces, and the resulting profile is more uniform across the tunnel than the steady-state profile. The velocity measurement would thus be slightly higher than the bulk flow. When the air is slowing, the deceleration is first noted in the layers near the wall (Ref. 9). In this situation, the measured velocity would be slightly low in relation to the actual bulk-flow velocity.

15.4.1 Tests With One Train

Due to a lack of sufficient tractive effort at speeds over 40 mph, at speed limitations in certain portions of the system, and at speed control sensitivity, the trains in the multi-junction tests were not able to maintain constant speed throughout each test. As a result, explicit train performance was used in the corresponding SES program simulations to duplicate the actual train performance. The train speed-time profile for test M-211, typical of all tests, is shown in Figure 15-20.

Comparisons of the field-measured tunnel and fan-shaft airflows and the corresponding SES program calculations for the one-train tests are shown in Figures 15-21 through 15-31. The initial airflow, on the order of 180 to 240 fpm, is the natural ventilation effect in the METRO system. This value was entered as an initial flow for the SES program simulations. The SES program calculations were consistently within the accuracy of the reduced field data, being within ± 10 percent for the steady-state airflows.

During the acceleration of the air, the SES program calculations show a slightly lower rate than the measured value, while the reverse occurs during deceleration of the air. These differences are at least partly attributable to the previously described effect of velocity profile distortion on the measured-to-bulk velocity relationship. Further differences were caused by various airflow leaks in the system. As stated previously, the system could not be sealed thoroughly due to leaking dampers in various shafts and doors that did not completely seal the entrance ways to the stations. These leaks did not materially affect the near-field tests, but they had large effects upon the multi-junction tests. In order to simulate the multi-junction tests, the magnitude of these leaks had to be determined.

Figures 15-23 through 15-25 demonstrate the order of magnitude of these system airflow leaks. The difference between the initial steady-state

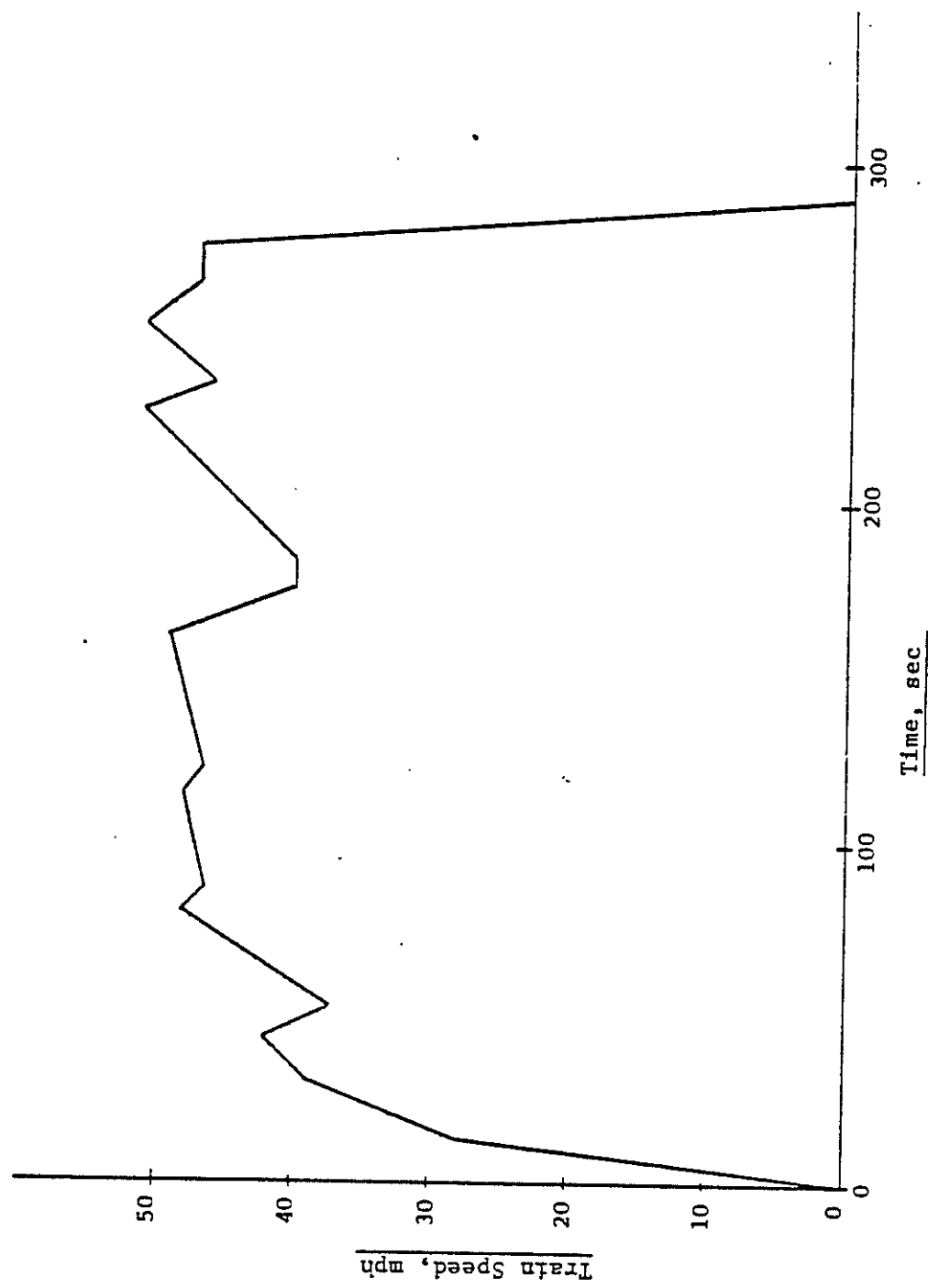


FIGURE 15-20. TRAIN SPEED-TIME PROFILE FOR TEST N-211

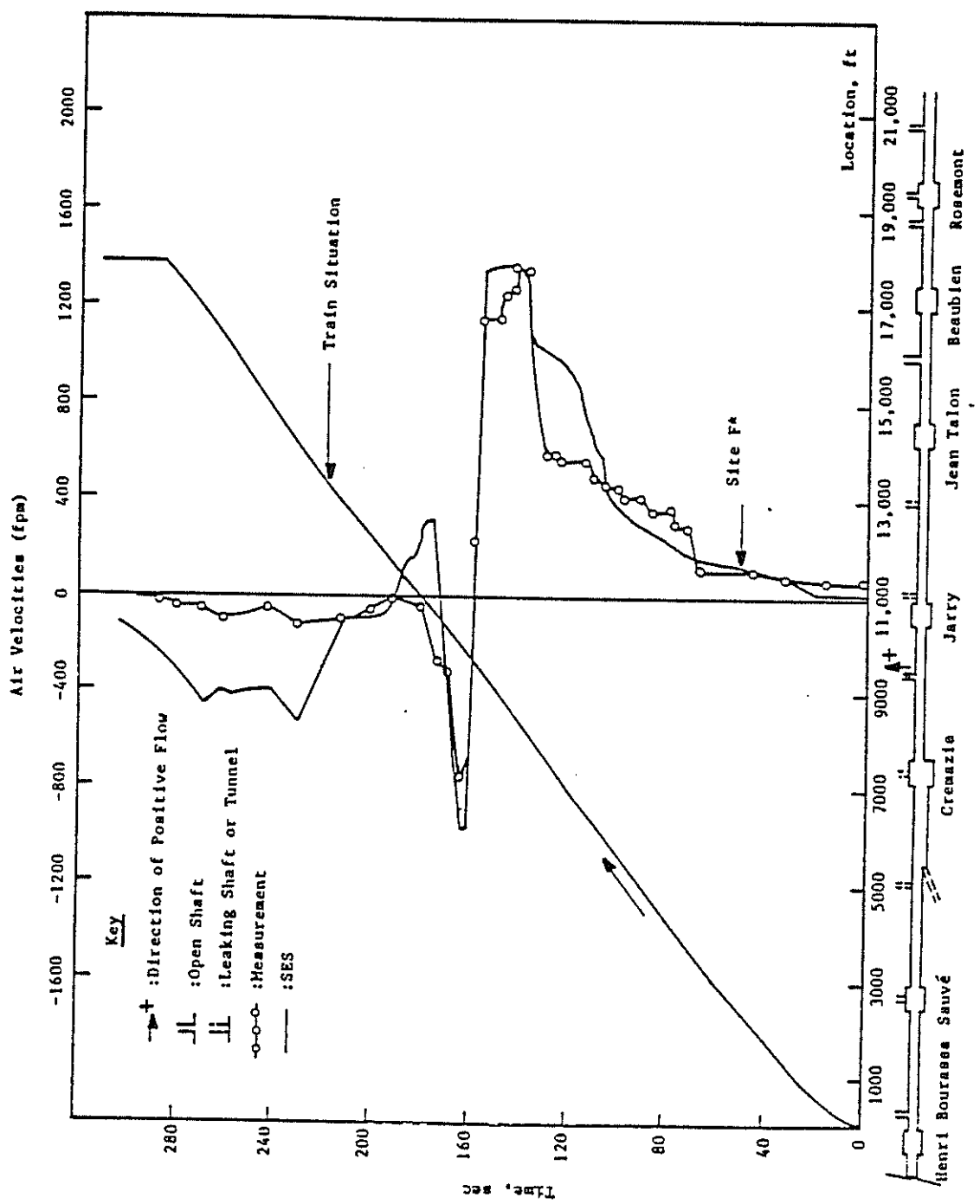


FIGURE 15-21. MEASURED VS SES AIR VELOCITY - TEST M-211 SITE F

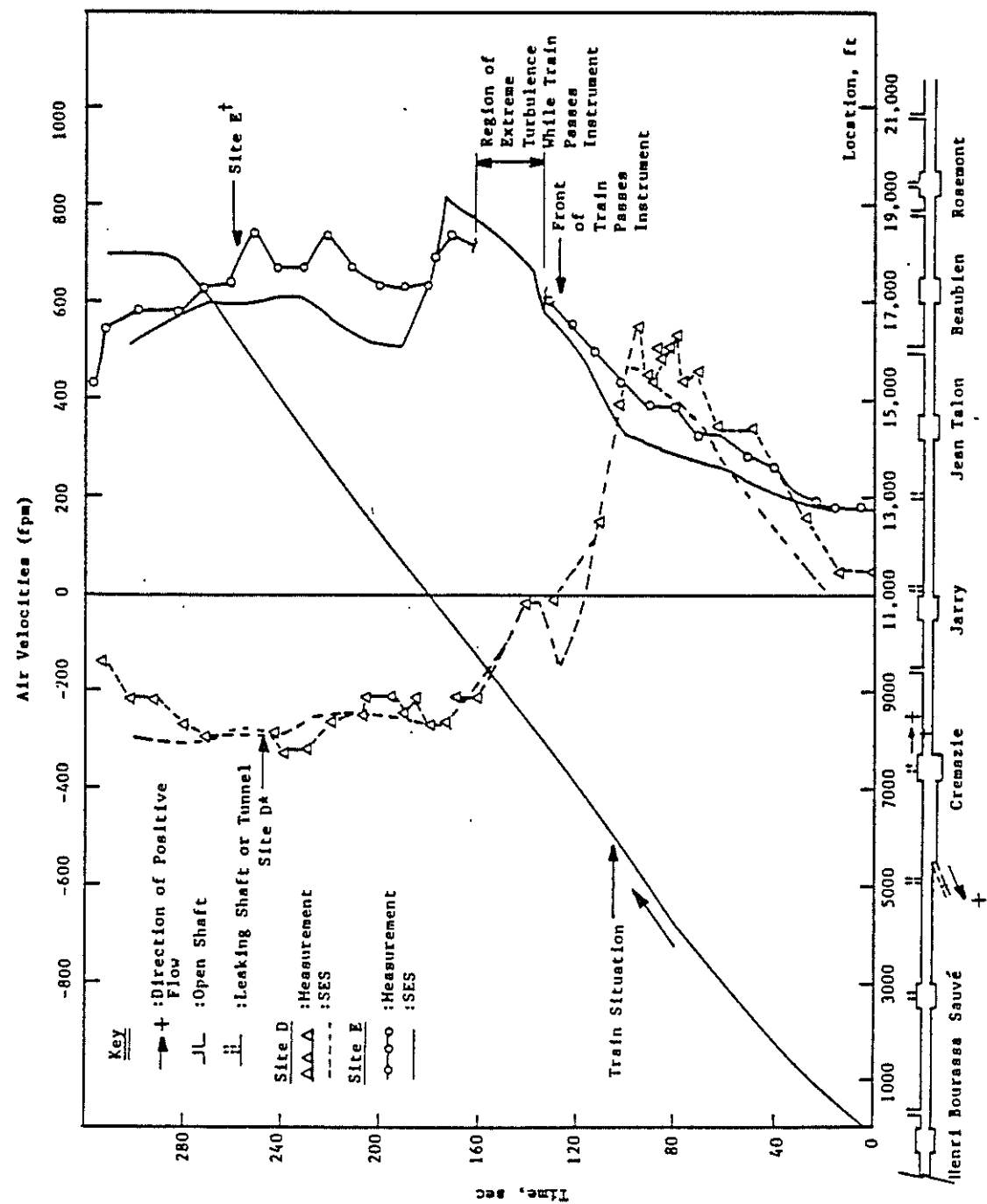


FIGURE 15-22. MEASURED VS SES AIR VELOCITY - TEST M-211 SITES D AND E

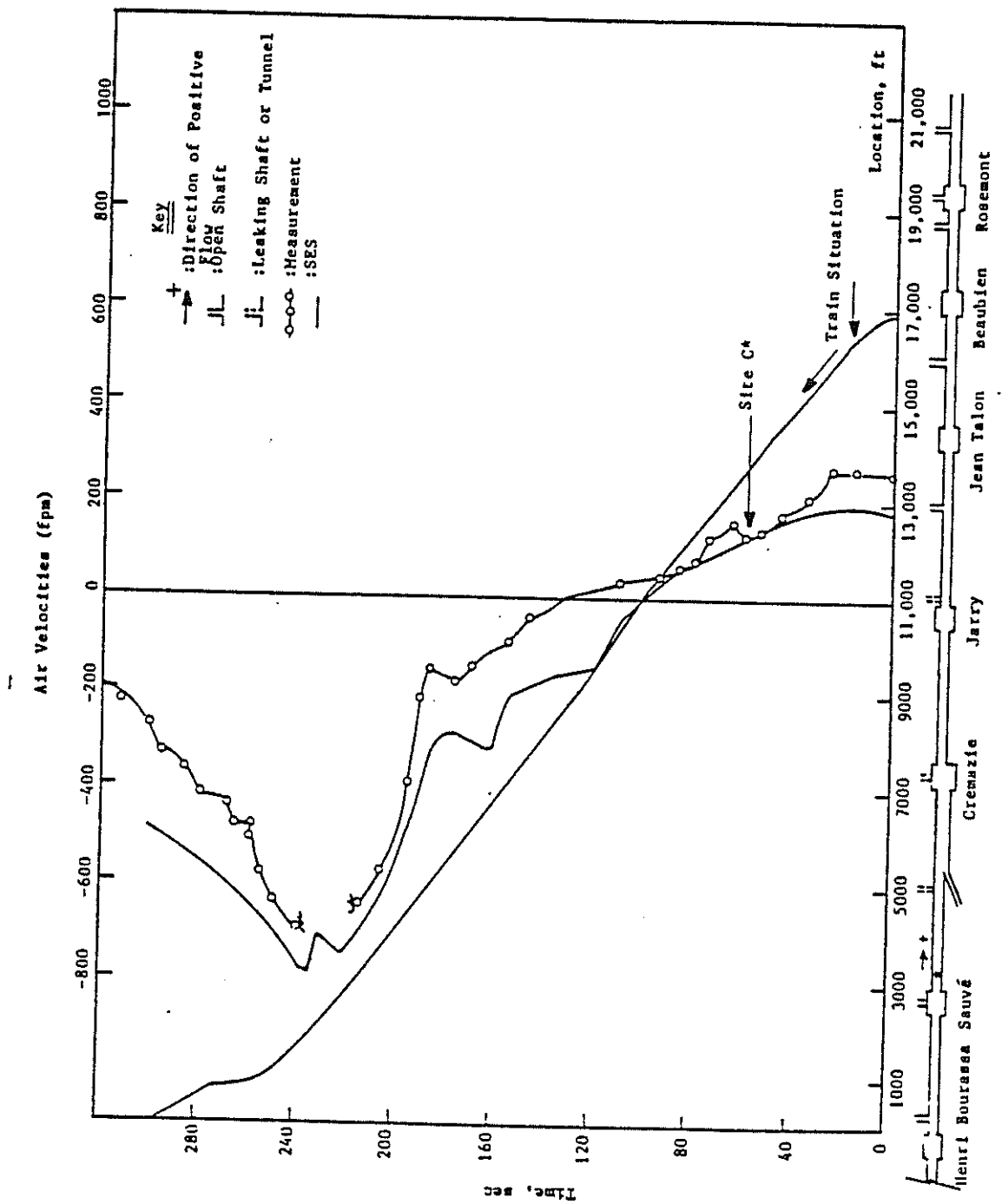


FIGURE 15-23. MEASURED VS SES AIR VELOCITY - TEST M-212 SITE C

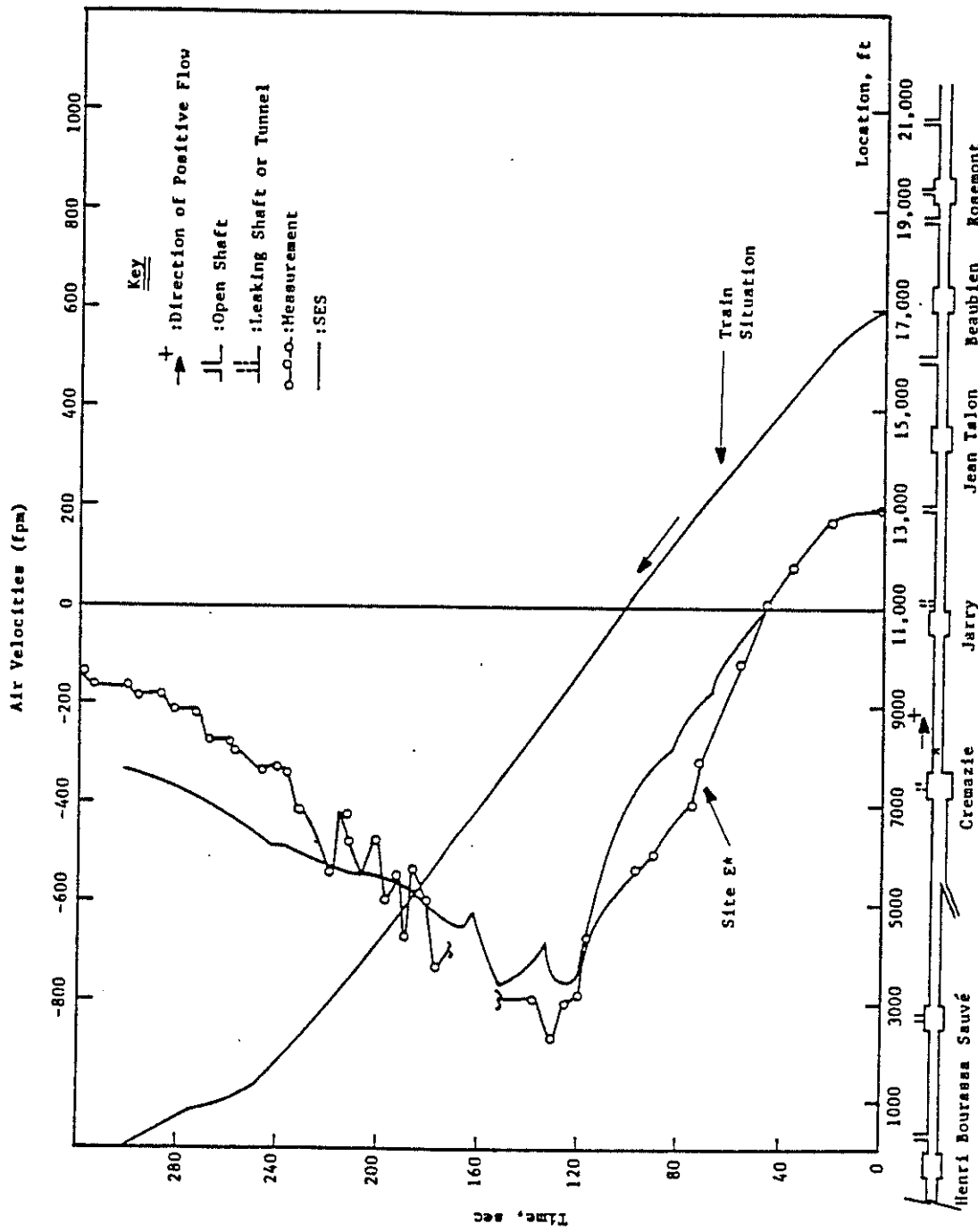


FIGURE 15-24. MEASURED VS SES AIR VELOCITY - TEST M-212 SITE E

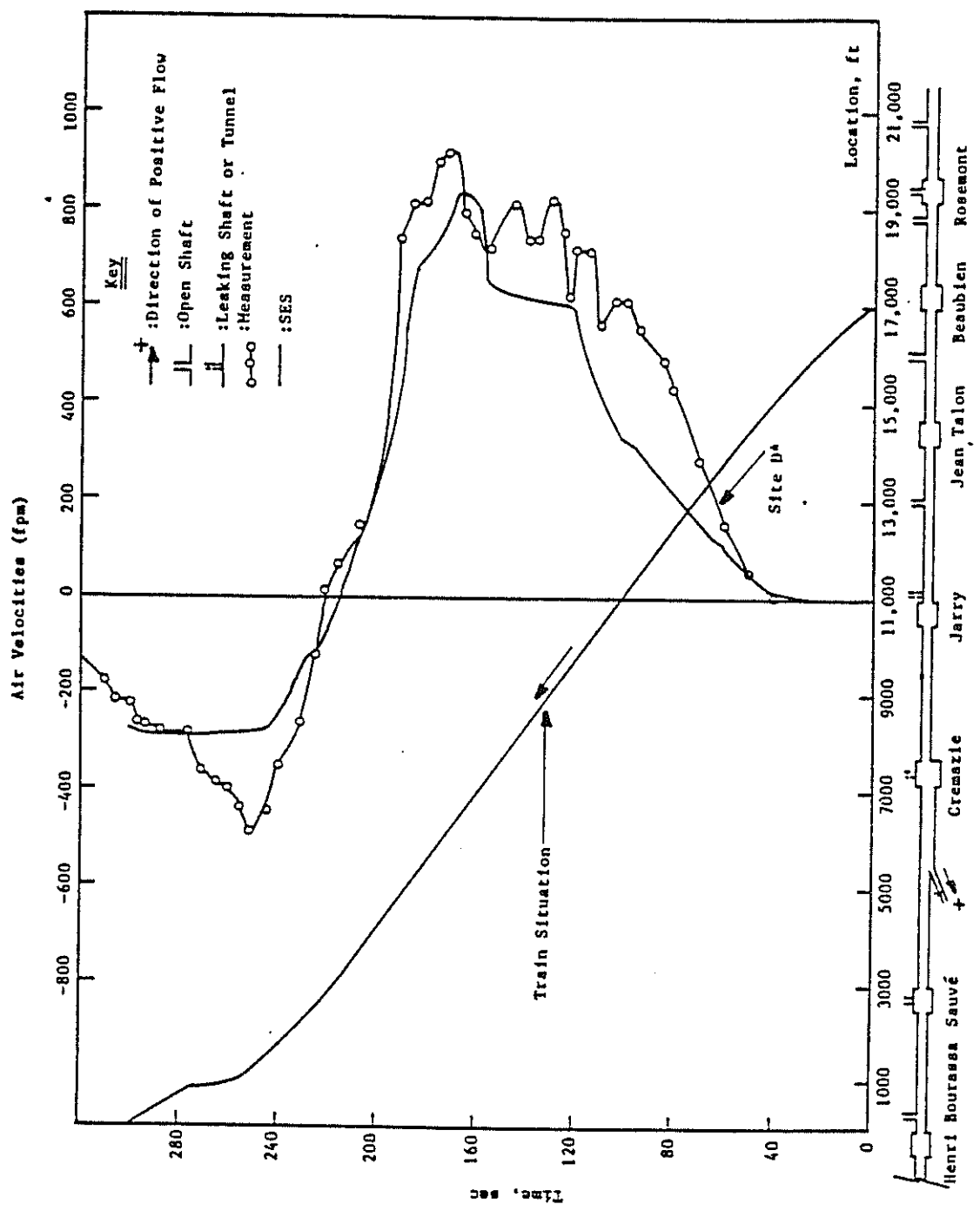


FIGURE 15-25. MEASURED VS SES AIR VELOCITY - TEST M-212 SITE D

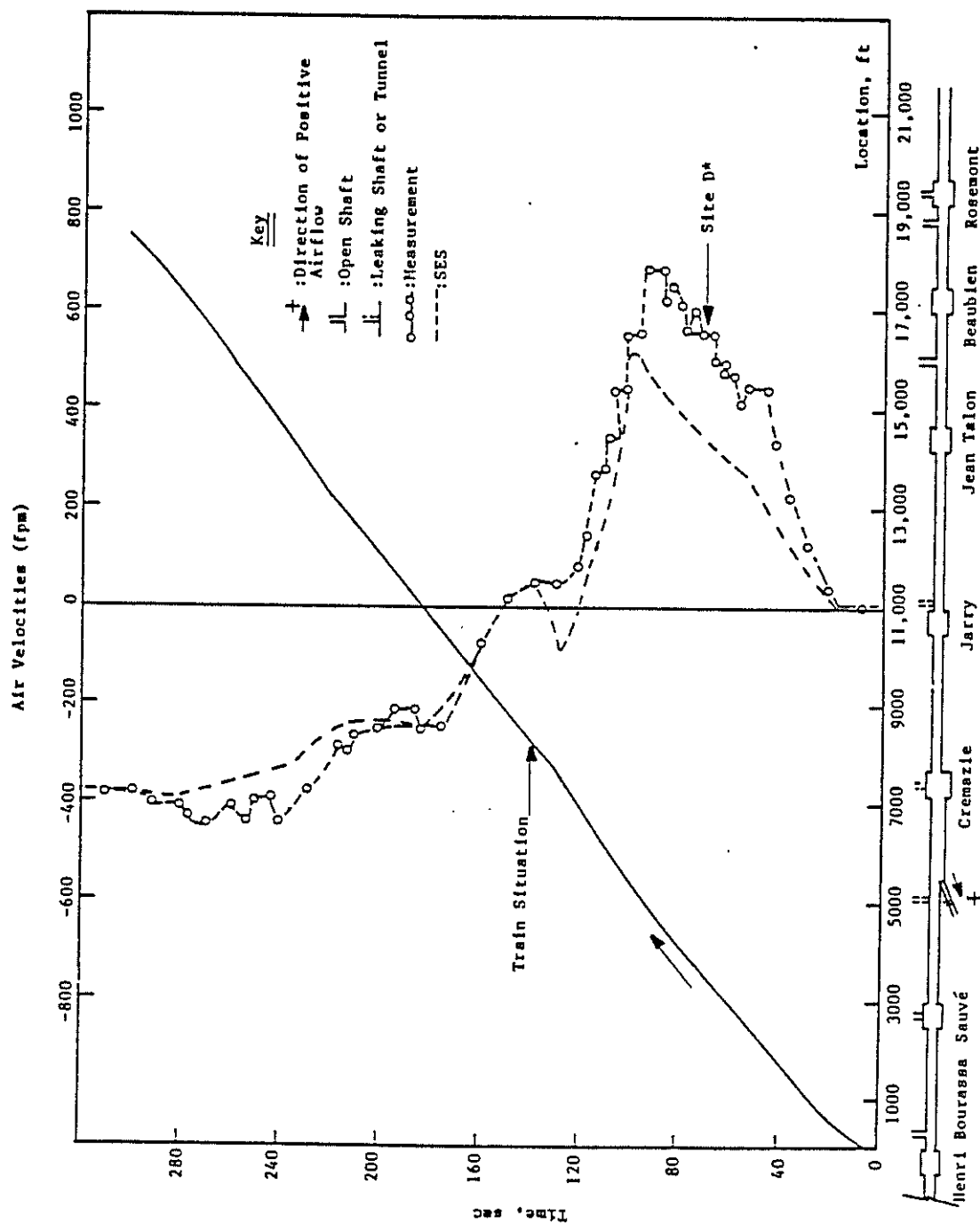


FIGURE 15-26. MEASURED VS SES AIR VELOCITY - TEST M-213 SITE D

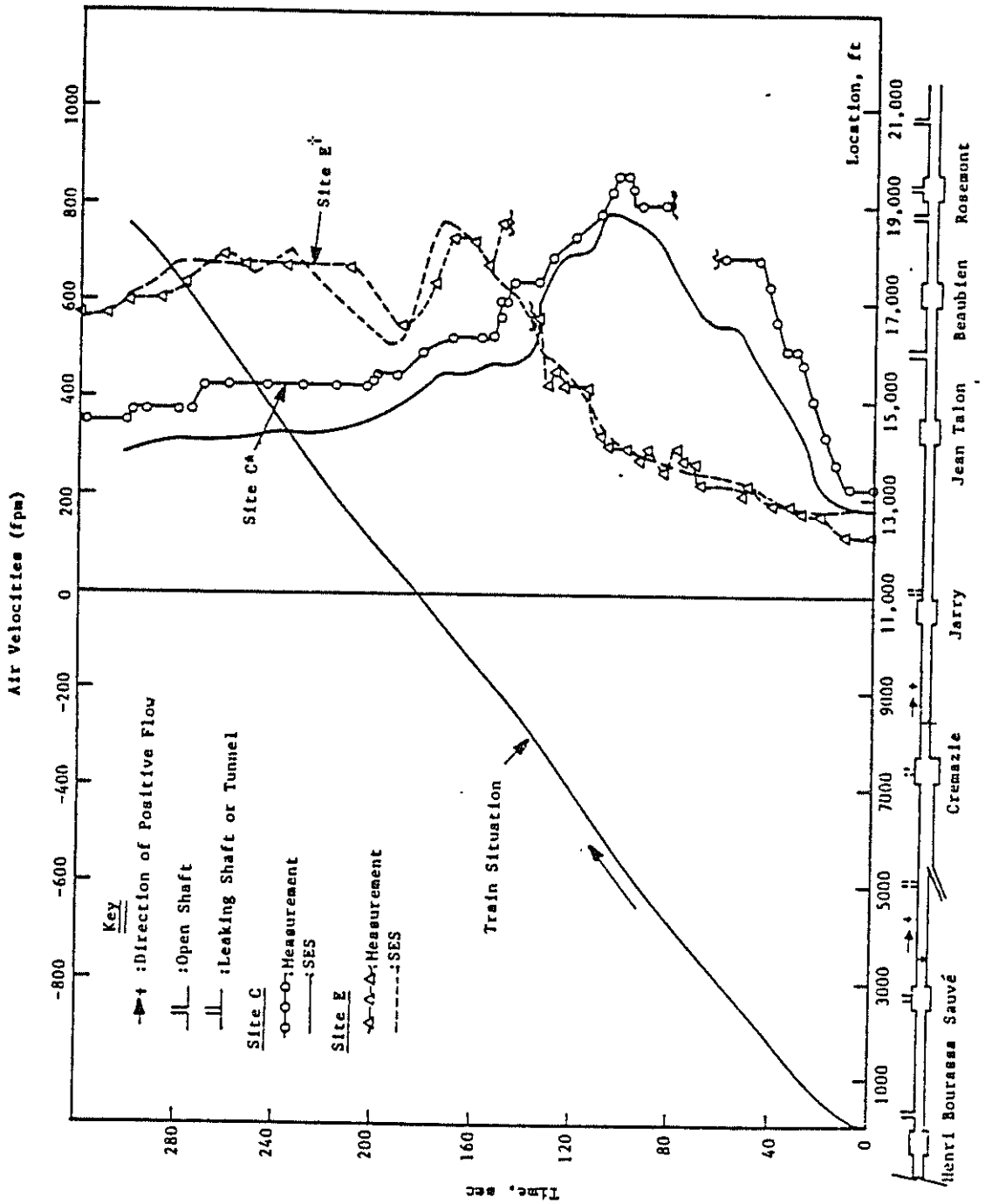


FIGURE 15-27. MEASURED VS SES AIR VELOCITY - TEST M-213 SITES C AND E

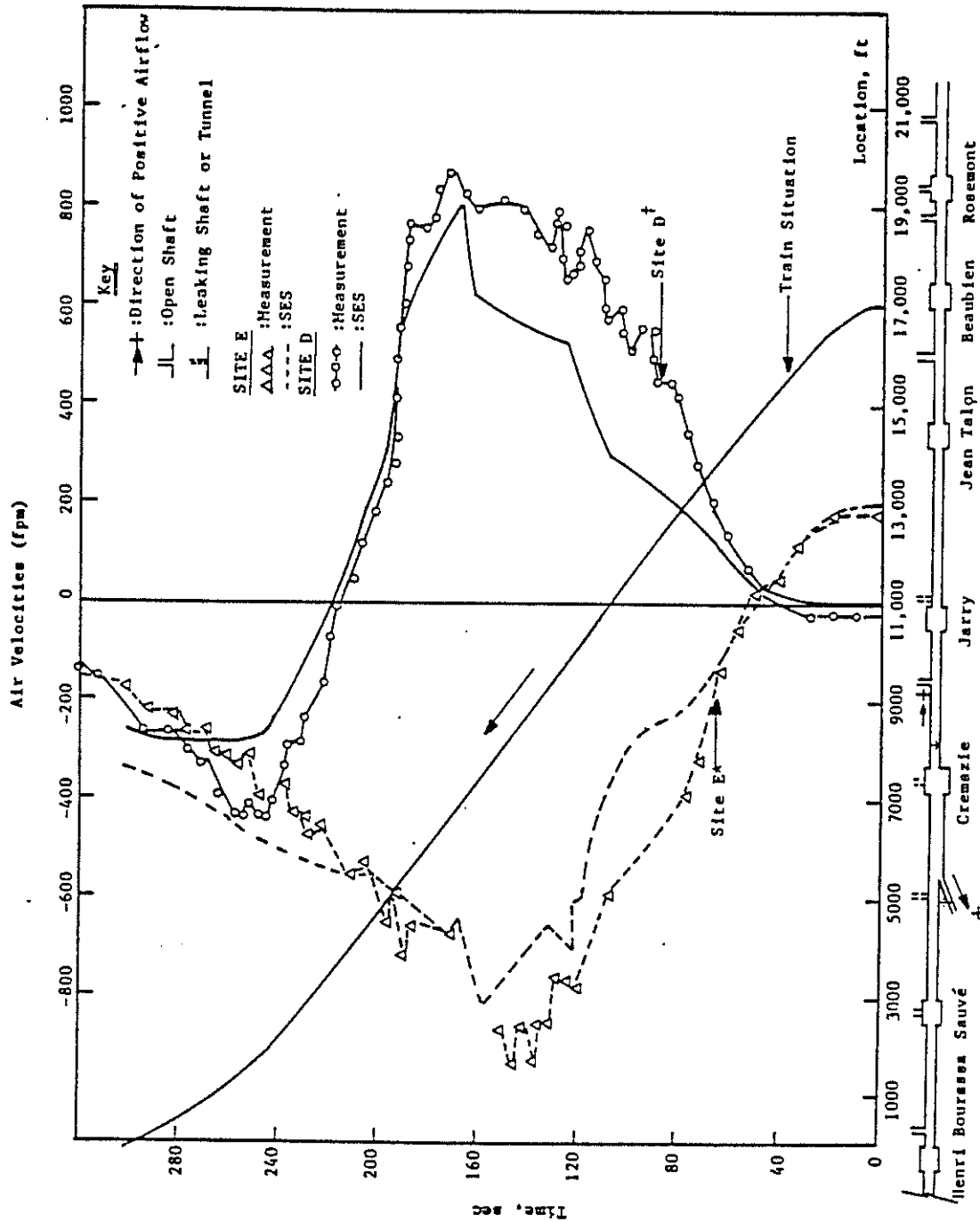


FIGURE 15-28. MEASURED VS SES AIR VELOCITY - TEST M-214 SITES D AND E

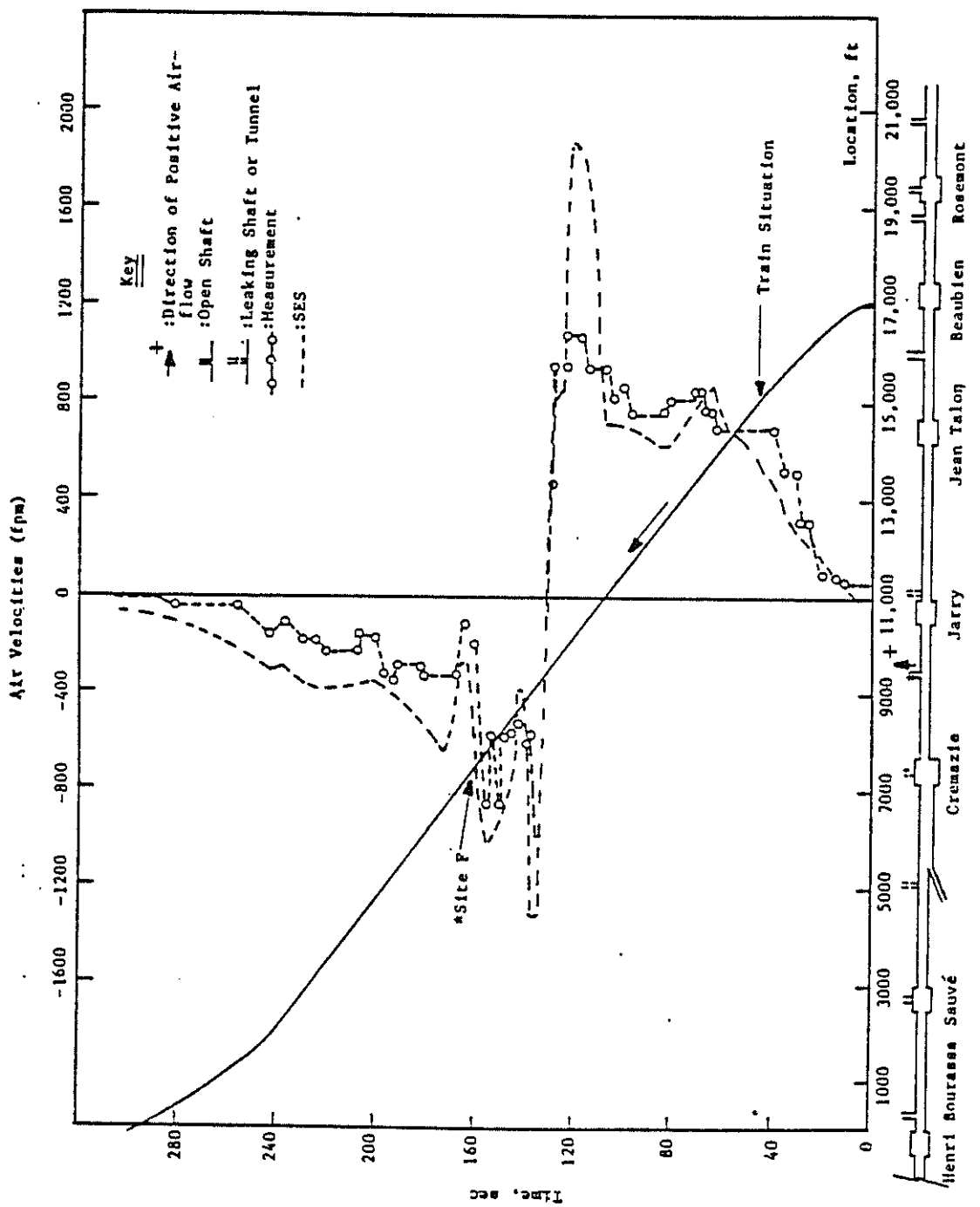


FIGURE 15-29. MEASURED VS SES AIR VELOCITY - TEST M-214 SITE F

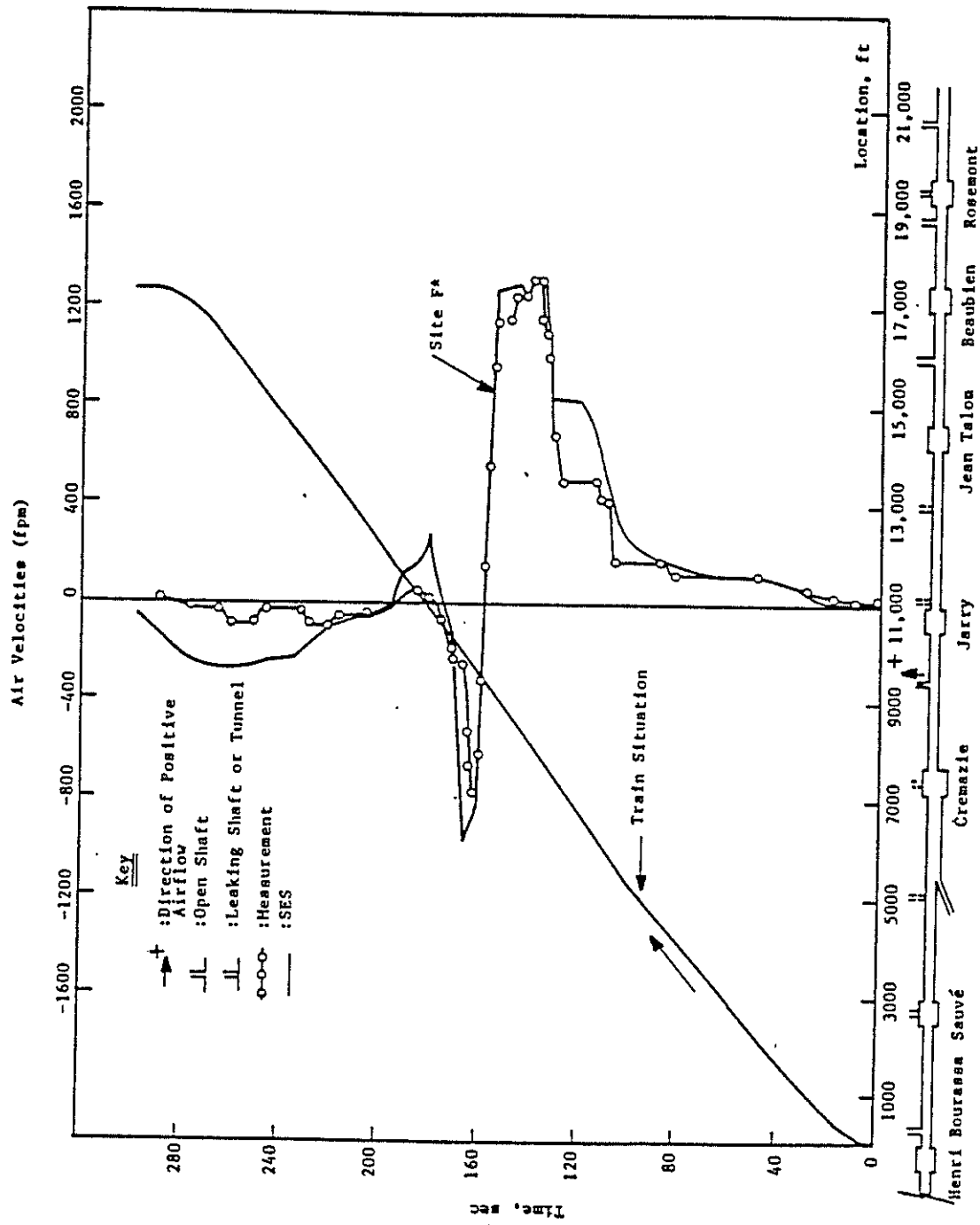


FIGURE 15-30. MEASURED VS SES AIR VELOCITY - TEST M-215 SITE F

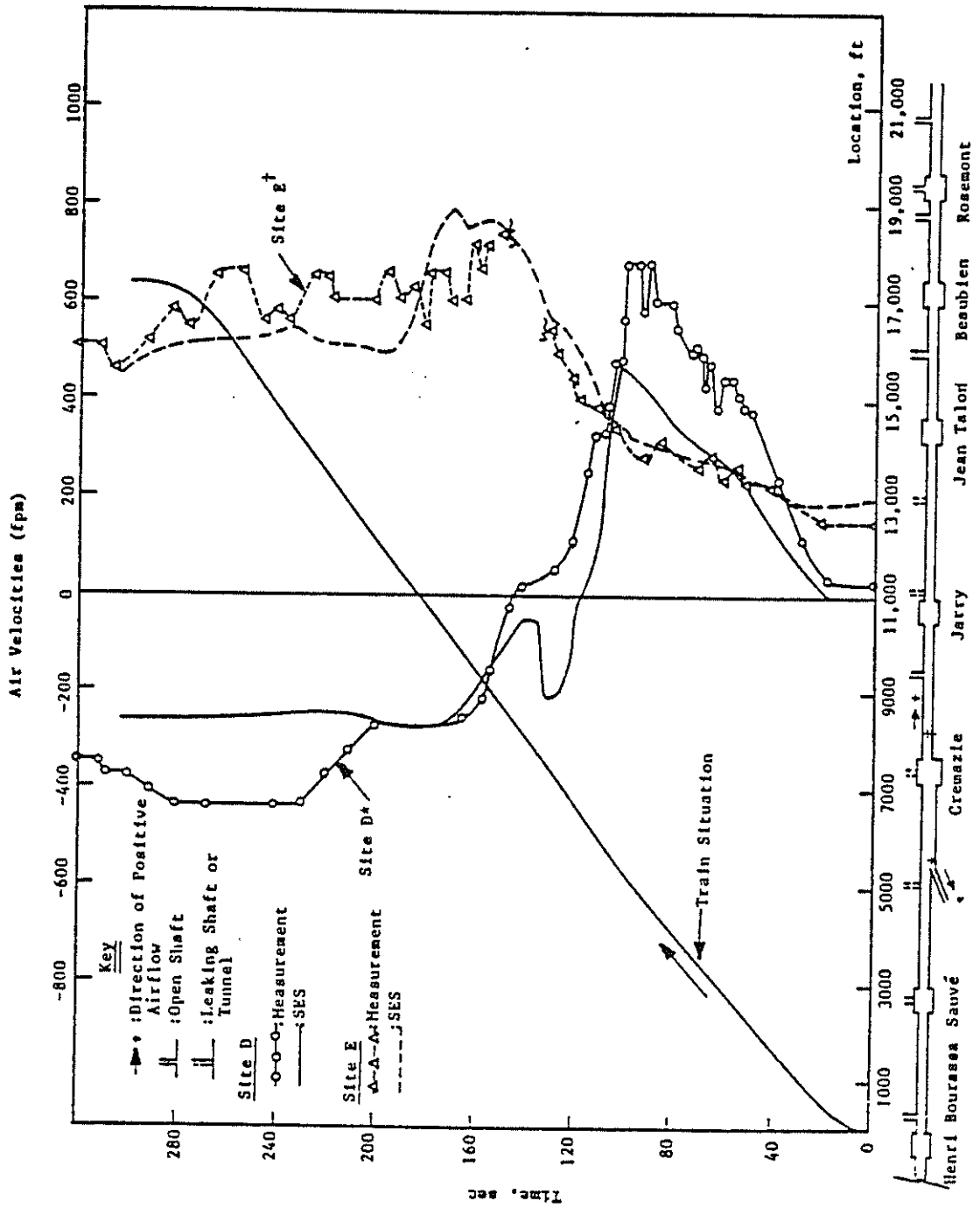


FIGURE 15-31. MEASURED VS SES AIR VELOCITY - TEST H-215 SITES D AND E

airflows at tunnel site E and tunnel site C is 60 fpm. The cross-sectional areas of both of these tunnel sites are the same. As shown in Figure 15-25, there was no flow in the single-track tunnel at site D. Therefore, from continuity considerations, some of the airflow through the tunnel at site C must have left the system between Sauve Station and the tunnel south of Cremazie Station. Through both field inspection and data reduction, it was determined that there was a leak in Cremazie station. The approximate magnitude of this leak in cfm is the difference in the tunnel flows at sites C and E times the cross-sectional area of the tunnel (338 ft^2). For the steady-state flow case cited above, the approximate magnitude of the leak was as follows:

$$(260 - 200) \text{ fpm} \times (338) \text{ ft}^2 = 20,280 \text{ cfm.}$$

Further data reduction in conjunction with the theory of continuity of flow revealed the time-dependent behavior of these airflow leaks. These airflow leaks were then accounted for in the appropriate SES program simulations by estimating the leak area and impedance.

To verify the method used to approximate the system airflow leaks, comparisons were made between the SES-predicted flows at a leak and the corresponding actual flow determined by observing flow continuity in the data. Figure 15-32 shows the comparison of the actual and the SES-predicted airflows through the leak in Cremazie Station for test M-212. This comparison is expressed in terms of equivalent tunnel-flow velocity to demonstrate the leak magnitude in relation to the tunnel-flow measurements (Figures 15-23, 15-24 and 15-25). Peak tunnel flows on the order of 800 fpm were recorded during these tests. The equivalent peak tunnel flow through the leak in Cremazie Station on the order of 400 fpm emphasizes the potential for error and the necessity for including a characterization of these leaks in the SES program simulations.

An additional possible source of error was introduced in the multi-junction tests at the fan shaft (site E) forming the "T" junction. This fan shaft had a free-floating counter-weighted damper at the top of the shaft (see Figure 15-33). This damper served two purposes, the first being to relieve the pressure in the tunnel when a train travelled beneath the fan shaft, and second to prevent cold ambient air during the winter from entering the system when trains were not in the vicinity of the fan shaft. Therefore,

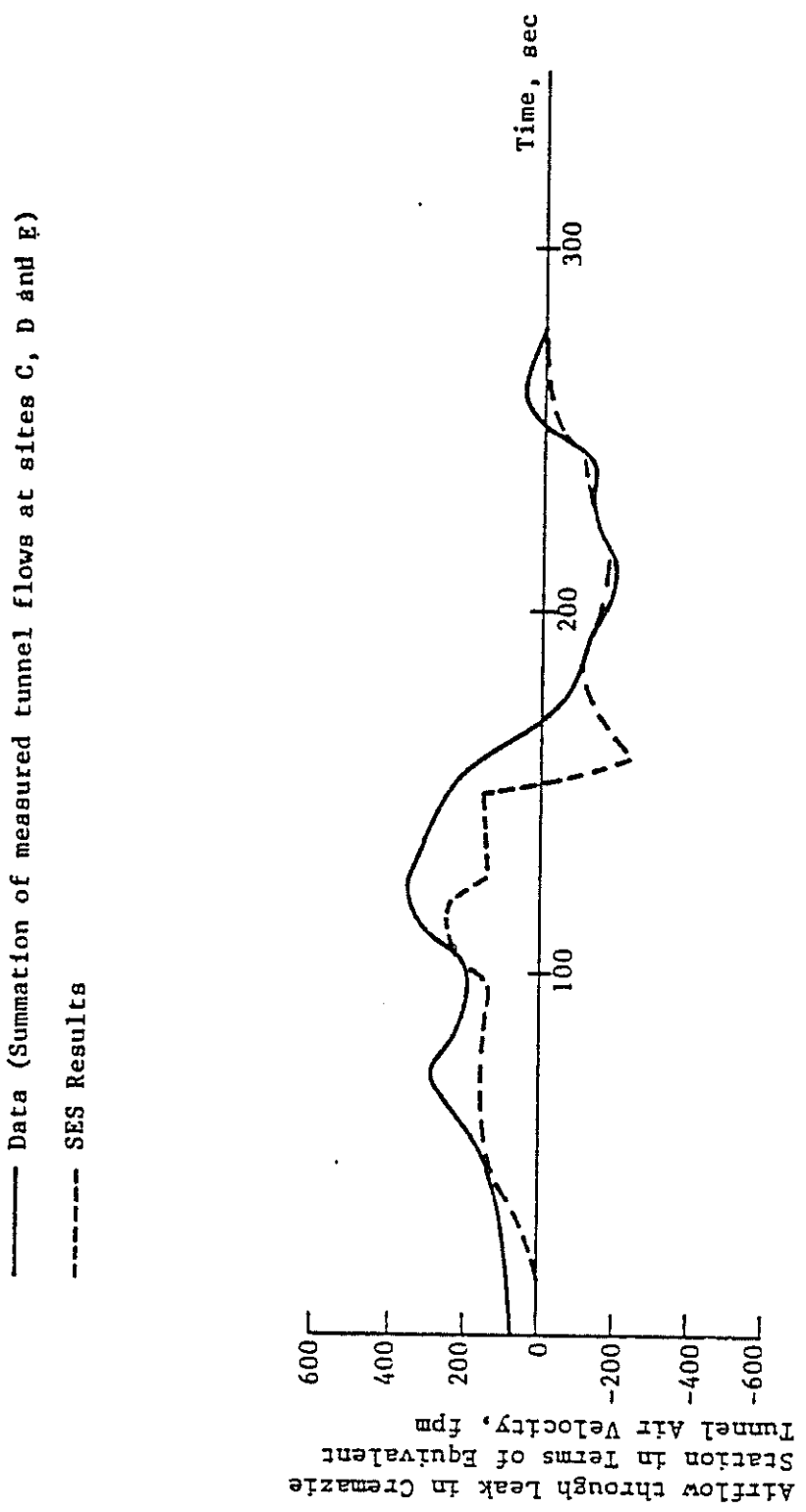


FIGURE 15-32. COMPARISON OF THE ACTUAL AND SES COMPUTED AIRFLOWS THROUGH LEAK IN CREMAZIE STATION FOR TEST M-212

FAN SHAFT 4504

Notes:

1. All dimensions not to scale
2. Fan is off during morning and evening rush hour
3. Counter-weighted damper is free floating and capable of 180° swing

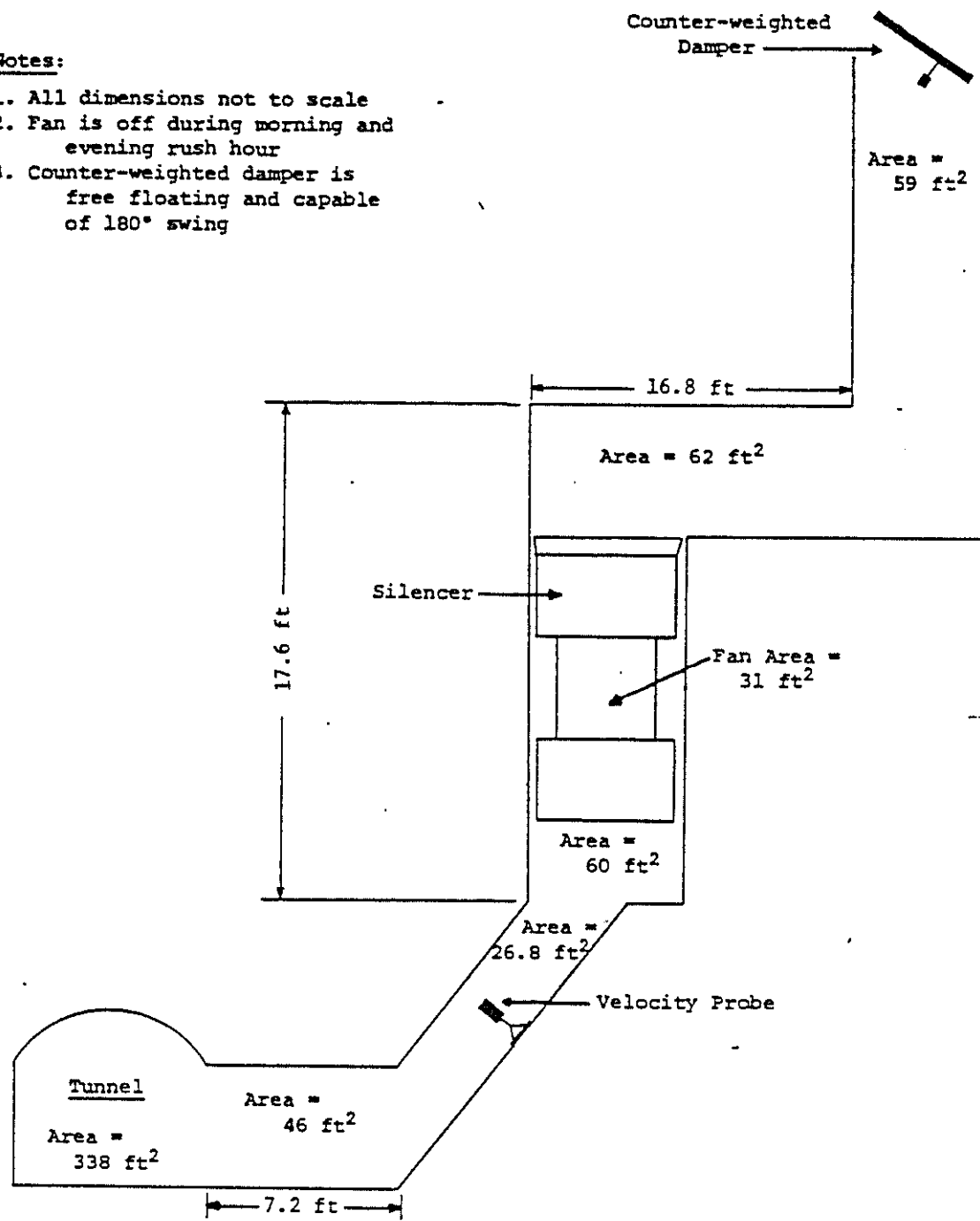


FIGURE 15-33. SCHEMATIC DRAWING OF FAN SHAFT 4504

this fan shaft acted as a closed shaft when no trains were in the vicinity of the "T" junction and as an open shaft when trains were in the vicinity of the "T" junction. The damper is locked open in the summer months to increase the system ventilation. A mathematization of the dynamic response of this damper had to be included in the SES program to enable comparison runs, and as stated previously, the complications caused by this free-floating counter-weighted damper added an additional potential for error into the SES program computations. The analysis of the dynamic response of the counter-weighted damper is given in Reference 5.

Tests M-211, M-214 and M-215 involved measuring the airflow at both the "T" and the "Y" junction. A schematic drawing of the fan shaft forming the "T" junction is given in Figure 15-33. As this figure shows, the cross-sectional areas of the fan shaft where the velocity probe was located is 26.8 square feet. The cross sectional area of the tunnel section forming this "T" junction is 338 square feet. Due to this large difference in cross-sectional areas between the fan shaft and the tunnel, the air velocities in the fan shaft would be almost 13 times greater than the air velocities in the tunnel for a given volumetric airflow. Therefore, a small error in the SES-predicted tunnel flows can result in a large error in the SES-predicted fan-shaft flows (a 10 fpm error in the SES-predicted tunnel air velocity can result in a 126 fpm error in the SES-predicted fan-shaft air velocity).

The SES-predicted airflows provided excellent agreement with the measured airflows, especially when considering the manner in which the system air leaks were approximated, the existence of the counter-weighted damper at the top of the fan shaft, and the large differences in cross-sectional area between the tunnel and the fan shaft. The SES-predicted tunnel air velocities at sites D and E were almost always within 100 fpm of the measured air velocities for tests M-211, M-214 and M-215 (see Figures 15-22, 15-28 and 15-31). The SES-predicted air velocities in fan shaft 4504 (site F) were also very close to the measured air velocities for tests M-211, M-214 and M-215 (see Figures 15-21, 15-29 and 15-30). As seen in these figures, the SES-predicted higher air velocities than were measured in the fan shaft after the test train had passed the fan shaft and the flow reversed from outflow to inflow. This overprediction of air velocity is mostly attributable to two of the factors mentioned previously-- namely, the existence of the counter-weighted damper at the top of the fan shaft and the gross difference

between the tunnel and the fan shaft cross-sectional areas. In addition, as seen in Figures 15-21, 15-24 and 15-30, the SES program appears to overpredict the magnitude of the abrupt flow changes (during both inflow and outflow) that occur when the test train traverses beneath the fan shaft. A partial explanation for this observation is the assumption of incompressible flow in the SES aerodynamic subprogram. When the train passes under the fan shaft into a region of relatively slower airflow, wave compressibility effects may become important for a short period of time, acting to dampen the abrupt flow changes.

An additional contribution to the difference between observed and predicted behavior traces to the time response of the anemometer used for these flow measurements (see Ref. 5). This response time is of the same order as the time span over which the abrupt flow changes occur. As a result, the measurements do not accurately portray the extreme flow changes which occur within a very short period of time.

Fan shaft 4504 was sealed for tests M-212 and M-213 and only the airflows at the "Y" junction were examined. As seen in Figures 15-23 through 15-27, the SES-predicted air velocities at sites C, D and E were generally within 100 fpm of the measured air velocities at these sites. The discrepancies between the data and the SES-predicted airflows in tests M-212 and M-213 are attributed for the most part to the previously mentioned air leaks in the system.

15.4.2 Tests with Two Trains

As in the tests with one train, the SES program comparisons employed explicit train performance to duplicate the actual train performance in tests M-226 and M-227. Comparisons of the field-measured tunnel and/or fan-shaft airflows and the corresponding SES program calculations for the two train tests are shown in Figures 15-34 through 15-38.

An additional source of error not existent in the single-train tests was introduced in the two-train tests by the relative train operation of the two test trains. In the single-train tests, any slight time shifts in train operation (± 2 seconds) between the data and the SES computations were insignificant because the resulting SES program airflows could be shifted in time to coincide with the data. Small shifts in the SES program results to

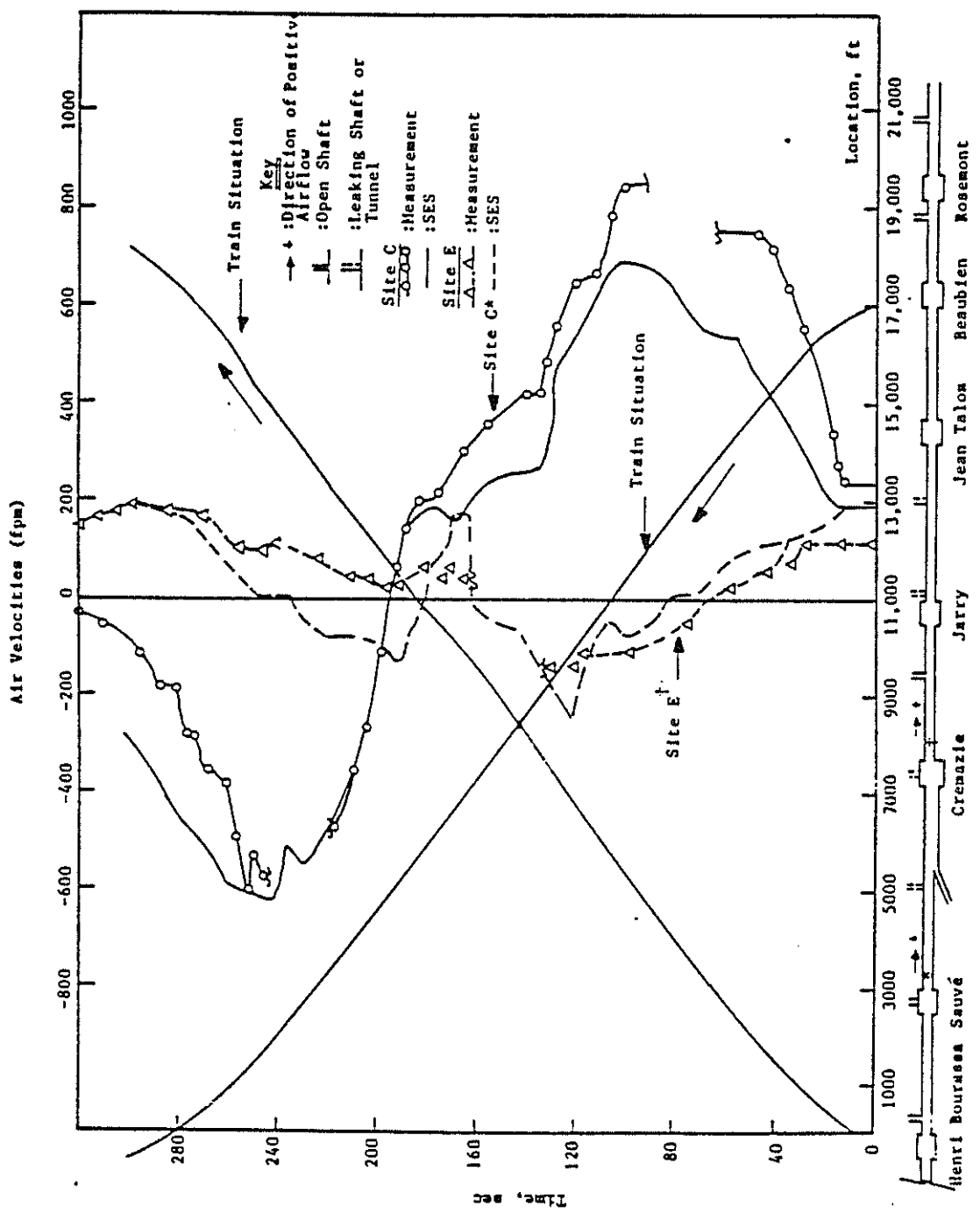
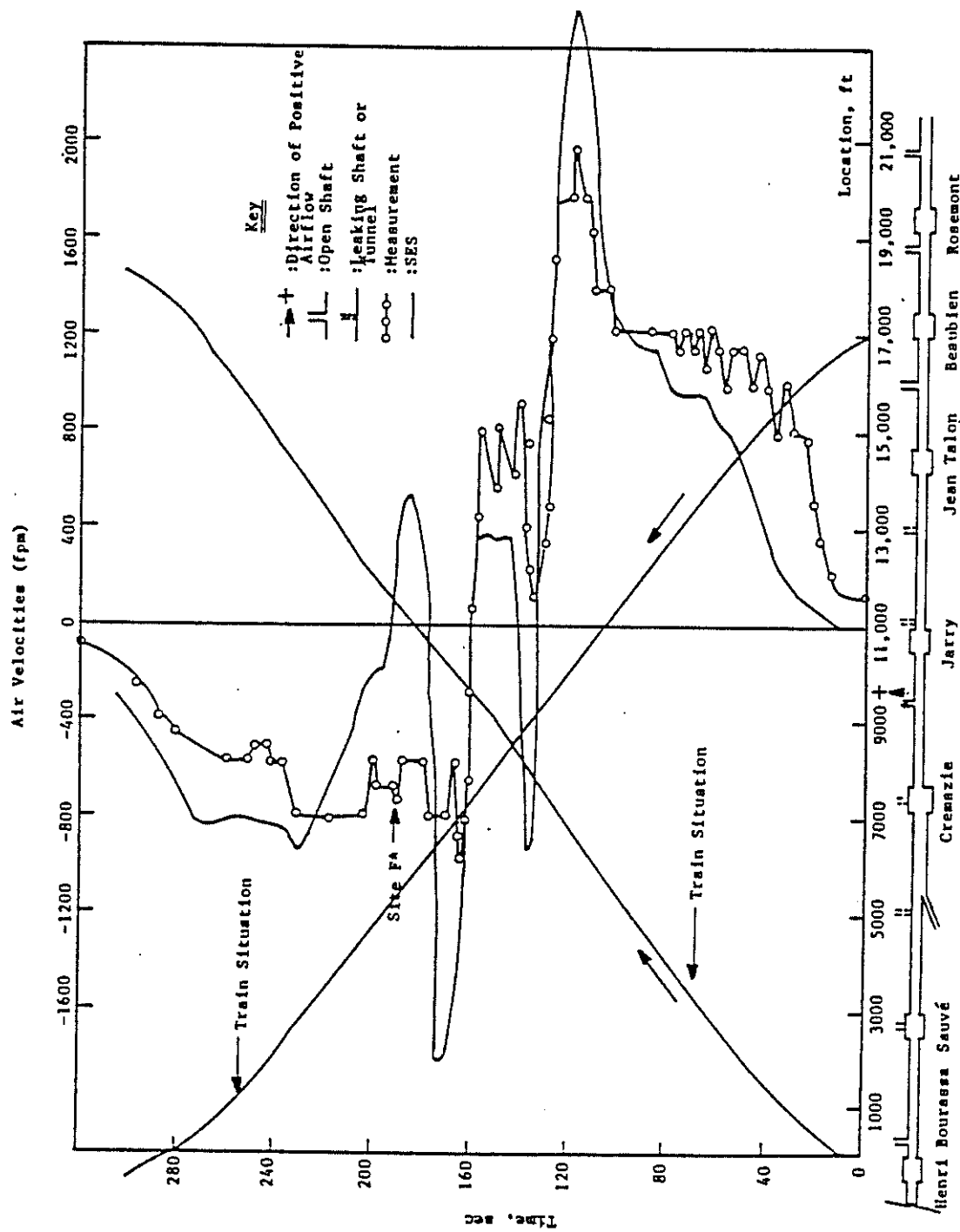


FIGURE 15-34. MEASURED VS SES AIR VELOCITY - TEST H-226 SITES C AND E



• FIGURE 15-35. MEASURED VS SES AIR VELOCITY - TEST M-226 SITE F

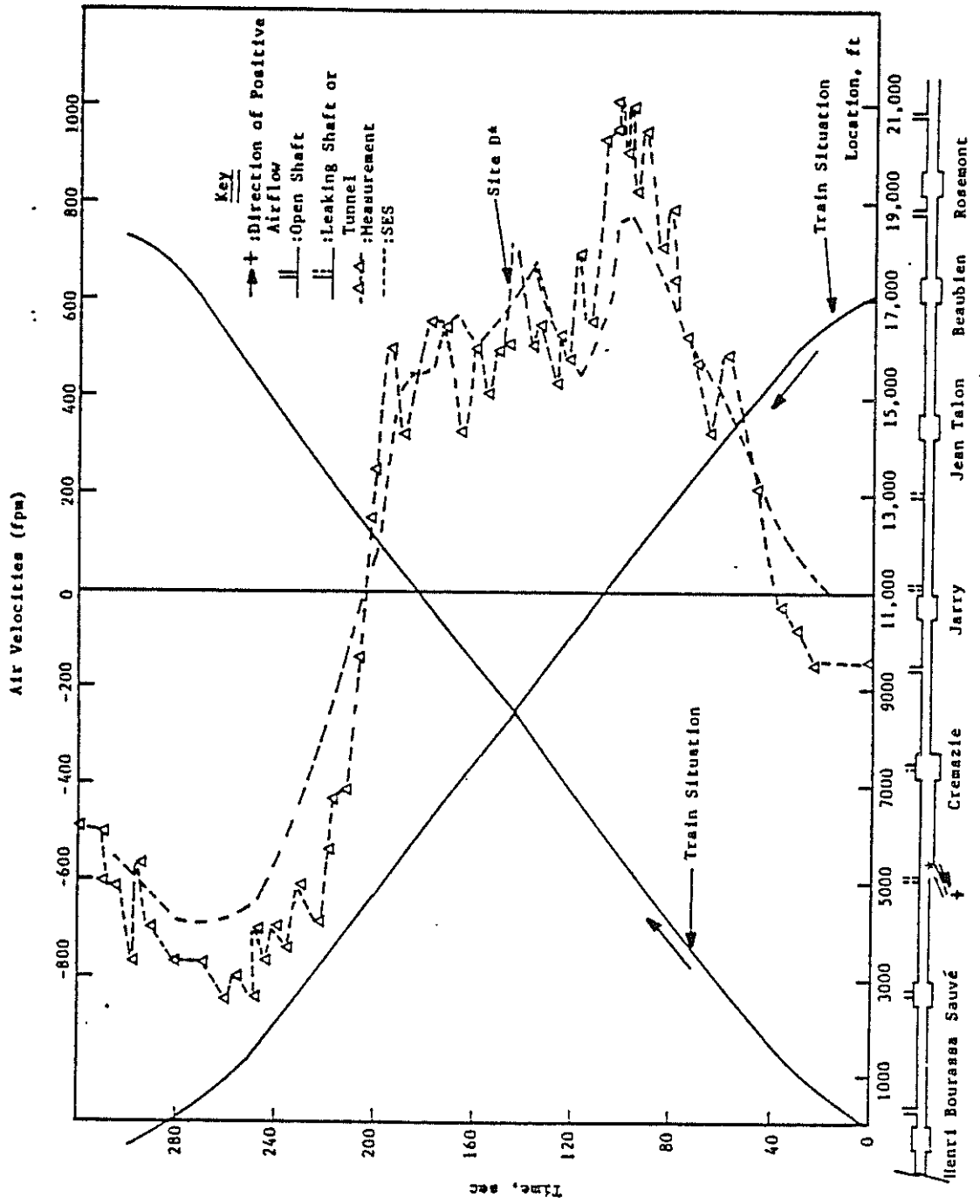


FIGURE 15-36. MEASURED VS SES AIR VELOCITY - TEST M-226 SITE D

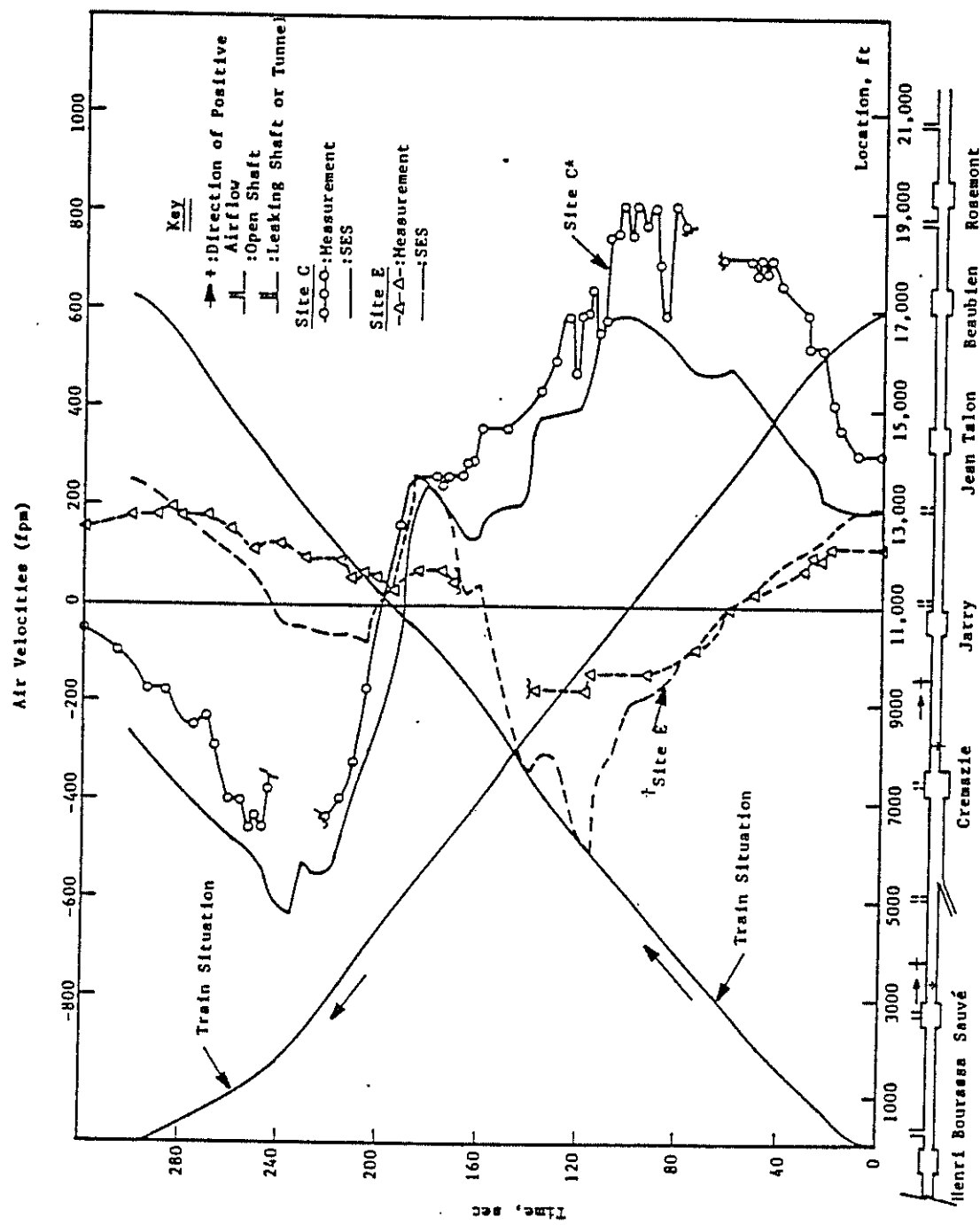


FIGURE 15-37. MEASURED VS SES AIR VELOCITY - TEST M-227 SITES C AND E

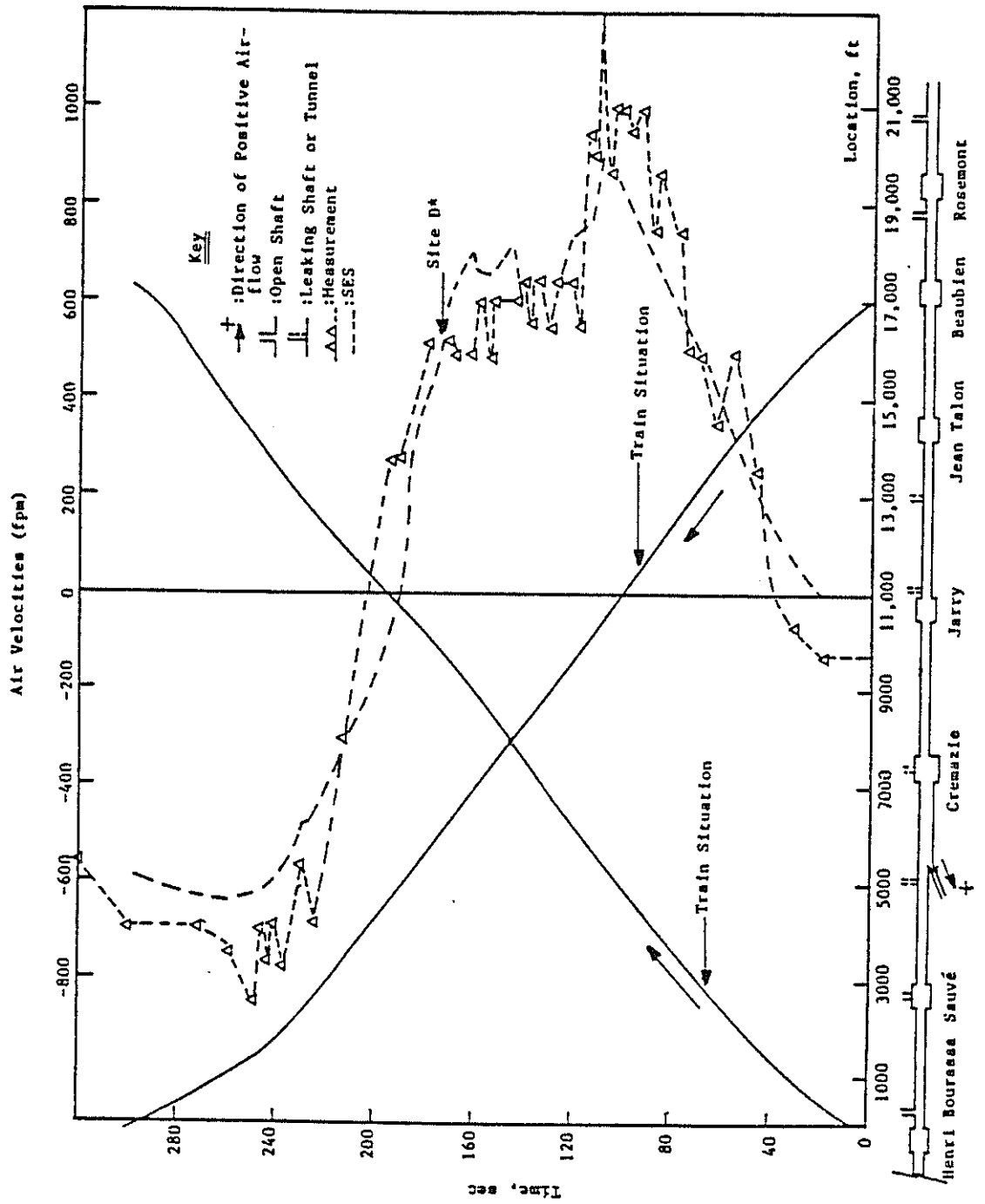


FIGURE 15-38. MEASURED VS SES AIR VELOCITY - TEST M-227 SITE D

account for such differences in train operation do not affect the comparisons as long as the time shaft is consistent throughout the comparison. In the two-train tests, time shifts in the train operation could not easily be compensated for because of the bi-directional train operation. This is due to the fact that when there is bi-directional train operations (and therefore opposing airflows), a shift in the relative train operations would affect the resulting airflows throughout the test. Such aforementioned small shifts in the relative train operation between the SES program comparisons and the data for tests M-226 and M-227 accounted for a relatively significant portion of the discrepancies found in the two-train comparisons.

Test M-226 measured the airflows at both the "T" and the "Y" junction. The comparisons of the SES-predicted airflows and the data for test M-226 at instrument sites C,D,E and F are given in Figures 15-34 through 15-36. The SES-predicted tunnel airflows were generally within 100 fpm of the measured tunnel flows. As in the single-train tests, errors were similarly introduced into the two-train SES-program comparisons by the system air leaks, the counter-weighted damper at the top of the fan shaft, the difference between the fan shaft and tunnel cross-sectional areas, and the incompressible flow assumptions in the SES aerodynamic model.

Fan shaft 4504 was sealed for test M-227 and only the flows at the "Y" junction were measured. The comparisons of the SES-predicted airflows and the data for test M-227 at instrument sites C,D and E are given in Figures 15-37 and 15-38. The SES-predicted airflows were generally within 100 fpm of the measured tunnel flows at sites C,D and E.

The results of these comparisons show the combination of the multi-junction and tunnel flow theories developed during the Transit Development Corporation's Subway Environment Research Project to be more than adequate for computations of the overall flow split at "T" and "Y" type junctions. The SES program incorporates four junction types other than the "T" and the "Y" junction, and the overall flow splits at these four junction types remain unchecked against any full-scale field data. However, a SES program user can still have a large degree of confidence in the SES program results due to the fact that, as explained previously, the overall flow split at a multi-junction is determined largely by the inertia of the branch flows and the relative impedances of the branches. The portion of the SES program that calculates the inertia of the airflows and the total pressure drops in the

various branches of the system has been thoroughly validated and shown to be very accurate. Therefore, any error in the junction theory for any of these four unchecked junction types should have very little influence on the overall accuracy of the SES-predicted airflows.

15.5 SYSTEM TESTS

The overall system validation required simultaneous measurements of airflow, temperature and humidity over the entire test section from Henri-Bourassa Station to the sump pump room at instrument site I (see Figure 15-6). These measurements were taken at various intervals throughout the daily cycle of operation (see Table 15-3), with particular emphasis on the morning and evening rush hours.

To provide a basis for direct comparison between the field data and SES program predictions, the SES-computed train operations must closely emulate the actual operation of trains through the test area. The field-observed variations in headway, dwell time and relative train position were simulated in the SES program computations through the use of the explicit train performance option which requires that a separate velocity-time history be developed for each train. Simulations using the implicit train performance option (internally computed train operation) were also undertaken to develop further information regarding the effect of train operations on SES-computed airflows and temperatures.

Due to the extensive effort involved in simulating the actual train operations that existed during a given interval of the system tests, the SES program comparisons were concentrated on one particular evening rush hour, with spot comparisons being performed in the off-hours and morning rush hours. The evening rush hour in general is the focal point of all the SES program mathematical models, and a validation of the SES program's evening rush-hour capabilities in principle validates the entire SES program.

The SES systems-validation effort was performed in two stages. The first stage of the systems validation involved the short-term capabilities of the SES program where the wall surface temperatures used in the heat sink computations are entered by the user (Ref. 10). The second stage of the SES systems validation involved the long term capabilities of the SES program where the wall-surface temperatures in the system are predicted by the SES

heat sink model using the results of the short-term SES program simulations (Ref. 10).

15.5.1 Short-Term SES Validation

Wall-surface temperatures throughout the test section were obtained by the AE engineers on three different occasions during the METRO full-scale field tests. These measured wall surface temperatures were used to approximate the wall-surface temperatures for the evening rush hour, and were subsequently used as the wall-surface temperatures in the SES short-term simulations (see Figures 15-52 through 15-55).

The actual train performance for a 12-minute segment of the November 19, 1974 Montreal METRO evening rush hour was approximated in the SES program comparison runs as closely as possible within the physical storage space limits of the computer used for the SES program simulations. The physical, machine-determined constraints upon the SES program allowed the specification of up to six separate velocity-time profiles. Each train which enters the system during the course of the SES program simulation must follow one of these prescribed profiles, or "routes." In this manner, each train can have a different dispatch time, different run time and speed between stations, and different dwell time in each of the stations. There were always eight trains actually operating within the test section during this 12-minute portion of the evening rush hour, and the SES program could closely emulate the operation of six of these trains. The operation of the remaining two trains was determined by comparing the field-measured train performance data for these two trains against the operation specified for the six other train routes, and the two additional trains were then placed into operation along one of the six routes that provided the closest approximation to the two trains actual operation. The resulting SES-predicted train performance closely, but not exactly, follows the field-measured train operations.

Figure 15-39 shows the comparison of the average system air temperatures obtained from the data and the SES-predicted average system air temperatures. In addition, the SES-predicted minimum and maximum air temperatures experienced at each of the instrument sites during the 12-minute interval are also given in Figure 15-39. As shown in this figure, the SES-predicted average air temperatures are, except in one instance (at instrument site H in the tunnel

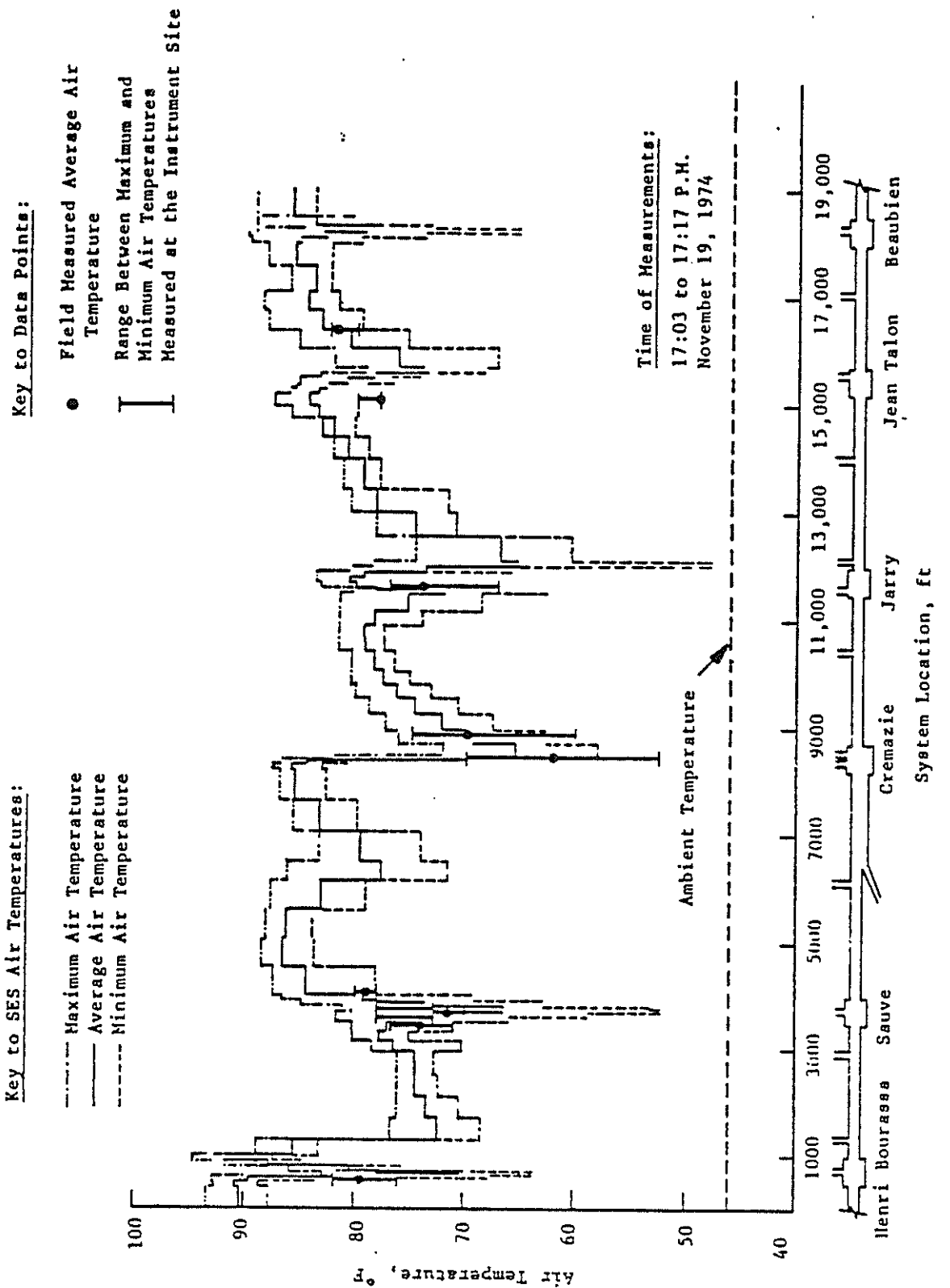


FIGURE 15-39. COMPARISON OF PREDICTED AND MEASURED SYSTEM AIR TEMPERATURES - TEST M-303

north of Jean Talon Station), always within $\pm 3^{\circ}\text{F}$ of the measured average air temperatures. To express this absolute accuracy value in terms of a relative, or percentage, accuracy requires the definition of a base against which the temperature difference can be compared. In order to do this, a basic understanding of how the SES program operates is necessary.

The SES program operates with the following basic information: the outside ambient air temperature, the wall-surface temperatures, the train operations, and the steady-state sources of heat within the system. The SES program then simultaneously calculates over short intervals in time the resulting airflows in each portion of the system due to buoyancy, fans (if operating) and the piston action of the trains, the net inflow or outflow of air through each opening to the atmosphere, and the net heat gain in each portion of the system due to the heat release from trains and steady-state heat sources, heat transfer to the walls, and the net influx of outside air. If the outside air is cooler than the air inside the system, the air temperature in a given portion of the system will rise if the heat gain in that portion of the system is not completely off-set by a sufficient influx of cool outside air and/or heat transfer to the walls (heat sink effect). Obviously, the resulting system air temperatures are directly affected by the net amount of outside air that enters the system and the temperature of the outside air. When the air temperatures throughout a system become "stabilized" (Ref. 11), the average heat entering the system equals the average heat leaving the system. The average system air temperature that exists in a system operating under these conditions can be expressed as a function of the rise in temperature above ambient, due to the fact that the ambient air temperature serves as the governing reference temperature in the SES program simulations.

As seen in Figure 15-39, the outside ambient air temperature was 46°F and the average system air temperature was approximately 80°F for test M-303. The temperature rise above ambient was therefore $80^{\circ}\text{F} - 46^{\circ}\text{F} = 34^{\circ}\text{F}$. The fact that the SES-predicted air temperatures were, except in one instance, within 3°F of the measured air temperatures implies that the SES program results for the M-303 were within 8.8 percent ($3/34 \times 100$ percent) of the actual conditions. Therefore, the accuracy of the SES program in predicting average system air dry-bulb temperatures for conditions encountered during test M-303 is well within 10 percent. The average air temperatures throughout a system are the most important parameters in the environmental design of a subway system, and

the above comparison indicates that the SES program more than adequately predicts these average air temperatures.

The relatively larger differences between the measured and the SES-predicted air temperature extremes at some of the instrument sites is attributed to the method in which the actual geometry of the system was approximated in the SES program simulations. The SES program requires the user to divide the system into discrete mathematical entities called "subsegments" wherein the "bulk" airflow and temperature is calculated over user-specified intervals of time. The air temperatures were measured at discrete points in the system, and these discrete point temperatures were not necessarily representative of the "bulk" air temperatures calculated by the SES program. This difference between the discrete point measurements and the SES bulk-flow calculations is most apparent in the stations. Many of the subsegments in the stations comprised large volumes of both the platform and mezzanine. Figures 15-40 and 15-41 illustrate the manner in which Sauvé and Cremazie Stations were broken into subsegments for the SES program comparison runs, and the actual positions along the platform where the temperature probes were located during the field tests. The SES-computed air temperatures in sub-segments 3, 4 and 5 in Cremazie Station (see Figure 15-41) reflect the overall bulk temperatures of the entire volume of air in each of these sub-segments, from the bottom of the station to the ceiling of the mezzanine. This is similarly true for subsegments 3 and 4 in Sauvé Station (see Figure 15-40). In the SES program comparisons runs, any inflowing outside air in Sauvé Station was immediately reflected in the bulk air temperatures in sub-segments 3 and 4. This was similarly true for subsegments 3, 4 and 5 in Cremazie Station. The temperature probes located along the middle of the platform in Sauvé Station, as with all the temperature probes in the system, measured only the air temperatures within the immediate vicinity of the probes. During the actual temperature measurements in Sauvé Station, all inflowing outside air had to pass through the mezzanine before reaching the platform area. The mezzanine therefore acted as a "buffer" between the inflowing outside air and the platform air, as the inflowing air generally mixed with the mezzanine air on its way to the platform area. As a result, due to the buffering action of the mezzanine, the temperatures measured along the Sauvé platform showed relatively little variation. This was similarly true for the other stations in the system where the air temperature were measured.

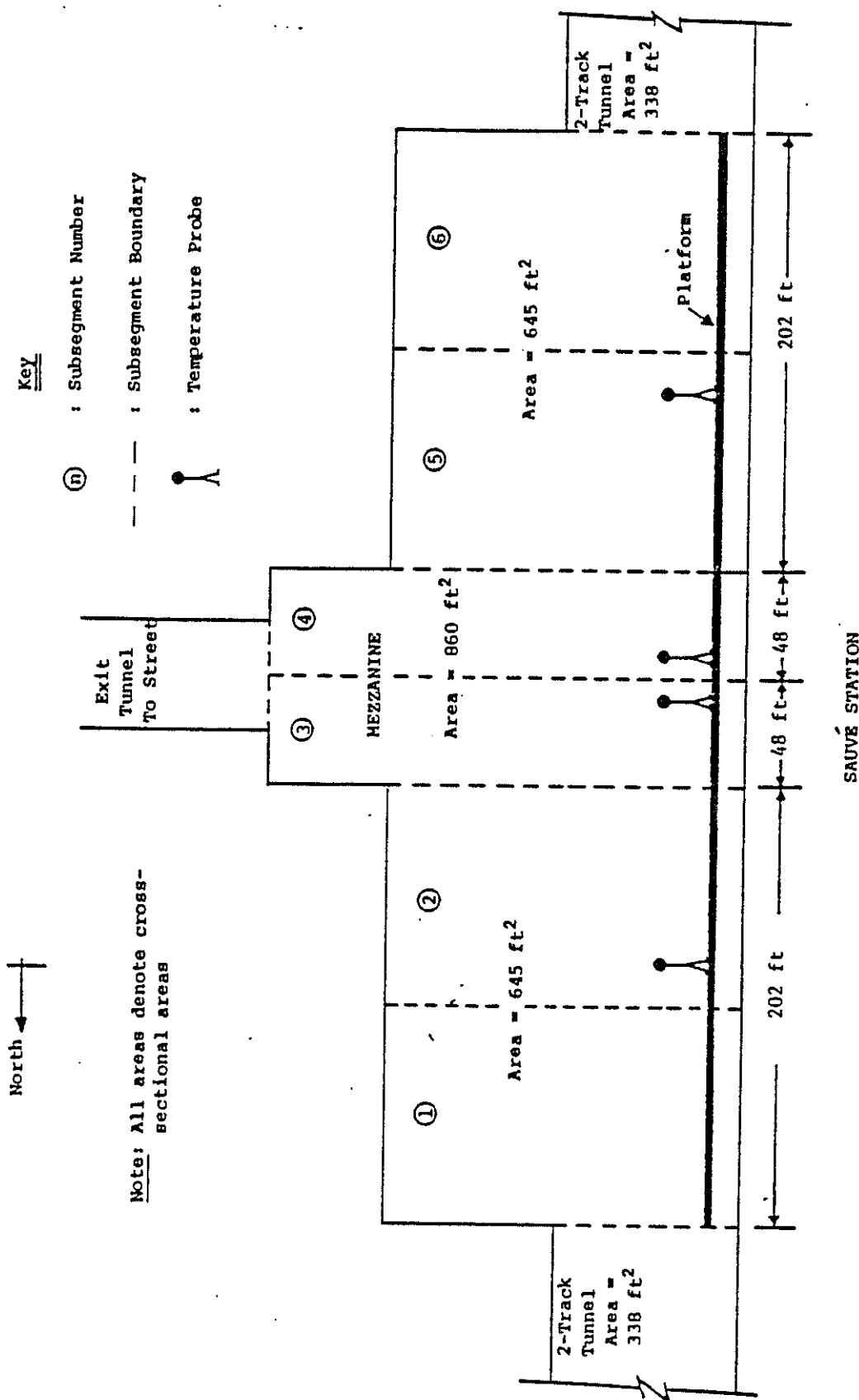


FIGURE 15-40. SCHEMATIC DIAGRAM OF THE SAUVÈ STATION GEOMETRY AS ENTERED IN THE SES PROGRAM AND THE CORRESPONDING ACTUAL LOCATIONS OF THE PLATFORM TEMPERATURE PROBES

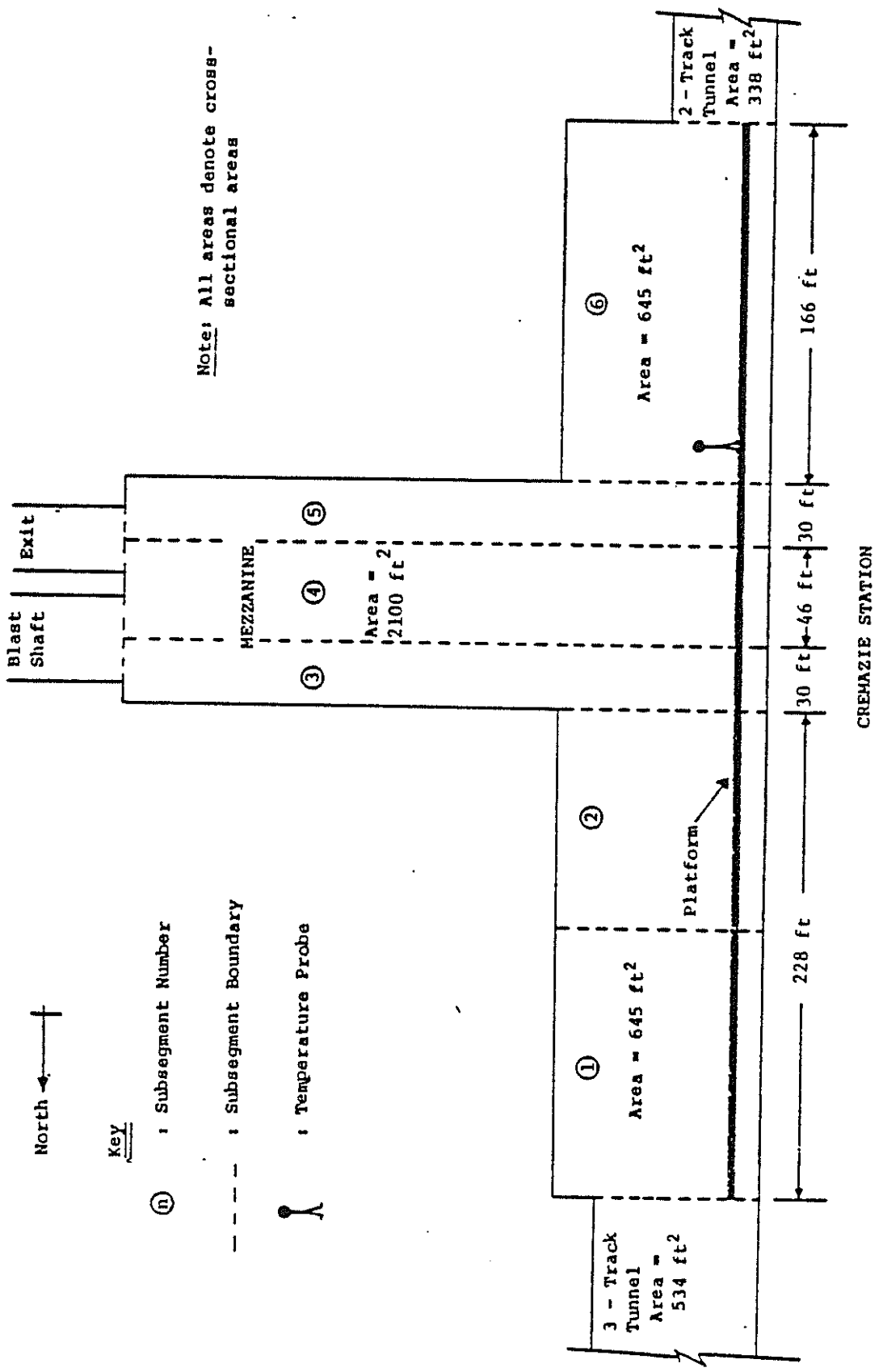
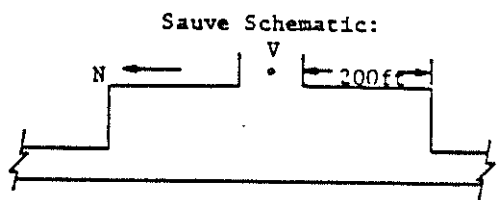


FIGURE 15-14. SCHEMATIC DIAGRAM OF THE CREMAZIE STATION GEOMETRY AS ENTERED IN THE SES PROGRAM AND THE CORRESPONDING ACTUAL LOCATION OF THE PLATFORM TEMPERATURE PROBE

Figures 15-42 through 15-46 show the comparisons of the data and the SES-predicted airflows and temperatures in Cremazie and Sauvé Station over a 300-second period of the November 19, 1974 Montreal METRO evening rush hour. In Figure 15-43 it can be seen that the SES-predicted station air temperatures in subsegment 4 (the location T_s) varies according to the direction of the airflow in the station. At time-equals-zero in Figure 15-43, air is moving northward into the station from the tunnel south of the station. The SES-predicted tunnel air, T_t , is warmer than the SES-predicted station air, T_s , and causes the SES-predicted air temperature in subsegment 4 to rise. At time-equals-80 seconds, the direction of the airflow reverses and the air in subsegment 4 flows southward out of the station via the tunnel south of the station. Cool outside ambient air flows down through the mezzanine and into the platform area to serve as part of the make-up air for the flow leaving the station. The remainder of the make-up air is composed of air from the north end of the station. The cool outside ambient air mixes with the air in subsegment 4 and lowers the SES-predicted air temperature in subsegment 4. The SES-predicted air temperature in subsegment 4 can be seen to similarly fluctuate over the remaining portion of the comparison according to the direction of the SES-computed bulk airflows in the station and surrounding tunnels. In comparison, the field measured air temperatures in both the tunnel and the station remained fairly constant over the entire 300-second comparison. This comparison serves as an excellent illustration of the above mentioned buffering effect the mezzanines had upon large variations in the field-measured discrete point air temperatures along the platforms. As a result, certain instantaneous values of the bulk air temperature computed by the SES program were often much lower than the corresponding measured air temperatures. It is for this reason that the SES-predicted minimum air temperatures throughout the test section (see Figure 15-39) were often much lower than the corresponding field-measured temperatures. It is very important to note that the SES-predicted minimum air temperatures in each of the subsegments almost always existed over only a very short instant in time, and therefore had only a relatively minor affect upon the average SES-predicted air temperatures (see Figure 15-39). As mentioned previously, the subway environmental designer is chiefly concerned with average air temperatures, and the SES-predicted average air temperatures were almost always within less than 9 percent of the measured air temperatures.

.... SES
 —— MEASUREMENT



Notes: 0 seconds corresponds
to 17:05:45 on
November 19, 1974

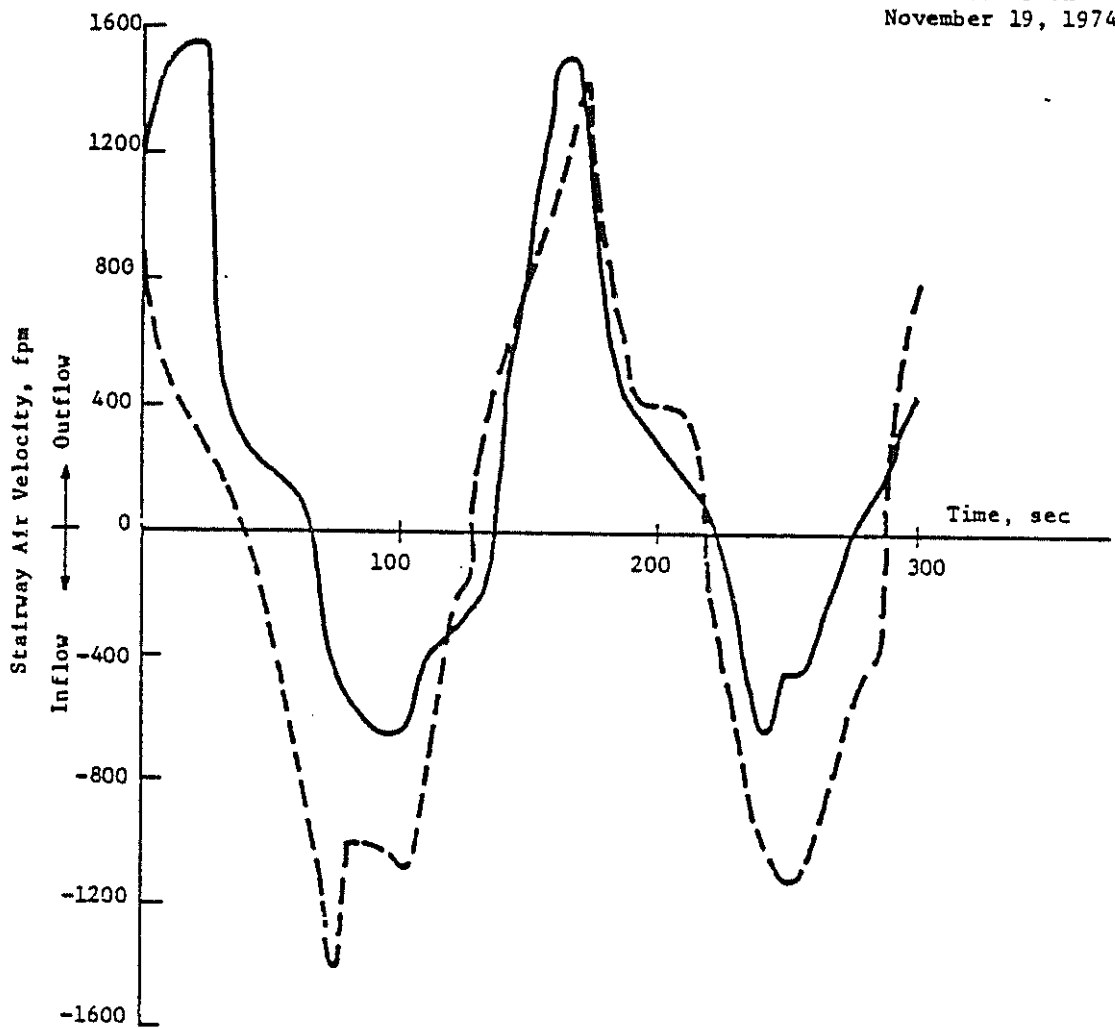


FIGURE 15-42. COMPARISON OF PREDICTED AND MEASURED AIRFLOW TRANSIENTS—
SAUVE STATION STAIRWAY, EVENING RUSH HOUR — TEST M-303

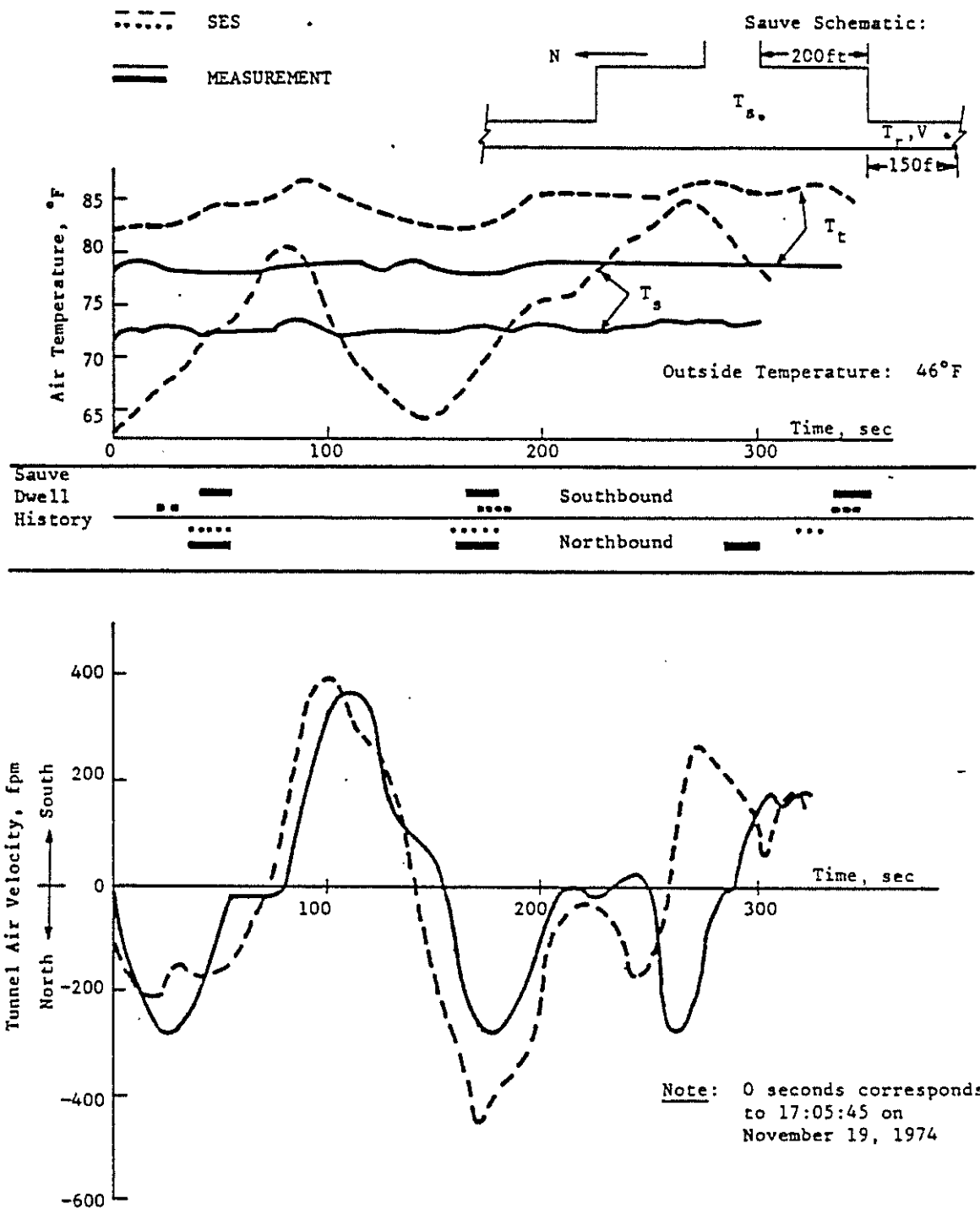
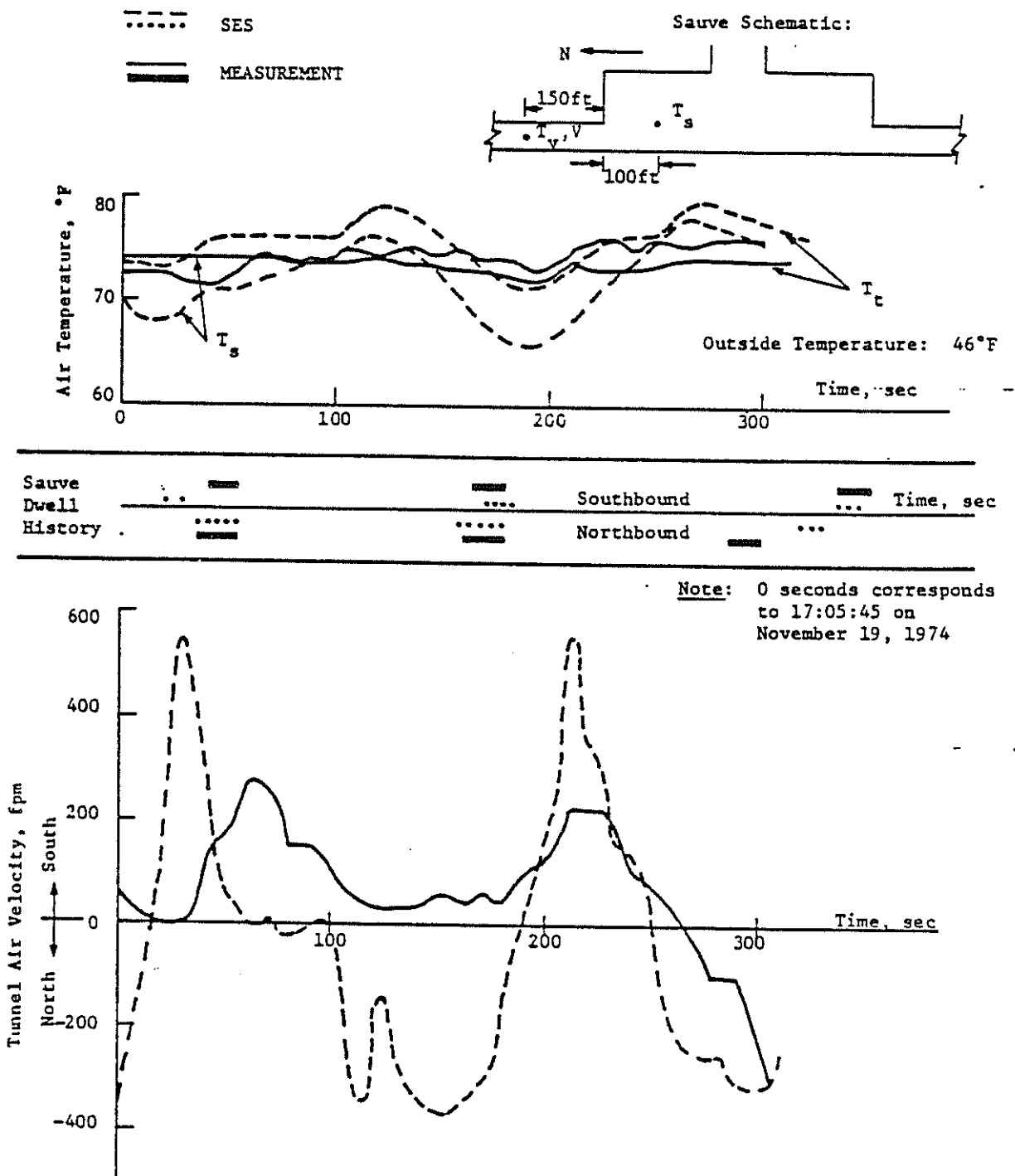


FIGURE 15-43. COMPARISON OF PREDICTED AND MEASURED AIRFLOW AND TEMPERATURE TRANSIENTS - SAUVE STATION, EVENING RUSH HOUR - TEST M-303



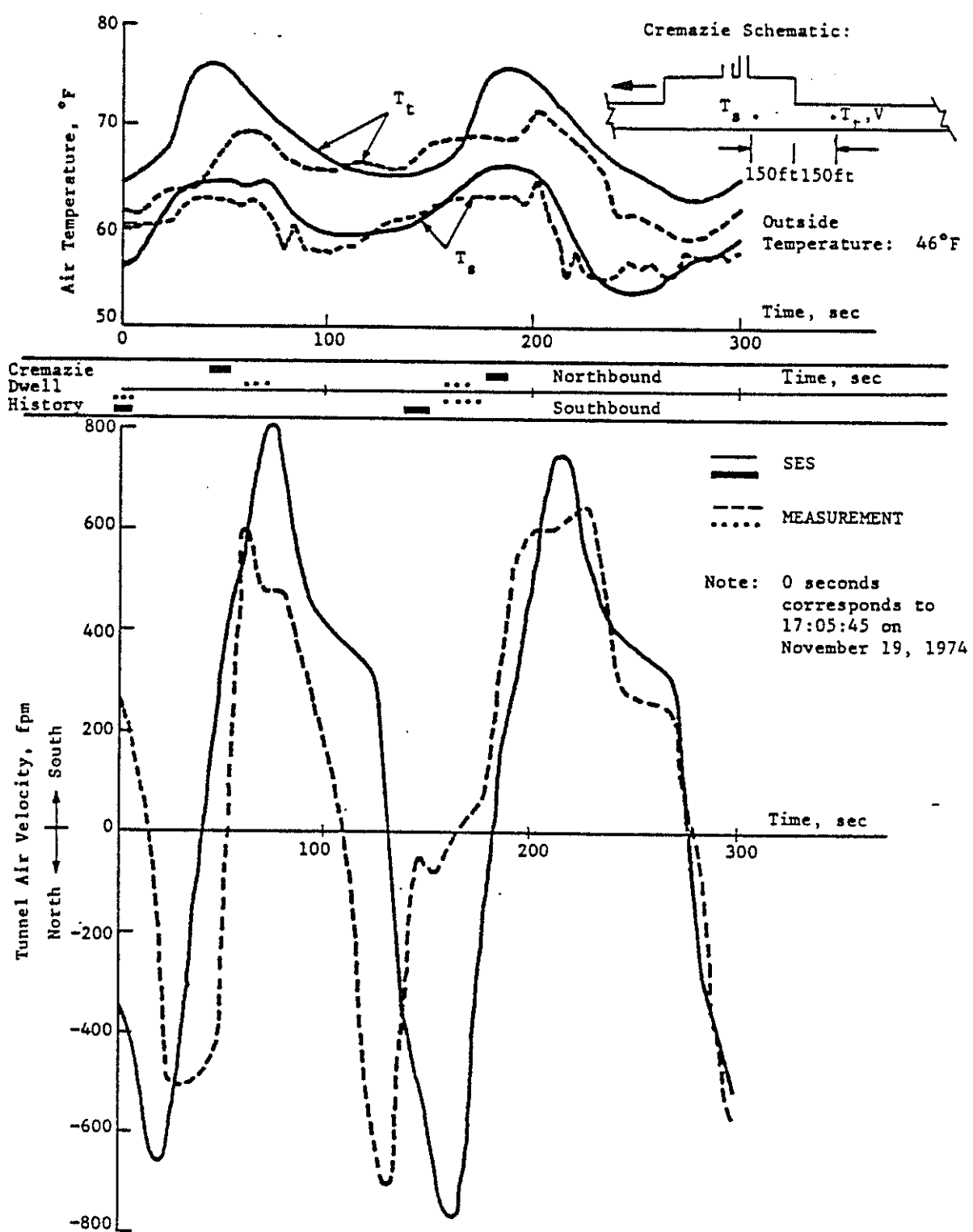


FIGURE 15-45. COMPARISON OF PREDICTED AND MEASURED AIR FLOW AND TEMPERATURE TRANSIENTS - CREMAZIE STATION, EVENING RUSH HOUR - TEST M-303

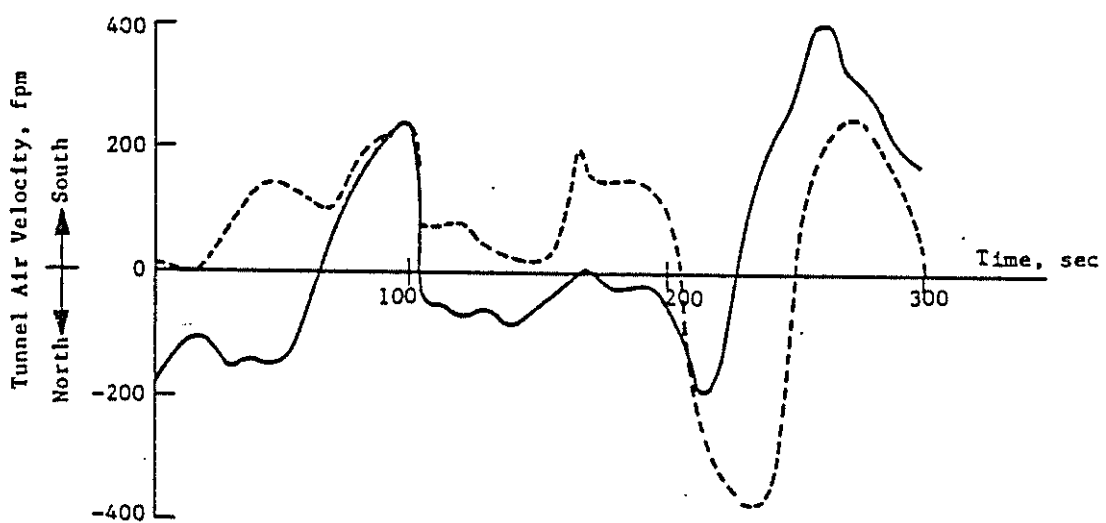
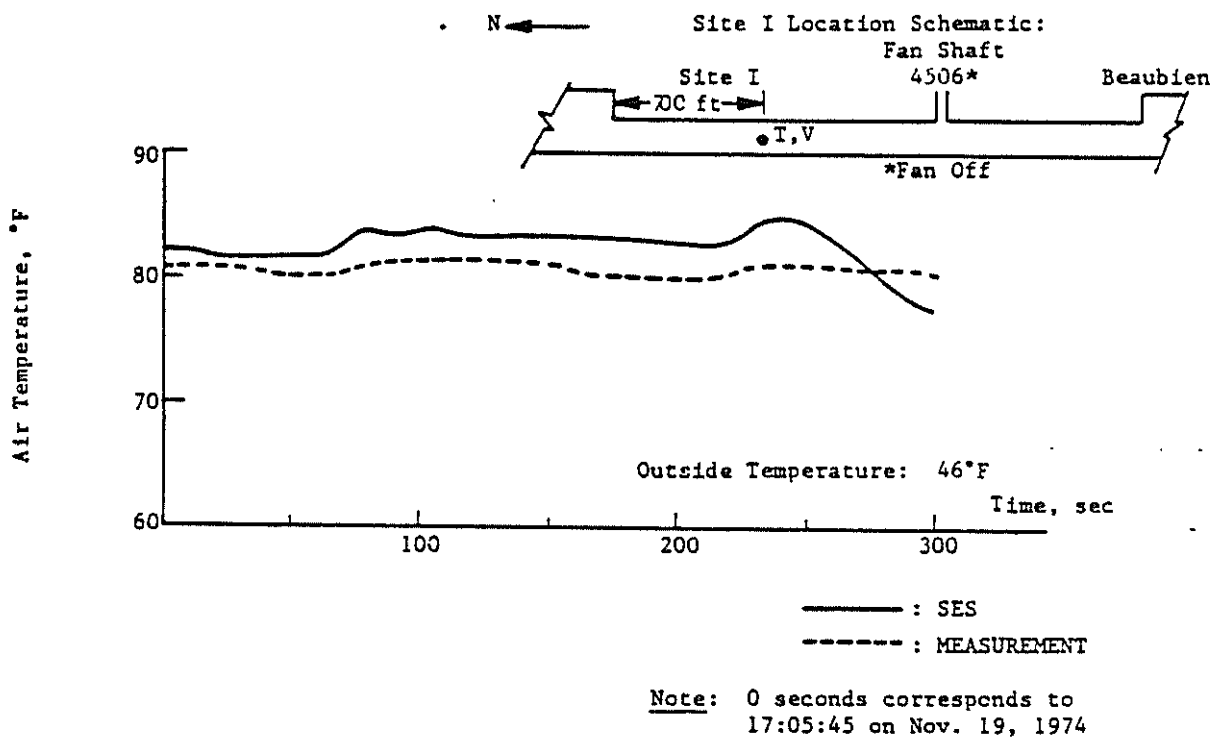


FIGURE 15-46. COMPARISON OF PREDICTED AND MEASURED AIRFLOW AND TEMPERATURE TRANSIENTS - TUNNEL SITE I, EVENING RUSH HOUR - TEST M-303

Figures 15-42 through 15-46 also serve as an excellent illustration of the differences introduced into the systems tests comparisons by the approximation of the actual train operation in the SES program. As explained previously, the actual train operations that existed during the systems tests could not be duplicated exactly in the SES comparison runs. As shown in Figure 15-42, at time>equals=20 seconds the SES train operations had a train just come to a stop in Sauvé Station along the southbound platform. The train dwelled in the station for 10 seconds. At the end of this 10-second dwell, the train accelerated away from Sauvé Station toward Cremazie Station. As also shown in Figure 15-42, the corresponding train in the actual test did not come to a hault along the southbound platform until time>equals=40 seconds. The actual train dwelled in the station for 17 seconds, and left towards Cremazie station at time>equals=57 seconds. It can also be seen in Figure 15-42 that the actual train operations and the SES train operations corresponded very closely for the train that just came to a stop along the northbound platform at time>equals=35 seconds. The comparison of the measured and the SES-predicted air velocities through the stairway in Sauvé Station over the period in time from 0 to 300 seconds (17:05:45 to 17:10:45 on November 19, 1974) is also provided in Figure 5-4. It can be seen that the influence these first two trains had upon the Sauvé Station stairway airflows decreased rapidly at approximately time>equals=100 seconds due to the fact that two new trains (one southbound and one northbound) were approaching the station. Almost all of the discrepancies between the measured and the SES-predicted Sauvé stairway airflows between 0 and approximately 100 seconds are due to the above mentioned differences in train operations along the southbound platform. As explained previously in Section 15.3, the airflow in a double-track system with opposing train operation is extremely sensitive to the relative operation of the trains, and a slight shift in the relative train operation can result in very large differences in the resulting transient airflows.

Further similar comparisons between the actual and the SES-predicted airflows in conjunction with the relative train operation such as the one performed above can be made for the tunnels on both ends of Sauvé Station, the tunnel just south of Cremazie Station, and the tunnel south of Jean Talon Station (site I) using Figures 15-43 through 15-46, respectively. As shown in these figures, the SES-predicted airflows in the systems tests comparisons

almost always followed the general directional trends of the measured airflows. In other words, when the actual airflow in a portion of the system was moving in a northward direction, the corresponding SES-predicted airflow was also moving in a northward direction and vice versa. In addition, the SES-predicted magnitudes of these airflows were, except in a few instances, close to the actual magnitudes of the measured flows. In conclusion, although some obvious discrepancy was introduced into the SES comparison runs by the approximation of the actual train operation, the degree of error introduced was relatively small in almost all instances.

15.5.2 Short-Term SES Program Using Implicit Train Performance

The implicit train performance in the SES program uses the train and motor characteristics specified by the manufacturer in conjunction with the track profile and speed restriction within the given system to calculate the theoretical speed of the train as it traverses the system. The user specifies the headway and the locations along the route where the train is to stop (if any). If two trains operating along a given route are of the same manufacture, both trains will traverse the given route in exactly the same manner. Therefore, if all trains are of the same manufacture, operate along the same route, and have the same specified headway, the SES-computed airflows and temperatures will cyclicly repeat over a period of one headway due to the invariance in train operations. In contrast, successive trains traveling through an actual subway seldom follow exactly the same velocity-time history. As will be explained in greater detail in Section 15.5.3, the resulting temporal and spatial changes in relative train operations on adjacent tracks within the subway give rise in turn to deviations in airflows and temperatures from the idealized, cyclic pattern. The purpose of this section is to demonstrate how the use of implicit train performance and the consequent elimination of randomness in train operations compares with real subway operations in terms of the predictions of subway environment.

An implicit SES program comparison run for test M-303 was performed to exemplify the relative differences between the SES implicit and explicit train performance options. Figure 15-47 shows the comparison between the results of this implicit SES program simulation and the explicit SES program simula-

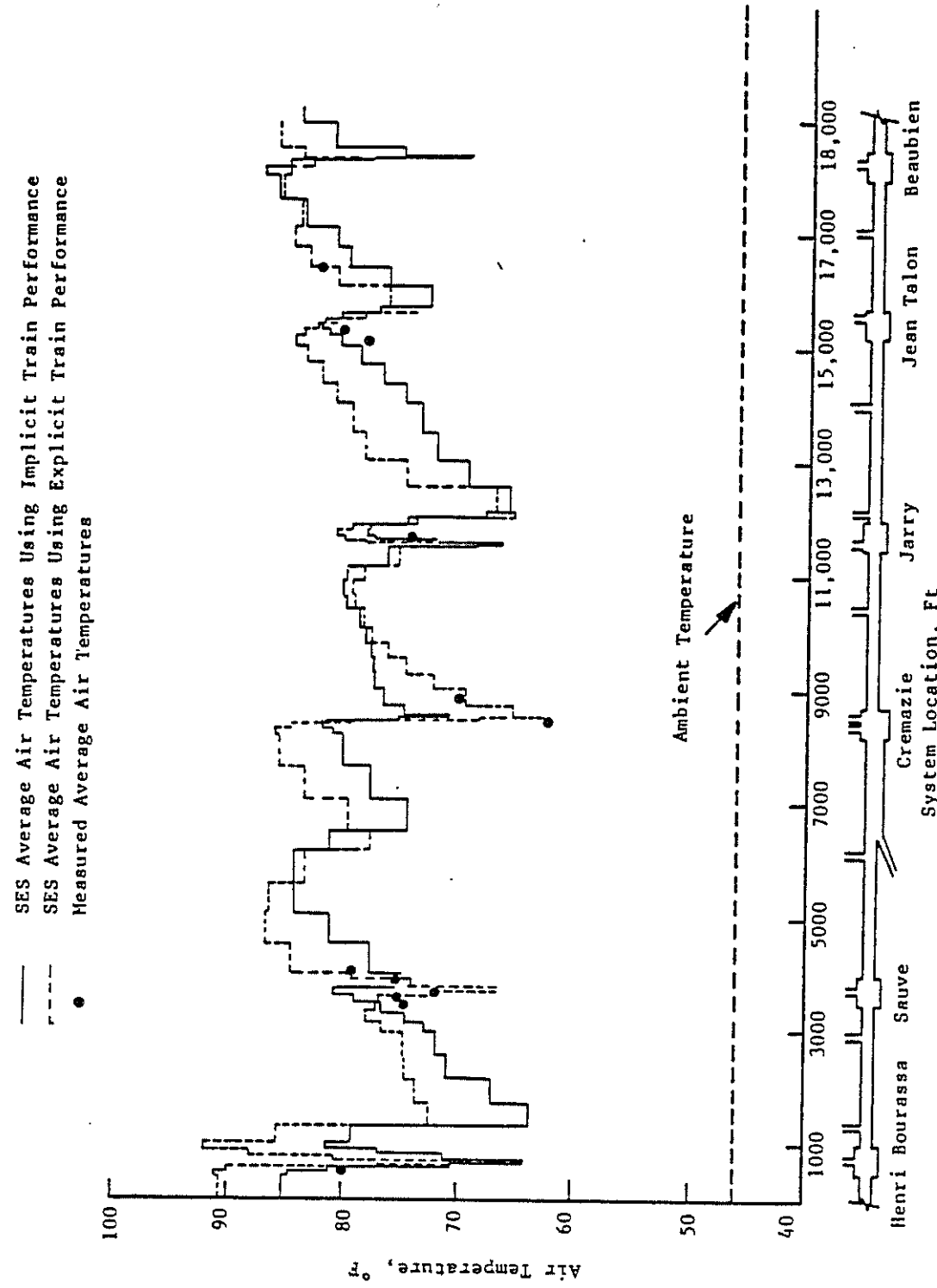
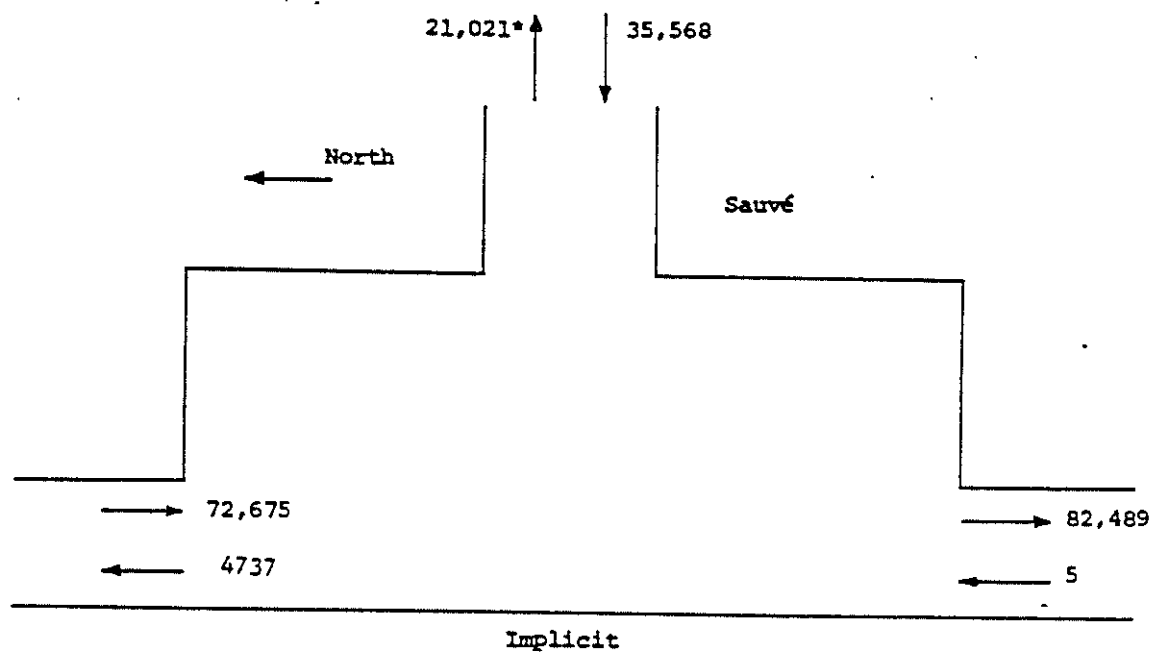


FIGURE 15-47. COMPARISON OF THE AVERAGE AIR TEMPERATURES PREDICTED BY THE SES IMPLICIT AND EXPLICIT TRAIN PERFORMANCE SIMULATIONS AND THE MEASURED AVERAGE AIR TEMPERATURES - TEST M-303

tion described in Section 15.5.1. As expected, the explicit SES program simulation compared somewhat more favorably with the field data than did the implicit SES program simulation. As explained in Section 15.5.1, the explicit SES program simulation for test M-303 utilized an approximation of the actual train performance, and it was this approximation that caused most of the discrepancies between the measured and the SES-predicted average air temperatures using explicit train performance.

The train headway during test M-303 ranged between 104 and 152 seconds, with the average headway being approximately 140 seconds. For comparative purposes, the implicit SES program simulation for test M-303 was performed with a constant headway of 140 seconds. As shown in Figure 15-47, the cyclicly repetitive train performance, airflows, and temperatures in the SES implicit comparison run yielded average air temperatures that differed slightly from the explicit SES program computations. The basic reason for the difference between the implicit and explicit SES program results is as follows: in a given specific tunnel section, bi-directional, repetitive train operations may have either a cancelling or an enhancing effect upon the piston-action ventilation, the degree of which depends on the details of the relative train operations. In general, the SES program predicts warmer average air temperatures in tunnel sections where the train operations tend to cancel the piston-action ventilation, and cooler average air temperatures in tunnel sections where the train operations tend to enhance the piston-action ventilation.

As an example, consider the comparison between the SES implicit and explicit average air temperatures for Sauvé Station shown in Figure 15-47. The implicit average air temperatures range from about 3°F warmer than explicit SES program predictions at the north end of the station to 3°F cooler at the south end of the station, although both the explicit and implicit calculations compare favorably with the field data. The reason for the difference in air temperature computations can be best illustrated by considering the difference in SES-computed average airflows through the station, shown by Figure 15-48. The airflows resulting from several headways of explicitly simulated train operations show no strong directional bias, whereas the airflow in the tunnels contiguous to the station show a strong southerly bias for the case of implicit simulation of train operations. As Figure 15-47 shows, the temperatures from the explicit-SES analysis exhibit a degree of symmetry about the station entranceway. In the implicit simulation, the north end of the station



*Average air flow, cfm

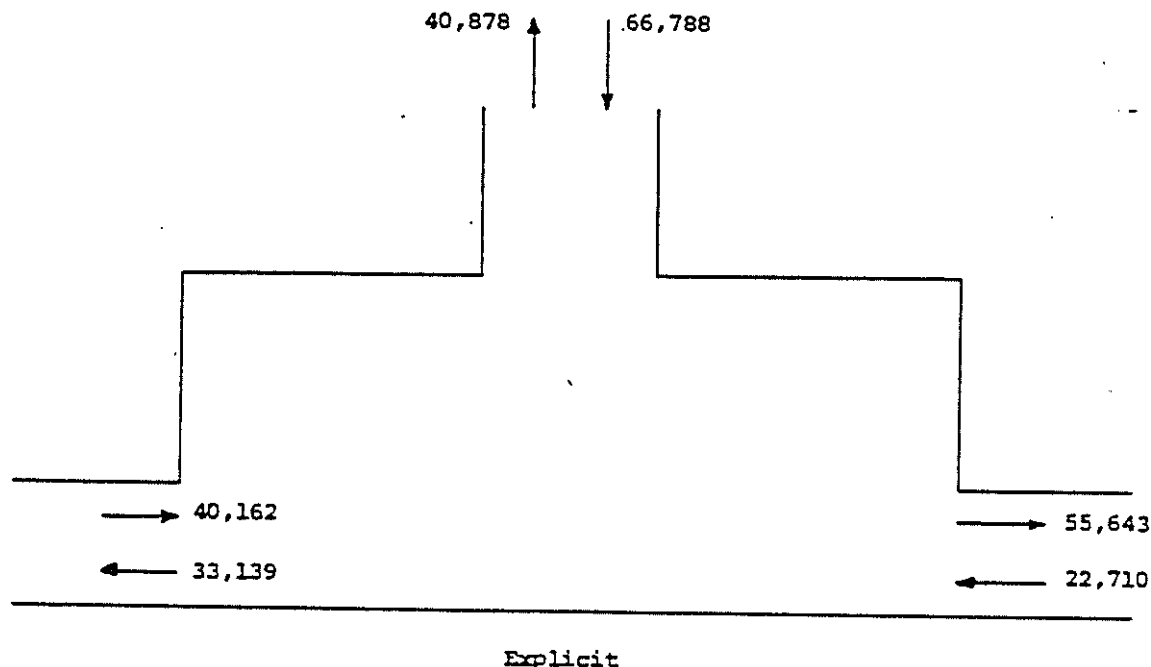


FIGURE 15-48. SES-COMPUTED SAUVÉ STATION VENTILATION: IMPLICIT AND EXPLICIT TRAIN PERFORMANCE SIMULATION

is ventilated primarily by inflowing air from the north tunnel. This results in relatively warmer air temperatures compared with the south end of the station which is cooled by inflowing air from the station entrance. However, the overall differences in average station ventilation and temperature are small.

Further differences between the implicit and the explicit SES program can be shown by comparing the explicit and the implicit SES-predicted transient airflow and temperatures in Sauvé Station. Figure 15-49 shows the comparison between the measurements and the implicit SES-predicted transient airflow and temperatures in Sauvé Station for test M-303, and Figure 15-43 shows the corresponding comparison between the measurements and the explicit SES-predicted transient airflow and temperatures in Sauvé Station for test M-303. The differences between the implicit SES-predicted tunnel airflow and the measured tunnel airflow is attributable to the previously explained implicit train operation. As shown in Figure 15-36, the trains in the implicit SES program simulation often came to a stop in Sauvé Station up to 35 seconds before or after the corresponding actual trains stopped in the station. The SES explicit train performance closely matched the actual train performance in Sauvé Station for test M-303 (see Figure 15-43) and, as a result, the explicit SES-predicted airflow in the tunnel south of Sauvé Station closely matched the corresponding measured tunnel airflow.

The transient air temperatures predicted by the implicit SES program near the sensor location just south of the Sauvé mezzanine and in the tunnel south of Sauvé compared favorably with the field measurements (see Figure 15-49), being closer in some respects than the explicit SES program prediction (see Figure 15-43). Similar comparisons between the SES explicit and implicit simulations can be made for Cremazie Station using Figures 15-45 and 15-50, respectively.

The SES implicit train performance option results in less accurate environmental calculations than the SES explicit train performance option only for the case of a user simulating a specific, given set of train operations. When performing a full-scale, field validation of the SES program, the actual train performance that existed in the field during a test must be simulated as closely as possible in the corresponding SES program simulation to facilitate one-to-one comparison with the data. When performing SES program simulations for design purposes, the implicit train performance option,

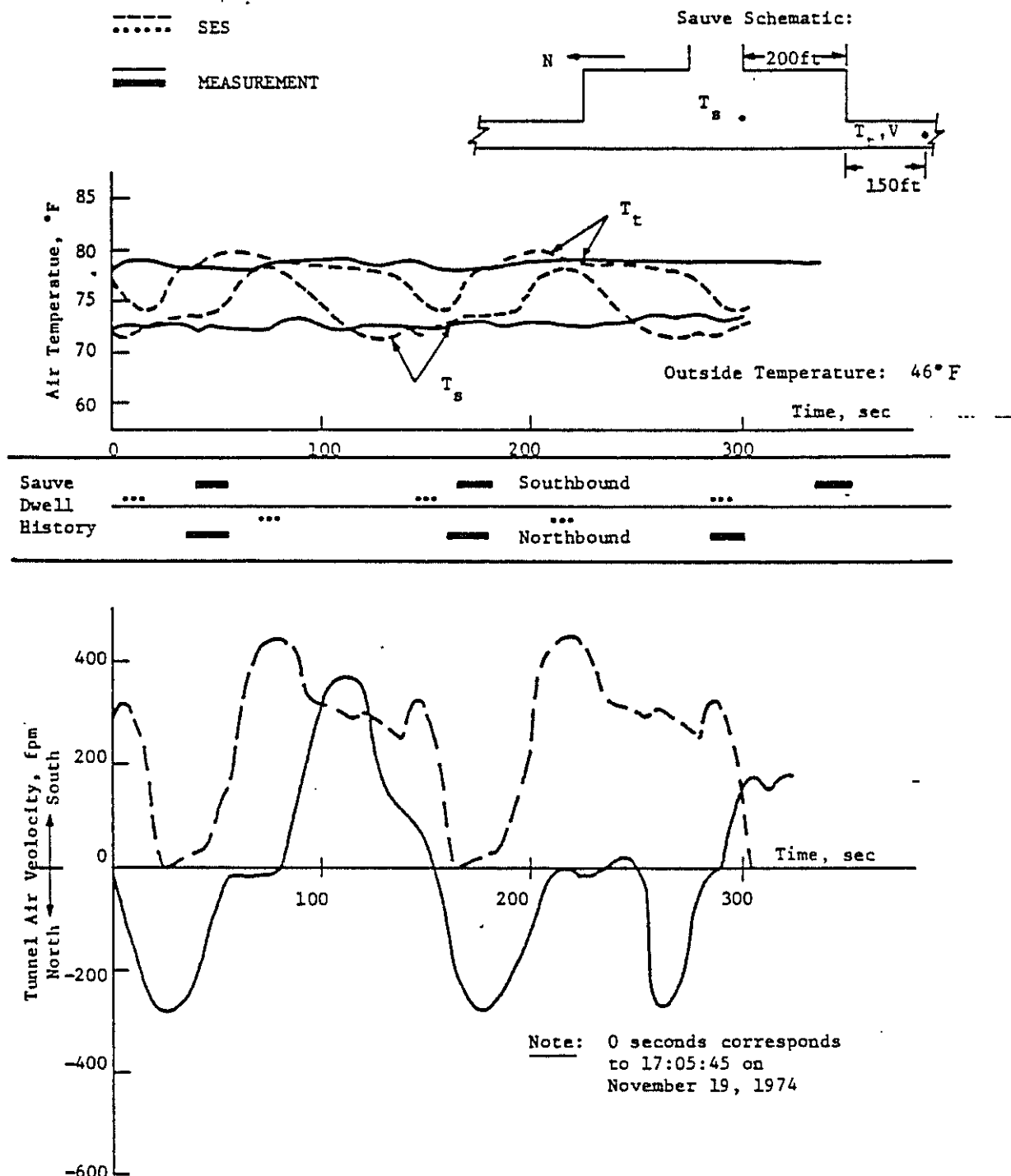


FIGURE 15-49. COMPARISON OF THE SES PREDICTED TRANSIENT AIRFLOW AND TEMPERATURES USING IMPLICIT TRAIN PERFORMANCE WITH THE CORRESPONDING MEASURED TRANSIENT AIRFLOW AND TEMPERATURE - SAUVE STATION, EVENING RUSH HOUR - TEST M-303

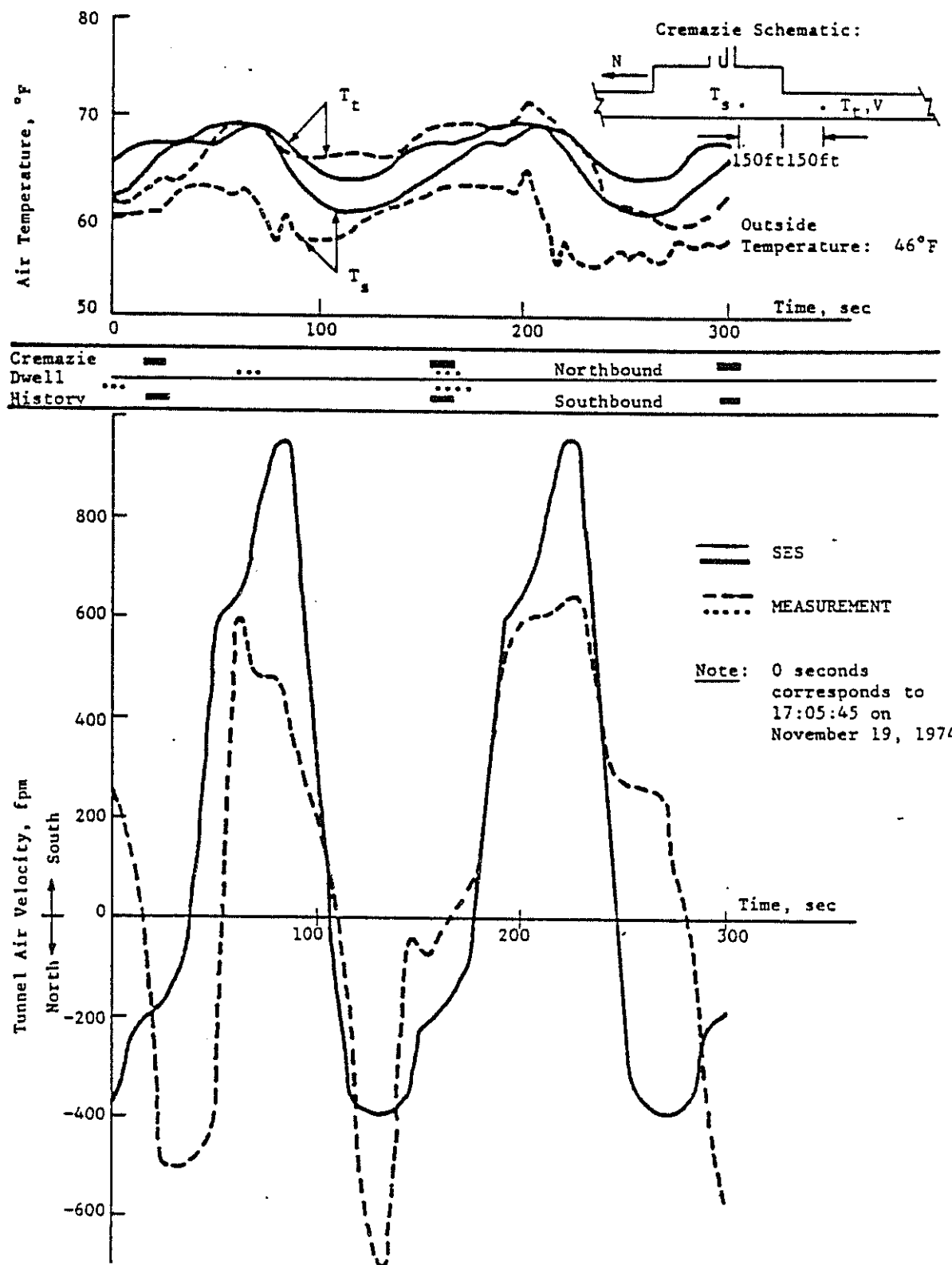


FIGURE 15-50. COMPARISON OF THE SES PREDICTED TRANSIENT AIRFLOW AND TEMPERATURES USING IMPLICIT TRAIN PERFORMANCE WITH THE CORRESPONDING MEASURED TRANSIENT AIR FLOW AND TEMPERATURES - CREMAZIE STATION, EVENING RUSH HOUR - TEST X-303

when implemented properly, results in environmental predictions which are as meaningful as those obtained using the explicit train performance option. As will be explained further in Sections 15.5.3 and 15.5.4, a user should evaluate a system with unknown train operation by performing at least two implicit SES program simulations, each one representing a different circumstance of relative train operations. This procedure greatly reduces the previously described possibility of the implicit SES program predicting warm and/or cool areas within the system because of one particular circumstance of cyclicly repetitive relative train operations. If warm or cool areas in a certain portion of the system are predicted by each of these implicit SES program simulations, the user can be confident that such a "hot spot" (or "cold spot") will actually occur in the real system.

In conclusion, it can be said that the implicit SES program, when properly implemented, is as accurate and meaningful as the explicit SES program for design applications. The possibility of inaccurate results with the implicit SES program due to invariance of train operation is greatly reduced by performing two or more implicit SES program simulations with different relative train operations. The explicit SES program is more accurate than the implicit SES program for special studies of systems where every detail of the train operation is known.

15.5.3 Long-Term Heat Sink

15.5.3.1 SES Heat Sink Analysis - For the wall heat transfer computations in the short-term, dynamic SES program simulations discussed to this point, the program uses an internally computed, air velocity-dependent heat transfer coefficient and the instantaneous difference between the air temperature and the user-input wall-surface temperature at discrete locations throughout the system. From a validation standpoint, this leaves one element of the SES program to be addressed-- the independent computation of wall heat flux and surface temperature computations by the SES heat sink subprogram (Ref. 11).

The heat sink subprogram has the function of computing the appropriate wall-surface temperature distribution as affected by subway heat gain and ventilation, daily and annual ambient temperature changes, and the thermal properties and "deep sink" temperature of the surrounding tunnel structure

and earth. The computations are performed for the user-specified time of the year, for either morning or evening rush hour. This constraint to rush-hour heat sink analysis traces to the need for extracting average heat gain and ventilation data from the short-term SES program simulation, then extrapolating these data such that the daily and annual fluctuations in subway environment and the consequent behavior of heat conduction in the surrounding materials can be estimated. A fundamental assumption in this extrapolation scheme, determined from measurements by several operating transit properties, is that the evening rush subway air temperature is the daily maximum, whereas the morning rush air temperature is approximately the daily mean.

The need for extrapolating the limited, short-term SES program data to longer time averages gave rise to a computation scheme within the subprogram called the Dynamic Thermal-Response Matrix (DTRM). Although mathematically complex, this tool is conceptually simple: taking the average thermal energy fractional splits at the multi-junctions (vent shafts, etc.) of the subway from the short-term simulation, the DTRM estimates subsegment air temperature changes resulting from changes in wall-surface temperatures and/or ambient temperature, for the same conditions of subway heat gain and ventilation as in the short-term simulation. The DTRM not only provides a method for estimating the impact of daily outside ambient changes on subway air temperature, required as input by the wall heat conduction analysis, but also enables the evaluation of the interactive behavior of subway air temperature and wall heat conduction.

The validity of the DTRM as a method of evaluating the subway thermal effects of ambient and wall-surface temperature changes has been checked by direct comparisons with short-term SES program simulations which considered a fixed subway geometry, ventilation and heat gain, but with different wall-surface temperatures and ambient temperatures. The results of this validation procedure, presented in Reference 12, confirm the DTRM computation scheme. It must be emphasized that the confirmation of the DTRM does not imply validation of the empirically-founded assumptions which guide the extrapolation of limited subway ventilation and heat gain data derived from a rush-hour simulation to obtain an estimate of the daily subway air temperature range. This important aspect of the subprogram will be addressed later in this section.

The heat sink subprogram also incorporates a mathematization of the heat conduction within the materials surrounding the subway. A closed-form analysis, the heat conduction model considers the material surrounding the subway tunnels to comprise two distinct regions in order to account for the possibility of marked differences between tunnel construction materials and the surrounding earth. This analysis evaluates the transient response of wall heat conduction to the periodic daily and annual tunnel air temperature variations. In addition, a long-term, warm-up analysis evaluates the annual average heat transfer between the subway air and the surroundings and the corresponding annual average wall-surface temperature to be expected after several years of subway operations at the design point. Heat sink temperature data recorded over a span of several years by the Toronto Transit Commission were applied in an assessment of the heat conduction model. The findings, documented in Reference 4, confirmed the validity of the heat conduction model.

The general confirmation of the DTRM and the heat conduction model by previous investigations leaves for validation the basic assumptions concerning the extrapolation of limited data from a short-term, rush-hour SES program simulation to other times of the day and year. The behavior of the heat sink depends on the cyclic variation of subway heat load and ventilation, yet an hour-by-hour evaluation of these parameters, and a commensurate heat conduction analysis which properly utilizes these data, would be prohibitively expensive to implement. The empirically founded approximation, taking morning rush as the mean and evening rush as the maximum subway air temperature condition, circumvents this problem at some expense of generality and accuracy. The field data on which this approximation is based were from systems where the ventilation configuration (shafts, fans, etc.) remained essentially invariant through the day and year. Thus the heat sink subprogram accuracy must suffer for subways with significant ventilation system changes on a daily and/or annual basis. As will be seen, the Montreal METRO falls into this latter category by virtue of the seasonal ambient temperature extremes and thus affords the opportunity to examine this source of inaccuracy more closely.

Another potential source of inaccuracy, inherent in the use of average ventilation data from the short-term SES program in the heat sink analysis, is the possibility that in a specific tunnel section, SES-simulated train operations may be such as to have a cancelling effect (or an enhancing effect) on piston-action ventilation. Although these short-term computations are

accurate, this condition may not persist on an average basis for prolonged periods due to the inherent randomness of relative train positioning on adjacent tracks. The extrapolation procedure does not recognize this fact and takes the low (or high) ventilation rate as a representative, repeating phenomenon. The heat sink analysis confronted with a poorly ventilated (or well ventilated) tunnel section, realizes that the heat sink must share a proportionately greater (or smaller) percentage of the heat load. The end result of the heat sink analysis in this circumstance is typically a "hot spot" (or "cool spot") within the subway, since the heat transfer to the sink, which depends on the air-wall temperature difference, is enhanced by higher air temperatures. Subway ventilation concept studies with the SES program (Ref. 12) confirmed this behavior, but also indicated that the circumstances leading to SES-computed average ventilation data not representative of long-term system behavior occur infrequently. In addition, subways in which mechanical ventilation contributes substantially to the tunnel airflow are less affected by this phenomenon. In any event, it is recommended that a user of the SES program should evaluate long-term heat sink for at least two separate conditions of relative train operations (accomplished by changing the relative dispatch times on opposing train routes in the short-term simulation) to obtain a complete assessment of the expected long-term heat sink behavior.

The application of the heat sink subprogram to the Montreal METRO is discussed in the following sections. The daily and annual operations of the METRO's ventilation system is presented first, in terms of the applicability of the subprogram assumptions. This discussion is followed by comparisons of field measurements and predictions of those parameters which directly influence the heat sink effect.

15.5.3.2 Montreal METRO Ventilation System Operation - The general scheme of ventilation in the METRO during normal operations involves piston-action enhanced by the use of mid-tunnel fans. These mid-tunnel fans combine with blast shafts and station entrances in providing for air exchange with outside ambient (see Figure 15-6 for location details). The fans in the test area of Line No. 2 are of a bi-directional, two-speed type with a nominal maximum capacity of 135,000 cfm in the exhaust mode, providing the METRO with a

substantial flexibility in controlling subway ventilation.

During the warmer months of the year, these fans operate in the full-speed exhaust mode almost continuously, the exceptions being morning and evening rush hour when all fans are shut down to reduce peak power demand utility charges. As the weather becomes cooler, fan operations are adjusted according to a pre-established schedule relating to the outside ambient temperature (see Ref. 13 for details). The fans are remotely operated from central control, where outside temperature is monitored and fan operations adjusted at several times during the day. A major checkpoint in the temperature/fan operations schedule is 40°F. Above this temperature, all fans within the test area are operated at high-speed exhaust. At 40°F and below, the fans are operated in specified combinations of low-speed exhaust and supply during revenue service, and all fans are off during non-revenue hours, except Chabane (4503) and Guizot (4504) which are operated in a low-speed exhaust mode.

Prior to and during the November test period, the ambient temperature generally dropped below 40°F during the nighttime hours corresponding roughly to the period of the non-revenue service, and the fan operations were tested accordingly during this period. Table 15-6, which gives the status of the fans within the test area during each of the system tests, shows all fans to be off during each of the rush-hour tests (M-301, 303, 305, 307). During the first day of testing the ambient temperature rose to 46°F, and the fans were operating in the high-speed exhaust mode during tests M-302 and M-304 (the fans at Faillon (4505) and St. Zotique (4506) were shut down for maintenance). On the second day of testing the ambient temperature was cooler, reaching a maximum of 42°F during tests M-306 and 308, and fan operations were adjusted to the low-speed configuration. The blast shafts within the test area were all open throughout the first day of tests. On the second day, the blast shaft in Cremazie Station (0-148) was closed after test M-307 because of inclement ambient conditions.

A summary of the subway air temperature measurements for each of the systems tests, demonstrating the general effects of fan operations, is presented by Table 15-7. The trend on the first day was for the subway air temperature measurements at noon to be less than during the morning rush hour, even though ambient temperature increased 7°F between the two tests. This observation is particularly true for test sites near blast shafts such as sites E and G, where significant quantities of ambient air were introduced

TABLE 15-6. FAN OPERATIONS DURING THE SYSTEMS TESTS

<u>TEST</u>	<u>SAURIOL (4502)</u>	<u>CHABANEL (4503)</u>	<u>GUILZOT (4504)</u>	<u>FAILLON (4505)</u>	<u>ST. ZOTIQUE (4506)</u>	<u>BELLCHAISE (4507)</u>
301	off	off	off	off	off	off
302	Full exh.	Full exh.	Full exh.	off	off	Full exh.
303	off	off	off	off	off	off
304	Full exh.	Full exh.	Full exh.	Full exh.	off	Full exh.
305	off	off	off	off	off	off
306	off	1/2 exh.	1/2 exh.	off	1/2 sup.	1/2 sup.
307	off	off	off	off	off	off
308	1/2 sup.	1/2 exh.	1/2 exh.	1/2 sup.	off	1/2 sup.

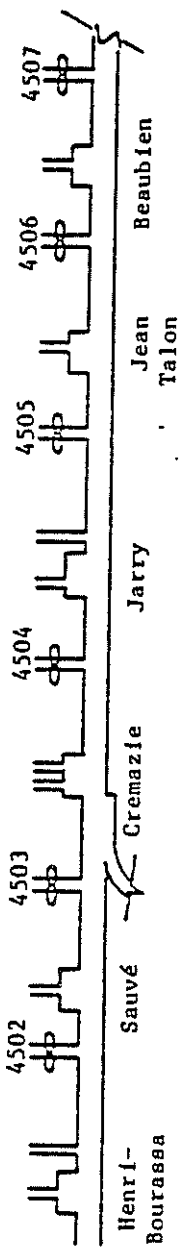
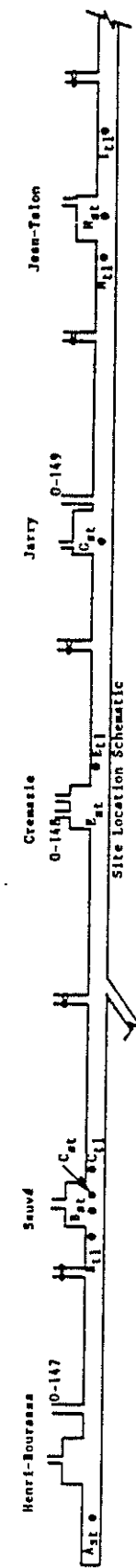


TABLE 15-7. SYSTEMS TESTS: AIR TEMPERATURE DATA SUMMARY

Test	Site								Site								Site														
	A _{st}	B _{st}	C _{st}	E _{st}	F _{st}	G _{st}	H _{st}	I _{st}	A _{st}	B _{st}	C _{st}	E _{st}	F _{st}	G _{st}	H _{st}	I _{st}	A _{st}	B _{st}	C _{st}	E _{st}	F _{st}	G _{st}	H _{st}	I _{st}							
	Min Max Avg	Min Max Avg																													
101	76	82	80	62	75	70	62	76	70	67	78	75	72	77	75	50	73	65	52	75	71	72	79	77	79	76	75	80	76	39	
302	76	82	80	64	71	68	64	72	68	73	76	75	75	78	77	48	60	53	51	65	55	51	73	67	73	77	79	78	78	46	
303	76	82	80	71	77	74	71	78	75	71	78	76	75	81	79	49	70	62	60	75	70	65	78	75	74	80	78	81	80	46	
304	75	83	80	62	70	65	63	72	68	65	72	69	70	75	73	50	71	56	50	65	57	60	75	74	77	79	79	83	82	46	
305	75	81	79	62	75	72	65	75	72	70	77	74	73	78	76	49	62	56	52	72	65	62	76	72	75	80	77	76	80	78	39
306	75	83	81	64	72	69	67	73	71	70	75	74	74	77	76	52	61	54	51	66	57	56	74	67	76	79	77	77	69	77	40
307	77	82	79	65	74	72	62	76	75	73	78	75	75	81	79	50	61	54	56	73	63	59	77	74	77	80	79	78	81	79	42
308	75	83	81	62	73	67	64	72	68	68	75	70	71	75	74	58	62	59	67	72	69	55	75	65	73	78	76	75	81	78	39



into the system by the mid-tunnel fans operating in the high-speed exhaust mode during the off-peak hours. Air temperature during the evening rush hour was consistently higher than morning rush conditions, averaging about 4°F hotter overall. Ambient conditions for test M-305 on the second day were essentially identical to the corresponding test on the first day (M-301), and average system air temperature measurements for the two tests generally corresponded to within 2°F or better, reflecting a reasonable degree of repeatability of the subway thermal behavior.

As the second day continued, ambient conditions changed significantly. During the off-hour tests (M-306 and 308) the temperature was at or below 40°F, resulting in the operation of fans in the low-speed configuration and measurable differences in system temperature compared with the first day. The ambient temperature at evening rush was only 3°F above the morning rush value, and subway air temperatures during evening rush averaged only slightly above the morning rush, with the site E evening rush temperature being 2°F cooler. The low-speed fan operations during the off hour also had a noticeable effect. During test M-306 subway air temperatures were much closer to the morning rush measurements than on the first day with exception of site I. The behavior of the site I temperature is explained by observing that the St. Zotique fan, adjacent to the site, was off for all system tests except M-306, when it was in the low-speed supply mode and providing cooler air past the test site. Other noteworthy behavior includes site E temperature during test M-308. Closing of the Cremazie blast shaft resulted in the highest station and tunnel temperatures of the day being recorded from 2200 to 2300 hrs. A contrasting behavior was noted at site C in Sauvé Station where temperatures on the second day followed those of the first day of system tests within 1°F. This finding suggests a relative insensitivity of subway air temperature in this area to transient daily changes in ambient conditions, perhaps caused by lower ventilation than in other parts of the system. A large percentage of the air exhausted by the nearby Chabane fan shaft appears to come through the adjacent single-track tunnel, providing a possible explanation. Air temperature at this site, recorded continuously for a 25-hour period, is presented by Figure 15-51.

From the foregoing discussion, it is clear that the operation of fans in the Montreal METRO is somewhat at odds with the SES heat sink subprogram

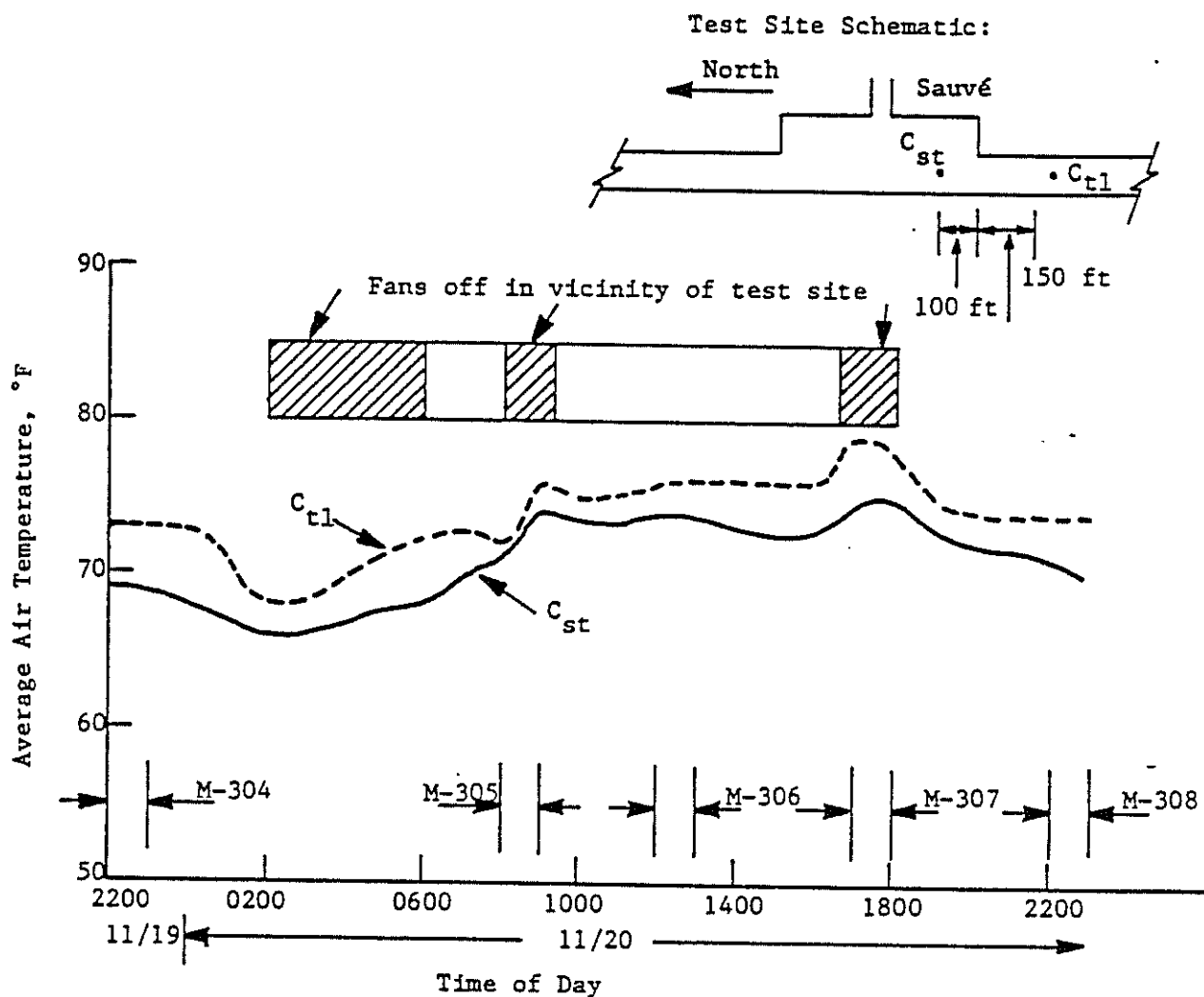


FIGURE 15-51. TWENTY-FIVE HOUR PROFILE OF SUBWAY AIR TEMPERATURE: SITE C

assumption regarding a time-invariant subway ventilation scheme. Differences become more pronounced as the weather becomes cooler, dictating major changes in fan operations. In November, however, the fans are still operating for over half of every 24-hour period, and it is expected that this degree of fan operation, together with the even greater use of fans during the preceding months, will have a very strong influence on the long-term aspects of the heat sink behavior during this time of the year.

15.5.3.3 Heat Sink Subprogram Application - In addition to the air temperature and flow rate data presented in Section 15.5.1, the SES program also tabulates average heat gain data on a segment-by-segment basis through the system. From this information, it was determined that the total SES-computed subway sensible heat gain during the rush-hour simulation was approximately 20,350 MBH from Henri-Bourassa to the St. Zotique fan shaft (4506). Approximately 95 percent of this heat traces to train operations, while the remaining 5 percent comes from fixed system auxiliaries. The spatial distribution of the train heat dissipation was significantly affected by the large mass of the friction-braking system. The steel wheels, comprising the bulk of the calculated 2770 lb/car braking system mass, operated in a relatively low-temperature range of 175-200°F (SES-computed average braking system temperature) within the test area and exhibited a significant thermal inertia. Free convection is the primary heat transfer mechanism from these wheels as trains dwell within the stations, and in this temperature range the free convection heat transfer coefficient is much lower than the forced convection coefficient which dominates when the train is in motion. Thus, although the primary dissipation of energy occurs in the vicinity of the stations, about 65 percent of the total, station-to-station, train heat release occurs within the tunnels (see Appendix D for typical vehicle power dissipation and heat release data).

Of the 20,350 MBH rush-hour sensible heat gain, the heat sink extracts approximately 40 percent based on the use of measured wall-surface temperature data in the short-term SES program simulation, while ventilation accounts for about 45 percent. According to the SES program analysis, the remaining 15 percent is converted to latent heat through adiabatic evaporation from small areas of free-standing water within the tunnels and stations (see Section 15.5.5 for a discussion of evaporation within the METRO). The

indicated heat sink magnitude during the evening rush is about twice that normally expected for November, and the increase is attributed to the intermittent operation of fans during the day.

To gain further insight regarding the effects of fan operations, a short-term SES program analysis of the hypothetical case of a METRO evening rush hour with continuous fan operations was implemented. This analysis showed the average inflowing ventilation air through shafts and entranceways from Henri-Bourassa to the St. Zotique shaft to be approximately 735,000 cfm. A simulation of the same train operations, but with all fans off (i.e., the simulation presented in Section 5.1), indicated an average ventilation airflow of 450,000 cfm. Thus the operation of fans in the hypothetical case increased the ventilation airflow within the test area by almost 65 percent. The increase ventilation air was accompanied by a reduction in subway air temperature on the order of 4°F to 6°F and a corresponding decrease in the heat sink effect to about 20 percent of the system heat gain, based on the measured wall-surface temperatures. This reduction in the heat sink effect was offset by an increase in the heat to the ventilation air to approximately 65 percent of the total heat gain. From this experiment it was concluded that the actual effect of intermittent fan operations in the Montreal METRO is to depress the subway air temperature for a significant portion of the day below that expected without fan operations. Since the heat sink is influenced more by long-term average air temperature conditions than by the short-term exposure to elevated temperatures such as occur during the rush hour when the fans are off, the depressed air temperature during fan operations results in a lower wall-surface temperature than would otherwise be achieved. As a final consequence, the lower wall-surface temperatures respond only slowly to increase in air temperature after the rush-hour cessation of fan operations, and the increased air-to-wall temperature difference results in a marked enhancement of the heat sink effect, limiting the air temperature rise. As noted earlier, this enhancement appears to effectively double the rush-hour heat transfer to the tunnel structure during November.

The complexity of the METRO's ventilation system operation and consequent heat sink behavior precludes a precisely corresponding application of the SES heat sink subprogram. Based on the foregoing reasoning, the conclusion was reached that the closest SES-approximation to METRO operations would be a heat sink analysis based on fans operating in the high-speed exhaust mode for

100 percent of the time, followed by a short-term SES program analysis with the fans off, but with wall-surface temperatures as computed by the prior application of the heat sink subprogram. It is emphasized that this approach represents a hypothetical situation which, by virtue of the heat sink evaluation based on continuous fan operations, should result in an overprediction of the heat sink effect with predicted wall-surface and air temperatures being lower than measured.

The results of the application of the heat sink subprogram to the hypothetical case of continuous fan operations is shown by Figures 15-52 through 15-55. Also shown on these figures, for comparative purposes, are the field measurements obtained with portable temperature sensors. These measured temperatures were adjusted upward 1°F when used for the SES validation runs of Section 15.5.1, to account for the daily wall-surface temperature swing.

The SES-computed wall-surface temperatures generally range from 5°F to 10°F below the measurements, and for the most part follow the spatial trends indicated by the field measurements. This relative behavior was expected by virtue of the assumed continuous fan operations in the SES-analysis. The largest divergence between the field data and predictions occurs near shafts and entranceways, where the assumed operation of fans in the high-speed exhaust mode introduces large quantities of low-temperature ambient air into the tunnels on a continuous basis. Air temperature measurements near these locations (site E_{st} on Table 15-7, for example) show these areas to be subject to large daily air temperature transients due to the intermittent fan operations and the cyclic nature of subway heat gain. These air temperature transients are accompanied by significant changes in wall-surface temperatures, characterized by the revenue-hours measurements of wall-surface temperatures shown on Figure 15-54. At the south end of Jarry Station, near the Jarry blast shaft, wall-surface temperature measurements showed a swing of about 3°F between 1300 and 1700 hours, and these measurements during revenue hours were from 2°F to 5°F below those made during non-revenue hours when the fans were off. Within Sauvé, on the other hand, similar wall-surface temperature measurements (see Figure 15-52) suggested only small daily changes.

Another source of difference in the comparisons of field-measured wall-surface temperatures and SES computations may be the effect of relative train operations and resulting piston-action on the overall balance of tunnel airflow toward the fan shafts. As was discussed previously, SES-predicted

Key to Field Measurements:

X - 0300 to 0440 hrs on 11/15/74
 □ - 0300 to 0430 hrs on 11/19/74
 ▲ - 1700 hrs
 ▼ - 1200 hrs
 11/20/74

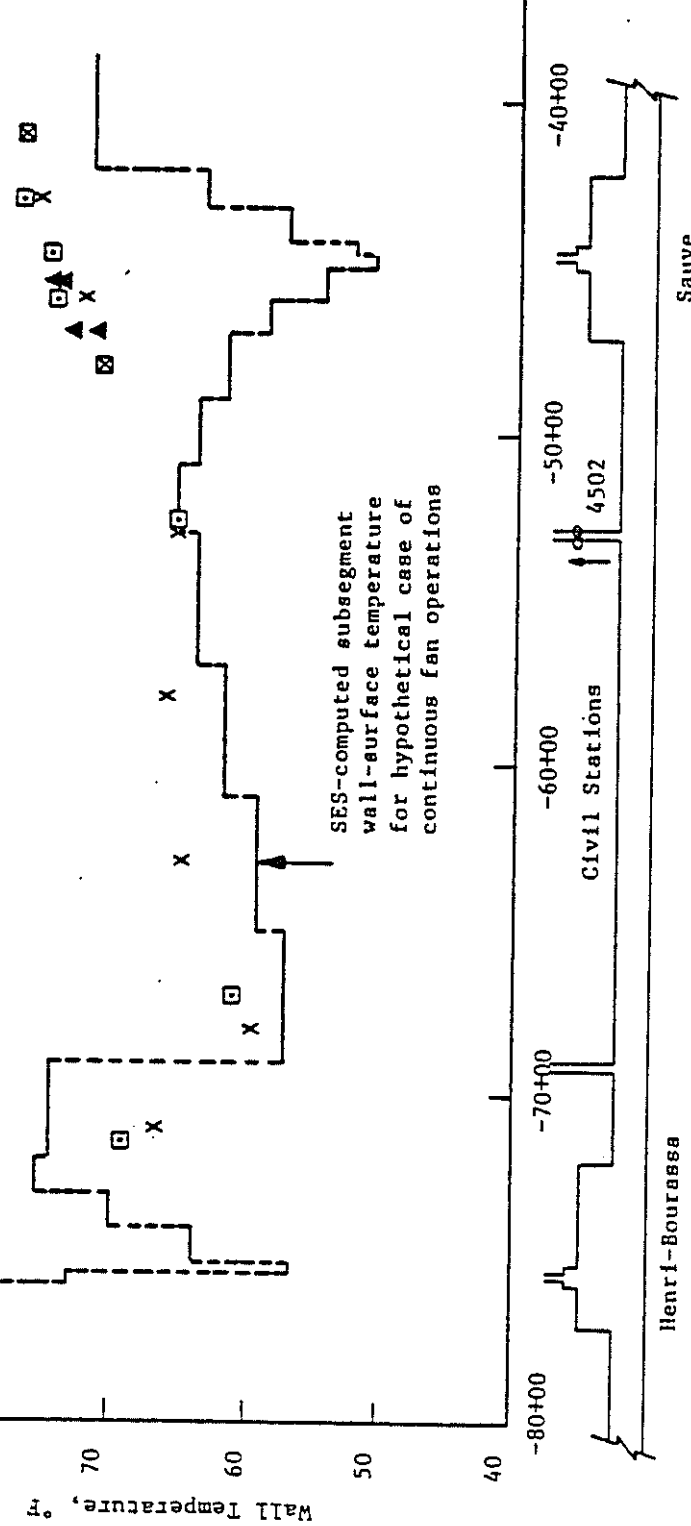


FIGURE 15-52. MEASURED AND PREDICTED WALL SURFACE TEMPERATURE: STA. -80+00 TO STA. -40+00

Key to Field Measurements:

- \times - 0300 to 0440 hrs on 11/15/74
- \square - 0300 to 0430 hrs on 11/19/74

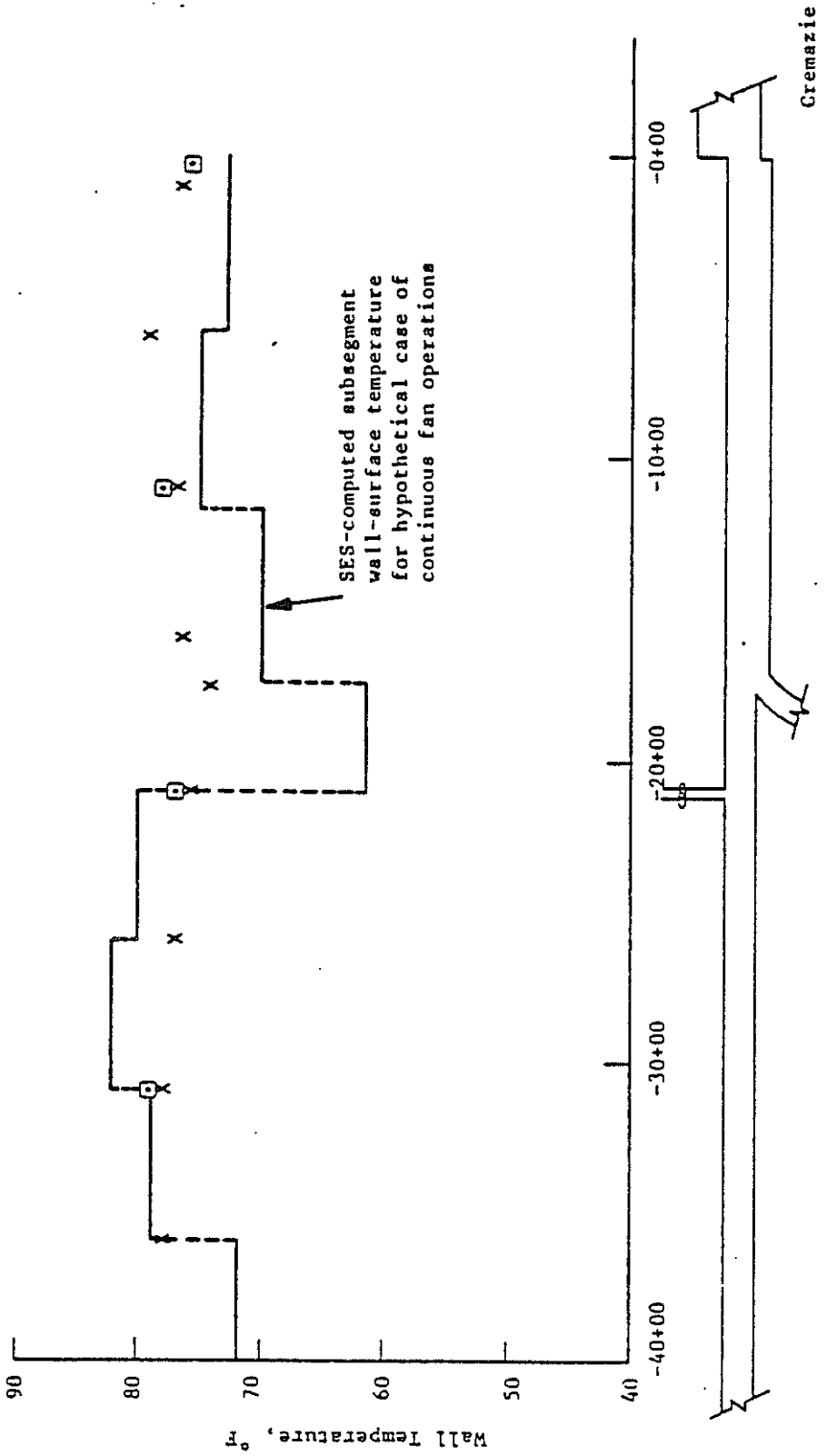


FIGURE 15-53. MEASURED AND PREDICTED WALL SURFACE TEMPERATURES: STA. -40+00 TO STA. 0+00

Key to Field Measurements:

- ◻ - 0300 to 0430 hrs on 11/15/74
- X - 0100 to 0200 hrs on 11/15/74
- ☒ - 0430 to 0440 hrs on 11/16/74
- ⊗ - 0250 to 0430 hrs on 11/19/74
- ▲ - 1700 hrs 11/20/74
- - 1300 hrs 11/20/74
- - 1300 hrs 11/19/74
- - 1700 hrs 11/19/74

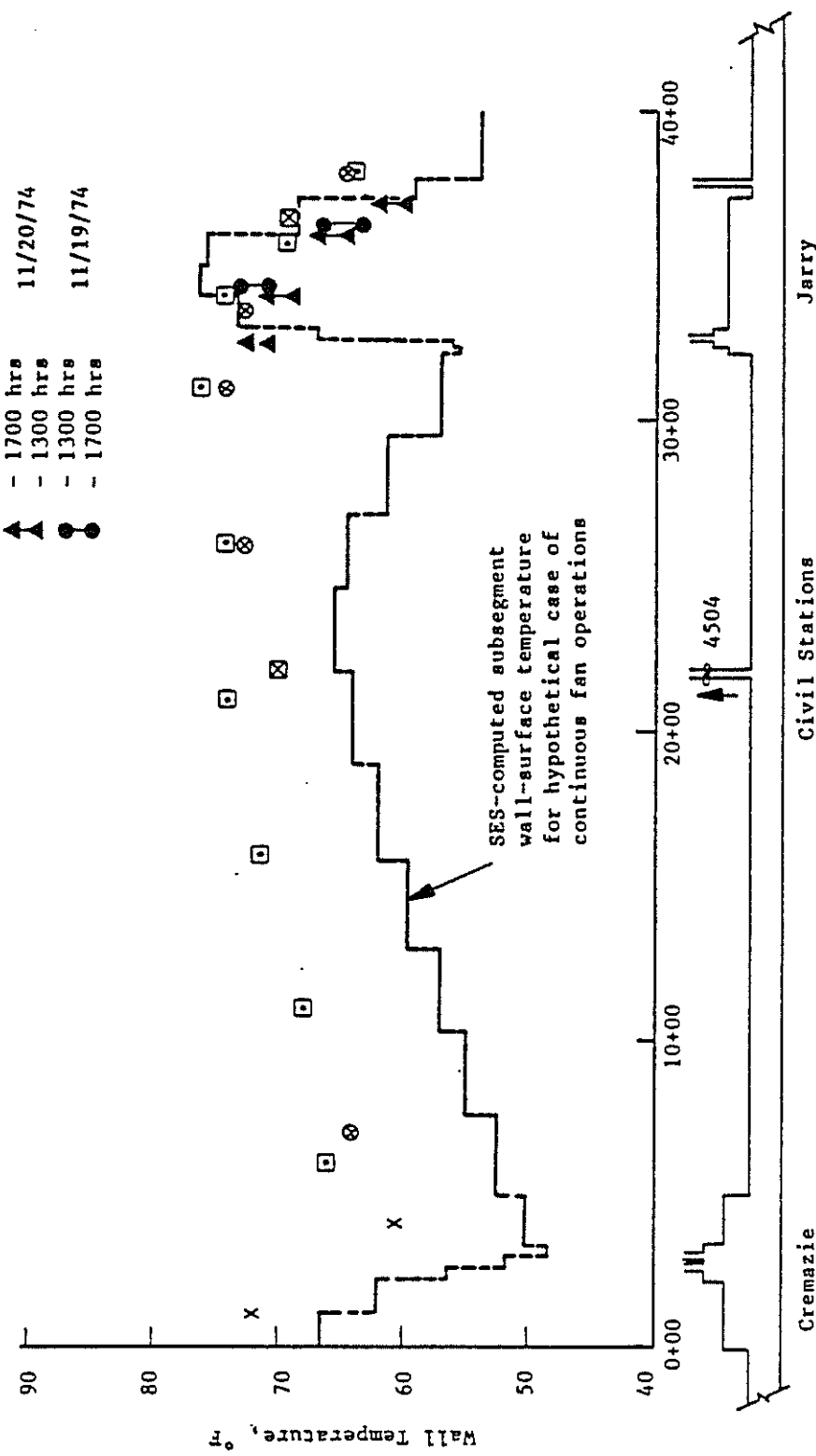


FIGURE 15-54. MEASURED AND PREDICTED WALL SURFACE TEMPERATURES: STA. 0+00 TO STA. 40+00

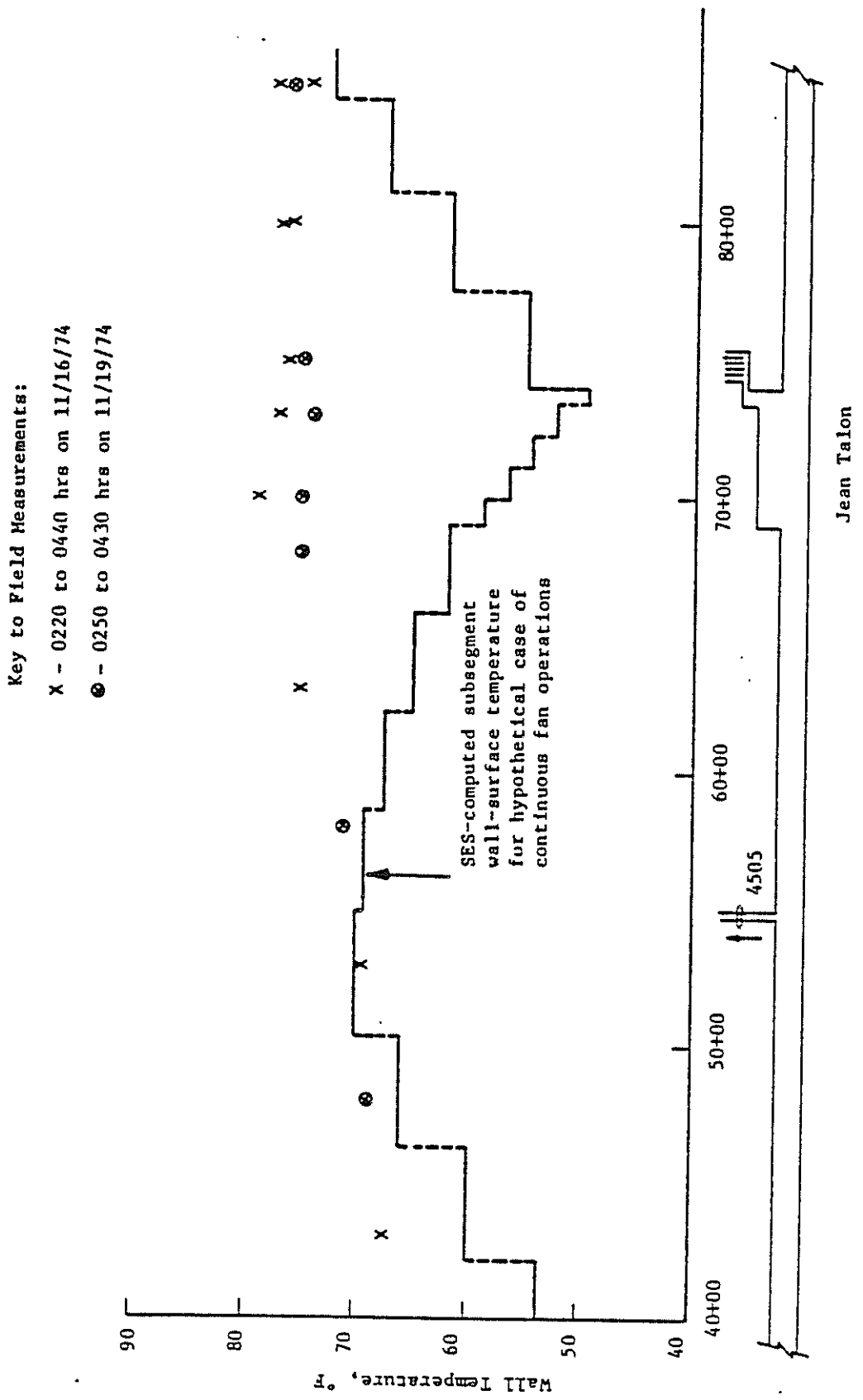


FIGURE 15-55. MEASURED AND PREDICTED WALL SURFACE TEMPERATURES: STA. 40+00 TO STA. 85+00

tunnel airflows associated with a specific case of relative train operations may not precisely represent the prevailing, long-term tunnel ventilation. When fans are a major factor, train operations affect the split of tunnel airflow in the two tunnel sections supplying the fan shaft. As seen in Figures 15-52 through 15-55, regions with relatively warmer SES-computed wall-surface temperatures resulting from a reduced ventilation (e.g., civil sta. -40+00 to -20+00 and 33+00 to 38+00) should in this circumstance be offset by regions with relatively cooler temperatures (e.g., -20+00 to 33+00). However, relatively warmer regions of the subway predicted by the SES program and SES heat sink subprogram may be only slightly affected by this situation. The air temperature measurements and wall-surface temperature measurements in the METRO bear out the SES program predictions of significant spatial variations in subway air and wall-surface temperature.

The heat sink subprogram wall-surface temperature predictions were applied in a short-term evening rush simulation identical in all other respects to the simulation discussed in Section 15.5.1.. A comparison of the resulting SES-predicted average system air temperature distribution with the original simulation using measured wall-surface temperatures for heat sink computations is shown by Figure 15-56. As expected, the lower wall-surface temperatures associated with continuous fan operations lead to lower air temperatures with the fans off, although generally the air temperatures from the two simulations are within 5°F. The one exception is the tunnel section between Cremazie and Jarry, where the difference reaches 7°F. Considering the hypothetical nature of the SES program simulation which produced the wall-surface temperature estimates for the short-term heat sink computations, these comparisons bear favorably on the validity of the overall heat sink subprogram.

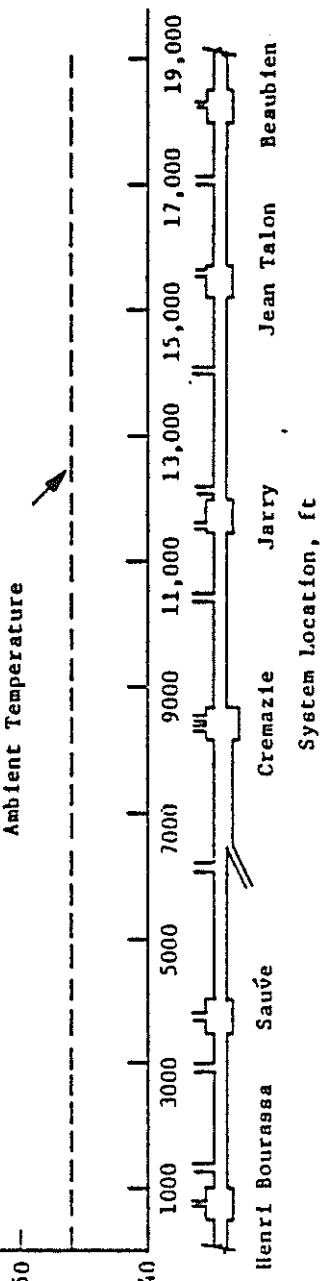
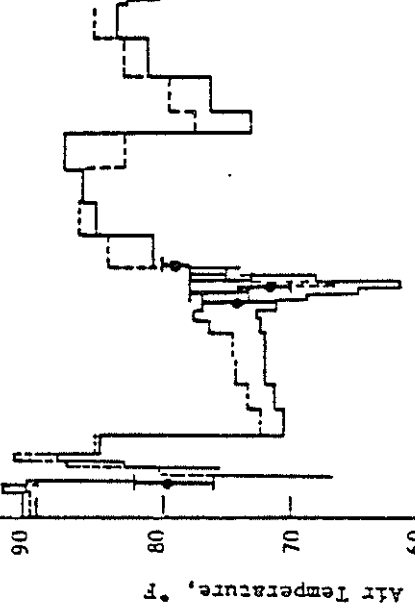
15.5.4 Long-Term Heat Sink Results Using Implicit Train Performance

A long-term SES heat sink analysis for test M-303 was performed using the results of a short-term SES implicit simulation of train operation with continuous fan operation. This implicit SES long-term heat sink analysis was performed to facilitate a one-to-one comparison with the explicit SES long-term heat sink analysis for test M-303 described in Section 15.5.3. As in the comparison between the explicit and implicit short-term SES program simulations described in Section 15.5.2, the implicit SES long-term heat sink

Key to SES Air Temperatures:

- Field-Measured Average Air Temperature

Range Between Maximum and Minimum Air Temperatures Measured at the Instrument Site



- Range Between Maximum and Minimum Air Temperatures Measured at the Instrument Site
- Field-Measured Average Air Temperature
- Average air temperature using field-measured wall-surface temperatures
- Average air temperature using Heat Sink Subprogram wall-surface temperatures from continuous fan operations analysis

FIGURE 15-56. EVENING RUSH SUBWAY TEMPERATURE DISTRIBUTION USING THE HEAT SINK SUBPROGRAM

simualtion was identical to the explicit SES long-term heat sink simulation in all respects except for the operation of trains.

As previously described in detail in Section 15.5.3, performing the long-term heat sink with fans in continuous operation (see Table 15-6) provides only a hypothetical approximation of the actual conditions within the METRO during the evening rush hour. The conclusions reached about the capabilities and constraints of the SES long-term heat sink subprogram discussed in Section 15.5.3 are equally valid here.

The results of the application of the SES heat sink subprogram to the hypothetical case of continuous fan operations in conjunction with implicit train performance are given in Figures 15-57 through 15-60 which show the comparisons between the measured and the implicit SES-predicted wall-surface temperatures throughout the test section. The corresponding SES explicit long-term heat sink wall-surface temperature predictions are shown in Figures 15-52 through 15-55, respectively.

The implicit SES-computed wall-surface temperatures generally exhibited the same trends with respect to the measured wall-surface temperatures as the explicit SES program computations. The largest divergence between the field data and the SES program predictions occurred in Sauvé Station and in the tunnel south of Jean Talon Station (see Figures 15-57 and 15-60). The implicit SES-predicted wall-surface temperatures in Sauvé Station were much lower than the corresponding measured wall-surface temperatures because in the SES program simulation the continuous operation of the fans in the high-speed exhaust mode introduced large quantities of low-temperature (46°F) ambient air into the station on a continuous basis. This was similarly the case with the explicit SES long-term heat sink wall-surface temperature predictions for Sauvé Station (see Figure 15-52). In addition, as previously explained in Section 15.5.3, the relative train operations may have had an effect upon the overall balance of the tunnel airflows toward the fan shafts, which in turn affected the amount of inflowing air through the blast shafts and station entranceways.

The implicit SES-predicted wall-surface temperatures in the tunnel south of Jean-Talon Station (see Figure 15-60) were significantly higher than both the corresponding measurements and the explicit SES program predictions shown by Figure 15-55. The reason for this difference is traced to a cancelling effect that the implicit train operation had on the average ventilation rate

Key to Field Measurements:

- \times - 0300 to 0440 hrs on 11/15/74
- \square - 0300 to 0430 hrs on 11/19/74
- \blacktriangleleft - 1700 hrs
- \blacktriangleright - 1200 hrs 11/20/74

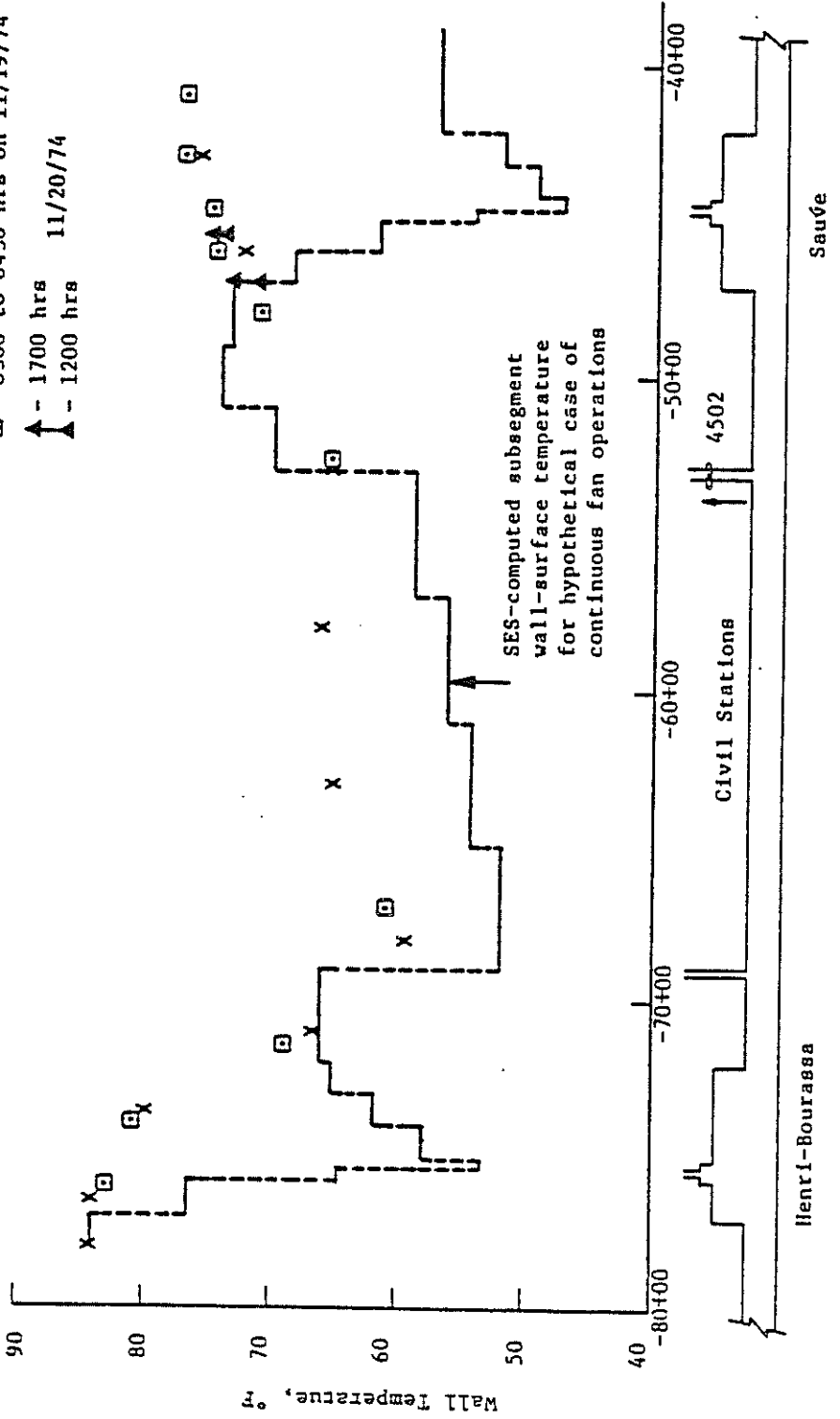


FIGURE 15-57. COMPARISON OF MEASURED AND SES PREDICTED WALL SURFACE TEMPERATURES USING IMPLICIT TRAIN PERFORMANCE: STA. -80+00 TO STA. -4000

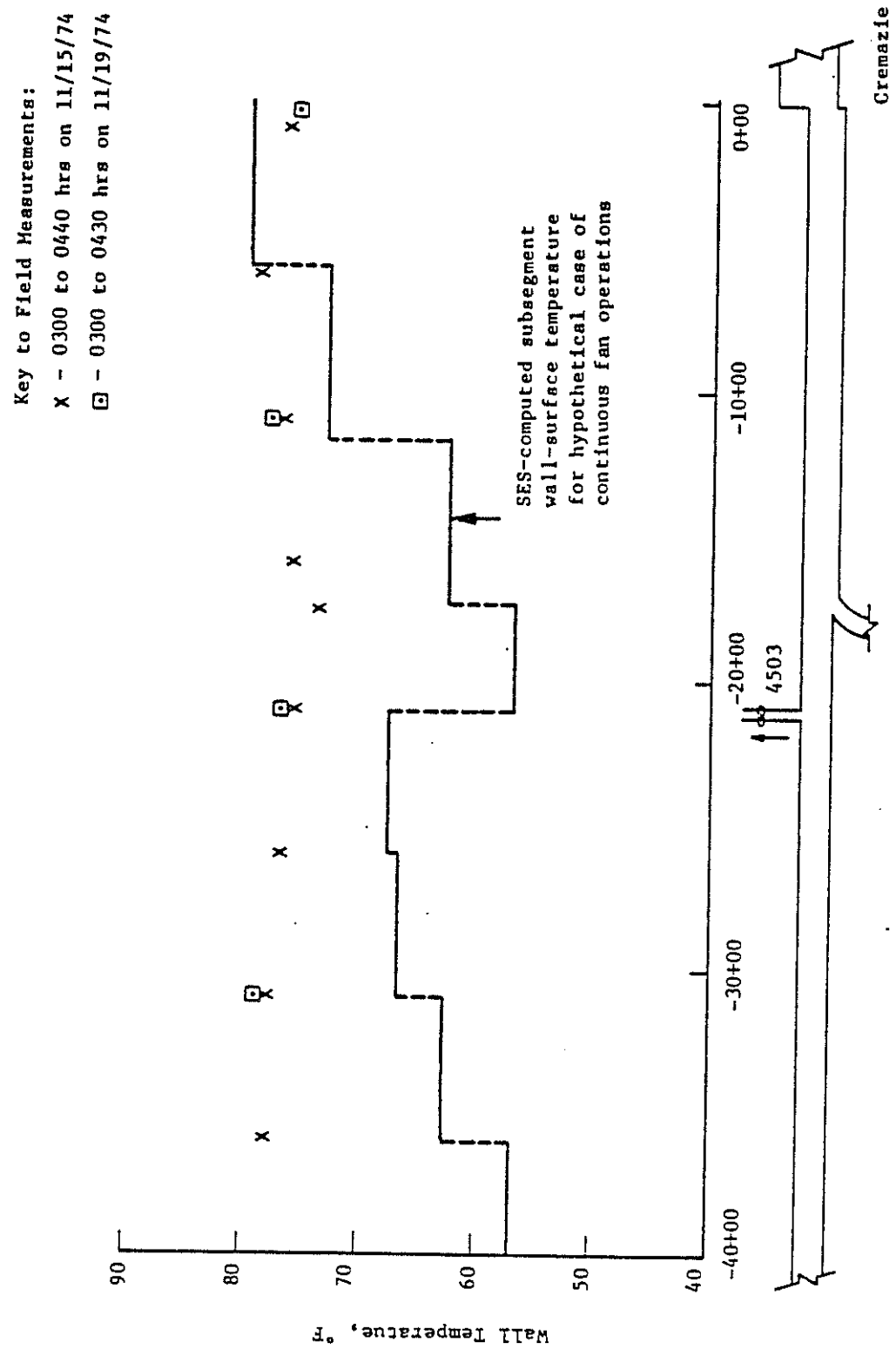


FIGURE 15-58. COMPARISON OF MEASURED AND SES PREDICTED WALL SURFACE TEMPERATURES USING IMPLICIT TRAIN PERFORMANCE: STA. -40+00 TO STA. 0+00

Key to Field Measurements:

- ◻ - 0300 to 0430 hrs on 11/15/74
- ✗ - 0100 to 0200 hrs on 11/15/74
- ☒ - 0430 to 0440 hrs on 11/16/74
- ⊗ - 0250 to 0430 hrs on 11/19/74
- ⊖ - 1700 hrs 11/20/74
- ▲ - 1300 hrs
- - 1300 hrs 11/19/74
- ◆ - 1700 hrs

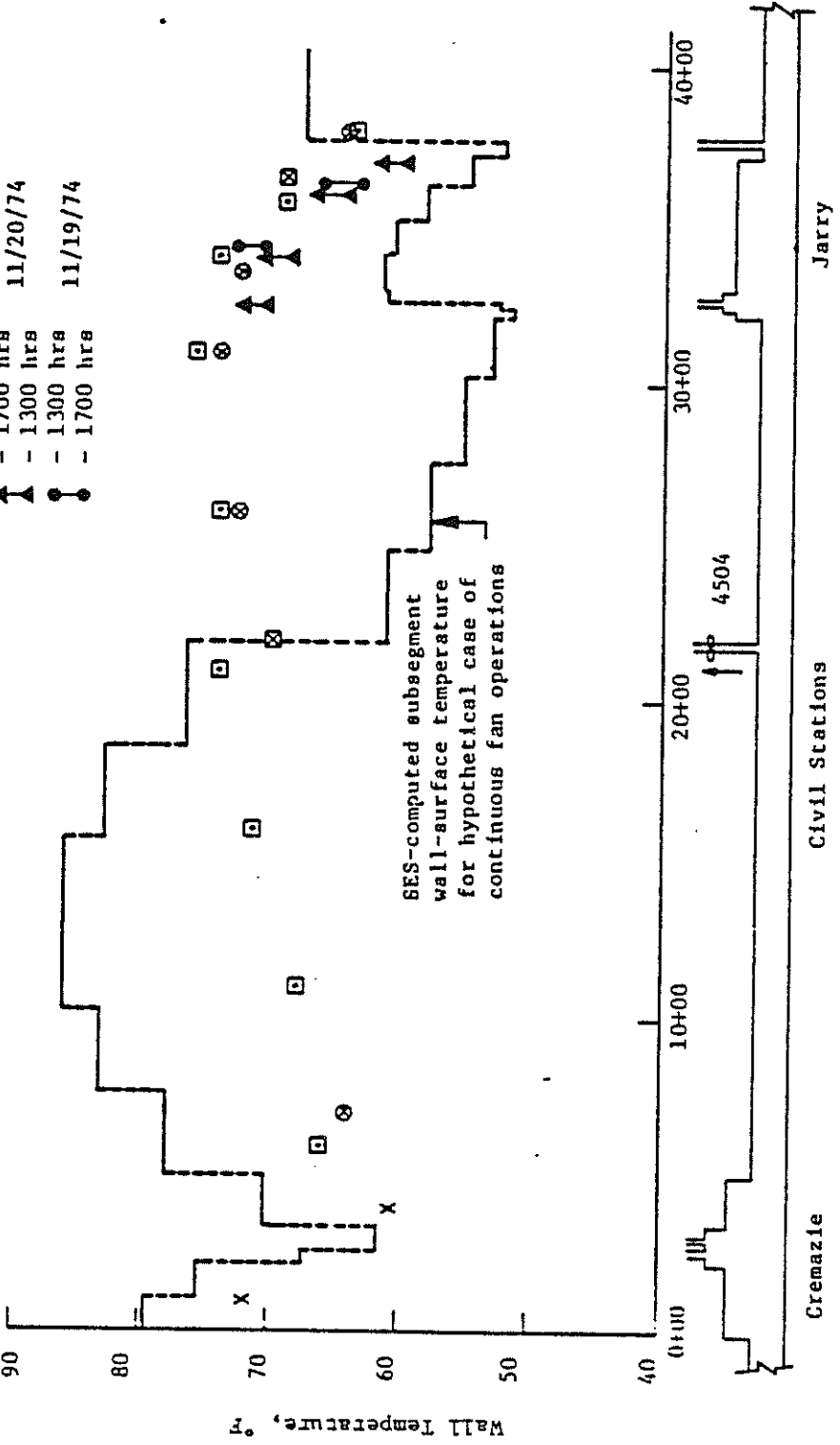


FIGURE 15-59. COMPARISON OF MEASURED AND SES PREDICTED WALL SURFACE TEMPERATURES USING IMPLICIT TRAIN PERFORMANCE: STA. 0+00 TO STA. 40+00

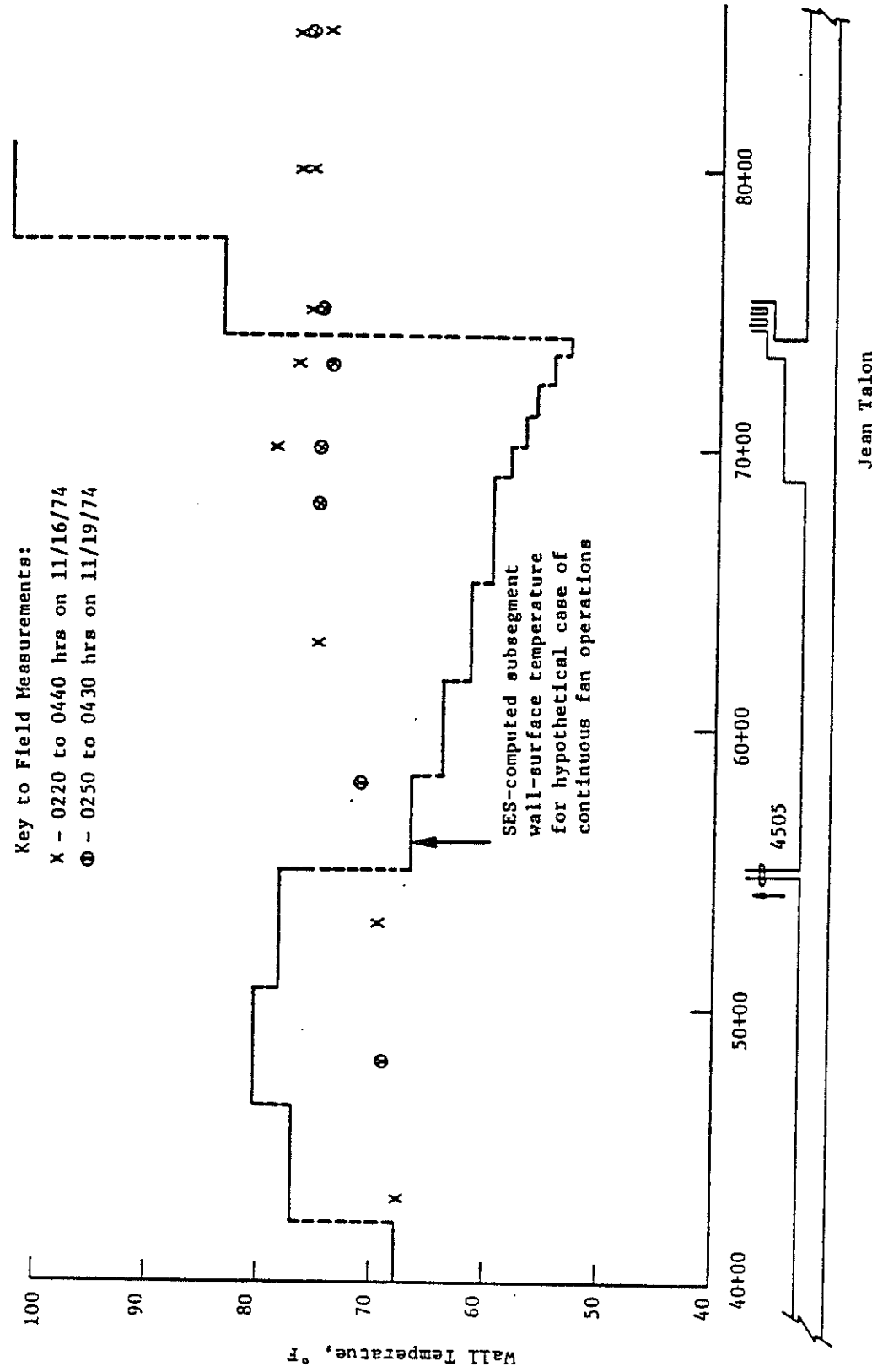


FIGURE 15-60. COMPARISON OF MEASURED AND SES PREDICTED WALL SURFACE TEMPERATURES USING IMPLICIT TRAIN PERFORMANCE: STA. 40+00 TO STA. 85+00

in that particular portion of the tunnel. To illustrate the magnitude of this cancelling effect, consider the following: in the explicit SES program simulation with continuous fan operation described in section 15.5.3, the computed average ventilation rates in the tunnel south of Jean Talon Station were 33,673 cfm in the southward direction and 9924 cfm in the northward direction. In the corresponding implicit SES program simulation with continuous fan operation, the average ventilation rates in the tunnel south of Jean Talon Station were 7334 cfm in the southward direction and 16,372 cfm in the northward direction. The difference in the net average ventilation rates between the SES implicit and explicit simulations is $23,747 - 9038 = 14,711$ cfm. Therefore, the SES implicit train performance caused a 62 percent reduction in the average airflow rate compared with the SES explicit simulation. As explained previously, the extrapolations of short-term averages required by the heat sink subprogram caused the heat sink subprogram to take this low ventilation rate predicted by the implicit SES program as a representative, repeating phenomenon. When the heat sink analysis is confronted with a poorly ventilated tunnel section, it realizes that the heat sink must share a proportionately greater percentage of the heat load. The end result of the heat sink analysis in this circumstance is typically a "hot spot," since the heat transfer to the sink, which depends on the air-wall temperature difference, is enhanced by higher air temperatures. The higher air temperatures result in higher wall-surface temperatures, giving rise to the predicted "hot spot" within the poorly ventilated tunnel.

Subway ventilation concept studies with the SES program (Ref. 12) indicate that the circumstances leading to SES-computed average ventilation rates that are not representative of long-term system behavior occur infrequently. Nevertheless, as exemplified above, it is important that the user perform two or more simulations, each with different relative train operations, when using the SES implicit train performance option.

In general, the accuracy of the heat sink subprogram depends upon the information supplied to it by the SES short-term simulation. When performing a short-term simulation of a system in rare instances when all phases of train operation are known, the explicit SES program simulation is more accurate than the implicit SES program simulation, and it follows that the resulting explicit SES long-term heat sink predictions are more accurate than the corresponding implicit SES heat sink analysis. The implicit SES program,

when implemented properly, is just as accurate as the explicit SES program for system design applications where the exact train operation is unknown.

Overall, the results of the SES heat sink subprogram application using data from a short-term analysis which employs the implicit train performance option emphasize the recommendation outlined herein regarding the need for evaluating long-term heat sink for more than one circumstance of relative train operations. The differences between wall-surface temperatures computed by the explicit and implicit SES programs are solely caused by the differences in train operations. Although the difference through most of the system are minor, the tunnel south of Jean Talon is an example of the "hot spot" which can be encountered with the SES heat sink subprogram.

The fact that the SES heat sink subprogram cannot directly address circumstances such as encountered in Montreal, where operation of the ventilation system undergoes substantial changes on a daily and annual basis, leads to the recommendation that the capabilities of the subprogram be broadened still further. The accurate evaluation of the heat sink effect is an important part of the overall environmental analysis, and the basic analytical models-- the heat conduction analysis and the DTRM-- have been proven valid. Additional research is warranted in the development of economical methods for estimating the effects of daily and annual changes in the subway ventilation configuration and translating these effects into data which can be applied in the proven models.

15.5.5 Evaporation

Within the test area, the METRO tunnels are bored and concrete lined. The tunnel surface is generally dry; however, significant seepage occurs at fault locations in the rock and concrete lining. This results in small areas of wet surface within the tunnels between the source of water and the open drainage troughs, estimated at 5 to 10 percent of the total tunnel surface area. The surface water provides the potential for evaporation; the actual degree of evaporation depends on the condition of the tunnel air. The rate of evaporation from surface water depends upon the wall surface convection heat transfer coefficient and the difference between the dry-bulb and wet-bulb air temperature, assuming that little of the heat for evaporation comes from the tunnel structure in contact with the water.

During the cooler months, the dry-bulb air temperature within the METRO subway is elevated significantly above ambient by virtue of ventilation system operations and annual heat sink behavior. The relative humidity of ambient air in Montreal is on the order of 70 to 80 percent during the cooler months. In November, this translates as a dry bulb-wet bulb temperature difference of 2°F to 4°F. However, as this ambient air is drawn into the subway and heated, the relative humidity falls sharply, with a corresponding increase in the dry bulb-wet bulb temperature difference. Taking test M-303 as an example, ambient conditions were 46°F db and 42°F wb. Assuming an average elevation in dry-bulb temperature within the tunnels to 75°F prior to considering the effects of evaporation, the wet-bulb temperature becomes 55°F corresponding to a relative humidity of about 25 percent. The temperature difference affecting the rate of evaporation from surface water is thus on the order of 20°F during November.

The conditions for the warmer months contrast with those described for the cooler months, because temperatures within the METRO tunnels are much closer to outside ambient from late April until early October. In fact, measurements by the METRO during 1971 and 1972 (Ref. 13) show the subway temperatures often to be slightly below ambient during the warmest part of the day for the months of May, June and July. Ambient humidity continues at a high level during the warmer months; ASHRAE recommends a value of almost 60 percent for design, and Montreal METRO measurements suggest an average value of closer to 80 percent. For an ambient dry-bulb temperature of 85°F, these relative humidities correspond to wet-bulb temperatures of 74°F and 81°F, respectively. Since the dry-bulb temperature in the tunnels increases little, if any, above ambient, the dry bulb-wet bulb temperature difference affecting the rate of evaporation is on the same order as ambient, or about 5°F to 10°F. Consequently, much less evaporation would be anticipated for the summer months. This supposition is borne out by the METRO's 1971-1972 measurement program. Their findings suggest that specific humidities within the tunnels is near, or even below, ambient during the warmer months.

The SES program simulations applied in the system validation discussed in Sections 15.5.1 and 15.5.3 used as input for evaporation calculations an average tunnel surface wetness of 10 percent. As mentioned in the Section 15.5.3 discussion of the heat balance within the METRO, this resulted in

approximately 15 percent of the SES-computed sensible heat gain being converted to latent heat during the November evening rush-hour test M-303. The corresponding computed and measured specific humidities at the test sites during this test are given by Table 15-8. Considering the uncertainty inherent in the estimation of wall-surface wetness and the complexity of the actual, dynamic evaporation process, the agreement is excellent.

Also shown on Table 15-8 are the humidity computations from the SES program simulation of continuous fan operations, implemented as a part of the Section 15.5.3 evaluation of the heat sink subprogram. Test M-302 was selected as being close to this SES program simulation in terms of METRO ventilation system operation and ambient humidity, and the humidity measurements from this test are also presented for qualitative comparison. The most noteworthy difference between SES program computations for the analysis of evening rush hour versus the hypothetical case of continuous fan operations is the marked reduction in subway specific humidity when the fans are operating. This behavior traces to the increase in subway ventilation when the fans are turned on: the higher quantities of air are exposed to evaporating surfaces for a shorter period of time, and the tunnel dry bulb-wet bulb temperature difference is smaller because of the lower subway temperatures resulting from the increased ventilation. The difference in subway humidity between tests M-302 and M-303 qualitatively substantiates the SES program computations.

TABLE 15-8. COMPARISON OF MEASURED AND PREDICTED SUBWAY AIR HUMIDITY

LOCATION	AVERAGE HUMIDITY, $\text{lb}_{\text{water}}/\text{lb}_{\text{dry air}}$			
	EVENING RUSH TEST M-303*	(FANS OFF) SES+	OFF-PEAK (FANS ON) TEST M-302**	SES+
Sauvé (site B)	0.0063	0.0065	0.0053	0.0052
Cremazie (site E)	0.0064	0.0063	0.0057	0.0050
Jean Talon (site H)	0.0070	0.0071	0.0059	0.0053
Pump Room (site I)	0.0069	0.0061	0.0064	0.0056

*Measured Outside Humidity: 0.0047 lb/lb

**Measured Outside Humidity: 0.0045 lb/lb

+SES Outside Humidity: 0.0047 lb/lb

NOTE: The test results represent the average of readings at 15 minute intervals. The range during test period averaged ± 0.0006 lb/lb.

REFERENCES

1. Parsons, Brinckerhoff, Quade and Douglas, Inc., "A Comparison of the ST-SES with the SAT", Technical Report No. UMTA-DC-MTD-7-72-21.
2. Parsons, Brinckerhoff, Quade and Douglas, Inc., "Comparison Between Computer Simulations and Scale Model Tests of Subway Tunnel Airflow", Technical Report No. UMTA-DC-06-0010-74-3, (PB 244-567).
3. Parsons, Brinckerhoff, Quade and Douglas, Inc., "Aerodynamic and Thermodynamic Validation Tests in Berkeley Hills Tunnel", Technical Report No. UMTA-DC-06-0010-73-1, (PB 226-898).
4. Parsons, Brinckerhoff, Quade and Doublas, Inc., "SES Heat Conduction Model Validation", Technical Report No. UMTA-DC-06-0010-74-2.
5. Parsons, Brinckerhoff, Quade and Douglas, Inc., "Comparisons of Computer Model Predictions and Field Measurements of Subway Environment in the Montreal Metro", Technical Report No. UMTA-DC-06-0010-75-3, (PB 249-119).
6. Developmental Sciences, Inc. - Aerospace Technology Division, "Subway Aerodynamic and Thermodynamic Test (SAT) Facility - Double Track Aerodynamics", Technical Report No. UMTA-DC-MTD-7-72-17, (PB 220-807).
7. DeLeuw, Cather & Company, "Development and Test of Simplified Methods to Predict Subway Air Pressure Transients", Technical Report No. UMTA-DC-06-0010-74-1.
8. Developmental Sciences, Inc. - Aerospace Technology Division, "Vent and Station Test (VST) Facility - Special and Complex Vent Shaft Testing", Technical Report No. UMTA-DC-06-0010-73-5.
9. Schlichting, Dr. Hermann, : "Boundary-Layer Theory", Sixth Edition, McGraw-Hill Co., New York, 1968.
10. Associated Engineers - A Joint Venture, "Subway Environmental Design Handbook; Volume II - Users and Porgrammers Manual", 1975.
11. Parsons, Brinckerhoff, Quade and Douglas, Inc., "A Model for the Prediction of Long Term Heat Sink Effects on Subway Thermal Environment", Technical Report No. UMTA-DC-MTD-7-72-22.

12. Parsons, Brinckerhoff, Quade and Douglas, Inc., "The Aerodynamics and Thermodynamics of Subway Design Concepts", Technical Report No. UMTA-DC-06-0010-74-4.
13. DeLeuw, Cather & Company, "Subway Environmental Survey Montreal Urban Community Transit Commission," Technical Report No. UMTA-DC-MTD-7-71-31, (PB 206-782).

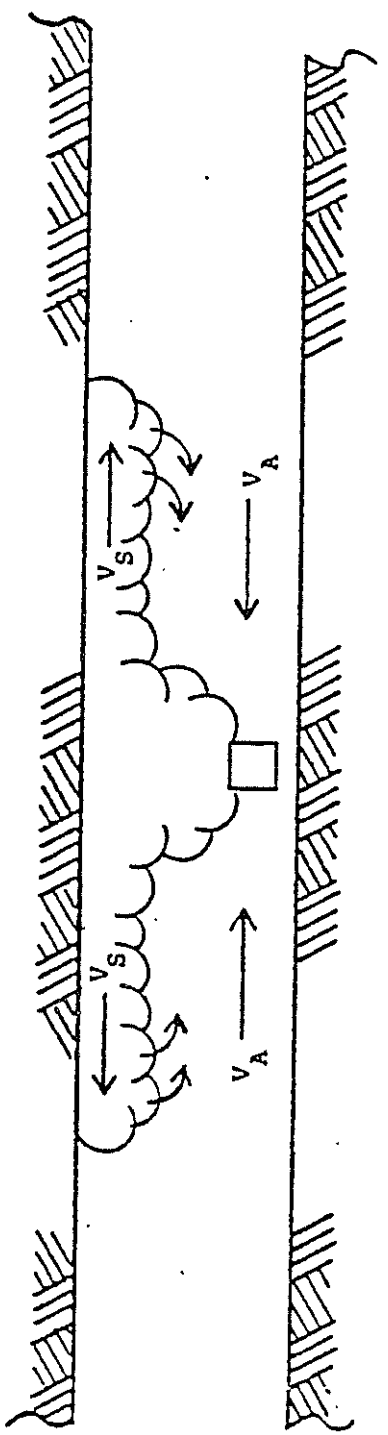
16.0 FIRE MODEL

Documented reports of tunnel fires (Ref...) show the behavior of the fire and associated tunnel air flows to differ significantly from more familiar fire situations outside the confines of a tunnel. The most noteworthy distinction is the buoyant effect which tends to create a layer of hot smoke and gases flowing away from the fire near the crown of the tunnel, while air supporting combustion moves toward the fire beneath the smoke layer. For example, in a horizontal (0% grade) unventilated tunnel with the fire near the longitudinal mid-point, the buoyant effect will establish a symmetrical circulation pattern with the hot, smokey air leaving both ends of the tunnel and air outside the tunnel drawn in beneath it. (See Figure 16-1)

A longitudinal ventilation system forcing air to flow through the tunnel will shift the balance of heated air in the direction of the forced flow. If the ventilation is of sufficient capacity, it will cause all of the heated air to flow towards the downstream direction. If the ventilation is weak, the upper layer of heated air may flow in a direction contrary to the forced ventilation (a phenomenon called "back-layering;" see Figure 16-2). Whether back layering occurs depends upon a number of factors which include the intensity of the fire, the grade and geometry of the tunnel, and the velocity of the ventilating airstream.

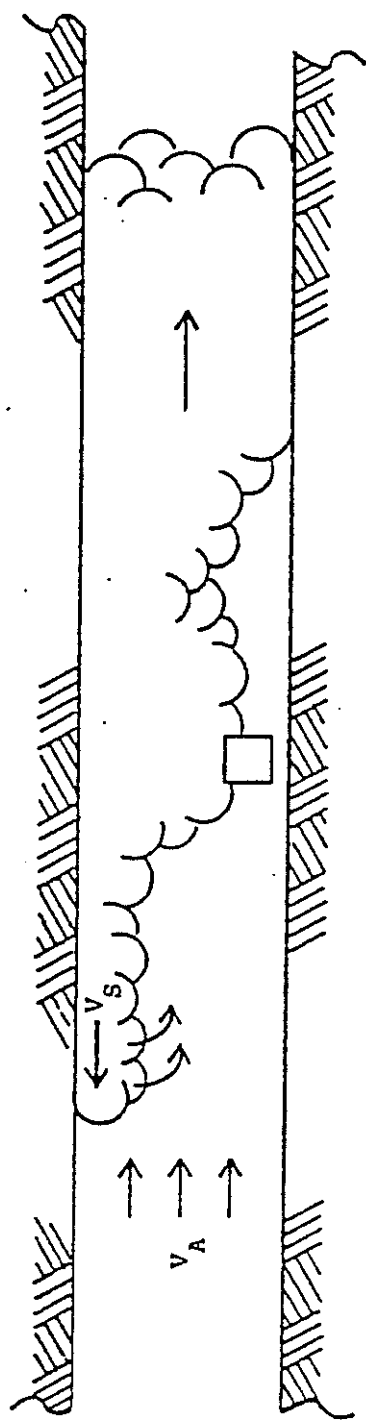
In the event of a subway fire involving a train disabled in a tunnel, the ventilation system should be able to control the direction of smoke movement in order to both provide a clear and safe path for evacuating people and to facilitate fire fighting operations. The ability to prevent back-layering therefore should be a major objective in the design of the ventilation system and its operation during an emergency. The fire model provides the system designer with an analytical tool for evaluating the performance of the ventilation system in this regard.

The fire model that has been developed reflects a compromise between satisfying the basic needs of the ventilation system designer and utilizing the latest state-of-the-art analytical treatment of fires in enclosed spaces in a manner which is compatible with the basic structure of the SES program. In formulating the analytical treatment of the problem, it was concluded that a direct simulation of the complex three-dimensional compressible flow

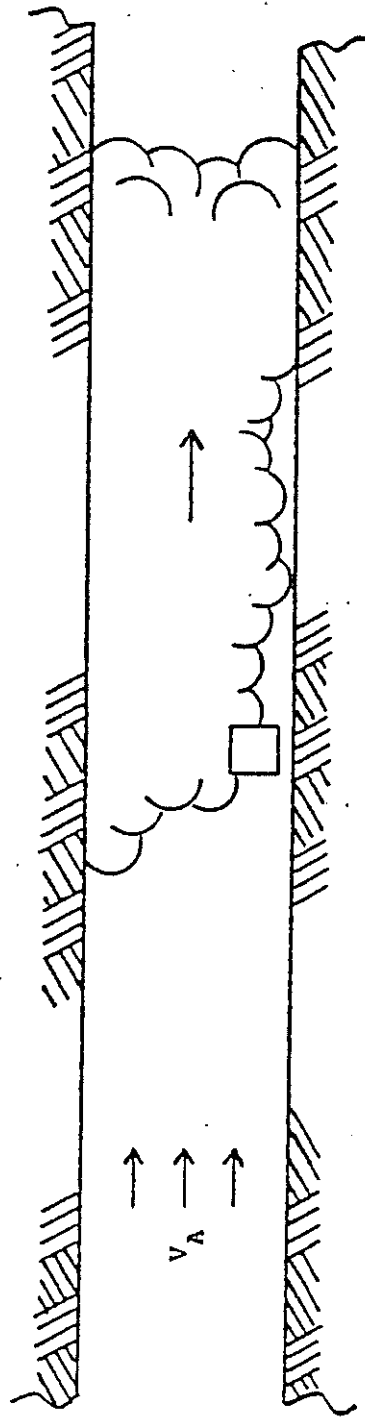


H6-2

FIGURE 10-1 SYMMETRICAL AIRFLOW PATTERNS TYPICAL OF AN UNVENTILATED TUNNEL FIRE



(A) Back-Layering Occurs -- Insufficient Ventilation



(B) Direction Of Smoke-Flow Controlled

FIGURE 16-2 TUNNEL FIRE WITH MECHANICAL VENTILATION

region of the fire was not required to be able to predict the occurrence of back-layering. Instead it was concluded that only the bulk flows and temperatures of the air moving toward and away from the fire, which are dependent on the coupled effects of the fire and the forced ventilation system, had to be simulated. Having done this, the occurrence of back-layering would then be determined by comparing the resulting velocity of the air moving toward the fire with a certain "critical velocity" above which back layering is precluded.

16.1 Critical Velocity

The method selected for treating the problem uses the results of a number of model and full-scale tests (References.....) which showed that back-layering will not occur if the velocity of the ventilating air moving toward the fire is equal to or exceeds a certain critical velocity. For a level tunnel, ($k_g = 1.0$), this critical velocity is determined from the following coupled equations:

$$V_c = K_g K \left(\frac{g H Q}{\rho_a C_p A T_f} \right)^{1/3} \quad (16.1.1)$$

$$T_f = \frac{Q}{\rho_a C_p A V_c} + T_\infty \quad (16.1.2)$$

where:

- V_c = critical velocity, ft/sec
- g = acceleration of gravity, ft/sec²
- H = tunnel height, ft
- Q = fire heat release rate, Btu/sec
- ρ_a = ambient air density, lbm/ft³
- C_p = specific heat of air at constant pressure, Btu/lbm-deg R
- A = net cross-sectional area of tunnel, ft²
- T_f = hot gas temperature, deg R
- K = 0.61 (dimensionless)
- K_g = grade correction factor (dimensionless)
- T_∞ = ambient temperature, deg R

For a tunnel in which the direction of ventilation is downgrade, the critical velocity is greater than that for a level tunnel. Although the effect of grade on the critical velocity has not as yet been specifically studied in connection with tunnel fires, related studies on the control of methane layers in coal mines (methane, being lighter than air tends to form layers along the crown of a mine gallery) have provided some useful data. Since the physical phenomena are similar in both cases, i.e., a low density fluid flowing over a higher density fluid, the data presented for methane layers has been used to develop a grade correction factor. This factor, is tentatively determined from Figure 16-3.

The simultaneous solution of Equations (16.1.1) and (16.1.2) determines the critical velocity. This criterion determines the minimum steady state velocity of the ventilating air moving toward the fire that would be required to prevent back layering. Note that this criterion determines the required air velocity during the fire and not the air velocity in the absence of the fire which can be substantially different. The velocity of the ventilating air moving toward the fire must therefore be known in order to apply this criterion. This velocity is provided by the SES fire model.

16.2 SES Fire Model

A fire in a tunnel can have a considerable effect on the air flow normally induced through the tunnel by the ventilation system. There is the buoyant effect of the hot gases which can either increase or decrease the air flow, depending on whether one is trying to ventilate upgrade or downgrade, respectively. There is a throttling effect which occurs as a result of the expansion and acceleration of gases at the fire site which retards the air flow. There is an increase in the viscous losses downstream of the fire due to the faster flowing hot gases. In addition, the operating characteristics of the downstream fans exhausting the heated air are also affected.

The above described effects are all interrelated with the thermal exchanges that occur at and downstream of the fire site. These exchanges include the direct transfer of heat from the fire to the tunnel air and the transfer of heat to the tunnel walls from the flame via radiation and from the air via both radiation and convection. The magnitude of heat transfer to the walls in the vicinity of a major fire is such that it causes the wall surface

Note: This curve has been adapted from data presented in, "Methane Roof Layers" by Bakke and Leach, S.M.R.E. Research Report No. 195, Sheffield, 1960.

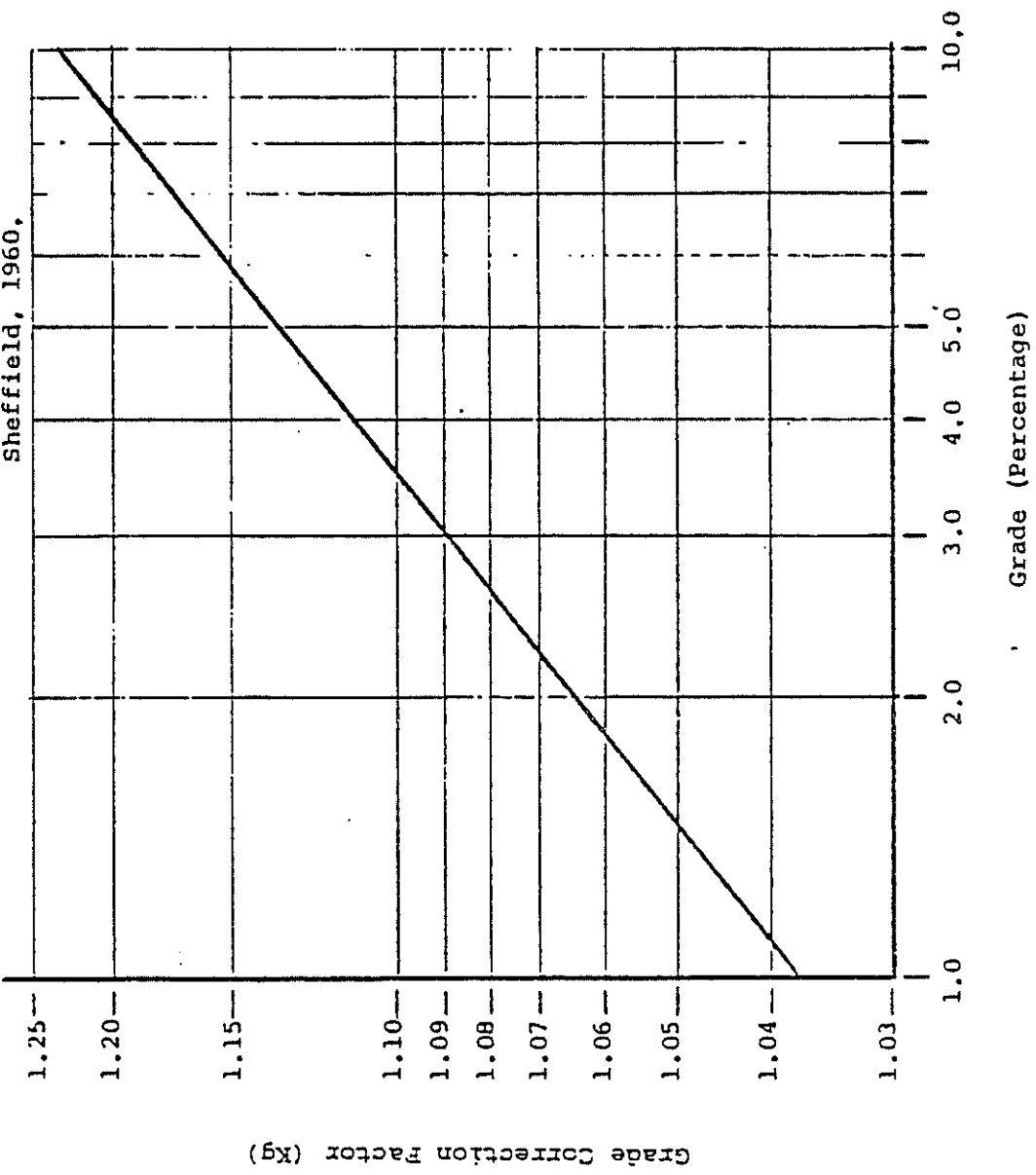


FIGURE 16-3 GRADE CORRECTION FACTOR

temperature to rise rapidly. This rise, in turn, reduces the cooling effect of the walls and increases the temperature of the air (for a constant heat rate fire) as the life of the fire progresses.

16.2.1 Methodology

The SES fire model is able to simulate the interaction of all these fire related effects while still maintaining the basic structure of the SES model, i.e., one-dimensional and incompressible. This was accomplished by: 1) creating a new type of line segment referred to as a "fire segment"; 2) modifying the operating characteristics of fans processing heated air and 3) expanding the capability of the unsteady state heat source to represent a fire. With this approach, the user only has to adjust the program printed CFMs to arrive at the actual flow rates in order to account for variations in air density throughout the system.

For those segments designated by the user as fire segments, the normally performed aerodynamic and thermodynamic computations have been modified to reflect the actual density and other temperature dependent properties of air as a function of the air temperature in the respective subsegments of the segment. In addition, computations relating to buoyancy and throttling effects as well as radiant heat transfer to the walls are also performed. Furthermore, a conduction model has been included to simulate the heating-up of the tunnel wall surface.

16.2.2 Model Limitations

The SES fire model is essentially a quasi-steady-state model that has been designed with the ability to simulate the "overall" effects of a tunnel fire on the air flow induced by the ventilation system. The level of detail is considered sufficient for evaluating the adequacy of the ventilation system and is consistent with the state-of-the-art in mining ventilation programs with the capability of simulating fires. Because the SES is a one-dimensional model, the results of a fire simulation will only indicate whether or not the ventilating air flows are sufficient to prevent back-layering when compared with the critical velocity, but not the extent of back-layering, which is a two-dimensional phenomena. In addition, the early stages of a fire, before the ventilation system is activated, generally cannot be simulated, since this period is dominated by buoyant recirculating air flows.

16.3 Fire Scenario

To reduce weight, cut costs, and provide greater aesthetic appeal and comfort, most modern day subway vehicles are constructed with more and more plastics and other potentially combustible materials than ever before. These materials can be found in the floor covering, wall panels, seats, light diffusers, window and door gaskets, wire insulation, and many other items. Consequently, the transit rider is being exposed to an increasing fire hazard.

A survey of fires which have occurred in subway systems has revealed three main causes:

1. An accident due to a derailment or a collision followed by an electrical short circuit
2. Electrical problems either in the vehicle interior or exterior
3. Arson (usually in the vehicle interior)

A typical fire development process for a transit vehicle is shown in Figure 16-4. The fire starts with some ignition (heat) source which may be in the interior or exterior of the vehicle. In order for a fire to develop, the ignition source must come in contact with flammable material. For an exterior fire, this will usually be beneath the floor, where electrical, equipment, wiring, and the propulsion motors and drives are located.

The floor of a typical transit vehicle is made by bonding thin metal sheets to both sides of a plywood core ("plymetal"). The metal cladding adds strength and increases the fire resistance of the flooring. The specifications for the transit vehicle will usually state the degree of "fire resistance" which is required of the floor. This will govern the selection of floor material and the requirements for sealing all openings (penetrations). Despite these precautions, some undercar fires manage to penetrate into the interior of the car.

Soon after penetrating the floor, the fire will spread to the interior of the car but will remain relatively small in size. This fire will increase the temperature of the car interior causing the interior plastic furnishings to melt. This results in the vaporization of flammable gases. When the concentration of these gases build up and then combine with a sudden increase in air entering the car, sudden ignition can occur.

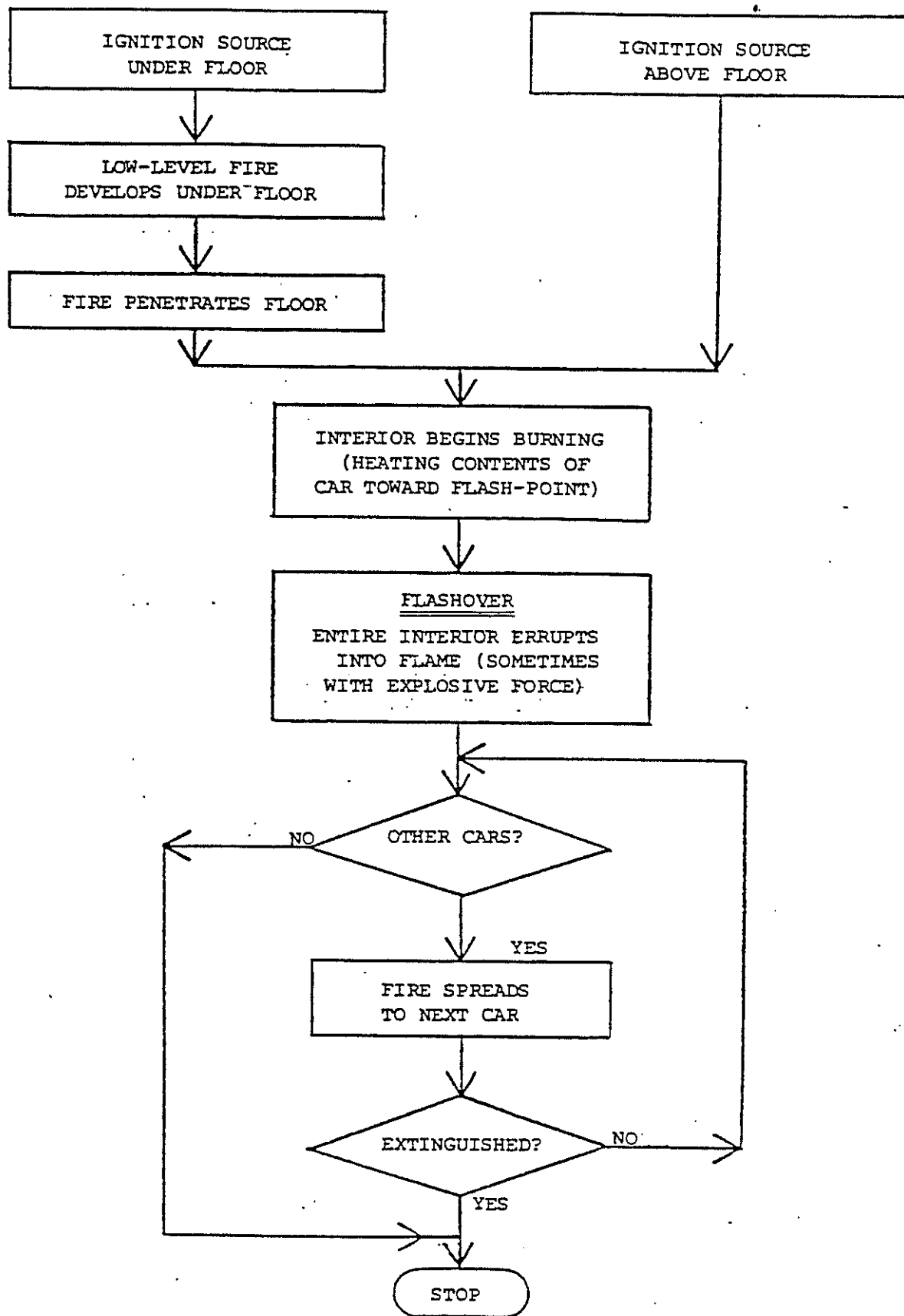


FIGURE 16-4 TYPICAL TRAIN FIRE DEVELOPMENT FLOW DIAGRAM

"Flashover" is an event when essentially the whole interior of the car erupts in flame. A dramatic increase in the fire heat and burning rate results from flashover.

The heat from one burning car is usually sufficient to spread the fire to adjacent cars. Several factors affect the spread of the fire, including the quantity and type of combustibles on each car and the fire resistance of the car ends.

Observations of actual subway fires have shown that the flame spread between cars occurs above the floor line. In most cases, the fire will be confined to the interior above the floor line for the second and subsequent cars. The fire resistant construction of the vehicle floor will usually prevent the fire from spreading to the undercar equipment or burning the floor itself. This has the beneficial effect of reducing the total quantity of combustible materials available to the fire, and thus reduces the heat generated from the burning of the second and subsequent cars.

In summary, a transit vehicle fire can go through many stages. Many fires will be prevented from spreading by the fire resistance of the vehicle construction or be extinguished in the early stages by subway patrons, transit personnel or the fire department. Most major fires can be subdivided into two distinct stages: the "before flashover" stage where the fire is relatively small and produces a small amount of heat, and the "after flashover" stage, when the fire is of major proportions, producing a large quantity of heat.

16.4 Design Fire Heat Release Rate

The key input parameter required by the fire model is the design fire heat release rate of the burning train. This value should be consistent with events observed during major subway fires involving a burning train and the overall design objectives of the subway ventilation system. One approach for estimating this value is to first develop an "inventory of combustibles."

A typical inventory of vehicle combustibles for a particular car is shown in Table 16-1. This table gives the quantity of combustible materials in the vehicle and their heat content broken down into three groups: above the floor level, the flooring material itself, and below the floor level. Having established the total amount of heat that could be liberated from the total consumption of the vehicle, an estimate of the time for this to occur is required to arrive at the average heat release rate from the fire.

TABLE 16-1 INVENTORY OF COMBUSTIBLES FOR SEPTA NEW BROAD STREET CAR*

<u>ITEM</u>	<u>MATERIAL</u>	<u>LBS</u>	<u>BTU/LB</u>	<u>BTU per car</u>
1. Seats (68)	Molded FRP			5,335,000
2. Floor cover	Rubber Sheet			3,200,000
3. Acous. insulation	Insulcoustic 943	200	4,000	800,000
4. Wall & Ceiling Insulation	Woven Glass Fiber (No Binder)			---
5. Liners	Plywood	200	7,900	1,580,000
	Melamine faced aluminum	200	11,100	2,220,000
6. Windows	Lam. safety glass			---
7. Glazing gaskets	Rubber			825,000
8. End caps	FRP	152	11,100	1,687,000
	Cardboard	5.3	7,800	41,000
	Fiberglass	20	11,100	222,000
9. Light diffusers	Polycarbonate			651,000
10. Wire insulation				201,000
<hr/>				
TOTAL ABOVE FLOOR				16,762,000
<hr/>				
11. FLOOR	Stainless steel sheet on 3/4" plywood			6,445,000
<hr/>				
TOTAL IN FLOOR				6,445,000
<hr/>				
12. Batteries	Polycarbonate	20	11,100	222,000
13. Oil (90W)		8 gal	22,000	176,000
14. Control covers	FRP	150	11,100	1,665,000
15. Wire Insulation		1000	11,100	11,100,000
<hr/>				
TOTAL BELOW FLOOR				13,163,000
<hr/>				
TOTAL FOR ENTIRE CAR				<u>36,370,000</u>

*Data prepared by Gage-Babcock & Associates

The following observations have been made concerning past fire incidents:

1. San Francisco-BART (January 17, 1979) - Five vehicles were involved in varying degrees. Estimates of the quantity and type of materials burned result in an equivalent of 3 vehicles burned in 3 hours, or approximately 1 vehicle per hour.
2. Montreal (January 3, 1974) - 4 1/2 vehicles burned in 2 1/2 hours, for an average burning rate of 90 million Btu/hr (22.7 million Kcal/hr) or approximately 1.7 vehicles per hour.
3. Montreal (December 1971) - 24 vehicles burned in 18 hours for an average burning rate of 70 million Btu/hr (17.6 million Kcal/hr) of approximately 1.3 vehicles per hour.

On the basis of the above observations, it seems that a burning rate of one to two vehicles burning per hour is reasonable. Note that this estimate does not necessarily mean that each vehicle is completely consumed each hour, but that a number of vehicles can become involved and partially burn simultaneously, liberating an average amount of heat equivalent to one or two vehicles burning per hour. The latter case is probably the more realistic situation.

To estimate the fire heat release rate in a multiple-car fire as the life of the fire progresses, certain critical times during the fire must be estimated. These times are: 1) The time for a low-level fire to reach flashover, 2) the time for most of the vehicle to be consumed by the fire (measured starting with flashover); and 3) the time for the fire to cause flashover in succeeding vehicles.

Figures 16-5 and 16-6 show the time-dependent fire heat release rates which result from two hypothetical fire scenarios, referred to here as case 1 and case 2. These scenarios were based on the following:

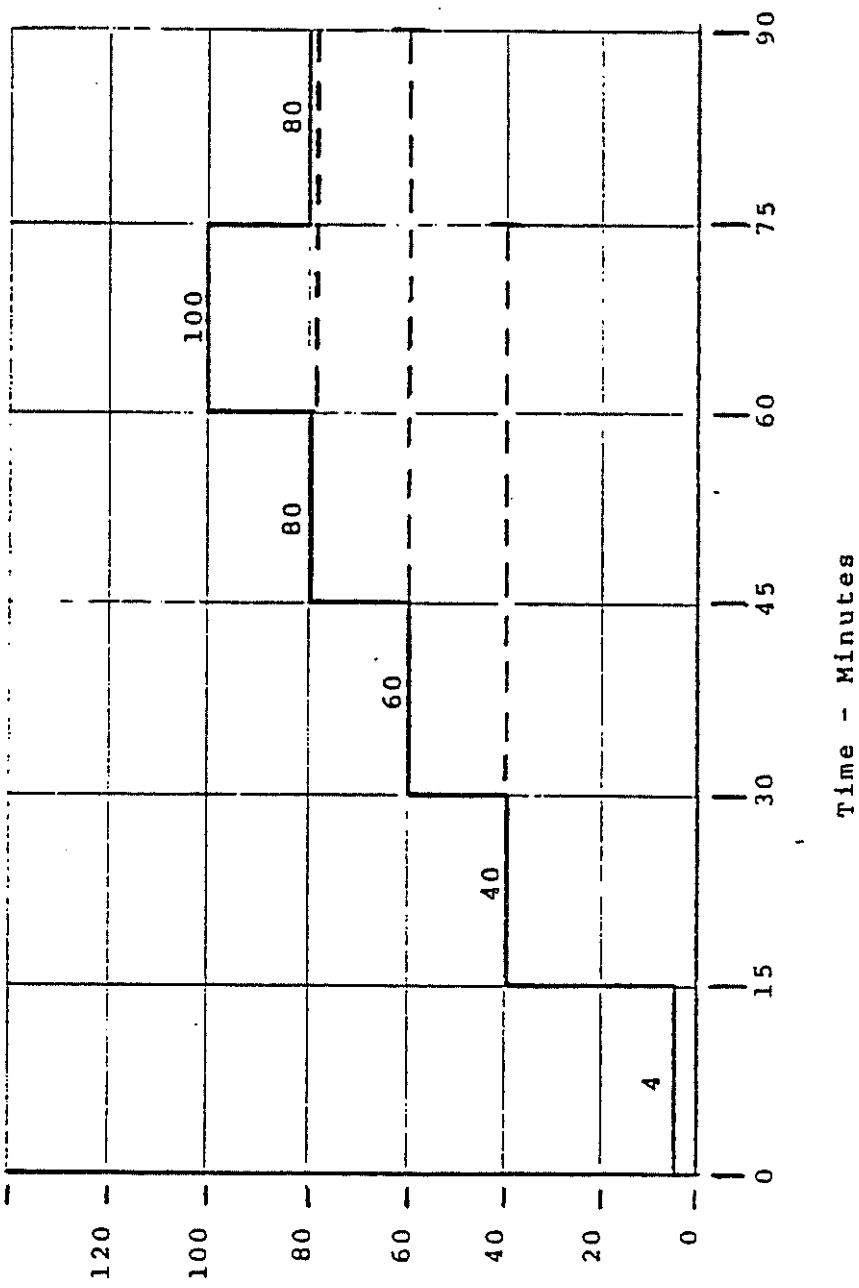
	<u>Case 1</u>	<u>Case 2</u>
Total Vehicle Combustibles - BTU	41×10^6	41×10^6
Vehicle Combustibles Above Floor Level - BTU	20×10^6	20×10^6
Vehicle Burn Rate, Undercar Fire, start to Flashover, BTU/HR	4×10^6	4×10^6
Vehicle Burn Rate, Flashover to Burnout, First Vehicle - BTU/HR	40×10^6	40×10^6
Succeeding Vehicles - BTU/HR	20×10^6	20×10^6
Time Between start and Flashover First Vehicle - Minutes	15	15
Time For Flashover to spread to Succeeding Vehicles - Minutes	15	45

In each of these cases it was assumed that no intervening action was taken to prevent the fire from spreading from car to car. It was also assumed that all the combustibles in the first car were consumed (above floor, floor itself, and below floor), but that the fire was confined to the-above-floor combustibles in the second and subsequent cars.

If the subway ventilation system is to be designed to always prevent back-layering, then the maximum fire heat release rate resulting from the fire scenario should be used as the design fire heat release rate. For case 1, therefore, 60 million BTU/HR would be used in the fire model, and for case 2, 100 million BTU/HR.

If the subway ventilation system is only required to prevent back-layering during the passenger evacuation process, then the maximum fire heat release rate during the time specified to complete this process should be used as the design fire heat release rate in the fire model. For a specified evacuation time of between 45 and 60 minutes, the design fire heat release rate for case 1 and case 2 would be 40 and 80 million BTU/HR, respectively.

Hypothetical Fire Scenario -
15 Minutes Between Flashover
Of Succeeding Vehicles



Fire Heat Release Rate - Million BTU/HR

Hypothetical Fire Scenario -
45 Minutes Between Flashover
of Succeeding Vehicles

